# NEWCASTLE UNIVERSITY

Thermo-economic analysis for optimal selection of desalination techniques based on combined cycle power plant

By

Nuri Mohamed Masoud Eshoul

B.Sc., M.Sc.

A thesis submitted to the School of Mechanical and Systems Engineering for the degree of

Doctor of Philosophy

In Mechanical Engineering

Supervised by

Professor Brian Agnew

Dr. Jack Hale

Dr. Sandy Anderson

November 2017

Abstract

Scarcity of water has become a challenging problem for countries in arid and semi-arid regions. Seawater desalination is considered to be one of the main sources of potable water in areas such as the Middle East and North Africa, with dependency on desalination reaching 90% in some of the Gulf Cooperation Council (GCC) countries. Libya is one of those counties which suffers from a lack of natural water resources. This study focuses on the prospect of coupling desalination plants with existing Combined Cycle Power Plant (CCPP) to produce potable water. This study was based on seawater in the north of Libya and on a source of brackish water in the south of Libya at Waddan City.

The study begins by considering the improvement that could be achieved in CCPP performance by cooling the inlet air using a waste heat driven Absorption Chiller (AC) and then continues to determine the optimal selection of the desalination technique suitable for the environmental conditions in Libya.

The methodology depends on validated simulation models developed from IPSEpro software. The CCPP model was validated against vendor data and the AC was validated against manufacturer data. Different desalination units, Multi-Effect Desalination with Thermal Vapour Compression (MED-TVC), two-pass Reverse Osmosis (RO) and Single Effect Desalination (SED) desalination systems were modelled and validated against actual operation data. After validation the performance of each model was investigated from energy, exergy and economic standpoints for design and off-design conditions using real Libyan environmental data.

This study has, for the first time, compared the exergy efficiency, power consumption and economic characteristics of different configurations of two-pass RO with energy recovery devices such as a Pressure Exchanger (PX) and an Energy Recovery Turbine (ERT). The results shows that when PX is used in the first and second stages of RO the exergy efficiency increases by 81% and the specific power consumption declines of more than 100%.

MED-TVC Gain Output Ratio (GOR) and exergy efficiency are improved by adding a preheater on the distillate water stream to increase the feed water temperature, and the amount of steam extracted from the CCPP is reduced.

A comparison between two-pass RO or MED-TVC coupled with a CCPP has been carried out using thermodynamic and economic analysis. The result shows that the

power plant exergy efficiency deceases by about 4% when MED-TVC desalination plant is coupled with a CCPP but only 0.5% when RO is coupled with a CCPP. Also the net power output declines by about 22.5MW when MED-TVC desalination is used but only 5MW when the CCPP is coupled with a RO with PX desalination plant. In addition, economic analysis shows that RO desalination is a better process compared with MED-TVC, either standalone or coupled with CCPP.

An exergy and economic analysis of two different desalination technologies to produce drinking water from brackish water was investigated. The analysis shows that the exergy efficiency of a single-pass RO unit is nearly double that of single effect desalination and the cost of water produced by a single effect desalination unit is higher than that of a single-pass reverse osmosis unit by about 60%. This confirms that reverse osmosis is the suitable desalination system in Libya.

IN THE NAME OF ALLAH
THE MOST GRACIOUS AND THE MOST MERCIFUL

ACKNOWLEDGMENT

At the beginning, I thank Almighty Allah for giving me the courage, determination and guidance to conduct this research work.

List of publications derived from thesis

Journal papers

1- Nuri Eshoul, Brian Agnew, Alexander Anderson and Mohanad Atab "Exegetic and economic analysis of two-pass RO desalination proposed plant for Libyan domestic water and irrigation" Energy, Vol. No. 122, 2017, 319-328.

2- Nuri Eshoul, Brian Agnew, Mohammed Al-Weshahi and Mohaned Sarari "Exergy analysis of two pass Reverse Osmosis (RO) desalination with and without Energy Recovery Turbine (ERT) and pressure exchanger(PX) "Energies" 2015,8, 6910-6925.

3- Nuri Eshoul, Brain Agnew, Mohammed A. Al-Weshahi and Fathi Latrash "Exergy analysis of two-passes Reverse Osmosis (RO) desalination with and without Energy Recovery Turbine (ERT) "International Journal of Exergy", Vol, 19, No. 1, 2016, 1-14.

Conference papers

1- Nuri Eshoul, Brian Agnew and Ratha Mathkor. Thermodynamic analysis of combined cycle power plant standalone and coupled with multi effect desalination with thermal vapor compression, 6th International Renewable Energy Congress IRCE, Sousse – Tunisia, March 24-26, 2015. IEE.

2- Nuri Eshoul, Brian Agnew, Mohammed A. Al-Weshahi, Ratha Mathkor. Validation and thermal analysis of combined cycle power plant standalone and with multi effect thermal vapour compression. International Conference on Environment Science and Engineering, (ICESE2015), Istanbul, Turkey, April 24-25.

3- Nuri Eshoul, Brian Agnew, Abdalbaset Mnider. Parametric study of multi-effect desalination with thermal vapour compression plant. 7th International Renewable Energy Congress IRCE, Hammamet – Tunisia March 22-24, 2016. IEEE.

4- Nuri Eshoul, Brian Agnew and Alexander Anderson. A comparison between single effect desalination and single reverse osmosis desalination plants using brackish water Waddan city – Libya, Heat Powered Cycles Conference Nottingham University, UK, 27-29 June 2016.

LIST OF CONTENTS

LIST OF FIGURES

LIST OF TABLES

ABBREVIATIONS

AC	Absorption chiller
ARH	Average relative humidity
BWRO	Brackish Water Reverse Osmosis
CCP	Condenser cooling pump
CCPP	Combined cycle power plant
COP	Coefficient of performance
cv	Control volume
CR	Concentration ratio
D	Destruction
DBT	Dry bulb temperature
dp	distillate product
E	Evaporator
ED	Electrolysis desalination
EES	Engineering equation solver
ERD	Energy recovery device
ERT	Energy recovery turbine
G/P	Gas/power
GCC	Gulf cooperation council
GOR	Gain output ratio
GT	Gas turbine
HPP	High Pressure Pump
HPT	High pressure turbine
HRSG	Heat recovery steam generator
HUF	Heat utilization factor
LHV	Lower heating value
LPT	Low pressure turbine
MDK	Model development kit
MED	Multi effect desalination
MED-TVC	Multi effect desalination with thermal vapour compression
MPT	Medium pressure turbine
MSF	Multi stage flashing
MVC	Mechanical vapour compression
N	Number of moles at salt
ORC	Organic Rankine cycle
PEC	Purchased equipment cost
p	Pressure (bar)
pp	Pumps
PSE	Process simulation environment
PWD	Product water disposal
PX	Pressure exchanger
RBWD	Rejected brackish water disposal
Rh	Relative humidity
RO	Reverse osmosis

RSWD	Rejected seawater disposal
SED	Single effect desalination
ST	Steam turbine
SWRO	Seawater reverse osmosis
SWT	Seawater temperature
TCI	Total capital investment
TDS	Total dissolvent salt
TRR	Total revenue requirement
V_1 and V_2	Volume (m^3)
V	Volume (m^3)
w	Water

Nomenclature

A_w	water permeability coefficient (m/s.pa)
b_1 to b_{10}	are constants
B_s	Salt permeability coefficient ($kg/m^2.s$)
C	Molar concentration, thermal capacity (J/K)
Ch	Chemical
cho	Chemical of component
C_f	Feed concentrate
Cf	Feed concentration (mol/m^3)
C_{min}	Minimum thermal capacity (J/K)
Cm	Membrane concentration (mol/m^3)
Cp	Permeate concentration (mol/m^3)
C_w	Water concentration in the membrane (mol/m^3)
D_s	Diffusivity of solute (m/s)
D_w	Water diffusivity (m/s)
Ed	Rate of exergy destruction (MW)
E_{input}	Rate of input exergy (MW)
e	Specific exergy of stream (kJ/kg)
$\dot{E}$	Total exergy rate (MW)
f	Circulation ratio
G	Gibbs energy (J)
g	Specific Gibbs energy (J/kg)
g	Acceleration gravity (m/s)
h	Enthalpy of the stream (J/kg)
J	Flux (m/s)
J_w	Water flux
J_s	Salt flux

Ks	Solubility of solute (m^2/s)
$\dot{m}$	Mass flow rate (kg/s)
p	Pressure of the stream (Pa)
Po	Pressure at dead state (bar)
$\dot{Q}$	Heat transfer rate (kW)
Q_p	Flow rate (m^3/day)
R	Gas constant (J/(mol.k))
Rr	Membrane recovery ratio
R_s	Membrane salt rejection ratio
s	Entropy of the stream (J/(kg.K))
T	Temperature of the stream (°C)
UA	Heat transfer conductance (kW/m^2)
V_w	water molar volume (m^3)
v	Specific volume (m^3)
w	Salinity of the stream (g/kg)
W_{min}	Minimum work of separation (kW)
$W_{net,GT}$	Net output power (kW)
$\dot{W}$	Work (kW)
$\dot{W}_{pp}$	pumps work (kW)
X	Concentration (%)
x	Relative reversibility
z	high (m)
z_i	High at inlet side (m)
z_e	High at outlet side (m)

Greek symbols

μ	Chemical potential
$\eta_{I,GT}$	Gas turbine thermal efficiency
$\eta_{I,ST}$	Steam turbine thermal efficiency
η_I	Thermal efficiency
η_{II}	Exergy efficiency
ε	Effectiveness
π	Osmotic pressure (bar)
Ø	Osmatic coefficient
ɣ	Chemical potential coefficient
Δm	Membrane thickness (m)
ΔT_{lm}	Log mean temperature difference

Subscripts

0	Dead state
B	Brine disposal
b	Boundary system

ch	Chemical
cv	Control volume
e	Exit
In	input
ke	Kinetic
max	Maximum
min	Minimum
P	Product disposal
ph	Physical
p_o	Potential
s	Salt
sw	Seawater
Out	outlet

Superscripts

I,1, 2,…,n	Stream number
w	Water
0	Dead state
*	Stream condition

CHAPTER 1. INTRODUCTION

1.1 Introduction

The shortage of fresh water has become a challenge in arid and semi-arid countries. Desalination techniques are the best solution [3, 4]. Libya is located on the south coast of the Mediterranean Sea and is one of these countries which suffers from lack of fresh water for drinking, irrigation and industry, with a climate of four seasons which effect the seawater temperature and salinity compared with other regions. The aim of this research is to meet the increasing demand for fresh water in arid and semi-arid regions (especially Libya in this instance), within the recognised global requirement to reduce CO_2 emissions, by exploiting available low-grade energy resources such as power plant waste heat or geothermal water. Concerns about global warming, carbon emissions and climate change have stimulated a great deal of research, often by simulation, of thermal system performance.

Water desalination treatment by different processes has been known since Antiquity [5]. From the fourth century evidence has been found of evaporation to produce drinking water and in the nineteenth century it was found that distillation of sea water in vessels made transiting the ocean economically feasible [6]. These were followed by continuous research until the 1950s when Professor Silver investigated Multi Stage Flashing Desalination (MSF). The desalination industries are considered to have a major role in supporting human life [7]. In the last decades the MSF technology has become widely distributed and its construction along coastal areas has been reported. Libya is one of these countries which are suffering from lack of underground water resources. Located on the Mediterranean it has a coast length of approximately 1950 km [7] (Figure 1-1). The Libyan government has built a number of desalination plants to produce potable water for human use, for agriculture (because the area near the coast is suitable for planting) and for industry.

In this study a Combined Cycle Power Plant (CCPP) is the chosen waste heat source due to its location close to seawater that is the desalination feed water. As a specific case study, this investigation will be based upon an existing gas turbine power plant in Zawya City in Libya which forms the base plant for evaluation purposes [8]. Steam can be extracted from the Heat Recovery Steam Generator (HRSG) to power, for example, a Multi-Effect Desalination plant with Thermal Vapour Compression (MED-TVC), or

alternatively electricity can be used for Reverse Osmosis (RO). These desalination plant alternatives have been selected based on previous studies, which showed that of the thermal desalination technologies MED-TVC has high thermal efficiency with low temperature and high exergy efficiency, low product cost and minimum corrosion risk. In addition, it can be used in small and large sizes compared with other thermal processes. Whereas RO is one of the most promising desalination technologies with reducing costs, high exergy efficiency and low power consumption [9]. Recently Reverse Osmosis (RO) desalination has motivated research because of its considerable increased utilization [10]. Also RO has benefits such as a small footprint, relatively low cost of water production, automatic process control and modular design [11]. This offers an alternative in which thermal and membrane desalination technologies can be compared.

Brackish geothermal water offers an alternative source for desalination which need not be located by the sea or require a power plant to provide waste heat. A potential geothermal source exists at Waddan City (200km from the Libyan coast) with geothermal water at a temperature about 73°C and salinity 1960 ppm [12].

1.2 Aims and Objectives

The aim of this work is to perform exergy, economic and environmental studies for combined cycle power plant integrated with two different desalination technologies, to assess the overall performance of the combined cycles. The work also introduces a new desalination plant application using geothermal renewable resources as energy input. Furthermore, this work provides comparison studies to enhance existing plant performance and improve cost effectiveness as well as reducing environmental impact. The objectives of this study are as follows:

a. Investigate the performance of an existing standalone combined cycle power plant (CCPP) located at Zawya City on the coast of Libya in order to identify possible design improvements (thermodynamic, environmental and economic).

b. Evaluate the performance of different desalination technologies, including in the analysis the impact of chemical exergy based on the latest published thermodynamic properties and investigate the environmental impact of the proposed systems using carbon dioxide

as an indicator. Methods of improving the performance of the desalination systems are a prime objective of this work.

    c. Assess the thermodynamic performance of the combined CCPP when combined with an inlet air cooler and with the desalination units. This analysis was based on both energy and exergy and economic factors.

    d. To consider the production of potable water from a geothermal source of brackish water situated close to Waddan City in the south of Libya.

To carry out these objectives, this study will progress through five stages:

➢ First, because of the difficulty to perform this research experimentally, standard plant simulation software (in this case IPSEpro [13]) will be used to model plant performance in the Libyan environment. It is necessary to validate the IPSEpro models for all the plant elements to be considered, against measured plant performance or vendor data. The plant elements considered are an Absorption Chiller (AC) air conditioning system and MED-TVC, Single Effect Desalination (SED) and RO desalination plants as well as a CCPP.

➢ Second, the CCPP is a source of significant waste heat but the initial step should be to improve the CCPP performance (eg cycle thermal efficiency, exergy efficiency, output power, economics) and reduce CO_2 emissions by adding an absorption chiller to cool the intake air and avoid output power degradation during seasonal high ambient temperatures. Although this is not an original concept, in this work the chemical exergy of the chiller working fluid will be taken into account. This has not previously been the case.

➢ Third, because of the two different desalination concepts to be compared, it is important to identify the best configuration for each of these. For MED-TVC the number of effects and the use of a preheater recovering heat from the distilled water output stream are considered. In the case of the two-pass RO a pressure exchanger (PX) or an energy recovery turbine (ERT) on the stage rejected brackish stream are considered. As with the absorption chiller above, the latest data on the chemical exergy of sea and brackish water conversion will be incorporated into the models, which has not previously been the case.

➢ Fourth, consequently a comparison between thermal and membrane desalination technologies with the selected two-pass RO and MED-TVC

configurations is possible. This will allow the impact of two-pass RO and MED-TVC plant on the CCPP performance to be explored.

➢ Fifth, a further comparison between the performance of thermal and membrane desalination systems, ie SED and single-pass reverse osmosis (SRO), utilising the brackish ground water data from Waddan City, will be made for the first time.

➢ Sixth, thermodynamics alone cannot ensure the validity of a multi-generation thermal system as economic considerations are important. This study will include economic criteria such as initial costs, total capital cost and life time cost.

All of these factors are considered in the research to find the optimal desalination method that could be used in the Libyan environment and economy context. This environment area has not been addressed before even though there are a number of desalination plants that exist in Libya, which use different operating techniques.

Figure 1-1: Libyan map location of Zawya and Waddan [14]

1.3 Outline of the thesis

The thesis contains seven further chapters organized as follows:

Chapter two contains the literature review covering studies of power and desalination plants, which has informed the development of the five objectives set above by identifying where original contributions can be made.

Chapter three discusses the methodology which includes the IPSEpro software used to model the main components of the final systems.

➢ A description of the IPSEpro simulation software package including the general power plant and refrigeration libraries is presented.

➢ The basic thermodynamic principles are summarised and the plant performance criteria are fully defined.

➢ The economic criteria are summarised and Libyan environmental data provide.

Chapter four covers the validation of the simulation models used in this study (CCPP, AC, RO, MED-TVC and SED) and explores the sensitivity of two of these to uncertainties in the input data used.

Chapter five presents:

• Further development of thermal desalination (MED-TVC) by introducing preheater concept.

• A comparison between five configurations of two-pass reverse osmosis desalinations systems: (standard, with ERT, or PX at 1st stage and with PX in 1st and 2nd stages).

• A comparison between MED-TVC and best RO configuration using Libyan environmental data (seawater salinity and temperature).

• Further comparison of thermal SED and membrane SRO for brackish geothermal water in Waddan City Libya.

Chapter six presents a parametric study based on energy and exergy analyses (for the Libyan environment) of a Combined Cycle Power Plant (CCPP) without and with a single effect lithium bromide-water (LiBr-H$_2$O) absorption chiller (AC) which is energized by the exhaust heat from the combined cycle power plant.

Chapter seven presents an economic evaluation in the Libyan context of:

• The case for adding the absorption chiller to the CCPP intake.

• The merits of different improvements to thermal (MED-TVC) and membrane (two stage RO) technologies.

• The comparison of these technologies when coupled to an existing CCPP for seawater desalination.

- A further comparison of thermal (SED) and membrane (single stage RO) desalination technologies using a brackish groundwater source.

Chapter eight presents the conclusions and future study recommendations from this thesis.

CHAPTER 2. LITERATURE REVIEW

2.1 Introduction

Water scarcity for countries in arid and semi-arid regions has become more acute due to population growth and limited natural water resources. Desalination of seawater is considered one of the main sources of potable water in areas such as the Middle East and North Africa, with dependency on desalination up to 90% in some of the Gulf Cooperation Council (GCC) countries [7, 9]. This review will start with a brief introduction to the most common desalination processes, including comparisons between these processes based on thermal and economic analyses. Finally, previous studies on thermally–powered desalination systems will be reviewed especially on waste heat utilisation and absorption chilling for the intake air.

2.2 Desalination

When desalination started in the 1850s, the cost was not so important, with the main objective to produce fresh potable water. Between the 1960s and 1970s, when thermal desalination was widely used, the cost was still high. In 1975 a membrane process started to compete, which led to the cost being taken in consideration which was around US $ 2.1/m^3 in Southwest Florida [15].

Demand for desalination plants encouraged companies to improve desalination technologies and reduce costs, with clear cost reductions through the years 1990 to 2010 [16]. With water demand increasing with population increase, desalination costs reduced dramatically mainly due to developments in desalination technologies. However, in some areas the water cost declined to US$0.5 /m^3 whereas at the same production elsewhere the cost was US$1/m^3 because of the difference in location. Most desalination costs are dependent on location due to aspects such as energy, raw materials, transportation and equipment. These will continue to affect decreases in cost in future [16].

Desalination technologies are classified by their separation mechanism into thermal and membrane based desalination (Figure **2**-**1**). Thermal desalination separates salt from water by evaporation and condensation, whereas in membrane desalination the water diffuses through a membrane permeable to water while the salt is retained [17]. The most common forms of thermal desalination technology are Multi-Stage Flash

(MSF) and Multi-Effect Distillation (MED). MED can be combined with Vapour Compression which may be externally powered (mechanical compression) or also thermally powered (TVC). Membrane desalination technologies such as Reverse Osmosis (RO) and Electrolysis Desalination (ED), are considered the most common type [18].
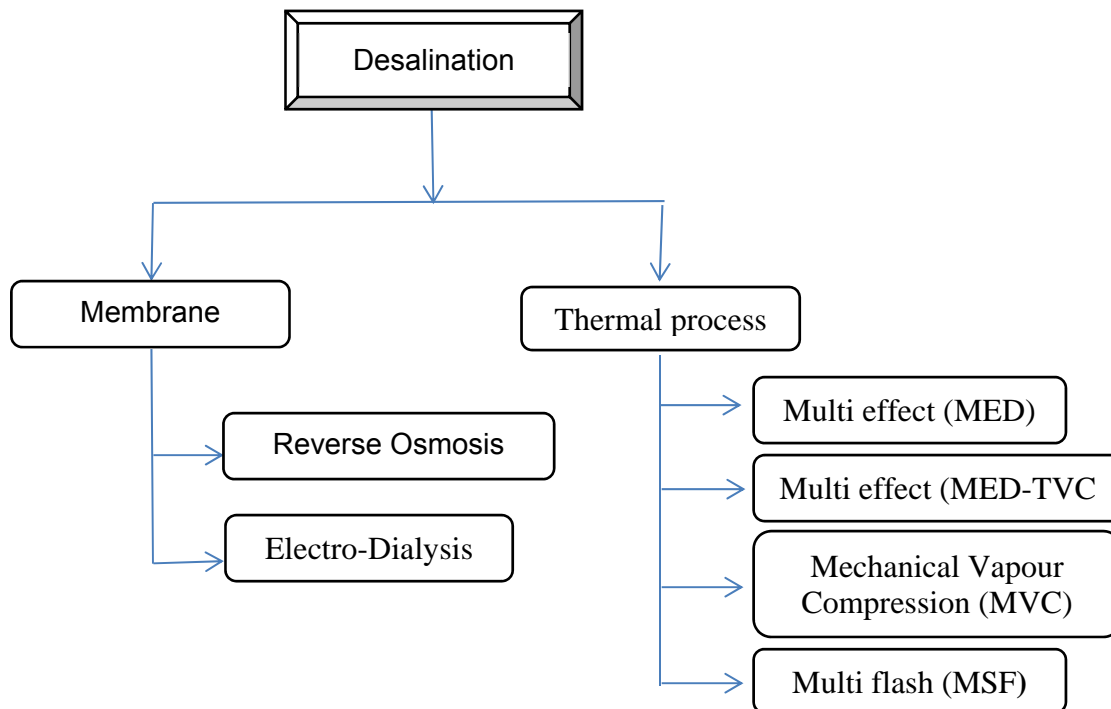
Figure 2-1: Desalination technologies

2.2.1 *Membrane processes*

2.2.1.1 **Electro-Dialysis (ED)**

William and Boby Ltd installed the first ED plant in Tubruk City, Libya in 1959 with a capacity of 55 m^3/day [19]. ED was known commercially 10 years before RO which was introduced in the 1970s [20]. ED is known as a powerful separation technology, but still has some limitations such as product purity, cleaning and limited maximum system temperature, although recently this has been improved to 60°C. The ED process consumes only electric power and the product cost is comparable to that of RO. The ED unit could be built with a capacity of up to 104,000 m^3/day [21]. In addition ED can produce pure and ultrapure water by electro-deionization (EDI) [22]. Eg. Zakia Amor et al [23] used electro-dialysis technology to reduce fluoride from brackish water.

Figure 2-2 shows the main parts of the ED process. Potable water is produced by applying an electrical potential, which is used to feed salt water through a membrane,

leaving potable water behind. In general ED plant consists of a pre-treatment unit, a relatively low-pressure circulation pump system, a membrane stack and a post-treatment unit. The membrane stack consists of hundreds of cells, which each combine two membranes and two spacers. The purpose of the spacers is to distribute the flow of the feed water and brine solutions and direct them into parallel cells [24, 25].
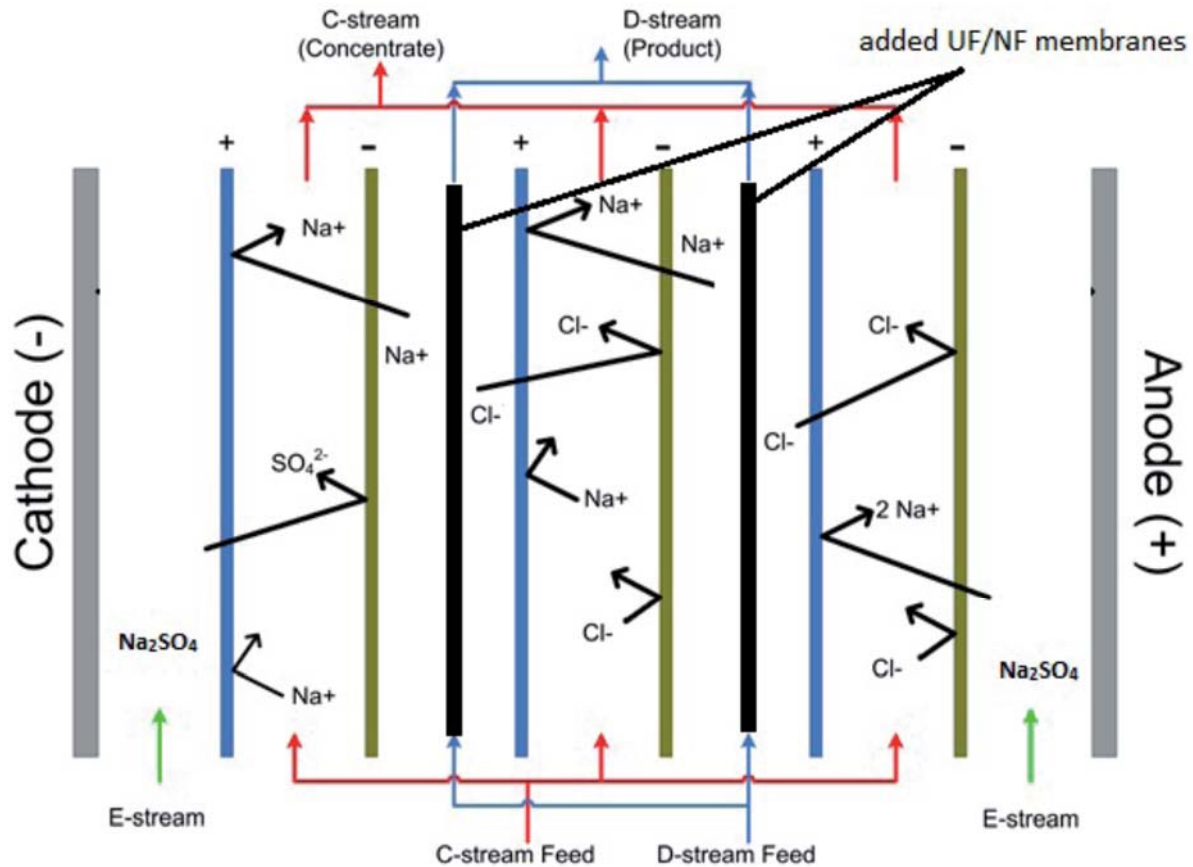
Figure 2-2: Electrolysis desalination process [26].

2.2.1.2 Reverse Osmosis (RO) desalination plant

RO is now a leading technology in the desalination industry worldwide, both in small and large scale applications [18, 27]. RO desalination is popular among fresh water supply companies due to its lower start up and delivery time, lower environmental impact, easier operation and maintenance, lower capital and operating costs, and a significant drop in energy consumption due to the latest energy recovery devices [5]. On the other hand, RO technology is not generally favoured for seawater desalination of high saline waters (45,000ppm) with high temperatures (40℃), such as occur in the Persian Gulf [28]. Membrane fouling is also a problem so pre-processing of the feed water is important.

The working principle of RO desalination depends on separating the solvent (pure water) from the solute (seawater) by using pressure to make the solvent flow in the opposite direction to the osmosis, leaving the solute on the high-pressure side of a semi permeable membrane. Unlike thermal desalination techniques, RO feed seawater should be passed through a pre-filtration system to remove suspended solids from the seawater before it reaches the membrane, which does not have mechanical filtration capabilities. A high-pressure pump is used to increase the filtered seawater pressure up to 65 bar to facilitate the separation of salts from the seawater. RO desalination could be designed for either better water quality or more product flow. For better product quality, a two pass RO is used, where the product from the 1st stage seawater RO (SWRO) is filtered again in a second Stage Brackish Water RO (BWRO). The rejected stream from the second BWRO can be directed to the 1st stage SWRO to increase the amount of the product (Figure **2**-**3**). Despite their drawbacks, the low energy requirements and low operating costs of membrane technologies make them attractive for seawater desalination as a first option, whether for new plants or hybridization in connection with existing MSF plants [18]. The behaviour of the membranes depends on feed pressure and concentration [29].

The main improvements in RO desalination technology have been focused on the membrane technology, to reduce the fouling and increase the membrane life, and on high pressure pumps to reduce their electrical power consumption [7, 18]. To mitigate some limitations, such as polarization, membrane fouling and hydraulic resistance to flow, energy recovery could be an option to reduce energy consumption and costs [1].
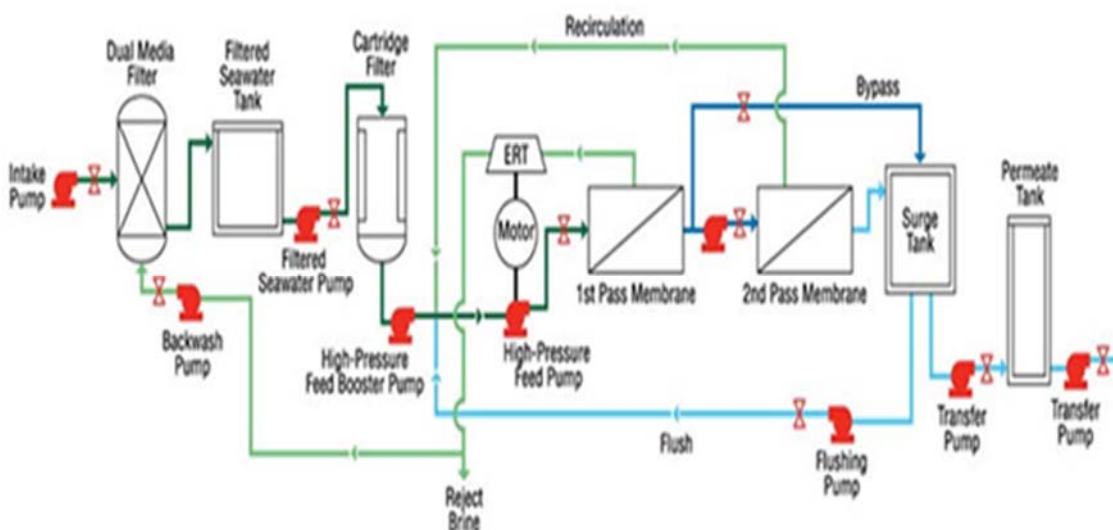
Figure 2-3: A schematic drawing of RO process [30]

2.2.1.3 Thermodynamic and economic analysis of RO plant

While first law of thermodynamic analysis focuses on the quantity of energy, second law analysis (exergy analysis) introduces energy quality as well as quantity [31]. Exergy analysis allocates the irreversibility in the system and suggests economical modification and enhancement [1, 32] However, only a limited number of studies have analysed seawater desalination exergy, due to the complexity of the determination of the seawater stream exergy [33]. The main source of exergy destruction or loss are the membrane modules, high pressure pump and throttle valves [18, 34-37] and rejected seawater [38].

A number of parameters such as seawater salinity, temperature and recovery ratio affects the efficiency of reverse osmosis. As the seawater temperature increases the saline water viscosity diminishes and the permeate flow and operating pressures increase. Moreover, the exergy efficiency increases [37, 39] as well as the recovery ratio [10]. As the feed water salinity increases the exergy efficiency increases [40] and permeate flow declines [18, 34] . Costs are therefore affected by these parameters as well as electrical costs [37]. As Recovery Ratio increases permeate flow increases and specific power consumption decreases from (2.8kW/m^3 to 0.8kW/m^3 when the Recovery Ratio changed from 30% to 60% respectively) [10], where the recovery ratio is defined as percent of feed flow to the permeate flow.

Most research in the area of RO desalination optimization has focused on either improving membrane technology or reducing power consumption. The power consumption of RO desalination per m^3 is between 2.5 and 7.9 kW/m^3 [41-43]. Reducing the energy consumption of the RO desalination technology by using an energy recovery device (such as pressure exchanger or energy recovery turbine) could save from 1.5% to 27% of the total power consumption by high pressure pumps [41] and improve the exergy efficiency and reduce specific energy consumption by about 30% to 50%, as well as life time cost [10]. The pressure exchanger appears to be the best energy recovery device [38, 44-46]. The effectiveness and reliability of these devices through recent advances in the energy recovery technology are considered to make a large scale RO economically viable. The energy requirement of SWRO is now at the range about 1.6 kWh/m^3, making the process energy competitive with the other traditional water supply sources. There has been evolution of SWRO energy recovery devices (ERD) some of which are briefly discussed below:

(a) Pelton turbine

Pelton turbines (tangential flow impulse turbine) were the first ERDs deployed in municipal scale SWRO process in the 1980s, instead of Francis turbines because they operate at higher efficiency for high pressure applications. The Pelton turbines are used widely in SWRO desalination process, because they have proven reliability and familiarity. The rejected seawater flow with high pressure is ejected through nozzles and directed against a series of spoon-shaped buckets mounted around the wheel. To keep the force on the wheel in balance and to ensure smooth, efficient momentum transfer of the fluid jet to the wheel, the buckets are mounted in pairs. The turbine wheel is connected to the high pressure pump shaft to reduce the motor power required to pressurise the SWRO system. The effect of feed water temperature, salinity, mass ratio and energy recovery turbine and pumps isentropic efficiency were also investigated and the results showed that salinity had the highest effect on second-law efficiency when the pressure exchanger was used [46]. Economic analysis of the desalination separation and thermal technologies were conducted. The results for thermal technologies showed that as the plant capacity increased, the overall unit production cost dramatically decreased. But the overall capital cost increased, whereas the RO unit product cost has almost the same percent of the fixed charge, membrane replacement and energy power costs [47]. Importantly, the cost of the system was found to be location specific and start from $0.5/m^3 to double [1, 16, 48].

The first and second laws of thermodynamics were used to analyse RO desalination plant with Energy Recovery Turbine (ERT) and economic studies were carried out at the different recovery ratios and different feed water temperature, the results showed that a large exergy destruction occurs at the membrane module followed by the high pressure pump by about 67.8% and 17.16% respectively, whereas, exergy destruction was reduced by about 35% when an ERT was used. Where the product cost was around 2.451$/m^3 and it reduced as the recovery ratio increased [37].

To improve RO desalination plant performance, a comparison between different Energy Recovery Devices (ERD) was conducted using single and two-pass RO. A pressure exchanger was found to be the best ERD [38, 46] The effect of feed water temperature, salinity, mass ratio and energy recovery turbine and pumps isentropic efficiency were also investigated and the results showed that salinity had the highest effect on second-law efficiency when the pressure exchanger was used [46].

b) Piston pressure exchange

To avoid the efficiency losses caused by the energy conversion process in centrifugal devices, the positive displacement piston was developed in the 1980s. Both feed water and rejected water contact with the intervening piston in pressure-equalising or isobaric chambers. A booster pump in series with the ERD is important to circulate high

Figure 2-4: The position of PX and ERT on RO plant [1]

pressure water through the membrane. The water pressurised by ERD combines with the discharge of high pressure pump entering to the membrane. These piston isobaric devices require control to operate their valves and to limit piston movement [49]. Figure 2-4 shows the location of the ERD that is connected to the electrical motor and used to recover work rejected with the brine as well as the PX that transfers the brine pressure to feed pressure.

The last two decades showed that the RO process has significantly decreased the cost of producing fresh water from saline water as shown by a number of researchers [10, 16, 37, 50, 51]. Indeed it was considered possible to reduce the water cost to less than US$0.8/m^3 [50]. The studies also indicated that 37% of the total plant capital cost was the membranes [51]. A comparison between different Energy Recovery Devices (ERD) was conducted using single and two-pass RO. A pressure exchanger was found to be the best ERD. For instance, using pressure exchanger device, Sarai Atab et al. [10] studied the operational and economic analysis of 15000 ppm brackish water to reduce the salinity to below 400ppm for drinking water and below 1600 ppm for irrigation. The results showed the total capital cost and lifetime cost were about £14.4 million, £0.11/m^3 and £11.3 million, £0.9/m^3 for drinking use and irrigation respectively. However, the study did not cover exergy analysis and only single-pass RO was considered. More so, Cerci Yunus [34] studied exergy analysis of existing 7250m^3/day

reverse osmosis desalination plant in California. The result showed that about 74% exergy loss occurred in the membrane modules, where the lowest value was in mixing chamber by about 0.67%. The exergy efficiency was very low at only 4.3%. This could be improved to 4.9% by adding pressure exchanger and two throttle valves. In Canary Island, Spain an exergy analysis of 21,000 m^3/day capacity reverse osmose desalination plant was conducted, the result showed that about 80% of the exergy destruction occurred at high pressure pump, the valves, membrane and energy recovery [35]. Adding pressure exchanger to the reverse osmosis increases the second law efficiency [40].

The exergy analysis of a two-pass Reverse Osmosis (RO) desalination unit with and without an energy recovery device was carried out. The results showed that the exergy efficiency of the RO desalination plant is equal to (27.3% and 32%) from using ERT and PX respectively. For the RO desalination system studied the total exergy destruction was reduced from 690 kW in the standalone to 411 kW with ERT and 324 kW with PX. The results also show that when the system operate without using energy recovery device. The rejected seawater represented around 42% of total exergy destruction, whereas the corresponding percentages were 0.07% and 0.64% with ERT and PX respectively. It is clear that the PX gives low power consumption, low exergy destruction and high exergy efficiency. In addition, RO with the PX involves higher minimum separation work and the smallest area compared to the other two configurations [38]. Leakage became the most serious problem on SWRO energy recovery device (ERDs) due to wearing of either rotating parts or stationary parts leading to decrease in efficiency. This issue could be solved by using Fully-Rotary Valve Energy Device (FRV-ERD). The results showed that there was an improvement on the ERD performance and a reduction of the pressure leakage with high system efficiency measured at about 99% [52].

A number of studies confirmed that RO has a better techno-economic performance due to the continuing advances made to reduce energy consumption which lowered the cost of water produced [53, 54]. Although many authors claim RO was the less expensive alternative, possible increases in energy costs have not been taken into account. Furthermore, RO is alone in its reliance on electricity, unlike the thermal processes, that could be more economical in their use of waste heat or solar thermal energy [53-55].

Recently, most of SWRO and BWRO research focus has been on reducing the power consumption, about 30 to 50% of the energy cost in the SWRO process from the total

production cost [56]. Using Isobaric ERDs, and PX pressure exchanger provided a number of benefits such as, minimal simple controls, fail-safe operation, low vibration, long life and corrosion avoidance [57]. A proposed reverse osmosis desalination plant which was to be built at Umm Qaser city in Iraq was studied using DEEP-3-2 software. Parametric studies were also carried out, the results showed that a production cost was 0.896 $/m^3 and water salinity (279 ppm), this cost was affected by a number of parameters such as seawater temperature, seawater salinity, and electrical cost. When the seawater salinity rose from 35,000 to 45,000 ppm the production cost increased by 2.5%. Moreover, the cost increased by 0.71% when the seawater temperature declined from 33°C to 20 °C, and increased by about 12% when the electrical price increased from 0.06% to 0.1% US$/kWh [58]. Lee et al [59] discussed the application of hybrid systems techniques for cleaning and replacement of a RO membrane using a number of factors such as water and salt transport permeability. Their results indicated that it could be feasible to optimize control using a dynamic hybrid method applicable to an operational cost saving for a SWRO desalination plant. MacHarg [45] studied the advantages of pressure exchanger (PX). His result showed that there was clear improvement for reducing the power consumption on SWRO plant by 75%. Seawater RO desalination plants consumption and membrane replacement have been investigated, the energy consumption was found to vary from 3.02 kW/m^3 to 9.38kW/m^3 [60]. Furthermore, Qureshi et al [61] investigated the energy consumption of a 2250 ppm water desalination plant in California. The plant consists of Nano-filtration, reverse osmosis and electro-dialysis connected to the same water source. The results showed that as the feed water salinity increases, the exergy efficiency increases due to the increment in the waste brine stream salinity. Importantly, the energy efficiency of nano-filtration, reverse osmosis and electro-dialysis were 0.087%, 0.066% and 0.078% respectively [61].

Table 2-1: Membrane desalination plant technology reverse osmosis (RO)

No.	Author	Parameters or subjects investigated	Main outcomes
1	Malek et al 1996 [51]	1. Feed water flow rate 2. Product recovery ratio	The results showed that, as the water flow rate increased the pump cost increased and also as the recovery ratio increased the product concentration increased. It can be concluded that about 37% of the total cost is related to energy costs.
2	Cerci Yuns 2002 [62]	Exergy analysis	The results showed that the exergy analysis could be improved by introducing a pressure exchanger and two throttle valves into the system.
3	MacHarg 2003 [45]	Use of pressure exchanger	The extremely high efficiency of pressure exchanger technology makes it is possible to significantly increase the capacity of existing systems and/or reduce their power consumption.
4	Romero-Terneo et al 2005 [63]	Exergy analysis	The main results indicated that about 80% of the exergy destruction depends on high pressure pump, valve regulation, and the membrane element and recovery devices.

No.	Author	Parameters or subjects investigated	Main outcomes
5	Stover 2007 [49]	Energy recovery devices for seawater reverse osmosis.	The results showed that using a pressure exchanger offered significant advantages such as reducing high pressure pump costs, fail safe operation, low vibration and long life.
6	Dashtpour and Al-Zubaidy 2012 [42]	Use of hydrostatic pressure	The results showed that the specific power consumption can be reduced to 2.46kWh
7	El-Elman and Dincer 2014[37]	1. Recovery ratio 2. Feed water temperature	The results showed that, as the recovery ratio increased, seawater flow rate, membrane area and product cost reduced. Whereas when the feed water temperature increased the total exergy destruction deceased. The highest exergy destruction occurred at the membrane and high pressure pump.
8	Eshoul et al 2015. [38]	Use of energy recovery devices	The results showed that using a pressure exchanger on SWRO has given high exergy efficiency compared with an energy recovery turbine.
9	Jamil et al 2016 [40]	1. High pressure pump efficiency 2. Feed water salinity 3. Comparison of ERT and PX.	The results showed that as the high pressure pump efficiency increased, the exergy efficiency increased and the specific power consumption decreased and when the feed water salinity increased the exergy efficiency increased. Also the results proved that using PX is more efficient than ERT.
10	Farooque et al 2008 [41]	1. Feed water temperature 2. Reject pressure	The results showed that, as the feed water temperature increased, efficiency decreased and specific power consumption increased, whereas when the rejected pressure increased, efficiency increased but the specific power consumption also increased.
11	Ludwig 2010 [43]	1. Recovery ratio 2. Membrane flux	The result showed that, as the recovery ratio increased, the specific power consumption decreased. Increasing the membrane feed pressure led to decrease the TDs permeate while revers accrue the average membrane flux.
12	Geisler et al 2016 [44]	Working pressure	The results showed that, as the working pressure increased, the specific power consumption increased.
13	Qureshi and Zubair 2016 [46]	1. Feed water salinity 2. Pump isentropic efficiency 3. Feed water temperature	The results showed that, as the feed water salinity increased, the exergy efficiency increased, whereas increases in pump isentropic efficiency led to increased exergy efficiency to increased and specific power consumption. Also exergy efficiency increased with feed water temperature.
14	Sarai Atab et al 2016 [10]	1. Feed temperature 2. Recovery ratio 3. Feed pressure	The results showed that, when increasing the feed temperature, the permeate flow rate, recovery ratio and concentration increased, but when the recovery ratio increased the permeate flow and power consumption increased but the specific energy decreased. In addition, when the feed pressure increased, the flux and power consumption increased whereas the permeate concentration and membrane area decreased
15	Stover2006 [49]	Uses of recovery devices	The results showed that the energy requirements of SWRO are now as low as 1.6kWh/m3, which makes the technology competitive with other desalination processes.
16	Avlonitis et al 2003 [60]	1. Total water cost 2. Membrane replacement cost	The results showed that the cost of water could be decreased by using energy devices, where the membrane replacement cost can be lowered if a hydrodynamic cleaning procedure is applied.
17	Al-Zahrani et al 2012 [9]	1. Feed water salinity 1. Feed water pressure	The results showed that as the feed water salinity increased the specific power consumption increased, whereas increasing the feed pressure will increase the permeate flow, recovery ratio and specific power consumption
18	Wilf and Bartels 2005[64]	Recovery ratio	The results showed that, as the recovery ratio increased the specific power and feed pressure increased.
19	Qureshi and Zubair 2016 [61]	1. Use of recovery devices 2. Feed water salinity	The results showed that the nano-filtration unit had the best efficiency. The exergetic efficiency increased with feed water salinity

2.2.2 *Thermal desalination process*

The thermal desalination technologies are dependent on heat to evaporate salt water and the evaporated steam condenses as the product. This process can be achieved using a number of technologies as shown in figure 2.1. Below are types of desalination systems.

2.2.2.1 **Multi Stage Flash Desalination (MSF)**

The MSF desalination process constitutes a number of stages which are located in series. Each stage is at a successively lower pressure which is maintained by a vacuum system, with the process repeated in each stage [65]. Figure 2-5 shows the process of MSF desalination plant, the main seawater pump delivers the seawater to the heat rejection stages, where most of this will be rejected again to the sea, meanwhile a part of it will pass as makeup to the deaerator. To avoid tube corrosion in the heat recovery stages oxygen is removed from the seawater by the deaerator. A brine cycle pump transfers recycled brine to the tube side of the heat recovery stages and the flashed brine at the condenser of each stage is gradually heated [28]. The fundamentals and costing of MSF desalination plants compared with other technologies were investigated. The results proved that MED and MSF, which were thermal technologies, gave very similar product water cost. On the other hand, all thermal technologies have an environment impact due to high temperature discharge [66].
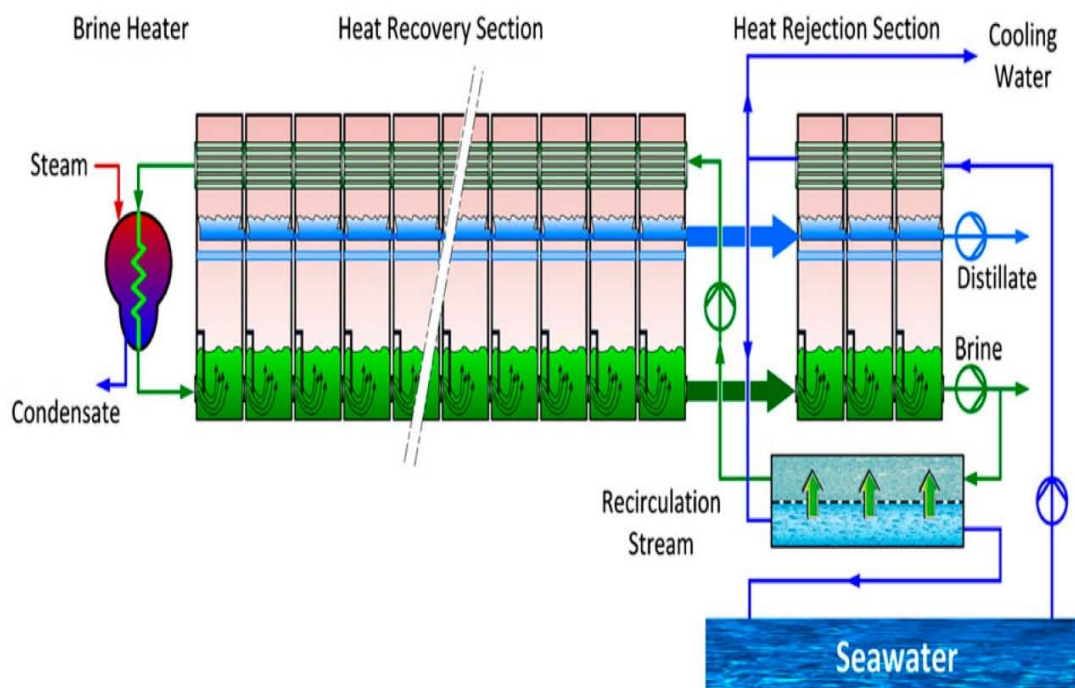
Figure 2-5: Schematic drawing of Multi stage flash (MSF) [30].

Nafey et al [67] studied in detail exergy and thermo-economic analysis of a 500 m^3/day existing MSF desalination plant. They found that the exergy destroyed was 6.46MW and exergy efficiency was only 1.83% which was very low, while the product cost per m^3 was $2.63. More so, exergy analysis of a MSF desalination unit by Al-Weshahi et al [68] show that the exergy input destruction of 55%, 17%, 14% and 4.3% occurs at heat recovery stage, brine heater, pump, and brine steams respectively. Besides, only 4.3% is lost at the heat rejection stages. In addition, recovering heat from the hot distillate water stages could economically improve the unit exergy efficiency from 5.8% to 14% with the resulting hot water suitable for powering other thermal systems such as an absorption chillier and multi-effect desalination. Al-Ghamdi and Mustafa [69] performed exergy analysis of a similar process in Yanbu, Saudi Arabia using Matlab. In this study, the production in the summer was 159 kg/s and 200 kg/s in the winter. The seawater temperature was 22.9°C in winter and 35.2°C in summer. The major exergy destruction reportedly occurred at the heat recovery section by about 74.9%. However, this can be reduced to 69.2% by increasing the number of stages from 25 to 31. Table 2-2 shows the summary of these studies.

Table 2-2: Thermal desalination plant technologies (MSF)

No.	Author	Parameters or subjects investigated	Main outcomes
1	Abdul-Wahab et al 2012 [65]	Number of stages	The results showed that flashing brine temperature, distillate temperature, flashing brine flow rate and cooling brine temperature declined in the summer and winter seasons over the stages progressed, whereas distillate flow rate increased in both seasons.
2	Nafey et al 2006 [67]	Number of stages	The results consistently show that the low exergetic efficiency of the first and last stages is mainly due to exergy destruction in these stages.
3	Al-Weshahi et al 2013 [68]	Number of stages	The results showed that the exergy efficiency was reduced gradually over the stages of heat recovery from high temperature to low temperature stages, whereas exergy destruction decreased.
5	Al Ghamdi and Mustafa 2016[69]	Number of stages	The results indicated that exergy destruction gradually decreased as the number of stages increased.

2.2.2.2 Multi Effect Desalination (MED)

MED is one of the thermal desalination technologies which depends on heating, evaporating and condensation for fresh water production. Figure 2-6 shows a schematic of MED desalination plant. High efficiency is the major goal in designing desalination plant, which includes not only energy efficiency, but also reliability, operation costs and maintenance [5]. There are similarities between the MED and MSF process configurations. Both technologies consist of a number of stages and the

method of evaporating the salt water is by reducing the pressure at each stage without any additional thermal or electrical energy. To evaluating the performance of thermal desalination, the gain output ratio (GOR) parameter was used and can be defined as the ratio of the potable water mass flow rate (kg/s) to the driving steam mass flow rate [25]. However in the last few years the MED technology has again become competitive with MSF with better (GOR). The efficiency of MED unit can be improved by many ways: increasing the number of effects which increases GOR, use of recovered heat or by coupling the MED with a solar plant. Wang et al [3] investigated MED driven by low grade heat. In the design, each stage contains a bundle of heat transfer tubes, where the seawater feed flow is sprayed over the evaporator tubes and the vapour formed outside the tubes is passed to the next effect. The first effect is heated by the steam supply then the steam produced from each effect heats up the next effect. The condensate from the first effect is then returned to the power plant, while the condensate from the other effects downstream forms the total potable water product. These results indicated that there were improvements of about 25 to 60% compared to the traditional distillation process. The authors also alleged that the technology has high thermal efficiency with low temperature, low operating cost, minimum corrosion risks and adaptable to different plant sizes. Their view is also corroborated by [70] who suggests the suitability of the configuration for both small and large scale plant.
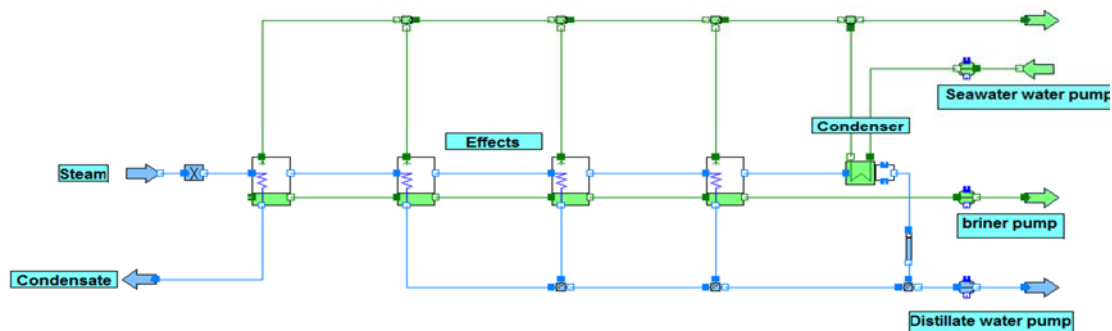
Figure 2-6: Multi effect desalination (MED) [13]

2.2.2.3 Multi-Effect Desalination with Thermal Vapour Compression (MED-TVC)

MED-TVC process consisted of single effect or number of effects similar to MED, the difference between MED and MED-TVC is that MED-TVC has a steam ejector to enhance plant performance as can be seen in figure 2-7. The steam ejector is widely

used in refrigeration and air conditioning, desalination, refining, petrochemical and chemical industries. Steam jet ejector models have been developed for design and evaluation [71]. The correlations developed were useful for design simplification and category calculation. They could be used to obtain the entrainment ratio and also to determine the motive steam flow ejector areas [71]. The main components of the MED-TVC are steam ejector (TVC), effects, condenser and pumps which are required for feed seawater, distillate water and brine water. The purpose of the ejector is to reduce the motive steam and boiling temperature by reducing the steam pressure. The operation of TVC process dependents on the Continuity and Bernoulli equations and it consists of five regions (steam inlet, suction, nozzle, mixing area and diffuser) as seen in figure 2-8. The motive steam at high pressure and low velocity enters the steam inlet and leaves the nozzle at high velocity above the sonic speed and produces a low pressure area which will allow the entrained vapour to be evacuted to the chamber and mixed with motive steam. The mixed steam moves through the diffuser and leaves the diffuser at the required pressure for boiling the seawater in the first effect of the MED.

Figure 2-7: Multi effect desalination (MED-TVC) [25]

Figure 2-8: Ejector components [72]

Thermodynamic analysis in single and MED-TVC desalination plants is investigated by [73]. Efforts were focused on improving all the components design and the results show that the steam ejector and effects were the main source of exergy destruction. Kamali and Mohebinia [74] studied possibilities of increasing desalination plant potable water product. Their results showed that temperature and pressure inside the system directly dependent on temperature and pressure inside the condenser. Moreover by increasing the surface area of the condenser, the GOR value would be increased as well as the plant life time. They optimized the thermodynamic design and conducted a parametric study of MED-TVC to achieve the best configurations for the desalination process to increase GOR, the results demonstrated that using a parametric study is an appropriate tool to estimate the optimum effective values [75]. More so, Hamed et al [76] were the first researchers to carry out exergy analysis to investigate the thermal performance of a four-stage MED-TVC plant located in the UAE. The plant operated at low temperatures with a performance ratio of 6.5. The authors contend that the maximum exergy destruction occurs at the first stage in the thermo- compressor. Alasfour et al [77], also presented a comparison study among three different configurations of a MED-TVC [8] and the results also reveal the occurrence of the highest irreversibility in the thermo-compressor and evaporators, whereas the first

effect constitutes approximately 50% of the total exergy destruction, due to high fuel exergy at this stage.

A parametric study of the impact of number of effects using a MATLAB algorithm was performed by [78]. The results showed that the GOR increases as the number of effects increases. The maximum GOR varied from 8.5 to 18 for 4 and 12 effects respectively. The top brine temperature varied from 55.8°C to 67.5 °C and the optimal range of compression and entrainment ratio were between 1.81 and 3.68 and 0.73 to 1.65, respectively. Furthermore, Choi, et al [79] , performed an exergy analysis on a MED-TVC plant manufactured by Hyundai Heavy Industries for different units with capacities of 4.5, 10, 16 and 20 million litres per day. The exergy destruction due to irreversibility and exergy losses of the MED-TVC was evaluated in order to reveal potential plant efficiency improvements; results showed that 70% of the total exergy destruction occurred in the TVC and effects.

Recently, Alamolhoda et al [80] carried out a parametric analysis on the Kavian desalination unit, which consists of four stages with a total plant capacity of 192 tonne per hour and the result shows exergetic efficiency of 3.95% which was considered too low compared with other thermal applications. The major sources of irreversibility occur in the thermo-compressor, heater and effects. The effect of input parameters on GOR and MED-TVC units during system operation showed that GOR and mass product increase with feed water temperature rise and declined with increase in feed water flow. On the other hand, increasing the flow rate of the steam entering the first effect caused a rise in product flow and reduced GOR and increasing the first effect thickness reduces both the GOR and production rate [80]. A parametric analysis of MED-TVC desalination systems based on the first and second laws of thermodynamics was performed by Samaké et al [81]. Their findings confirmed the insensitivity of plant performance to concentration factor. The ejector compression ratio played a great role in reducing the amount of required input thermal energy and exergy destruction. The authors recommended a higher value for the compression ratio. The specific exergy destruction increased as motive pressure increased, where the first effect has the largest exergy destruction ratio and the total exergy destruction declined as the number of effects increased [82]. Thus, higher value for the compression ratio was recommended by the authors. In the same vein, TVC has been found to be the main part controlling the overall process efficiency of MED-TVC and the area ratios of primary nozzle and mixing has been argued to have a great effect in the ejector's performance Yang et al [83].

There have been many attempts to improve MED-TVC desalination plant by coupling MED-TVC with combined cycle power plant to reduce power and water cost [84]. However, these studies did not include chemical exergy. Sayyaadi et al [85] presented a thermo-economic optimization of a multi effect distillation desalination system with Thermal Vapour Compressor to reduce the total levelized cost. An economic model was developed using the total revenue requirement method, the result showed that improvement in all costing elements. Three different configurations of MED-TVC, with regenerative feed water (MED-TVC, FH), and ME-TVC coupled with MEE system (MED-TVC + MEE) were investigated by [86]. The results indicated that this system integrated with a power plant could reduce the fuel energy cost by about 30% whereas, the first configuration had the highest water cost. Similarly, Esfahani et al [87] conducted an exergy analysis and optimization using a genetic algorithm based multi-objective function to minimize total annual cost and maximize the gain output ratio (GOR) of the ME-TVC desalination system. The results show that maximum GOR and minimum product cost were achieved by using the highest number of effects (six). This was later confirmed by Eshoul et al [88]. Thermal and economic analysis was conducted on a combined cycle power plant with and without MED-TVC desalination plant. Engineering Equation Solver (EES) was used to analyse the results. The results concluded that a cogeneration plant that produced electricity and water was more economical than using separate processes. This would save power and reduce water total annual cost and could increase the annual net cash flow by about 20% and 118%, respectively [89]. However, despite availability of numerous studies on MED-TVC desalination systems, there has been no study made to explore the impact of treating seawater as a real mixture. A real mixture is defined from a thermodynamics point of view, as a mixture in which molecules of different species that make up the mixture are similar in term of mass or structure or both and though their property changes with composition. Their deviation from ideal behavior is often expressed using the equation of state, where the chemical potential is a function of the partial pressure. A real mixture is also homogeneous and heterogeneous [90].

No work has been reported on the exergy analysis of the effect of using a feed water preheater. This presents a gap which this work aims at cover. Table 2-3 shows the summary of most researches studies of MED-TVC.

Table 2-3: Thermal desalination plant technologies (MED-TVC)

No.	Author	Parameters or subjects investigated	Main outcomes
1	Kamali and Mohebinia 2008 [74]	1. Feed water temperature 2. Effect of Pressure on heat transfer coefficient 3. Total capacity 4. Performance ratio	There is strong relationship between the effect of the temperature and pressure and the conditions inside the condenser. The heat transfer area of the condenser decreases as the pressure and temperature inside the condenser are reduced. GOR increased with decreasing top brine temperature. The system depended directly on the temperature and pressure inside the condenser.
2	Kamali et al 2008 [75]	1. Inlet steam pressure to TVC 2. Number of effects 3. Feed water temperature 4. Concentration factor 5. Steam temperature	The GOR increased with increasing inlet steam pressure, number of effects, feed water temperature and concentration factor but decreased with increasing steam temperature.
3	Ameri et al 2009[91]	1. Number of effects 2. Heating steam temperature 3. Boiler outlet pressure	The results showed that the performance ratio increased with number of effects increased where the inlet steam mass flow rate decreased, and the specific heat transfer area decreased with increasing steam temperature. As the boiler outlet pressure increased, the performance ratio also increased.
4	Alamolhoda et al 2015 [80]	1. Seawater temperature 2. Feed water flow rate 3. Steam flow rate	The results showed that, as the seawater temperature increases, the GOR and potable water increase, whereas an increase in feed flow rate leads to reductions in total product flow rate and GOR. The total product increased with increasing steam flow rate but the GOR decreased.
5	Choiel et al 2005 [79]	1. Number of effects 2. Entrainment ratio	The temperature difference for each effect with different entrainment ratios are almost the same. Whereas estimated total heat transfer area is reduced with increasing entrainment ratio. It was also concluded that TVC effects are responsible for 70% exergy destruction.
6	Mistry et al 2013 [92]	1. Number of effects 2. Recovery ratio 3. Steam temperature	As the number of effects and recovery ratio increased the performance ratio and specific area increased, but they decreased with increasing steam temperature.
7	Al-Shammiri and safar 1999 [5]	Discussion of the general features of existing commercial MED plants and associated technical aspects	The results showed that there are two ways to increase the GOR, by increasing the number of effects or coupling the MED with a heat pump, Also combination MED with solar power is recommended to improve the efficiency of the water plant not only energy but also operation costs reliability and maintenance.
8	Bin Amer 2009 [78]	1. Number of effects 2. Top brine temperature 3. Entrainment ratio	The GOR increased with number of effects and the optimal top brine temperature between 55.8 and 67°C and with the entrainment ratio between 0.73-1.65
9	Kamali et al 2009. [93]	1. Number of effects 2. Concentration 3. Steam temperature	The performance ratio increased with number of effects and with concentration factor but decreased as steam temperature increased.
10	Hamed et al 1996 [76]	1. Top brine temperature 2. Number of effects	The results showed that, as the top brine temperature increased, the performance ratio decreased and the specific exergy losses increased, whereas the performance ratio increased number of effects. Also the exergy analysis showed that the MED-TVC is the most exergy–efficient when compared with the MVC and MED
11	Samake el al 2014 [81]	1. Ejector compression ratio 2. Increased ejector motive steam pressure	The ejector compression ratio played a great role in reducing the amount of input thermal energy required and exergy destruction.
12	Binamer 2012 [84]	1. Top brine temperature 2. Motive steam flow 3. Temperature drop per effect. 4. Number of effects	The results showed that as the top brine temperature increased, specific heat consumption and specific exergy consumption increased but the GOR and potable water decreased, whereas when the motive steam flow increased the potable water production increased and specific exergy destruction was reduced. Also the specific exergy destruction significantly reduced by increasing the number of effects and the specific heat transfer area declined by temperature drop between the effects.

No.	Author	Parameters or subjects investigated	Main outcomes
13	Esfahani et al 2012 [87]	1. Effect of temperature difference between ∆T effects 2. Effect of number of Effects.	As the ∆T between effects increased the GOR increased, whereas the total annual cost deceased. The GOR Increased with number of effects increased.
14	Eshoul et al 2016 [88]	1. Seawater temperature 2. Seawater salinity 3. Effect of number of effects.	The results showed that, as seawater temperature, seawater salinity and number of effects increased, the exergy efficiency and GOR also increased.
15	Alasfour and Bin Amer 2006 [86]	1. Plant size capacity 2. Fuel price 3. The effect of the net thermal efficiency	The results showed that the fuel energy cost decreased with increasing plant size capacity or net thermal efficiency, but significantly increased when the fuel price increased.
16	Alasfour et al 2005 [77]	1. Motive steam pressure 2. Temperature difference between effects ∆T 3. Top brine temperature 4. Feed water temperature	The results showed that, as motive steam pressure increased, the gain ratio and total exergy destruction increased, but the specific heat consumption decreased. When the ∆T increased the specific heat transfer area and gain ratio deceased but specific exergy destruction and specific heat consumption increased. As the drop in the top brine temperature increased transfer area and gain ratio decreased but heat consumption and exergy destruction increased. As the feed water temperature increased, the performance of desalination increased by reducing the specific heat transfer area and increased gain ratio. The steam ejector and the effects are the main sites of exergy destruction.
17	Almutairi et al 2016 [94]	1. Feed water temperature 2. Number of effects 3. Entrainment ratio	The results showed that, as the feed water temperature and number of effects increased, the exergy efficiency and minimum work increased. The entrainment ratio should be adjusted to a low value. The results also showed that the first effect is responsible for the highest exergy destruction.

2.2.2.4 **Mechanical Vapour Compression desalination (MVC)**

The only difference between this process and the MED-TVC technologies is that the steam produced by evaporation is recompressed using diesel or electrical power to drive a mechanical steam compressor as shown in figure 2-9. The advantage of this process is that it could be economically operated on small and medium scale sizes. In addition, MVC could also be suitable for inland applications such as, industrial wastewater, brackish water and concentrate from RO. The greatest advantage of this process is that it does not need cooling water, which would normally be complicated and have a high cost. Also it is operated at low temperature which is a great advantage. Corrosion risks were also reduced.
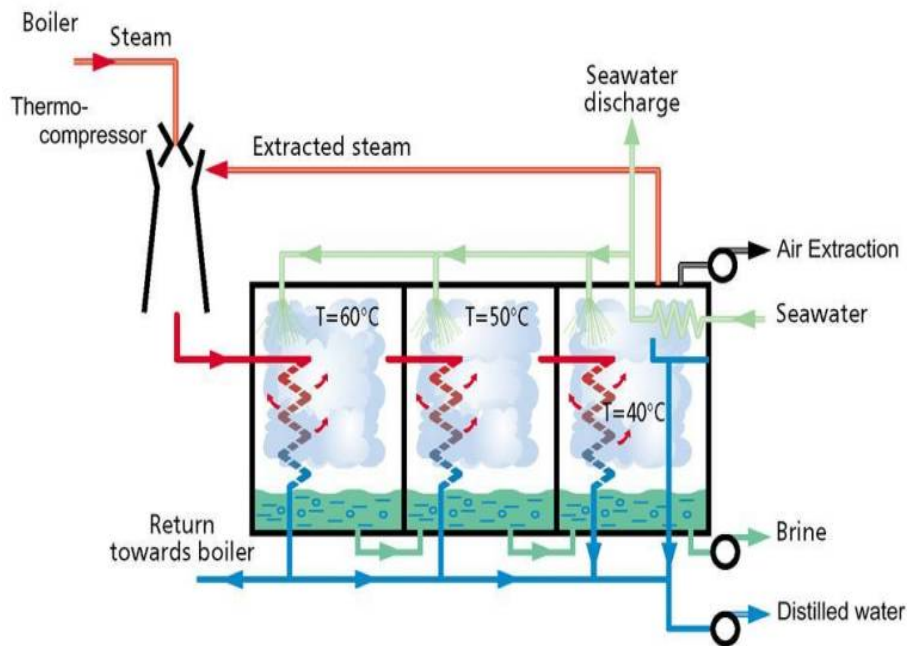
Figure 2-9: Schematic drawing of mechanical vapour compression (MVC) [30]

2.3 Comparison between the most common desalination techniques

Figure 2-10 shows the proportion of desalination processes types in use presently [2]. As can be seen, the RO and MSF are the dominant desalination processes, which constitute 53.0% and 25% of the worldwide capacity, respectively. The feasibility of each technology depends on specific conditions, such as energy price, water quality, and the technical resources of the region.
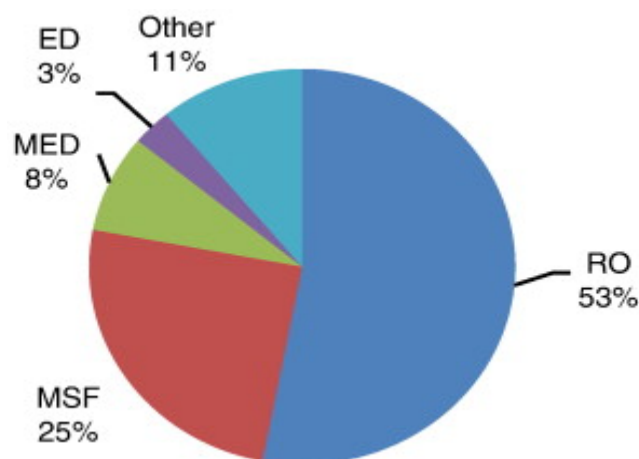
Figure 2-10: Desalination technologies distribution [2]

Recently, significant improvement has been made in MED-TVC desalination plant by SIDEM. This technology has shown a clear competition with Multi Stage Flash (MSF) as thermal desalination processes suitable for large scale production at lower operation temperatures. The GOR of MSF is limited to 13 whereas that of MED-TVC can reach to 20. The specific power consumption of MSF is about four times that of RO [95]. Small scale desalination, such as single stage desalination multi effect desalination multi stage flash desalination, vapour compression desalination and solar evaporation, produce fresh water for small factories, laboratories and any emergency use. The results of various studies of these units indicated that these methods were acceptable for these purposes and were most economical for small scale [96].

Thermo-economic analyses of some existing desalination technologies such as MSF, MEE-MVC, MEE, MEE-TVC, and RO were investigated using Visual Design Software (VDS). The results showed both RO desalination and MEE-MVC were the most promising technologies [97].

Mistry et al [98] studied different desalination technologies: MSF, MED, RO, Mechanical Vapour Compression (MVC), Direct Contact Membrane (DCM), and Humidification-Dehumidification (HD). These studies revealed that RO desalination delivered the best exergy efficiency among them with 31.9%, while other technologies were typically 2.9% (MSF), 5.9% (MED), 8.5% (MVC), 1% (DCM), and 2.4% (HD). They analysed exergy in three types of desalination: Reverse Osmosis (RO), Multi-Effect (MED), and MSF. They found typical exergy efficiencies were 30.10%, 14.27%, and 7.73% for RO, MED, and MSF, respectively. The CO_2 emission from MED was 5.22 and only 2.91kgCO_2eq/m^3 [33]. Furthermore, RO and MED consumed less power to produce water (3.29 kWh/m^3 and 5.9 kWh/m^3 respectively). All the above studies of desalination exergy assumed the seawater to be an ideal mixture. However, in reality it is a highly electrolyte filled substance [99]. The significant difference between both assumptions was demonstrated by Sharqawy et al [100] after the results from a study by Kahraman and Cengel [101].

Roberto el al [102] investigated a comparison between MSF, MED as a thermal technologies and RO technology which are used in desalination plant and assumed to produce the same amount of potable water 205,000 m^3/day. Their results showed that both MSF and MED have very similar water cost. On the other hand RO application give certain advantages without considering any risk effect due to the high sensitivity

of this type of plan to raw sea water quality, while MSF and MED have a higher environmental impact due to temperature discharge except when they were coupled with power generation plant.

Khawaji el al [103] reviewed desalination technologies and provided an overview of the research and development activities and outlined future prospects for RO and MSF systems. Their results indicated that much research and development needed to be done in order to make seawater desalination techniques affordable worldwide. The results also proved that the overall exergy efficiency of the units is lower than accepted. The impact of desalination technologies to the environment was also examined. The results indicated that RO has a lower effect on the environment than the thermal technologies. However, the environmental impact from the thermal desalination technologies could be reduced if integrated with other processes [104]. Although there are a number of seawater desalination plants currently available on the market, research has demonstrated that MSF and RO are the two main technologies, which have successfully achieved quantity production and low cost [4]. However MSF has an exergy efficiency lower than MED [98].

Wade [105], studied the effect of distillation plant development on cost in three main distillation processes (MSF, MED and RO). The results concluded that improvement in the process and energy efficiency reduce the potable water product cost by about 50% to the range between 0.7 to 0.9 US$/m^3. The MSF process had a high energy cost and it was only competitive in large scale when it had lower energy cost, and the MED had lower power consumption and faster development, whereas, the RO distillation process has clear significant cost saving for both capital or operating.

The cost for the major desalination technologies, MED, MSF and RO has decreased in the last decades. Furthermore, RO techniques may compete soon with conventional water supplies for potable purposes even in non-water stressed regions [106]. As population increases, the water demand increases as well. Desalination cost has reduced dramatically due to development in desalination technologies, in some areas the water lifetime cost has declined to 0.5 US$/m^3 whereas at the same potable water production the cost is 1US$/m^3 because of different local incentives or subsidies. Most of the desalination cost results were focused on their local area and there are some aspects that affect this analysis, such as; energy cost, raw materials cost and transportation. The rapid improvements in the existing technologies, raw materials and equipment may reduce the cost in future [16].

Thermal processes become more economical when cogeneration plant is used, which is called a dual purpose plant [32]. Previous research included parametric studies to study the influence of environmental parameters on the system performance. Where [12] has included the utilisation of an existing geothermal low temperature heat source to provide power, air conditioning and heating for an isolated community in southern Libya.

Tables 2-4 shows a comparison between different desalination techniques based on product cost, electrical power consumption, environmental impact and quality. As can be seen from this table reverse osmosis is the optimum selection from membrane technology, where the multi-effect with thermal vapour compression is the optimum selection from thermal desalination technologies [107]. Whereas table 2-5 shows comparison between thermal and membrane desalination.

Table 2-4: Comparison between different desalination technologies [28, 107]

	MED	MVC	MED-TVC	MSF	RO	ED
Thermal energy (kJ/kg) [107]	150-220	-	220-240	250-300	-	-
Electrical energy (kWh/m^3) [107]	1.5-2.5	11-12	1.5-2	3.5-5	5-9	2.6-5.5
Distillate quality [108] ppm	<20	<20	<20	<20	<500	20-500
Total electrical equivalent (MW) [107]	8-201	11-12	21.5-22	5-9	2.6-5.5	2.6-5.5
Unit product cost (US $/m^3 [107]	0.52-1.01	2-2.6	0.827	0.52-1.75	0.52-0.56	n.a

Table 2-5: Comparison between thermal and membrane desalination process

No.	Author	Parameters or subjects investigated	Main outcomes
1	Darwish 2014[95]	Studied two types of thermal desalination MSF and MED-TVC	The results showed that these technologies can compete with RO technologies, and the situation of MED/ME is better than that of MSF.
2	Saidur et al 2011 [96]	Small size desalination technologies	The results indicated that all of these technologies are acceptable for the production of fresh water, but more is recommended research to increase system efficiency.
3	Mabrouk et al 2007 [97]	A comparison of MED, MED-TVC, MED-MVC, and RO	The Thermo-economics results showed that cost is reduced if the exergy destruction in the jet ejector, condenser, and evaporator is reduced. A comparison among the processes considered shows that the unit product cost of the RO process is the lowest.

No.	Author	Parameters or subjects investigated	Main outcomes
4	Mistry et al 2011 [98]	Second law efficiency	RO has substantially higher second law efficiency than the other desalination processes considered in this paper.
5	Borsani and Silvio 2005 [66]	Installation cost, technical specifications	Thermal technologies have an higher environmental impact due to the high temperature discharge, and are reasonable only when coupled with a power generation plant.
6	Khawaji et al 2008 [4]	Review of research and development activities for MSF and RO technologies.	It is recommended that more research and development should be carried out to improve performance.
7	Wade et al 2001. [105]	Water cost and the plant capacity (for MED, MSF and RO)	MED is a flexible technology and had lower energy consumption compared with MSF. RO technology led to significant savings in both capital and operating costs.
8	Gude et al 2010 [107]	Existing and emerging desalination technologies and possibility to combine them with renewable energy sources to drive them and reduce desalination costs. Costs of renewable energy sources for small-scale applications suggest a hybrid energy source comprising both grid-powered and renewable energy.	It is suggested that a holistic approach to coupling renewable energy sources with technologies for the recovery, reuse, and recycling of both energy and water can be a sustainable and environmentally friendly approach to meeting the world's energy and water needs. High capital

2.4 Powering desalination

The desalination process could be powered by either electricity or heat and the main sources of these energies are renewable sources or from a heat or waste heat supplying plant, e.g. cogeneration plant.

2.4.1 *Geothermal heat*

Coupling renewable energy (such as geothermal, thermal solar, photo-voltaic and wind) with desalination processes is a promising solution to water shortages and environmental issues such as global warming gases [109]. The proportion of desalination plants driven by renewable energy is MED and MSF 10%, VC and ED 5%, RO 62% and the others is 4% are widely used in the world. Most of these, approximately 43% are powered by solar photo-voltaic, followed by solar thermal, wind and hybrid technologies, 27%, 20% and 10%, respectively [107]. However, the product cost of renewable desalination is still high compared to conventional desalination plants (above 2 US $/m^3), because of the high capital cost of renewable equipment, the cost of maintenance and low availability factor [107, 110]. Geothermal spring water can be used to power thermal desalination. The water at Waddan City in Libya has a temperature of 73°C which is acceptable to power MED desalination [12].

2.4.2 *Cogeneration plant*

When one plant produces two different products such as, electrical power and thermal energy it is known as a cogeneration process. This type of plant, sometimes called

dual purpose plant, can be used to produce electricity and water [28]. There are many advantages of cogeneration plant compared with standalone power plants and MED-TVC desalination plants. They have higher thermal efficiency, lower CO_2 emission per unit product, less fuel consumption per unit product, flexible operation, lower investment per unit product and require less manpower per unit product [111-113].

In cogeneration plant GTs are used to produce electrical power through a Brayton cycle, but the high temperature GT exhaust is utilized to produce steam through a Heat Recovery Steam Generator (HRSG). This steam is used to generated additional electrical power from a steam turbine [114], while at the lower pressure stage, part of it is used to power a thermal plant, such as desalination by MED-TVC.

For arid countries in general and Libya specially, power demand varies significantly through the year, whereas water demand remains constant [36]. Thus, a cogeneration plant should be designed to meet all possible scenarios resulting from power and water demand variations. Therefore, some cogeneration plants provide supplementary firing (SF) to maintain water production from MED-TVC desalination in case of reduction of GT load or shut down [37]. In addition, for such a plant in the winter season, where the power demand is low and the steam turbine is shut down, a pressure reduction station option is provided to supply the steam required for the MED-TVC [38].

2.5 Combined Cycle Power Plant Thermal Analysis

Combined cycle power plants (CCPP) are widely used for producing electricity, especially in oil producing countries where fuel is readily available and the CCPP situated on the sea coast where the fuel is provided through the pipe line from the oil and gas companies. This type of cogeneration power plant becomes more efficient when coupled with desalination. This plant is used in arid and semi-arid countries where there is shortage of water, both for drinking and industry uses.

2.6 Thermodynamic and economic analysis of cogeneration plant

Saidur et al [115] used an exergy analysis to determine the equipment performance a conventional boiler, the result showed that energy and exergy efficiencies were 72% and 24% respectively. The authors suggested the use of variable speed fan to reduce exergy destruction of the unit. The addition of the fan only has one year payback period. Ameri et al [116] studied exergy destruction in the Neka CCPP plant. They found out that the combustion chamber was the main source of irreversibility due to

large temperature difference between the working fluid and the burner cases and the chemical reaction. This was followed by the heat recovery steam generator (HRSG). More so, energy and exergy analysis were performed [117] for each component in a steam turbine power plant at three different loads: 100%, 75% and 50%. The results showed that the maximum energy losses occurred in the condenser at about 40% at maximum load and the maximum exergy destruction was at the turbine followed by the condenser. Thermal efficiency was 43% and exergy efficiency varied from 44% - 48%.

Exergoeconomic analysis at three different plant loads, 40%, 60% and 85% of full load were investigated at Tripoli gas turbine unit. The result showed that as the load increased the exergy efficiency increased from 20% (at 40% load) to 29% (at 85% load). Moreover, the study showed that the average cost per unit exergy decreases as load increases, $7.1/GJ and $4/GJ at 40% and full load, respectively. The main contributor of exergy destruction at the three different loads was found to be the combustion chamber [118] . This was corroborated by Almutairi et al [119]. However, a reheat gas turbine showed a lower cost of electricity production, as a result of improving the power turbine performance due to reheating.

 Almutairi et al [119] performed exergy, exergoeconomic and sustainability analyses for two advanced gas turbine at different loads to study the effect of CO_2 emissions to the environment (ambient temperature). The results showed that the combustion chamber is the main source of exergy destruction, due to temperature difference, friction and chemical reaction. Also as the ambient temperature increased the exergy efficiency and output power decreased due to more power being consumed by the compressor. However, a reheat gas turbine showed a lower cost of electricity production, as a result of improving the power turbine performance due to reheating. Ganapathy et al [120] studied the exergy analysis of operating lignite fired power plant. Their results showed that the maximum energy losses occurred at the condenser by about 39% where about 43% of exergy losses occurred at the combustor. The effect of inlet ambient temperature on gas turbine power was studied using different techniques. The results showed that a reduction of 1°C ambient temperature produces an increase in the turbine power by about 0.7%.

Ameri and Hejazi [121] studied the enhancement of gas turbine behaviour by reducing ambient air temperature using a steam-powered absorption chiller. The results indicated that cooling the inlet air to the gas turbine could improve the output power by

11%, when the inlet air temperature to the gas turbine decreased from 38°C to 15°C. Moreover, the results showed that the influence of inlet air cooling on raising the energy and exergy efficiency along with evaporative after-cooling was significant compared with cogeneration without this cooling equipment [122]. To improve the output power and keep it on steady state and to avoid the degradation during ambient temperature increase, a media evaporator cooling system was installed in the gas turbine at Fars Iran using different geometric shape, sizes and depth of the media. The practical and analytic results showed that when the ambient temperature decreased from 28°C to 19°C, the gas turbine output power increased the output power by about 14.6% (11MW). In addition, the payback period would be about 48 months [123]. El-Nashar [124] studied the design of a cogeneration plant with desalination taking equipment reliability into consideration. His results indicated that the introduction of reliability leads to higher product costs, which meant that reliability considerations were important and should be carried out in any cogeneration system design. Ahmadi and Dincer [125] conducted a comprehensive modelling of a dual pressure combined cycle power plant using a thermodynamic and exergy-environmental analyses and multi-objective optimization. The results indicated an increase in compressor isentropic efficiency, exergy efficiency and increased gas turbine isentropic efficiency.

Mehta parth et al [17] investigated how to improve the cogeneration plant efficiency and reduce the exergy destruction using an existing power plant in Izmir Turkey. The results indicated that to improve cogeneration plant efficiency and reduce exergy destruction some improvement should be made to the heat exchanger and combustion chamber.

Farzaneh-Gord and Deymi-Dashtebayaz [126] made a comparison between two air cooling methods, an evaporative media with a mechanical chiller and turbo-expanders to evaluate which could improve gas turbine performance at high ambient temperature. They found that the turbo-expander was beneficial economically and improved the gas turbine performance. Moreover, gas turbine performance enhancement using intake air coolers was investigated using two different types of cooling, namely cooling coils and a water spraying system. The results showed that the spray coolers improved gas turbine power and efficiency and were much cheaper than cooling coils. The cooling coils worked more efficiently at dry and hot climate conditions [127].

Because of the gas turbine output power was designed at ISA condition and the performance of gas turbine is affected by the change of inlet air temperature, Boonnasa et al [128], investigated how to improve the performance of a combined cycle power plant in Thailand by reducing the intake air temperature to International System Atmosphere (ISA) condition around 15°C and 100% relative humidity (off design point) before entering the compressor, using a steam powered absorption chiller. The result showed that, by cooling the compressor intake air, the gas turbine output power increased by about 11%. The combined cycle total power increased only 6% due to a steam turbine output decrease by about 2%. The estimated net electricity production could be increased by 70GWh/yr. IPSEpro software was used to develop the Sabiya combined cycle power plant and energetic and exergetic analyses were investigated [122]. The results showed that improving the thermodynamic performance has good impact on both environment and economics. Table 2-6 shows the summary of literature review.

Table 2-6: Combined cycle power plant

No.	Author	Parameters or subjects investigated	Main outcomes
1	Saidur et al 2010 [115]	Energy and exergy analysis	Exergy efficiency is lower than energy efficiency, and the boiler represented the major site of exergy destruction. The use of fan with variable speed could reduce the payback period.
2	Ameri et al 2008 [116]	First and second laws of thermodynamics	The results show that if a duct burner is added to the HRSG, first and second efficiencies could be reduced to 46% and 44% respectively. However, the results also show that the CCPP output power increases by 7.38% when a duct burner is used.
3	Fellah et al 2010 [118]	Power plant loads	The results of the exergoeconomic analysis showed that the per unit exergy decreased as the power plant load increased.
4	Almutairi et al 2016 [94]	1. Ambient temperature 2. Load %	Exergy efficiency decreased when ambient temperature increased, whereas exergy efficiency increased with load.
5	Gabapathy et al 2009 [120]	Energy losses and exergy destruction	The maximum energy losses were found at the condenser, whereas the maximum exergy destruction was at the combustor.
6	Ameri and Hejazi 2004 [121]	1. Ambient temperature 2. Fuel consumption	Cooling the inlet air temperature improved the output power and using an absorption chiller would very useful.
7	Khaliq et al 2004 [122]	1. Turbine inlet temperature 2. Pressure ratio 3. Process heat pressure	The largest exergy destruction takes place during the combustion and heat recovery processes, The exergy destruction in gas turbine components increased significantly with increasing in pressure ratio but decreases the same in water heater. The energy and exergy efficiency of the cycle was significantly influenced by the overall pressure ratio and turbine inlet temperature but only slightly by the process pressure
8	Farzaneh-Gord and Deymi-Dashtebayaz 2011[126]	Effect of ambient temperature	The result showed that the gas turbine inlet air temperature could be reduced by using which will enhance the gas turbine efficiency.
9	Alhazmy and Najja 2004 [127]	Relative change of ambient temperature	The results showed that using mechanical chiller will reduce the inlet temperature and enhanced the power
10	Boonnasa et al 2006 [128]	Inlet air temperature	The results showed that cooling the inlet air temperature increased the total output power. Nevertheless, the power of steam turbine reduced.

No.	Author	Parameters or subjects investigated	Main outcomes
12	Talbi and Agnew 2000 [129]	Efficiencies of components	The load in the condenser is slightly higher than that in the evaporator due to primarily superheating of the inlet vapour to the condenser.
13	Khaledi et al 2005 [130]	Effect of inlet air temperature	The results showed that as the inlet air temperature increased the GT exhaust temperature increased, where the inlet mass flow rate and fuel flow decreased.

2.7 Absorption Chiller (AC)

The increased cost of electricity, environment concerns and the climate condition especially in hot country have made the heat-operated cycle more attractive for both residential and industrial applications. One of the solution to these issues are Absorption chillers which are using heat instead of mechanical energy to provide cooling and use water as refrigerant and lithium bromide salt solution as absorbent. The absorption system working fluid proposed in this study, because water is vaporised at 100°C in the desorber where LiBr boiling point is 1265°C [131]. The advantage of the absorption chiller unit over other refrigeration systems is that it can operate with low-grade heat energy, as indirectly or directly, as steam, as gas, oil or hot exhaust gases, or solar energy, mechanical [131].

Recently the absorption chiller became important in the industry, especially for power plant located in hot areas, which benefit from cooling the inlet air. Many researchers focus on studying the performance of absorption chillers [129, 130, 132, 133]. Exergy analysis of single effect absorption chiller components using H2O-LiBr as working fluid was studied [129]. Waste heat from a diesel engine was used to power the absorption chiller where the ambient temperature was 35°C. The result showed that the absorber recorded the highest exergy destruction ratio by about 59% followed by the generator and evaporator at 27% and 8% respectively, whereas the solution pump had the lowest ratio of only 0.2%. However, the chemical exergy was not taken into consideration.

Kaushik and Arora [133] investigated energy and exergy analysis of single and double effect absorption chillers. Their results showed that COP increased with generator temperature increase. On the other hand, the absorber had the highest exergy destruction compared with the other components. Rahah [134] studied a two stage half effect absorption system. His results indicated that the COP of the cycle increased with an increase of generator temperature and decrease with increasing condenser

temperature. Moreover when the evaporator and absorber temperature was maintained at 4°C and condenser and absorber temperature varied from 28°C to 38°C the maximum COP relative change varied between 0.408% to 0.435% and the maximum exergetic efficiency was in the range of 14.7% to 22.6%. A similar study of single effect and double effect units showed that the coefficient of performance of the single effect system lies in range of 0.6 to 0.7 and the corresponding double effect system lies in the range of 1 to 1.28. The effect on the performance of such parameters as temperature difference between heat source, generator and evaporator and cold room have also been investigated. Irreversibility was found to be highest in the absorber in both systems when compared to the other system components.

Recently research has been carried out [135] to improve performance of absorption systems. Energy and exergy analyses and effect of temperature were considered. The results showed that at low temperature a high COP and energy efficiency on the desorber and the absorber was obtained for both single and double effect H_2O-Libr systems. Popli et al. [136] a thermo-economic completed analysis of a single effect absorption chiller (H_2O-LiBr) and compared this with an evaporative cooler. The results showed that to reduce the inlet ambient temperature from 55°C to 10°C the absorption chiller has more advantages than evaporative coolers. In order to reduce the compressor inlet ambient temperature to 10°C the absorption chiller utilized 17MW from the gas turbine exhaust heat and could provide about 12.3MW cooling to cool the compressor inlet air. However, at the same ambient condition the evaporative coolers would only provide about 2.3MW. Moreover the mechanical vapour compression chillers required additional power about 2.7MW to provide the same amount of cooling.

2.8 Summary

The results of the literature review has been summarised in the tables 2-1 to 2-6, in which the referenced papers are listed alongside remarks about their main outcomes. In the context of the objectives of the thesis, this review showed that there is increasing demand for potable water [7, 25]. The main sources of energy used in the production of distilled water are still fossil fuels, which have a negative impact on the environment. Many efforts by researchers have been attempted to ameliorate this issue, in areas including applications for power plants and their performance, absorption chillers and desalination technologies. A number of guidelines have been drawn up from this literature review to be applied as a part of this study:

Firstly, few comparisons have yet been made between different reverse osmosis configurations, especially with a PX in the first stage and an ERT or PX in the second stage. Moreover, the limited analyses so far performed have not considered chemical exergy or economic considerations.

Secondly, the exergy analysis approach is shown be the most suitable method for use with cogeneration plants which produce more than one product, such as electricity with distillate water. However, the number of studies that have evaluated a combined cogeneration power and water plants using the exergy approach is very small.

Thirdly, it has been shown that the exergy efficiency of thermal desalination plant is low compared with membrane plants. The MED-TVC is one of the most reliable and common thermal desalination technologies, which has the advantage of operating economically as well as with high effectiveness. Therefore MED-TVC technology was chosen for comparison with the membrane (RO) process on the basis of energy, exergy and economics. The input power was derived from steam for the MED-TVC and from electricity for the RO.

Fourthly, the heat recovered from the MED-TVC distillate water could be further utilized by heat recovery technologies. No attempts have been found in the literature to address this point so as to improve the GOR and exergy efficiency and to reduce the steam consumption of the MED-TVC system. The present study will fill this gap.

Fifthly, it is well established that waste heat from combined cycle exhaust gases could be utilized to power an AC to cool the compressor inlet air temperature. It is proposed that an AC be used to improve the power plant performance so as to avoid any degradation in output power during the summer in Libya. Exergy analysis will be carried out along with an economic analysis of this case.

Sixthly, ORC units have been investigated in previous studies to produce electrical power by using brackish geothermal water; for instance, in the City of Waddan, Libya. A similar system could be used to power a single effect desalination plant, as the power produced from the ORC can be also used to drive a single-pass reverse osmosis unit. This could provide fresh water which is required in cities such as Waddan. Previous studies did not include a comparison between SED and RO using exergy and economic analyses in this area.

CHAPTER 3. METHODOLOGY

3.1 Introduction

This chapter covers a number of aspects of the methods such as the IPSEpro software, with its power plant, desalination, and refrigeration libraries. Then the First and Second Laws of thermodynamics are described including methods of calculation for enthalpy, entropy, and energy and exergy efficiency, which are necessary to calculate the energy and exergy in each numbered stream of the models which are required to compare the results of the simulations. Furthermore, because this study is concentrated in the environment of Libya, this chapter also covers weather data for Zawya City in Libya where the combined cycle power plant is located**.**

3.2 IPSEpro Software

Many studies now use modelling and simulation as a key part of the testing and design of equipment. These methods have many advantages, such as flexibility, and speed, and a number of configurations can be considered [25]. In this study IPESEpro software [137] was used. The modelling results produced using IPSEpro have been validated against real-world data in many previous studies that show good agreement between the two [14, 25, 28, 138]. These results encourage use of this software in this study. This software can perform mathematical calculations with economic implications for many relevant engineering processes [139]. Based on the comparison between a number of softwares [140] also a number of previous publication which the IPSEpro has advantage when it used on thermal process. IPSEpro has flexibility at two levels, known as the component and process levels. It allows one to build and simulate from a single element up to a model of the complete plant [141]. IPSEpro allows single components to be changed or new components can be integrated into the program. IPSEpro is COM-based and interacts with other software programs [25, 139]. In addition, since this software is very flexible in many aspects of thermodynamic processes, it is attractive to industrial and research companies, such as Rolls-Royce. This software can calculate all the thermodynamic properties of the process streams, which helps the user to calculate energy and exergy. Only three Libraries of the software were used in this study.

3.2.1 *Model development kit (MDK)*

To build up a model in IPSEpro the MDK is used which provides the model description language (MDL). Full customization of all of the components allows the model built to exactly match the user's application requirements. The model building process is easy and interactive and designs can be represented graphically. Within the MDK, it is also possible to modify and customize existing model libraries [14, 137]. In the present study, three different types of libraries were used: the power plant library, desalination library, and refrigeration library. These were used to build a combined cycle power plant using multi-effect desalination with thermal vapour compression (MED-TVC), a reverse osmosis desalination plant (RO), and a single effect lithium bromide absorption chiller.

3.2.2 *Process simulation environment (PSE)*

The core of IPSEpro is the PSE, which combines the model library components to build a process model. The process model consists of various different component models which are connected on the flowsheet. This simulates the process using mathematically optimized methods with accurate and fast calculations. The components required can be easily selected from the library menu by the user and connected together with streams to represent the plant configuration. In a model library, the component models consist of fundamental or first principle models. They are based on fundamental laws of thermodynamics, such as conservation of mass and energy. Such models can be developed and tested for correctness. The equation balances in the software are accurate up to the inherent numerical calculation error. This numerical calculation error is considered for parameters (like isentropic efficiencies, pressure drops) and characteristics curves or tables. The underlying property models of the physical property functions used within a model library formulation give details on the uncertainties for the individual calculated properties.

From the applied numerical approach to solve a process model, it is assumed that the equations contained in the individual component models are correctly fulfilled when the system is solved and the solver converges to solution. If any limits or test conditions are violated at the solution point, an error message will be given. When there are no errors after the calculation run, all equations are correctly fulfilled, using Newton Raphson method [13].

3.2.3 *Libraries*

Three IPSEpro libraries were used for this study:

a) *Advanced power plant library*

This library consists of 49 units which represent most power plant equipment, such as compressors, turbines, boilers, pumps, heat exchangers, motors, and valves. One of the advantages of IPSEpro is that a new unit can be built using the MDK. In addition, a database of chemical and physical properties for many liquids used in the process is available, for example, seawater, pure water, steam, and combustion gases [137]. This library is used to build Combined Cycle Power Plant (CCPP).

b) *Desalination process library*

In this library all of the necessary equipment which is required for membrane and thermal desalination plants are available. The library also includes the auxiliary equipment required for desalination plants (such as heat exchangers, pumps, and ejectors) and a database of the fluids used in the desalination process (eg steam, seawater and distillate water) used in this study to build:

> ➢ Reverse Osmosis (RO).

> ➢ Multi Effect Desalination with Thermal Vapour Compression (MED-TVC).

> ➢ Single Effect Desalination (SED).

c) *Refrigeration process library*

The modelling process allows for a number of thermodynamic processes to use more than 50 refrigerants, referring to data obtained from the United States National Institute of Standards and Technology. The physical properties database covers a large range of refrigerants and refrigerant mixtures for both absorption and compression [25, 139]. The refrigerant library thus helps designers and researchers to build any advanced vapour compression system and absorption refrigeration system since it includes all of the components required. In this study this library was used to build a single stage lithium bromide absorption chiller.

3.3 Basic CV equations

In the steady state, a control volume around the components of the modelled cogeneration plant can be with multiple inlet (i) and outlet (e) mass flows balanced at steady state [112]:

$$\sum \dot{m}_i = \sum \dot{m}_e \tag{3-1}$$

The energy can be transferred into and out of the control volume by mass flux, work, and heat:

$$\dot{Q}_{in} + \dot{W}_{in} + \sum \dot{m}_i \left(h_i + \frac{v_i^2}{2} + gz_i \right) = \dot{Q}_{out} + \dot{W}_{out} + \sum \dot{m}_e \left(h_e + \frac{v_e^2}{2} + gz_e \right) \tag{3-2}$$

This study was carried out with no significant changes in potential and kinetic energy assumed [142, 143]. Therefore, equation 3.2 can be reduced to:

$$\dot{Q}_{in} + \dot{W}_{in} + \sum \dot{m}_i h_i = \dot{Q}_{out} + \dot{W}_{out} + \sum \dot{m}_e h_e \tag{3-3}$$

When it moves from state one to state two the entropy balance in the closed system can be written as follows [68, 142]:

$$(S_2 - S_1) = T_0 \int_1^2 \left[\frac{\delta Q}{T} \right] - T_0 S_{gen} \tag{3-4}$$

where T_0 and S_{gen} are the temperature of the environment and entropy generated, respectively.

Combining the first and second laws of thermodynamics leads to [142]:

$$(U_2 - U_1) + T_0(S_2 - S_1) = \int_1^2 \delta Q - T_0 \int_1^2 \left[\frac{\delta Q}{T} \right] - W - T_0 S_{gen} \tag{3.5}$$

By rearranging, the closed system balance can be written as:

$$(E_2 - E_1) = \int_1^2 \left[1 - \frac{T_0}{T_b} \right] \delta Q - \left[W - p_0(V_2 - V_1) \right] - T_0 S_{gen} \tag{3.6}$$

where:

$\Delta E = E_2 - E_1$ is the exergy change in the control volume system, where each E describes the maximum reversible work that can be obtained.

$E_q = \int_1^2 \left[1 - \dfrac{T_0}{T_b}\right]\delta Q$ is exergy transfer, which is associated with heat transfer of the energy by the heat crossing the system boundary.

$E_w = \left[W - p_0(\Delta V)\right]$ can be interpreted as the transfer of exergy by work.

$E_D = T_0 S_{gen}$ represents the destruction of exergy due to the irreversibility in the system. It is also commonly referred to as availability destruction and may be termed the Gouy-Stodola theorem [112].

The exergy balance of the closed system can be expressed in rate of change of exergy form as follows [142]:

$$\frac{dE}{dt} = \int_1^2 \left[1 - \frac{T_0}{T_b}\right]\delta \dot{Q} - \left[\dot{W} - p_0 \frac{dV}{dt}\right] - \dot{E}_D \tag{3.7}$$

Like mass, exergy is an extensive property that can be transferred to the system. Because most industrial engineering systems can be treated as control volume systems, Equation 3.7 can be rearranged to describe the control volume:

$$\frac{dE_{cv}}{dt} = \sum_j \left[1 - \frac{T_0}{T_b}\right]\delta \dot{Q}_j - \left[\dot{W}_{cv} - p_0 \frac{dV}{dt}\right] + \sum_i \dot{m}_i e_e - \dot{E}_D \tag{3.8}$$

In the steady state, the two terms $\dfrac{dE_{cv}}{dt}$ and $\dfrac{dV}{dt}$ equal 0, and equation 3.8 is simplified to:

$$0 = \sum_j \left[1 - \frac{T_0}{T_b}\right]\delta \dot{Q}_J - \dot{W}_{cv} + \sum_i \dot{m}_i e_i - \sum_e \dot{m}_e e_e - \dot{E}_D \tag{3.9}$$

This can be expressed as:

$$0 = \sum_j \dot{E}_{q,j} - \dot{W}_{cv} + \sum_i \dot{E}_i - \sum_e \dot{E}_e - \dot{E}_D \tag{3.10}$$

The total inlet $\dot{E}_i$ and exit $\dot{E}_e$ exergy can be determined as a sum of physical exergy $\dot{E}_{ph}$, chemical $\dot{E}_{ch}$, potential $\dot{E}_{po}$, and kinetic $\dot{E}_{ke}$ exergies in the absence of magnetic, electrical, and nuclear exergies [68].

$$\dot{E} = \dot{E}_{ph} + \dot{E}_{ch} + \dot{E}_{po} + \dot{E}_{ke} \tag{3.11}$$

$\dot{E}_{po}$ indicates the total potential exergy rate due to the change in elevation of the stream from that of the environment, although it is usually ignored if the environment and stream elevations difference is assumed to be small [142, 144].

$\dot{E}_{ke}$ is the total kinetic exergy rate, representing different velocities at the stream inlet and outlet. This is ignored in many studies of exergy if it is assumed that a velocity gradient is absent [142, 144].

Neglecting the small potential and kinetic exergy terms.

$$\dot{E} = \dot{E}_{ph} + \dot{E}_{ch} \tag{3.12}$$

$\dot{E}_{ph}$ is the total physical exergy required to change the stream from present state to the dead state as described above. The specific physical exergy for the stream can be written as [68, 100, 143]:

$$e_{ph} = (h_i - h_0) - T_0(s_i - s_0) \tag{3.13}$$

where T_0, h_0, and s_0 are the dead state of values temperature, enthalpy and entropy, respectively.

$\dot{E}_{ch}$ is the total stream chemical exergy rate due to differences in composition between the stream state and the dead state. The specific chemical exergy of the stream is determined from:

$$e_{ch} = \sum x_k e_{k,cho} + RT_0 \sum x_k \ln \gamma x_k \tag{3.14}$$

Where x_k represents the concentration of components, $e_{k,cho}$ is the specific chemical exergy of component k, and γ its chemical potential coefficient, which is equal to one

for an ideal mixture [142]. Note that x_k is ignored if the fluid composition remains constant [144, 145].

3.4 Performance Criteria

Energy analyses is used to calculate the losses in the system by concentrating on the amount of energy in each process stream but without any information about the quality of the energy content. On the other hand exergy analysis clearly shows the location of energy degradation by focusing on the quality as well as quantity of energy [146].

The exergy efficiency is defined as the ratio of the net-work output to the fuel exergy input to the thermal system:

$$\eta_{II} = \frac{\dot{W}_{net,out}}{\dot{E}_{in}} \qquad (3.15)$$

However, in cogeneration systems where useful heat generated in addition to the net-work is available for other processes, exergy efficiency is defined as follows [142]:

$$\eta_{II} = \frac{\dot{W}_{net,out} + \dot{E}_{useful}}{\dot{E}_{in}} \qquad (3.16)$$

The gas turbine thermal efficiency (η_I) and its components are calculated based on the latest ASME standards [139, 147, 148].The thermal efficiency of the gas turbine (GT) and steam turbines (ST) respectively can be expressed as:

$$\eta_{1,GT} = \frac{\dot{W}_{net,GT}}{\dot{m}_{GT,fuel}\,LHV} \qquad (3.17)$$

$$\eta_{I,ST} = \frac{\dot{W}_{net,ST}}{\dot{m}_i\left(\dot{h}_e - \dot{h}_i\right)} \qquad (3.18)$$

where LHV (MJ/kg) is lower heating value.

The heat rejected steam generation (HRSG) thermal efficiency can be obtained as the division of HRSG output, which is high pressure (HP) steam, by the input, which is the fuel energy from the gas turbine exhaust [139, 147, 148]:

$$\eta_{I,HRSG} = \frac{\dot{m}_i\left(\dot{h}_e - \dot{h}_i\right)}{\left(\dot{m}_{GT,e}\,LHV\right)} \qquad (3.19)$$

The overall thermal efficiency of the standalone CCPP is obtained by:

$$\eta_{I,overall} = \frac{W_{net,GT} + \dot{W}_{ST} - \dot{W}_{pp}}{\left(\dot{m}_{GT,fuel} LHV\right)} \tag{3.20}$$

The exergy destruction ratio can be determined in terms of either the total input exergy of the fuel y_D , or the total exergy rate y_D^* as in equations 3.21 and 3.22

$$y_D = \frac{\dot{E}_D}{\dot{E}_{fuel,tot}} \tag{3.21}$$

$$y_D^* = \frac{\dot{E}_D}{\dot{E}_{D,tot}} \tag{3.22}$$

The overall exergy efficiency of the MED-TVC and RO defined as the W_{min} divided by E_{input} as expressed in equation (3.23):

$$\eta = \frac{W_{min}}{E_{input}} \tag{3.23}$$

where W_{min} is the minimum work of separation required to changing the chemical composition from sea to fresh water .

The heat utilization factor (HUF) of the cogeneration plant which is producing both power and potable water can be evaluated as follows [139, 149, 150]:

$$HUF = \frac{\dot{W}_{net,GT} + \dot{W}_{ST} + \dot{m}\left(h_i - h_e\right)_{MED-TVC} - \dot{W}_{pp}}{\left(\dot{m}_{GT,fuel} LHV\right)} (\%) \tag{3.24}$$

3.5 Desalination

The performance of MED-TVC is indicated by Gain Output Ratio (GOR) and the concentration ratio (CR). The GOR can be defined as the amount of distillate product per amount of the mass steam consumed [139, 149, 151]:

$$GOR = \frac{\dot{m}_{dp}}{\dot{m}_{steam}} \tag{3.25}$$

The exergy analysis of desalination systems will be based on the latest thermodynamic properties of seawater, which were obtained experimentally [68, 99, 100]. The latest

thermodynamic properties is not available in the IPSEpro software. A special calculator using Excel is used to calculate for equations (3.26 to 3.37):

Equation 3.13 is used to calculate the physical exergy of the seawater streams. For water and seawater the enthalpy is calculated by [99, 100, 139]:

$$h_{sw} = h_w - w_s[b_1 + b_2 w_s + b_3 w_s^2 + b_4 w_s^3 + b_5 T + b_6 T^2 + b_7 T^3 + b_8 w_s T + b_9 w_s^2 T + b_{10} w_s T^2 \quad (3.26)$$

b_1 to b_{10} are seawater enthalpy is given by (constants presented in appendix 3-A) where the pure water enthalpy is calculated by:

$$h_w = 141.355 + 4202070T - 0.535T^2 + 0.004T^3 \qquad (3.27)$$

The effect of stream pressure on its enthalpy of the stream is then added:

$$h_{sw}(T, p, w_s) = h_{sw}(T, p_0, w_s) + v(p - p_0) \qquad (3.28)$$

For the water and seawater the entropy is given by (constants presented in appendix 3-A1):

$$s_{sw} = s_w - w_s[c_1 + c_2 w_s + c_3 w_s^2 + c_4 w_s^3 + c_5 T + c_6 T^2 + c_7 T^3 + c_8 w_s T + c_9 w_s^2 T + c_{10} w_s T^2] \quad (3.29)$$

The pure water entropy S_w is:

$$s_w = 0.1543 + 15.383T - 2.99610^{-2}T^2 + 8.19310^{-5}T^3 - 1.37010^{-7}T^4 \qquad (3.30)$$

where T is temperature in degrees Celsius:

The chemical exergy of a pure water and seawater stream is produced when it has a salt concentration different from that of the dead state, and is determined by equation 3.31:

$$e_{ch} = \sum_{i=1}^{n} w_s \left(\mu_i^* - \mu_i^0 \right) \qquad (3.31)$$

where μ_i^* and μ_i^0 are the chemical potentials of the i component at (T_0, p_0, w_s^*) and (T_0, p_0, w_{s0}) respectively. With combined pure water and seawater, the chemical potential is formed by differentiating the Gibbs function:

$$\mu_w = \frac{\partial G_{sw}}{\partial m_w} = g_{sw} + (1 - w_s)\frac{\partial g_{sw}}{\partial_{ws}} \qquad (3.32)$$

$$\mu_s = \frac{\partial G_{sw}}{\partial m_s} = g_{sw} + (1-w_s)\frac{\partial g_{sw}}{\partial w_s} \tag{3.33}$$

where g_{sw} is the specific Gibbs function at T $^\circ$C given by:

$$g_{sw} = h_{sw} - (T + 273.15)s_{sw} \tag{3.34}$$

Differentiation of the specific Gibbs function gives:

$$\frac{\partial g_{sw}}{\partial w_s} = \frac{\partial h_{sw}}{\partial w_s} - (T+273.15)\frac{\partial s_{sw}}{\partial w_s} \tag{3.35}$$

When the salt concentration changes, the enthalpy and entropy also change. This change can be calculated by the following equations, for which the constants b and c are given in appendix 3-A [68]:

$$-\frac{\partial h_{sw}}{\partial w_s} = b_1 + 2b_2 w_s + 3b_3 w_s^2 + 4b_4 w_s^3 + b_5 T + b_6 T^2 + b_7 T^3 + 2b_8 w_s T + 3b_9 w_s^2 T + 2b_{10} w_s T^2$$

$$\tag{3.36}$$

$$-\frac{\partial s_{sw}}{\partial w_s} = c_1 + 2c_2 w_s + 3c_3 w_s^2 + 4c_4 w_s^3 + c_5 T + c_6 T^2 + c_7 T^3 + 2c_8 w_s T + 3c_9 w_s^2 T + 2c_{10} w_s T^2 \tag{3.37}$$

3.6 Reverse Osmosis (RO)

The membrane process is used to reduce the salinity of seawater and brackish water to an acceptable range. This process is controlled by parameters such as osmotic pressure and flux. The osmotic pressure π is calculated using the Van't Hoff equation [152]:

$$\Delta\pi = \text{CRT} \tag{3.38}$$

where T is absolute temperature, C is molar concentration, and R is the gas constant. Equation 3.38 gives an acceptable level of accuracy for practical cases of RO, but it is considered weak in predicting the osmotic pressure in a solution of macromolecules [152]. Earlier researchers concluded that osmotic pressure was an inappropriate measure for solutions whose molarity was measured in millimoles. However, this argument proved to be incorrect and the following empirical expression can be applied [10, 153]:

$$\Delta\pi = RT\sum(n/v) \tag{3.39}$$

where R = 0.083 J/mol-K, and $\sum(n/v)$ = the sum of ionic concentrations, and T is the absolute temperature

To calculate the water flux J_w and salt flux J_s at the membrane from the diffusion of the solution the following equations were used [29, 154]:

$$J_w = \frac{Q_p}{A_w} = A_w(\Delta p - \Delta\pi) \tag{3.40}$$

where A_w is water permeability coefficient [m/(s.bar)] and calculated by using equation 3.41 [29, 155]:

$$A_w = \frac{D_w C_w V_w}{\delta_m RT} \tag{3.41}$$

$$J_s = B_s(C_m - C_p) \tag{3.42}$$

where B_s is salt permeability [kg/(m^2.s)] coefficient and calculated as [10, 155, 156]:

$$B_s = \frac{D_s K_s}{\delta_m} \tag{3.43}$$

where:

D_s Diffusivity of solute, (m/s).

K_s Solubility of solute, m^2/s.

δ_m Membrane thickness, m.

J_s Solute transport, (m/s).

Δp Trans-membrane pressure, (bar).

C_m Membrane concentration surface, (mol/m^3).

$\Delta\pi$ Osmotic pressure gradient across the membrane, (bar).

Membrane salt rejection percentage is defined as the difference between the feed concentrations and permeate concentration [157]:

$$R_s = [1 - \left(\frac{C_p}{C_f}\right)].100\% \tag{3.44}$$

where C_p and C_f are permeate and feed water concentration, respectively (mol/m^3).

Salt passage percentage =100 – Salt rejection percentage. (3.45)

$$\text{Recovery ratio} = \frac{(Q_p)}{(Q_f)} x100 \tag{3.46}$$

where Q_p and Q_f are permeate flow and feed flow respectively.

3.7   LiBr – H$_2$O Absorption Chiller

This study considers the use of waste heat from a power plant to power a single effect LiBr-H$_2$O AC. This section describes the energy and exergy analysis of the AC. A schematic of the cycle is shown in figure 3-1, with major components labelled and the streams numbered for subsequent state analysis.

At steady state, the net mass flow into each component is equal to zero and controlled by overall mass balance as shown by equation 3.1. In this cycle, the refrigerant is water and the absorbent is LiBr-H$_2$O, and thus the mass balance of j is used to describe the process [158].

The variable mass flow is used to describe the ratio of the strong solutions flow to that of the refrigerant. This is the mass circulation ratio (*f*) which can found from [159]:
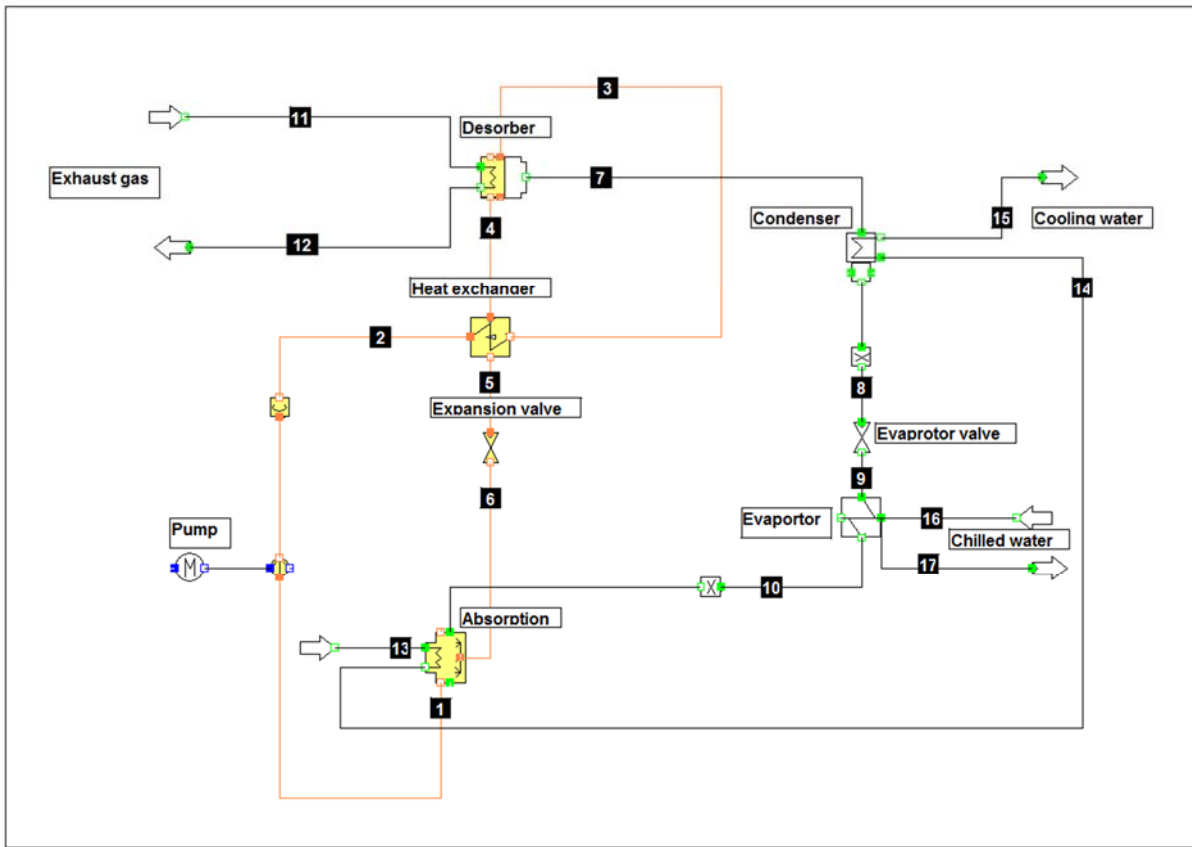
Figure 3-1: Schematic drawing of LiBr-H₂O AC IPSEpro model

$$f = \frac{\dot{m}_3}{\dot{m}_7}$$ (3.47)

Determining the energy balance for each component is a vital step in checking that the model output is correct. The energy balances of the evaporator and condenser can be written as:

$$\dot{Q}_E = \dot{m}_{10}h_{10} - \dot{m}_9 h_9$$ (3.48)

$$\dot{Q}_C = \dot{m}_7 h_7 - \dot{m}_8 h_8$$ (3.49)

The desorber energy balance can be expressed by:

$$\dot{Q}_D = \dot{m}_7 h_7 + \dot{m}_4 h_4 - \dot{m}_3 h_3$$ (3.50)

And similarly for the absorber:

$$\dot{Q}_A = \dot{m}_{10}h_{10} + \dot{m}_6 h_6 - \dot{m}_1 h_1$$ (3.51)

The energy balance of the heat exchanger can be formed in the steam table, and the enthalpy and entropy of LiBr according to concentration and temperature (x, T) can be determined using the experimental correlation conducted by Feuercker et al [160]:

$$h(T,x) = \sum_{n=0}^{4} a_n x^n + T \sum_{n=0}^{3} b_n x^n + T^2 \sum_{n=0}^{2} c_n x^n + T^3 d_0 \tag{3.52}$$

The above correlation constants and validation ranges are listed in second table second appendix 3- A:

The entropy of the LiBr-H$_2$O solution is calculated from equation 3.53, which has been validated by Kaita [161] for $40 \leq X$ (wt. %) ≤ 65, and $0 \leq T$ (°C) ≤ 210 (coefficients given in appendix table 3-A3).

$$S = \sum_{i=0}^{3} \sum_{j=0}^{3} B_{ij} X^j T^i \tag{3.53}$$

Absorption chiller performance is measured by evaluating the COP, which is the ratio of absorbed heat by the evaporator to released heat by the desorber [158]:

$$COP = \frac{\dot{Q}_E}{\dot{Q}_D} \tag{3.54}$$

The exergy of the LiBr-H$_2$O solution is derived by summing the physical and chemical exergies where the potential and kinetic exergies have negligible effects. Physical exergy is determined using equation 3.13, enthalpy and entropy are calculated and found using the methods described above (eqs. 3.52 and 5.53).

From equation 3.14 the chemical exergy of the LiBr-H$_2$O solution is derived for different concentrations. This parameter has been ignored in most studies or the solution assumed to be ideal. However, in this study the chemical exergy of the LiBr – H$_2$O is the difference in the ideal solution (standard chemical exergy) and the chemical exergy destruction is due to dissolution of the LiBr and H$_2$O. The standard chemical exergy of LiBr– H$_2$O at various concentrations has been reported in several previous studies [162-164]:

$$e_{H_2O}^{CH} / LiBr_0 = \frac{1}{M} \left(y_{H_2O} e_{H_2O,0}^{ch} + y_{LiBr} e_{LiBr,0}^{ch} \right) \tag{3.55}$$

where M is molecular weight and y is the mole fraction and $e^{ch}_{H_2O,0}$, $e^{ch}_{LiBr,0}$ are the standard chemical exergies for water and LiBr which are equal to 0.9 kJ/mol and 101.6 kJ/mol respectively [28]

The right hand side term in equation 3.14 is called exergy destruction due to dissolution and it can be reduced to:

$$RT_0 \sum x_k \ln \gamma x_k = RT_o \sum x_k \left(a_{H_2O/LiBr} \right) \tag{3.56}$$

where $a_{H_2O/LiBr}$ is called the H_2O - $LiBr$ activity.

In molar fraction forms, the equation can be rearranged to:

$$e^{ch}_{dis} = \frac{RT_0}{M_{H_2O/LiBr}} \left[\left(y_{H_2O} \ln \left(a_{H_2O} \right) \right) + \left(a_{H_2O} \right) + y_{LiBr} \ln \left(a_{LiBr} \right) \right] \tag{3.57}$$

where:

$$\ln \left(a_{H_2O} \right) = -\Phi.v.m M_{H_2O} \tag{3.58}$$

where Φ represents the osmotic coefficient derived by Kim and Infante Ferreira [165, 166]:

$$\phi = 1 + \sum_{i=1}^{6} a_i.m^{i/2} + \frac{p}{2.v} \sum_{i=1}^{2} i.b_i.m^{i/2} \tag{3.59}$$

With a_i and b_i obtained from:

$$a_i = \sum_{j=0}^{2} a_{ij}.T^{-J} \tag{3.60}$$

$$b_i = \sum_{j=0}^{2} b_{ij}.T^{-j} \tag{3.61}$$

a_{ij}, b_{ij} are listed in appendix 3-A4.

The term M is molality, which is defined as the number of moles of solute per kilogram of solvent. This is calculated from:

$$m = \frac{x_{LiBr}}{(1 - x_{LiBr}).m_{LiBr}}$$

(3.62)

The chemical activity for the LiBr component can be obtained by:

$$\ln(a_{LiBr}) = -v.\left[\ln(m) + \sum_{i=1}^{6} \frac{(i+2)}{i}.\left(a_i + i.\frac{p.b_i}{2.v}\right).(m)^{i/2}\right]_m^{m_{sat}}$$

(3.63)

3.8 Heat exchangers

Cogeneration plants and heat recovery technologies use a variety of heat exchangers, including boilers, condensers, evaporators, and brine heaters. The heat gained by a heat exchanger can be defined as a product of the overall heat transfer coefficient "U", the heat exchanger area A, and the logarithmic mean temperature difference ΔT_{LM}:

Q absorbed or released = U A ΔT_{LM}

(3.64)

$$\Delta T_{LM} = \frac{[(T_{hot,in} - T_{cold,out}) - (T_{hot,out} - T_{cold,in})]}{\ln\left[\frac{T_{hot,in} - T_{cold,out}}{T_{hot,out} - T_{cold,in}}\right]}$$

(3.65)

IPSEpro uses the same method with an iterative procedure to calculate the characteristics of the inlet and outlet streams in order to derive a convergent solution for absorbed or released heat [167-169]. The effectiveness and Number of Transfer Unit ($\varepsilon - NTU$) method is used to validate the modelled heat exchangers [167, 168] and was used throughout the present research. Effectiveness (ε) is the ratio of the actual heat transfer rate of the heat exchanger to the maximum possible heat transfer rate [168, 169]:

$$\varepsilon = \frac{\dot{Q}_{actual}}{\dot{Q}_{max}}$$

(3.66)

The actual heat transfer rate can be determined from the expression:

$$\dot{Q}_{actual} = \varepsilon.c_{min}(T_{hot,in} - T_{cold,in})$$

(3.67)

For any heat exchanger [167, 168]:

$$\varepsilon = f\left[NTU, \frac{c_{min}}{c_{max}} \right] \tag{3.68}$$

where: $\dfrac{c_{min}}{c_{max}}$ is known as the heat capacity ratio (C_r) which is C_{cold}/C_{hot} or C_{hot}/C_{cold} according to the relative size of the hot and cold fluid heat capacity rates. The NTU is a dimensionless variable commonly used in heat exchanger analysis [167, 168]. It is found from:

$$NTU = \frac{UA}{c_{min}} \tag{3.69}$$

It is more convenient to work with $\varepsilon - NTU$ relations of form:

$$NTU = f\left[\varepsilon, \frac{c_{min}}{c_{max}} \right] \tag{3.70}$$

c_{min} equals a smaller $\left(\dot{m}_{cp} \right)_{smaller}$ and thus:

$$C_{min} = \frac{\dot{Q}_{actual}}{\Delta T_{larger}} \tag{3.71}$$

Therefore [167-169].

$$NTU = \frac{UA\Delta T_{larger}}{\dot{Q}_{actual}} \tag{3.72}$$

3.9   CO$_2$ Footprint Estimation

Many researchers have assessed the role of CO_2 in global warming. Estimating the CO_2 footprint from the standalone power plant and the proposed cogeneration power plant in this study is crucial because it is an important criterion for comparing the three heat recovery technologies. The CO_2 footprint is calculated using two methods which calculate from either energy or exergy.

The CO_2 emission energy base for a natural gas standalone power plant can be obtained by [25]:

$$CO_2 Emission \left(\frac{g}{kWh} \right)_{energybase} = \frac{3600 * \alpha * \dot{m}_{natura\,lg\,as}}{\left(\dot{W}_{net} \right)} \tag{3.73}$$

Whereas, at the proposed cogeneration plant it is:

$$CO_2 Emission \left(\frac{g}{kWh} \right)_{energybase} = \frac{3600 * \alpha * \dot{m}_{natura\,lg\,as}}{\left(\dot{W}_{net} + \dot{Q}_{useful} \right)} \tag{3.74}$$

where α is 3124 kg CO_2 per tonne of natural gas and $\dot{Q}_{useful}$ is the heat recovered from the process, which may be diverted to other thermal applications, such as powering AC, or domestic heating. Note that $\dot{Q}_{useful}$ cannot be converted completely to any type of work, due to the Second Law of Thermodynamics. Furthermore, the conversion value will depend on the temperature of the useful heat with conversion lower at low temperatures.

The CO_2 emission exergy base is:

$$CO_2 Emission \left(\frac{g}{kWh} \right)_{exergybase} = \frac{3600 * \alpha * \dot{m}_{natura\,lg\,as}}{\left(\dot{W}_{net} + \dot{E}_{useful} \right)} \tag{3.75}$$

where $\dot{E}_{useful}$ is the maximum useful exergy that can converted to real work, which is measured logically in $\left(\frac{g}{kWh} \right)$. Here the unit in the denominator represents real electrical power, which is not the case in the energy base equation 3.74.

3.10 Economic Analysis

To assess economic analysis for the CCPP and desalination systems and at different scenarios, the payback period, net present value, average rate of return and profitability index are calculated as follows:

3.10.1 *Payback period (PBP)*

The PBP takes account of the period of investment before breaking even and making a profit. The PBP can be defined as the period required to return the Total Capital Investment (TCI) [142]. This can be calculated as follows:

$$TCI = \sum_{j=1}^{PBP} CFN_j$$

(3.76)

where: TCI is the Total Capital Investment and CFN is the recurrent Net Cash Flow.

3.10.2 *Net Present Value (NPV)*

The net present value is known as the difference between the sum of all the net cash inflows and the initial investment cost over the project lifetime discounted so that all values are compared at single point in time (the present). The value of NPV can be positive or negative. A positive value means that the income to the project is greater than the investment, which is preferable in any project. On the other hand, a negative value shows that the project could not recover the investment costs and should be avoided. The NPV is calculated mathematically as follows [142]:

$$NPV = \sum_{j=1}^{t} \frac{CFN_j}{(1+r)^j} - TCI$$

(3.77)

where CFN is the net cash flow over the lifetime t and r is the discount rate, which represent the revenue minus the outgoing expenses.

3.10.3 *Average Rate of Return (ARR)*

The average rate of return is defined as the ratio of the average annual net profit to the total capital investment. It can be worked out as follows [142]:

$$ARR = \frac{\overline{NP}}{TCI}$$

(3.78)

where $\overline{NP}$ is the average annual net profit.

3.10.4 *Profitability index (PI)*

The profitability index is defined as the net present value of the future net cash flow to the total capital investment [138]:

$$PI = \frac{NPV}{TCI}$$

(3.79)

Bejan et al [142] considered that using profitability index over the net present value adds no particular advantages to the profitability evaluation as the negative value of PI indicates that the NPV is less than the initial investment, which shows same result.

3.11 Energy recovery device: Energy recovery turbine and Pressure exchanger

To reduce the power consumption of the high pressure pump using the rejected brine pressure an energy recovery turbine (ERT) or pressure exchanger (PX) can be installed. The cost is based on purchased cost as a function of power produced [170]:

$$\log_{10}(ERD) = 2.2476 + 1.4965 \log_{10}(\dot{W}_{ERD}) - 0.1618 \left[\log_{10}(\dot{W}_{ERD})\right]^2 \qquad (3.80)$$

The cost of operation and maintenance of the ERT and PX are around 4% of the total capital investment (TCI) of RO desalination plant [63, 171]. The total annual operation and maintenance cost of the RO plant were calculated using the formula presented by [105]:

$$\dot{c}_{O\&M} = 0.126 f.\dot{Q}_p \quad (\$) \qquad (3.81)$$

where $\dot{Q}_p$ is the annual volume flow rate of product water and f is the plant load/year.

3.12 Meteorological Data

Power or desalination plants are affected by environmental change. Therefore the appropriate meteorological factors, Dry Bulb Temperature (DBT), Relative Humidity (RH) and Sea Water Temperature (SWT), should be taken into consideration in the engineering design of thermal systems such as air conditioning, heating, and ventilation systems. Libya has four seasons, summer, autumn, winter and spring [172, 173]. A general approach to defining these is to select the four highest long term monthly average DBTs as the summer period and the three lowest average DBT months as winter months [173].

3.12.1 Dry bulb temperature (DBT) and relative humidity data.

The data of meteorological DBT and Average Relative Humidity (ARH) were collected on a daily average basis from the meteorological centre, Zawya City in Libya. This city is located (Figure 1-1) on the Mediterranean Sea to the west of Tripoli, which is the capital city of Libya, and is classified as in a humid-arid zone which is quite hot and humid during the summer season. On the other hand, the temperatures decrease in

winter season to as low as five degrees Celsius. Figure 3-1 shows the monthly maximum and minimum DBT temperatures and the DBT temperature for each month of the year. The highest and lowest monthly DBTs were 36.8°C and 9.1°C in Jun and December respectively while the annual average was 21.45°C. Moreover, from January the monthly average temperature starts to rise and reaches its highest temperature in August after which it declines. Appendix 3-C shows the ambient temperature and relative humidity readings for Zawya City, Libya for 2010. Figure 3-2 shows the daily average dry bulb temperature for 365 days in 2010. As can be seen the temperature fluctuates from about 5°C to around 37°C.
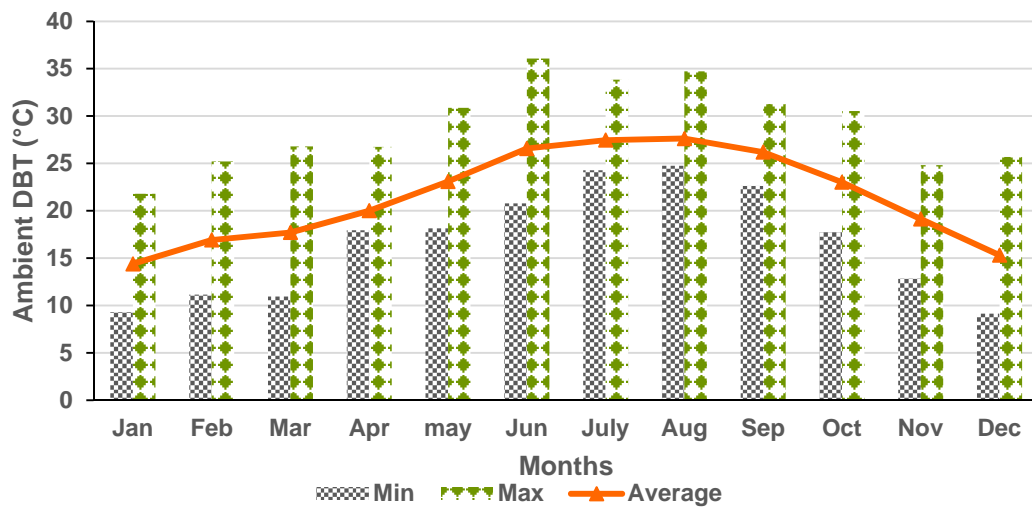
Figure 3-2: Monthly maximum, minimum and average DBT temperature Zawya City, Libya 2010 [174]

.
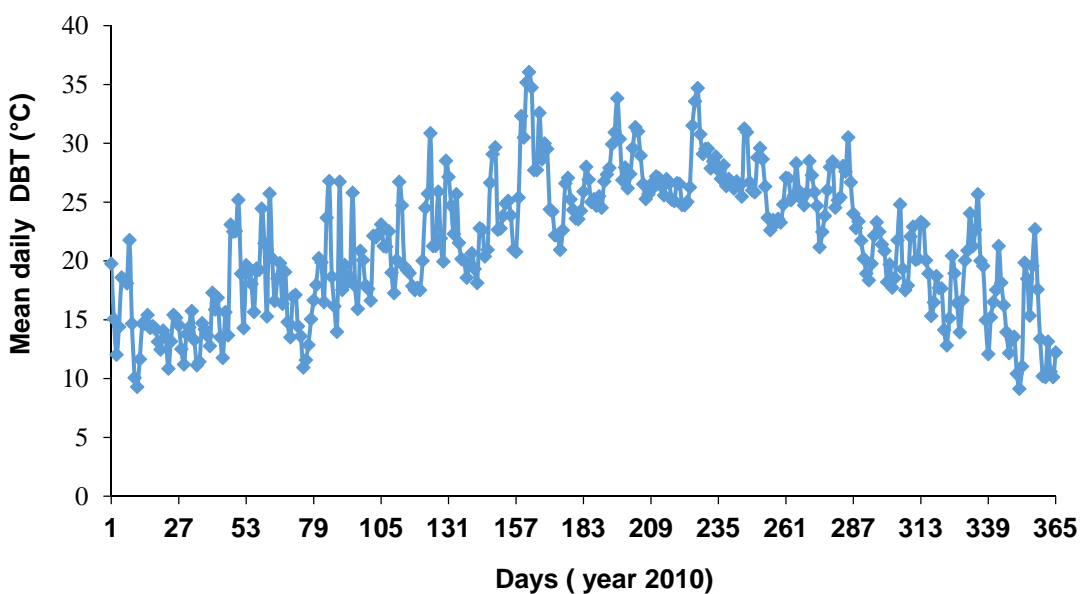
Figure 3-3: Mean Daily DBT average variation for Zawya City Libya (2010)

Figure 3-4 shows daily average RH where figure 3-5 shows the monthly minimum, maximum and average RH variation for Zawya City [174]. The highest and lowest values for this year were 93.75% and 31.125% respectively. During most of the year the RH has a similar daily pattern being high at night and lower during the daytime.
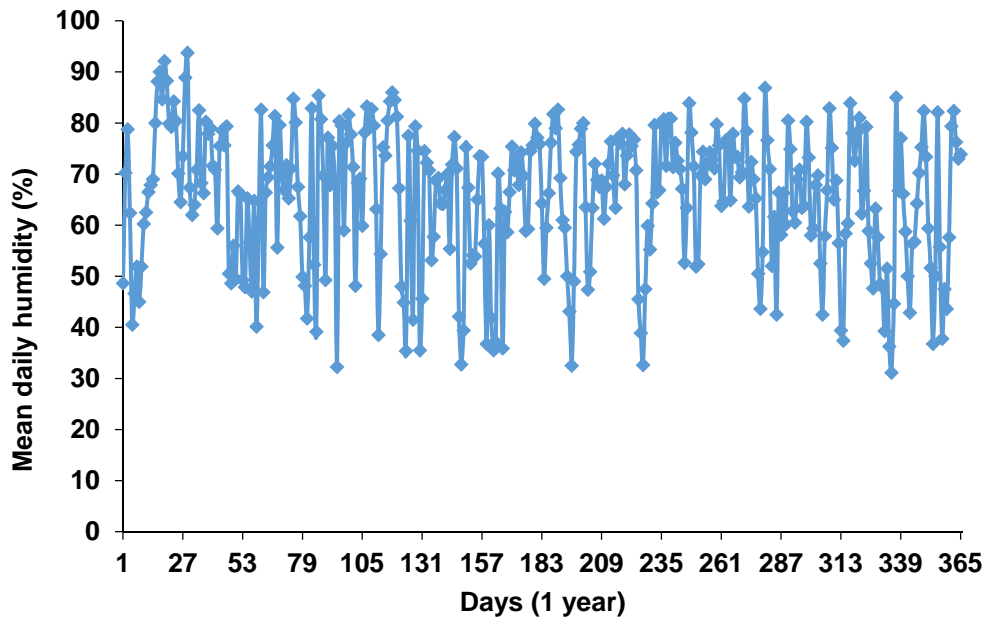
Figure 3-4: Mean daily RH variation for Zawya City (2010)
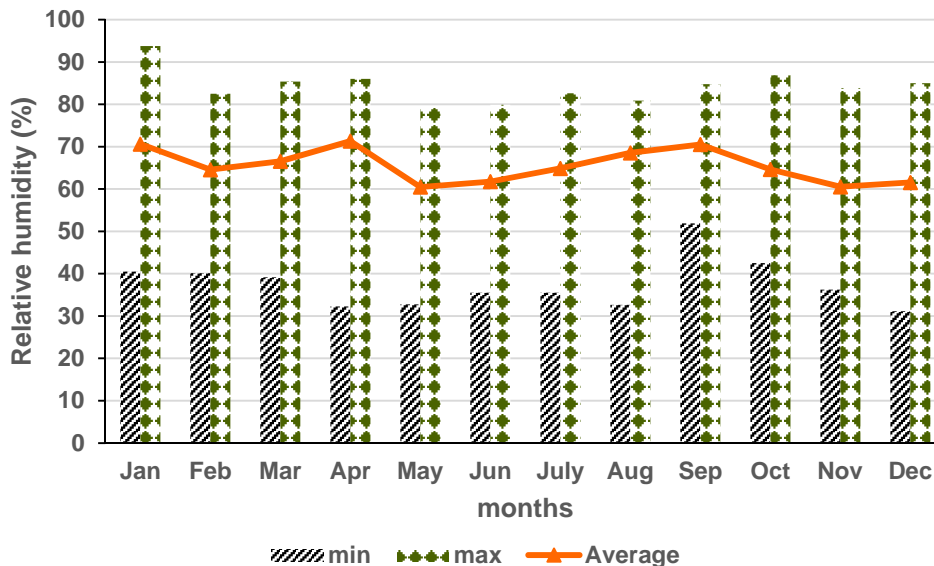
Figure 3-5: Monthly maximum, minimum average RH variation for Zawya City (2010)

3.12.2 *Sea water temperature (SWT) data.*

It is important to know the SWT and salinity levels in the present plant design, as sea water will used in the MED-TVC and RO desalination plants. It has been reported that SWT affects the performance of desalination plants [25, 175]. Figure 3-6 shows monthly minimum, maximum and average SWT. As can be observed the maximum SWT was recorded in August at 26.2°C and the minimum in February at 14.7°C, with an annual average SWT of 20°C. The monthly variation in water temperature is typical for the Mediterranean [176].
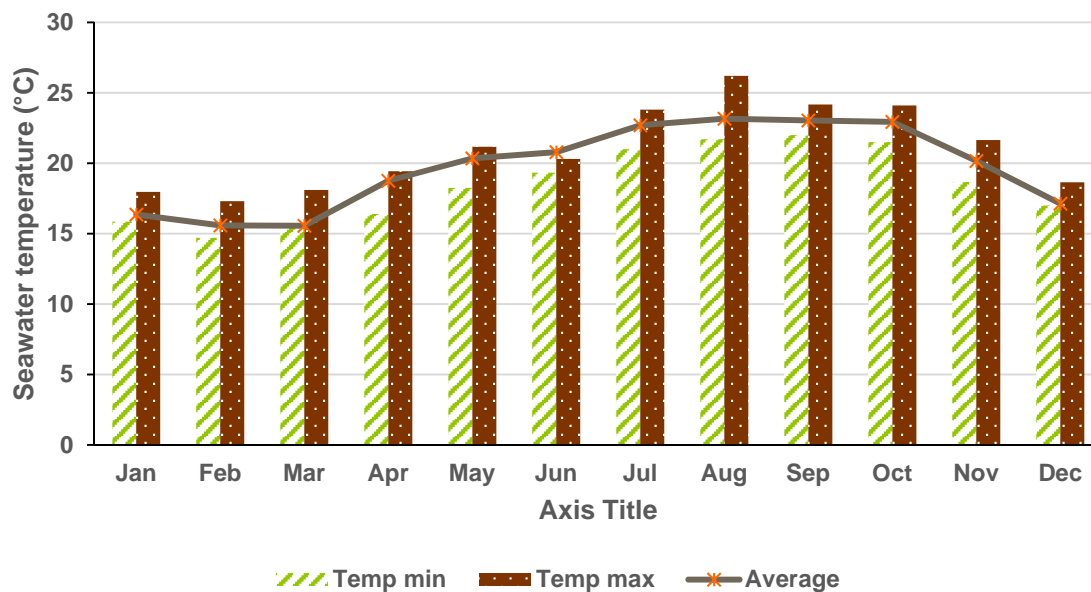
Figure 3-6: Monthly minimum, maximum and average variation in SWT, Zawya City (2006) [176]

3.12.3 *Seawater and brine salinity data*

Figures 3-7 shows the minimum and maximum and monthly average salinity, which were recorded to be 34.6g/kg in February and 38.6g/kg in July respectively, with annual average value of 37.03g/kg .This variation in salinity values between months is caused by environmental factors [176].
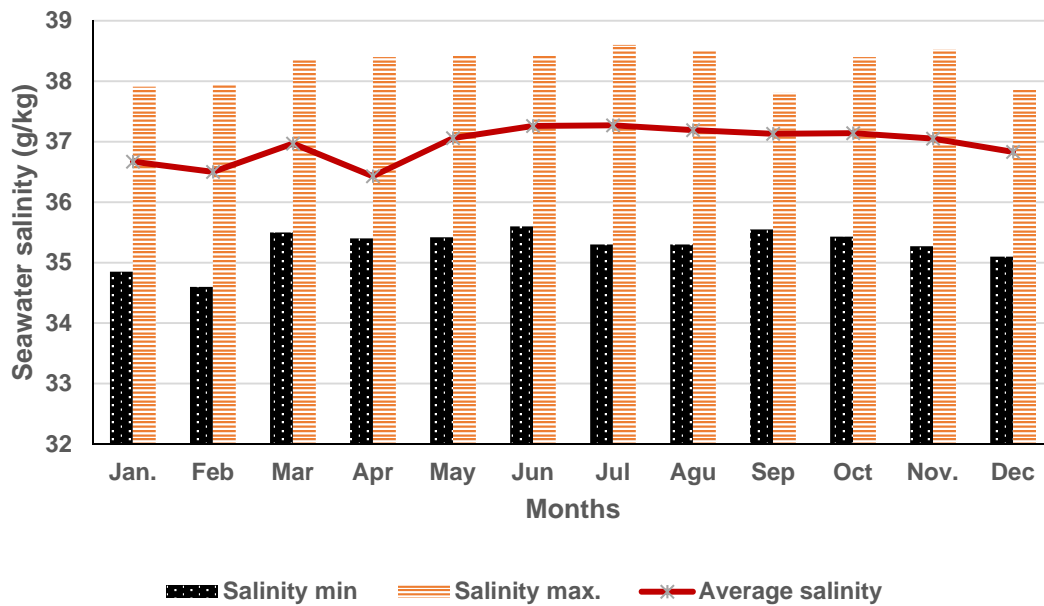
Figure 3-7: Monthly minimum, maximum and average sea water salinity Zawya City (2006) [176].

3.13 Geothermal Water

Waddan and its surrounding villages are located in a region favourable for date palm tree culture. Part of Waddan's economy is reliant on this agriculture sector as the main commodity from Waddan is dates [14].

The main source of palm tree irrigation water comes from naturally cooled geothermal artesian hot water wells (the irrigation hot water takes sometimes three days to cool down from 73°C to less than 40°C). The geothermal sources are surrounded by several shallow cold water reservoirs (the feed water temperature and salinity are 25°C and 1.96 g/kg respectively) [12], which are used for general irrigation and cooling some industrial components such as central air-condition wet cooling towers for Waddan City.

3.14 Summary

Different topics were introduced in this chapter covering the tools used in the study. These included the simulation and modelling software IPSEpro with all of its modules and libraries. The first and second law performance parameters and the latest thermodynamic properties were presented. The performance of a combined cycle power plant, absorption chiller and desalination units has been discussed. This chapter also includes criteria for calculating the PBP, NPV, ARR and PI. Finally weather and seawater data for Zawya City for one year in Libya were also included and then used during the parametric study. All of this information is used in the following chapters to perform energy, exergy and economic analyses.

CHAPTER 4.   VALIDATION

4.1   Introduction

It is essential to validate the IPSEpro models used in this study: Combined Cycle Power Plant (CCPP), Absorption Chiller (AC) and Multi-Effect Desalination with Thermal Vapour Compression (MED-TVC), two-pass Reverse Osmosis desalination (RO) and Single Effect Desalination plant (SED). IPSEpro software libraries will be used to build the models. These models will be validated against operational or vendor data, with input parameters selected from the unit or vendor data then model calculated compared with the measured or design values. All the models will be validated before carrying out subsequent parametric studies.

4.2   Combined Cycle Power Plant (CCPP) Modelling and Validation

A combined cycle power plant located on the sea coast at Zawya City in Libya is selected for validation because of its relevance and appropriateness for desalination technologies [8]. The input and output data are available [177]. The IPSEpro software power plant library [141] was used to build the standalone combined cycle power plant model (Figure 4.1). The CCPP consists of two gas turbines (GT1 & GT2) and two Heat Recovery Steam Generators (HRSG1 & HRSG2), each with a Boiler Feed Pump (BFP), feeding High, Medium and Low pressure steam turbine stages (HPT, MPT and LPT), with a Condenser Cooling water circulation Pump (CCP) and deaerator. In IPSEpro the equipment models [141] are linked by connectors that represent the working fluids moving from one component to another. All of the streams are numbered and the thermodynamic properties of the working fluid are included in Table 4.1. Table 4.1 identifies the model input data used for validation between the vendor data and model results. Table 4.2 shows the composition and thermodynamic properties of all of the numbered streams, either as values set by the user as model inputs or as calculated (Cal) values output by the model. These calculated values are used for the subsequent energy and exergy analyses. For the validation the corresponding input values allow a comparison to take place between the calculated output and reported measured values. For CCPP model Streams 39 and 19 would be the inlet to and outlet steam from the MED-TVC desalination plant, respectively, where the steam could be

extracted from CCPP to power the MED-TVC. These streams mass flow rate values are set to zero set when the CCPP is running standalone, as in this validation.

Table 4-1: Power plant input parameters at 60% relative humidity for CCPP standalone

Gas flow	(streams 2 and 21)	kg/s	10.4
Gas pressure	(streams 2 and 21)	bar	24
Inlet air temperature	(streams 1 and 22)	°C	15, 20, 25, 30 and 37
Inlet air pressure	(streams 1 and 22)	bar	1.013
HRSG exhaust temperature (streams 4 and 24)		°C	116
HP steam temperature	(streams 5 and 25)	°C	489.9
HP steam pressure	(streams 5 and 25)	bar	92
Condensate steam flow	(stream 19)	kg/s	0
Condensate steam pressure (stream 19)		bar	0
Condensate steam temperature (stream 19)		°C	70
LP steam pressure	(stream 27)	bar	8.7
Cooling water mass flow	(stream 33)	kg/s	3600
Cooling water temperature	(stream 33)	°C	25
Cooling water pressure	(stream 33)	bar	1.4
extracted steam flow	(stream 39)	bar	0
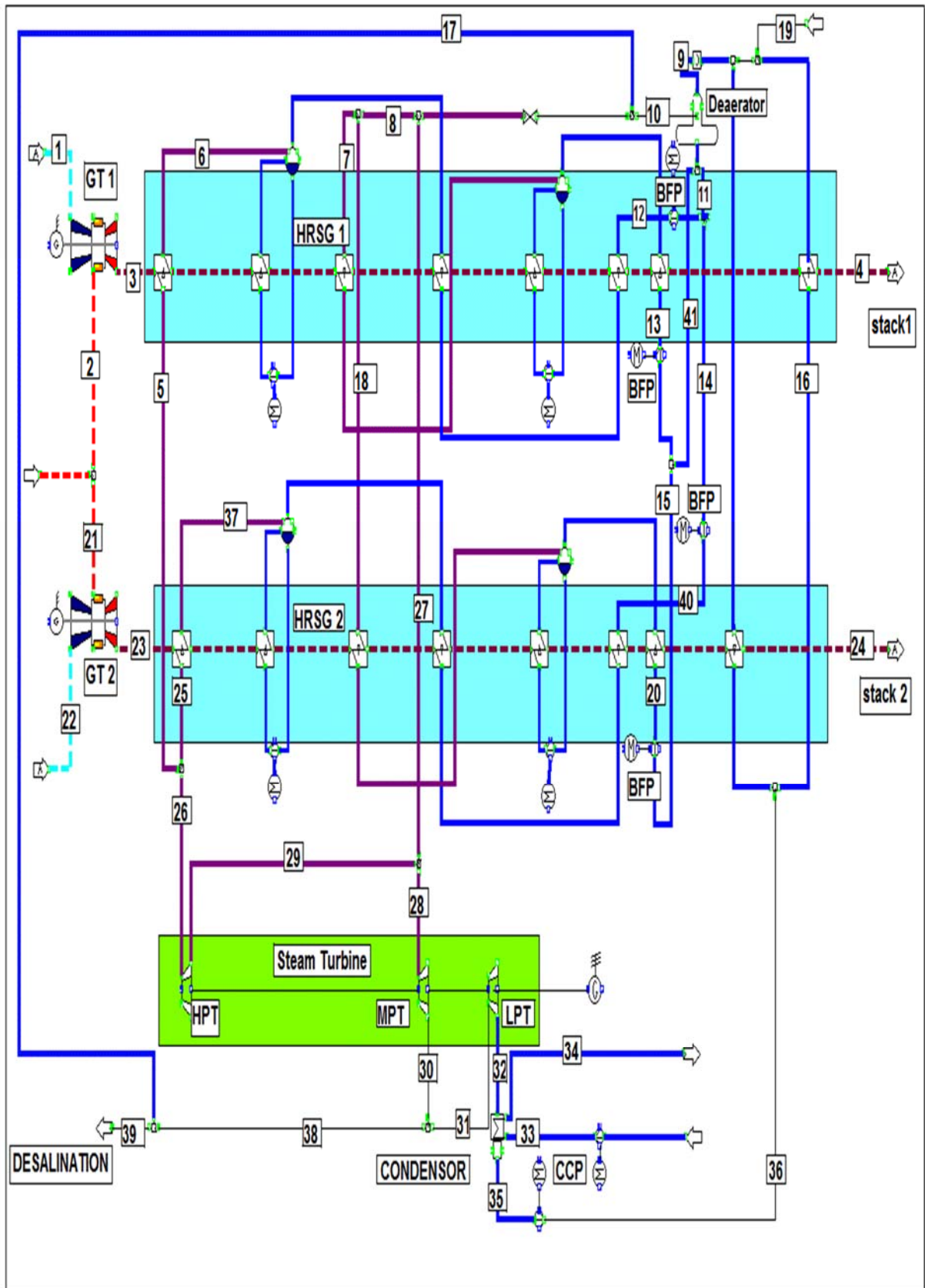
Figure 4-1: Schematic of CCPP IPSEpro model for validation

Table 4-2: Set/ Calculated values in CCPP model

Stream No.	Composition	Flow	Temperature	Pressure	Enthalpy	Entropy	Specific volume
1, 22	Air	Cal	Set	Set	Cal	Cal	Cal
2, 21	Natural Gas	Cal	Set	Set	Cal	Cal	Cal
3, 23	GT exhaust	Cal	Cal	Cal	Cal	Cal	Cal
4, 24	HRSG exhaust	Cal	Set	Cal	Cal	Cal	Cal
5, 25	HP steam	Cal	Set	Set	Cal	Cal	Cal
6, 37	HP steam	Cal	Cal	Cal	Cal	Cal	Cal
7, 18	LP steam	Cal	Cal	Cal	Cal	Cal	Cal
8	LP Steam	Cal	Cal	Cal	Cal	Cal	Cal
9	Condensate	Cal	Cal	Cal	Cal	Cal	Cal
11	Water	Cal	Cal	Cal	Cal	Cal	Cal
12, 40	Water	Cal	Cal	Cal	Cal	Cal	Cal
13	Water	Cal	Cal	Cal	Cal	Cal	Cal
14	Water	Cal	Cal	Cal	Cal	Cal	Cal
15	Water	Cal	Cal	Cal	Cal	Cal	Cal
16	Condensate	Cal	Cal	Cal	Cal	Cal	Cal
17	Steam	Cal	Cal	Cal	Cal	Cal	Cal
19	Return steam	Set	Set	Set	Cal	Cal	Cal
26	HP steam	Cal	Cal	Cal	Cal	Cal	Cal
27	LP steam	Cal	Cal	Set	Cal	Cal	Cal
28	LP steam	Cal	Cal	Set	Cal	Cal	Cal
29	LP steam	Cal	Cal	Cal	Cal	Cal	Cal
30	LP steam	Cal	Cal	Cal	Cal	Cal	Cal
31	LP steam	Cal	Cal	Cal	Cal	Cal	Cal
32	LP steam	Cal	Cal	Cal	Cal	Cal	Cal
33	Water	Set	Set	Set	Cal	Cal	Cal
34	Water	Cal	Cal	Cal	Cal	Cal	Cal
35	Condensate	Cal	Cal	Cal	Cal	Cal	Cal
36	Condensate	Cal	Cal	Cal	Cal	Cal	Cal
38	LP Steam	Cal	Cal	Cal	Cal	Cal	Cal
39	Extracted steam	Set	Cal	Cal	Cal	Cal	Cal
41	Water	Cal	Cal	Cal	Cal	Cal	Cal

A comparison between model results and power plant vendor data for the CCPP validation was carried out based on the effect of ambient temperature on output power (Table 4.3) and GT efficiency (Table 4.4). The model results were assessed by

calculating the relative percentage difference between the vendor data x_i and the model results y_i [28, 178].

$$e_i = \left[\frac{x_i - y_i}{x_i} \right] . 100$$ (4.1)

Table 4-3 shows agreement between vendor data and model results output power varying ambient temperature and 60% relative humidity with a maximum difference of -1.9%. This difference is because of the model assumption of constant heating value and its inability to represent detailed physical plant layout features [28]. Importantly, the model responds to ambient temperature variation with the same trend as the vendor data.

Table 4-4 shows that the gas turbine thermal efficiency decreases with increase in temperature as expected with a maximum difference from measure of <1%.

Table 4-3: Comparison between vendor output power and model results at 60% relative humidity and different ambient temperatures

Air ambient temperature °C		15	20	25	30	37
Vendor output power	MW	166.18	160.94	155.70	150.46	142.33
Model output power	MW	163.07	157.95	152.82	147.71	140.41
Differences	(%)	1.9	1.9	1.9	1.8	1.9

Table 4-4: Comparison between vendor thermal efficiency and model results at 60% relative humidity and different ambient temperatures

Ambient temperature	(°C)	15	20	25	30	37
Vendor GT Efficiency	(%)	35.65	35.27	34.89	34.89	33.98
Model GT efficiency	(%)	35.35	35.17	34.80	34.43	33.94
Differences	(%)	0.84	0.28	0.26	0.23	0.13

To make sure the model is working properly, sensitivity analysis was carried out to establish the effect of data uncertainty on the model output results. The input conditions of the combined cycle power plant were changed in a systematic way to determine the sensitivity of the plant (efficiencies, output power, fuel consumption and CO_2 emissions) to change in these parameters.

 The input parameters that were changed one at a time are as follows:

- Ambient temperature
- Fuel temperature

- Condenser pressure

- Relative humidity

- Fuel pressure

- Cooling water mass

- Cooling water temperature

- Stack temperature

- High pressure steam turbine efficiency

- Compressor pressure ratio

The input parameters were changed by ±5% (around the ISO standard condition for ambient parameters, where the ambient temperature is in Celsius). This percentage will consider a good indicator about the behaviour of the system and the impact of input parameter change, however any change at ±5% gives the same trend at any other variation.

Table 4.5 shows the summary of the results obtained. The compressor pressure ratio has greatest influence with the only response greater than the ±5% variation in it. These are the GT and hence net powers (9.2% and 13.1%, respectively). It also has a significant impact on CO_2 emissions (at 4%) because these are directly related to output power. Of the other input parameters, only ambient air temperature has any noticeable impact on the outputs (GT net output powers and consequently CO_2 emissions) but always < 5%.

This is because as ambient inlet air temperature decreased the compressor consumes less power for compression, but as the efficiency increase the steam turbine produce more power from the same input steam.

Table 4-5 shows the summary of the mode sensitivity for ±5% of the input data on the gas turbine performance.

Table 4-5: Summary of CCPP mode sensitivity to variation in input data at (±5%)

	GT thermal efficiency	GT1 + GT2 power	GT1 +GT2 gas consumption	Thermal Cycle efficiency	Net output power	CO$_2$ emission	Exergy efficiency
Percent	%	%	%	%	%	%	%
Effect of ambient temperature	0.1	1.8	0.1	0.0	2.1	3.6	0.053
Effect of Fuel temperature	0.0	0.0	0.0	0.0	0.0	0.0	0.000
Effect of Condenser pressure	0.0	0.0	0.0	0.0	0.6	0.6	0.001
Effect of relative humidity	0.0	0.0	0.0	0.0	0.6	0.0	0.000
Effect of fuel pressure	0.0	0.0	0.0	0.0	0.0	0.0	0.000
Effect of cooling water mass	0.0	0.0	0.0	0.0	0.0	0.0	0.000
Effect of cooling water temperature	0.0	0.0	0.0	0.0	0.0	0.1	0.000
Effect of stack temperature	0.0	0.0	0.0	0.0	1.3	1.3	0.001
Effect of HPST efficiency	0.0	0.0	0.0	0.0	1.9	2.0	0.002
Effect of compressor pressure ratio	0.7	9.2	0.4	0.4	13.1	4.0	0.040

4.3   Absorption Chiller Modelling and Validation

A LiBr-H$_2$O single-effect AC energized by the hot exhaust gas leaving the HRSG provides a cooling effect that can be used to reduce GT inlet temperature from ambient thus augmenting the cogeneration plant power produced. The single-effect AC model was built using the refrigeration library of the IPSEpro software package [141], then validated against an existing unit [179]. Working data for an existing unit were obtained from the literature [28, 179]. Table 4-6 presents the specification uploaded into the IPSEpro model described in figure 4-2. The labelled components are linked by the numbered streams used to indicate the thermodynamic properties of the fluid transferring from one component to another. Some of these properties were fixed in the model (called set values) as they were obtained from the unit specification and the remainder calculated by the model (represented as calculated values in Table 4-7). These calculated values are used for the subsequent energy and exergy analyses.

Table 4-6: Single effect AC specification and data [179]

Description		Units	Specification
Manufacture		-	Carrier Sanyo
Model		-	LJ
Heat source		-	Hot water
Cooling type		-	Series (absorber/condenser)
Working fluid		-	LiBr-H_2O
Capacity		kW	2213
Inlet and outlet data			
Li-bromide temperature	(stream 1)	°C	33
Li-bromide pressure	(stream 2)	bar	0.037
Hot water temperature	(stream 11)	°C	90
Hot water pressure	(stream 11)	bar	2
Hot water temperature	(stream 12)	°C	85
Cooling water temperature	(stream 13)	°C	28.5
Cooling water pressure	(stream 13)	bar	1.6
Cooling water temperature	(stream 15)	°C	34.5
Chilled water temperature	(streams 16/17)	°C	16/6.0
Chilled water pressure	(stream 17)	bar	1.4
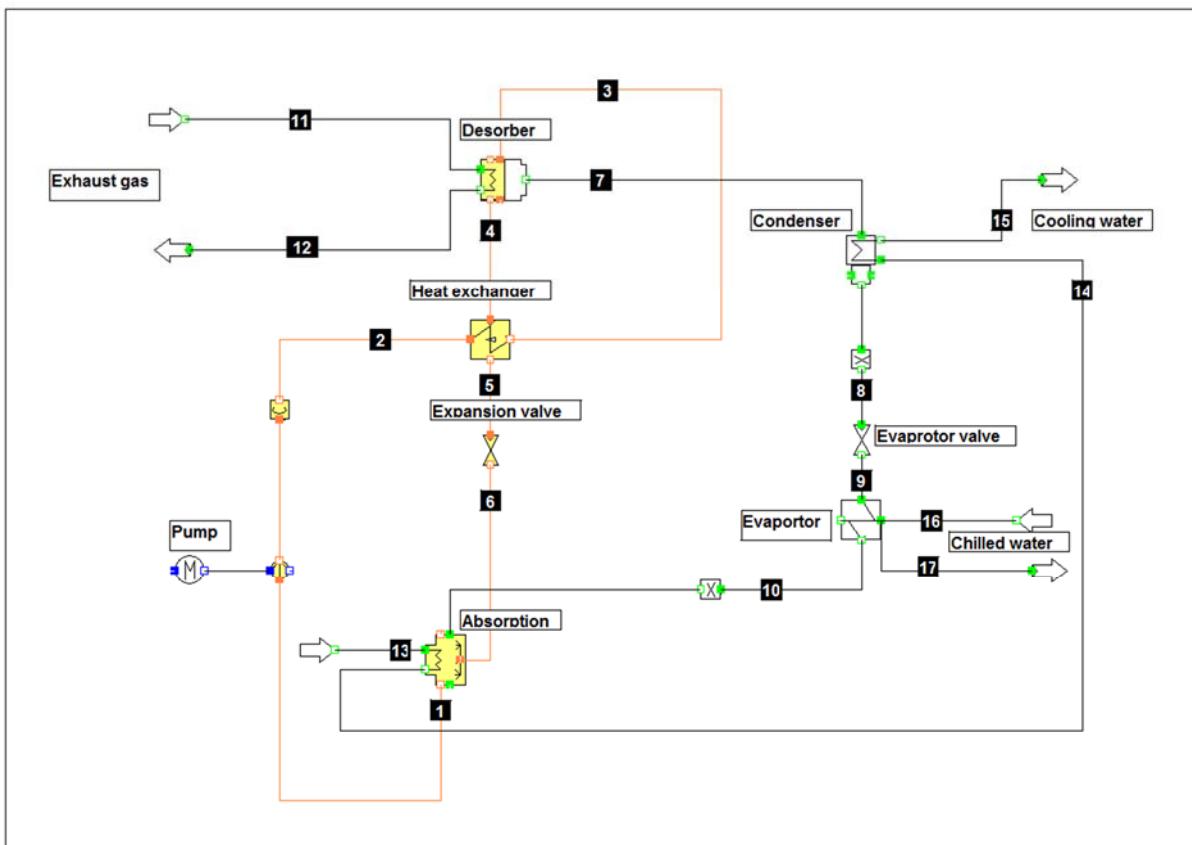
Figure 4-2: Schematic drawing of LiBr-H_2O AC IPSEpro model

Table 4-7: Set/ Calculated values in AC model

Stream No.	Composition	Flow	Temperature	Pressure	Enthalpy	Entropy	Specific volume
1	Li-bromide	Cal	Set	Cal	Cal	Cal	Cal
2	Li-bromide	Cal	Cal	Set	Cal	Cal	Cal
3	Li-bromide	Cal	Cal	Cal	Cal	Cal	Cal
4	Li-bromide	Cal	Cal	Cal	Cal	Cal	Cal
5	Li-bromide	Cal	Cal	Cal	Cal	Cal	Cal
6	Li-bromide	Cal	Cal	Cal	Cal	Cal	Cal
7	Water	Cal	Cal	Cal	Cal	Cal	Cal
8	Water	Cal	Cal	Cal	Cal	Cal	Cal
9	Water	Cal	Cal	Cal	Cal	Cal	Cal
10	Water	Cal	Cal	Cal	Cal	Cal	Cal
11	Hot water	Cal	Set	Set	Cal	Cal	Cal
12	Hot water	Cal	Set	Cal	Cal	Cal	Cal
13	Cooling water	Cal	Set	Set	Cal	Cal	Cal
14	Cooling water	Cal	Cal	Cal	Cal	Cal	Cal
15	Cooling water	Cal	Set	Cal	Cal	Cal	Cal
16	Chiller water	Cal	Set	Cal	Cal	Cal	Cal
17	Chilled water	Cal	Set	Set	Cal	Cal	Cal

Table 4-8 shows the compared values have a maximum difference of with +3.3% for chilled water flow and +3.1% for refrigeration capacity and +4.3% for COP (all related quantities), while the other parameters have closer agreement between the vendor data and model results. In addition, Sanyo AC suggest an energy balance requires that the heat amount coming into the chiller cycle (heat transfer to the desorber and evaporator) should be equal to the heat rejected from the cycle (heat rejected to cooling water of absorber and condenser) [28]. The model energy balance result reflected exact matching between both these heat amounts but a 7kW difference can be observed for the existing unit. This small difference could be due to the assumption of specific heat values for the heat calculations from the measured temperatures or minor heat losses to atmosphere (which are neglected in the model) or measurement uncertainties in the unit data provided (table 4-6).

Table 4-8: Single effect AC validation

Parameter	Unit	Existing unit data [28]	Model result	Differences (%)
Coefficient of performance (COP)	-	0.74	0.77	+4.30
Refrigeration capacity	kW	2213	2283	+3.10
Generator heat transfer	kW	2987	2957	-1.00
Generator and evaporator heat transfer	kW	5200	5240	+0.77
Absorber and condenser heat transfer	kW	5193	5240	+0.91
Cooling water flow	kg/s	211	209	-0.92
Chilled water flow	kg/s	52.60	54.30	+3.30

Any proposed AC cycle should be checked for thermal practicality by superimposing the thermodynamic state points on a Dühring chart [12, 158], as this helps avoid a number of pitfalls, such as avoiding crystallization [12]. On figure 4-2, flows 1, 4 and 8 are saturated liquid; 10 is saturated vapour; 2, 3 and 5 are sub-cooled liquid; 7 is superheated vapour; and the other two 6, 9 are the two-phase vapour-liquid phase. These thermodynamic state points drawn on the Dühring chart figure 4.3 show (as would be expected for a real plant) a practical thermodynamic working AC cycle with working parameters away from the crystallization line.
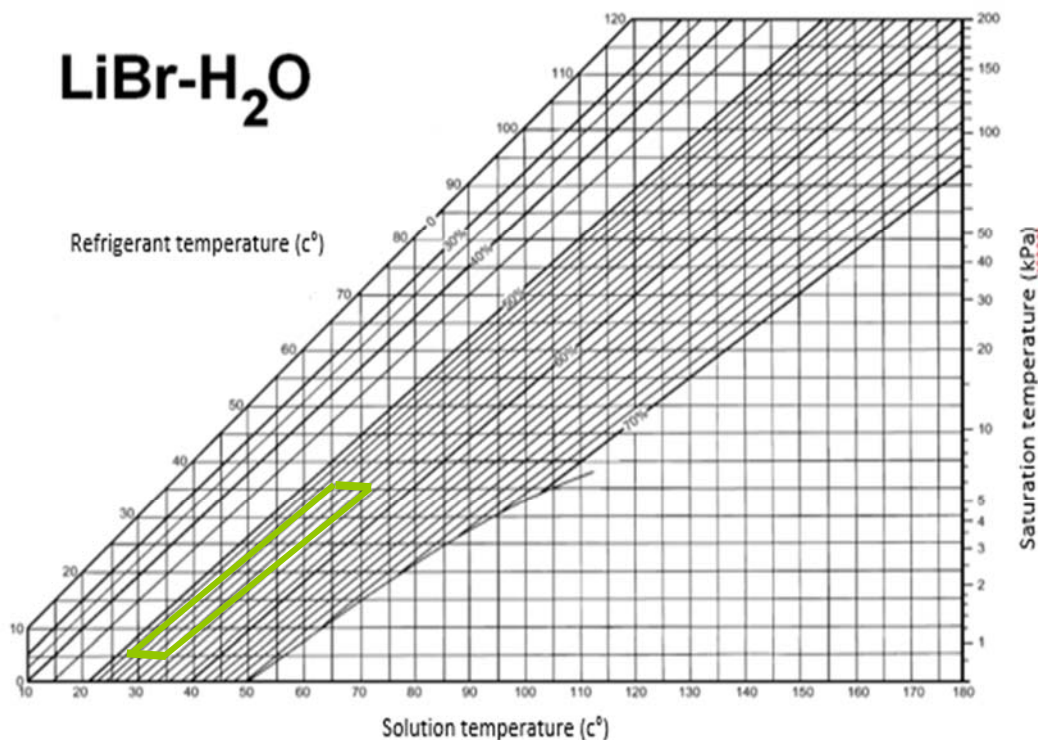
Figure 4-3: Single-effect AC[28] powered by CCPP hot water on Dühring Chart

4.4 Single Effect Desalination Plant (SED)

In this study Waddan City in Libya will be chosen as a case study (chapter 5) where a source of geothermal brackish water is available with temperature between 70 to 73°C which is acceptable to power SED desalination plant with the hot water cooled down at an open tank to 25°C [12]. SED is characterized by its ability to recover waste heat from 100°C down to 65°C [3]. It is believed that this is the first time the concept of powering desalination plant in this way with the SED producing fresh water from brackish water has been discussed. In the literature, there are few studies [3] on SED or MED powered by hot water; normally, it is powered by power plant LP steam [180]. The IPSEpro desalination library was used to develop a model using actual data from an SED (available in Alfa Laval Marine & Diesel product catalogue) [3] adapted from Wang et al [3] (Figure 4-4). Model inputs (set values) were obtained from the catalogue, whereas the model output (the SED water production, represented by stream 14 in figure 4-4) was considered as a calculated value. Tables 4-9 and 4-10 show input and output data and the model set and calculated values respectively.

Table 4-9: SED input and output data

Inlet and outlet data			
Feed water feed temperature	(stream 1)	°C	25
Feed water pressure	(stream 1)	bar	1.013
Feed water pressure	(stream 2)	bar	1.5
Feed water temperature	(stream 3)	°C	32
Rejected water pressure	(stream 4)	bar	1.5
Feed water pressure	(stream 5)	bar	1.5
Brine water pressure	(stream 6)	bar	0.0107
Brine water pressure	(stream 7)	bar	1.5
Seawater pressure	(stream 8)	bar	1.5
Geothermal water temperature	(stream 10)	°C	65
Geothermal water temperature	(stream 11)	°C	55
Distillate water pressure	(stream 14)	bar	2
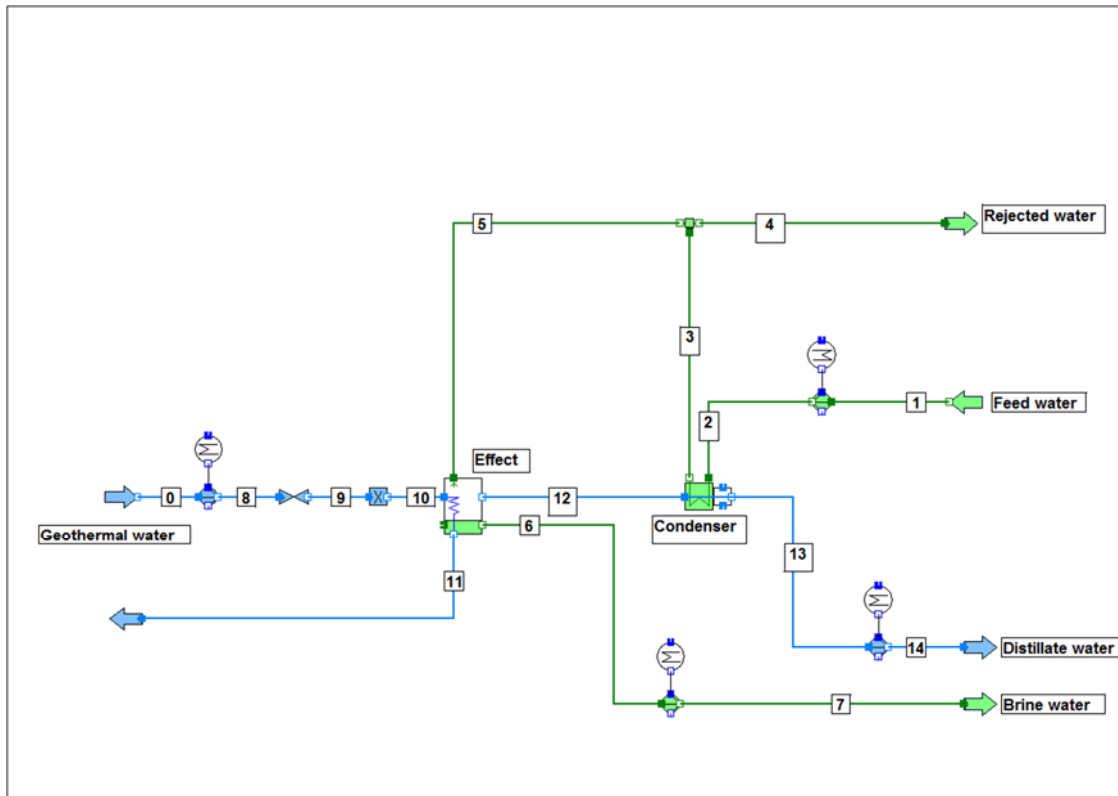
Figure 4-4: Single Effect Desalination plant model (SED)

Table 4-10: A comparison between actual fresh water yield and model yield result

Actual (m³/day)	model (m³/day)	Differences (%)
2	2.1	3.4
2	2.1	3.7
3	3.0	0.3
3	3.1	3.5
4	4.1	2.0
4	4.1	1.7
5	5.0	0.1
5	5.1	1.9
7	7.1	0.8
7	7.0	0.5
10	10.1	0.6
10	10.1	1.0
15	15.1	0.8
15	15.2	1.3

Table 4-11 shows the composition and thermodynamic properties of all of the numbered streams, either as values set by the user as model inputs or as calculated

(Cal) values output by the model. These calculated values are used for the subsequent energy and exergy analyses.

Table 4-11: Set/ Calculated values in SED model

Stream Number	Composition	Flow	Temperature	Pressure	Enthalpy	Entropy	Specific volume
1	Feed water	Cal	Set	Set	Cal	Cal	Cal
2	Feed water	Cal	Cal	Set	Cal	Cal	Cal
3	Feed water	Cal	Set	Cal	Cal	Cal	Cal
4	Feed water	Cal	Cal	Set	Cal	Cal	Cal
5	Feed water	Cal	Cal	Set	Cal	Cal	Cal
6	Feed water	Cal	Cal	Set	Cal	Cal	Cal
7	Brine water	Cal	Cal	Set	Cal	Cal	Cal
8	distillate water	Cal	Set	Set	Cal	Cal	Cal
9	Geothermal water	Cal	Cal	Cal	Cal	Cal	Cal
10	Geothermal water	Cal	Cal	Cal	Cal	Cal	Cal
11	Geothermal water	Cal	Set	Cal	Cal	Cal	Cal
12	Vapour steam	Cal	Cal	Cal	Cal	Cal	Cal
13	Condensate vapour	Cal	Cal	Cal	Cal	Cal	Cal
14	Distillate water	Cal	Cal	Set	Cal	Cal	Cal

Model validation compared actual performance and the model result for water production. To ensure the model validation covers an acceptable range of data, a number of cases were selected for validation at different hot powering water flow (m10), geothermal water powering temperature (T10), geothermal water return (11) and brackish water feed mass flow rate (m1). Brackish water salinity (w1) and feed water cooling temperature were maintained at 35000 ppm and 32°C, respectively. Table 4-10 shows the comparison between actual data and model result, with an average difference of 3.7%, a lower difference compared with the previous study conducted by Wang et al for same SED unit [3].

4.5 Multi-Effect Desalination with Thermal Vapour Compression (MED-TVC)

In this study the effect of the Libyan environment on the performance of a proposed multi-effect desalination plant has been used to build a simulation model of the plant

which is validated against actual data [28, 75, 179]. This model is powered by steam flow extracted from an existing CCPP low steam pressure turbine. This desalination plant is proposed to provide 24000 m^3/day fresh water to Zawya City in Libya.

The model validation is carried out using the input data [74] which are seawater temperature and salinity, steam pressure, mass flow. The model was built and then validated against operational data [74]. Table 4-12 shows the operational data used as model inputs. Table 4-13 shows the composition and thermodynamic properties of all of the numbered streams, either as values Set by the user (model inputs) or as calculated (Cal) values output by the model. These calculated values are used for the subsequent energy and exergy analyses.

Table 4-14 represents a comparison between the model results and operational data. As can be seen there is agreement between the model results and the operational data with very small differences.

Table 4-12: Input data[75]

Input and output data			
Feed water temperature	(stream 1)	°C	35
Feed water pressure	(stream 1)	bar	1.013
Feed water salinity	(stream 1)	g/kg	38
Feed water pressure	(stream2)	bar	1.5
Feed water temperature	(stream 3)	°C	39
Distillate water pressure	(stream 9)	bar	0.3
Distillate water pressure	(stream 10)	bar	2
Motive steam pressure	(stream 16)	bar	10
Steam pressure	(stream 17)	bar	0.329
Steam flow	(stream 17)	kg/s	17.78
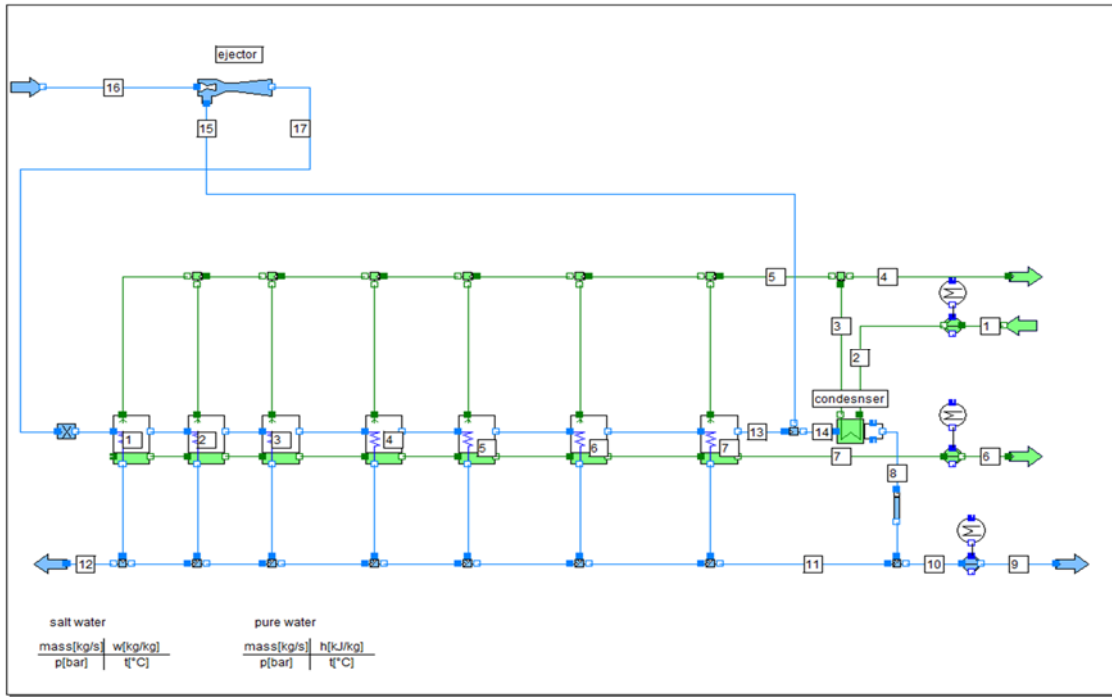
Figure 4-5: A schematic MED-TVC IPSEpro model

Table 4-13: Set/ Calculated values in MED-TVC model

Stream No.	Composition	Flow	Temperature	Pressure	Enthalpy	Entropy	Specific volume
1	Seawater	Cal	Set	Set	Cal	Cal	Cal
2	Seawater	Cal	Cal	Set	Cal	Cal	Cal
3	Seawater	Cal	Set	Cal	Cal	Cal	Cal
4	Seawater	Cal	Cal	Cal	Cal	Cal	Cal
5	Seawater	Cal	Cal	Cal	Cal	Cal	Cal
6	Seawater	Cal	Cal	Cal	Cal	Cal	Cal
7	Seawater	Cal	Cal	Cal	Cal	Cal	Cal
8	Condensate steam	Cal	Cal	Cal	Cal	Cal	Cal
9	Condensate steam	Cal	Cal	Set	Cal	Cal	Cal
10	Condensate steam	Cal	Cal	Set	Cal	Cal	Cal
11	Condensate steam	Cal	Cal	Cal	Cal	Cal	Cal
12	Condensate steam	Cal	Cal	Cal	Cal	Cal	Cal
13	Steam	Cal	Cal	Cal	Cal	Cal	Cal
14	Steam	Cal	Cal	Cal	Cal	Cal	Cal
15	Steam	Cal	Cal	Cal	Cal	Cal	Cal
16	Steam	Cal	Cal	Set	Cal	Cal	Cal
17	Steam	Set	Cal	Set	Cal	Cal	Cal

Table 4-14: Comparison between the actual data and model outputs [75]

Output data		Operational	Model	Difference (%)
Total water product	(tonne/day)	1536	1536.1	+0.013
First effect temperature	°C	67.5	67.5	0.00
Condenser temperature	°C	48	48	0.00
GOR	%	7.7	7.7	0.00

Sensitivity analysis of the MED-TVC model is carried out after validation to estimate the uncertainty of the model output results due to uncertainties in the model input data. The input conditions of the MED-TVC were changed in a systematic way to determine the sensitivity of plant parameters such as efficiencies, GOR, output capacity, etc. to uncertainties in input conditions. The main input parameters that affect MED-TVC performance are:

1- Seawater salinity (g/kg). 2- Seawater temperature (°C).

The target input parameters were varied over ±5% to find which parameter has more effect on the performance. Table 4.15 shows the summary of the results where appendix (5-A) shows the rest of the results obtained. Table 4-15 indicates that the model is generally more sensitive to seawater temperature than seawater salinity, except for exergy destruction and exergy efficiency which are directly altered by the changes in chemical exergy caused by changes in salinity. Other than these, the only sensitive outputs (change > 5%) are the seawater rejected and feed flows, which are strongly influenced by changes in seawater temperature in this relatively low temperature process. As the temperature increases or decreases the water product will also increase/decrease, which means the feed flow will also increase or decrease as well as the condenser UA. Other parameters are less sensitive to temperature change.

Table 4-15: Summary of MED-TVC sensitivity

Performance Parameters	Effect of change of feed water temperature (±5%)	Effect of change of feed water salinity (±5%)
Gain Output Ratio GOR	±1.46	±0.03
Specific Heat Consumption	±1.44	±0.03
Fresh Water Production	±1.47	±0.03
Seawater feed flow	±6.69	±0.30
Seawater rejected flow	±10.10	±0.47
Total pumps power consumption	±3.67	±0.14
Exergy efficiency	±1.62	±5.86
Total exergy destruction	±2.47	±5.86

4.6 Reverse Osmosis two-pass (RO) model

In this study a two-pass (RO) model was built and validated against operational data from an actual RO desalination unit (Table 4-16) [181]. The IPSEpro model illustrated in Figure 4-6. Table 4-17 shows the composition and thermodynamic properties of all of the numbered streams in figure 4-6, either as values set by the user as model inputs or as calculated (Cal) values output by the model. These calculated values are used for the subsequent energy and exergy analyses. As can be seen in table 4-18 there is agreement between model and operational data, the maximum difference is only 0.2%.

Table 4-16: Characteristics of the actual RO unit studied[181]

Data input and output (SWRO)			
Seawater feed temperature	(stream 1)	°C	25
Seawater feed flow	(stream 1)	t/h	327
Seawater feed salinity	(stream 1)	g/kg	36
Seawater feed pressure	(stream 1)	bar	1.013
Seawater feed pressure	(stream 2)	bar	1.5
SWRO feed pump discharge pressure	(stream 3)	bar	65.00
Brackish water pressure	(stream 5)	bar	2
SWRO osmotic pressure		bar	30.60
SWRO recovery ratio		%	45
Salt Rejection		%	98.60
Salt Passage		%	1.40
Rejected brine flow from SWRO		t/h	179
Rejected seawater salinity from SWRO	(stream4)	g/kg	65
Permeate water flow from SWRO	(stream 5)	t/h	147
Permeate water salinity from SWRO	(stream 5)	g/kg	0.486
Data input and output (BWRO)			
Brackish water flow to BWRO	(stream 6)	t/h	147
Brackish water salinity before BWRO	(stream 6)	g/kg	0.486
BWRO osmotic pressure		bar	0.41
BWRO feed pump discharge pressure	(stream 6)	bar	18
BWRO recovery ratio		%	85
Salt Rejection		%	99.7
Salt passage		%	0.31
Rejected brine flow from BWRO	(stream 7)	t/h	127
Rejected brine pressure	(stream 7)	bar	17
Permeate salinity	(stream 8)	g/kg	>0.020
Permeate pressure	(stream 8)	bar	1.5
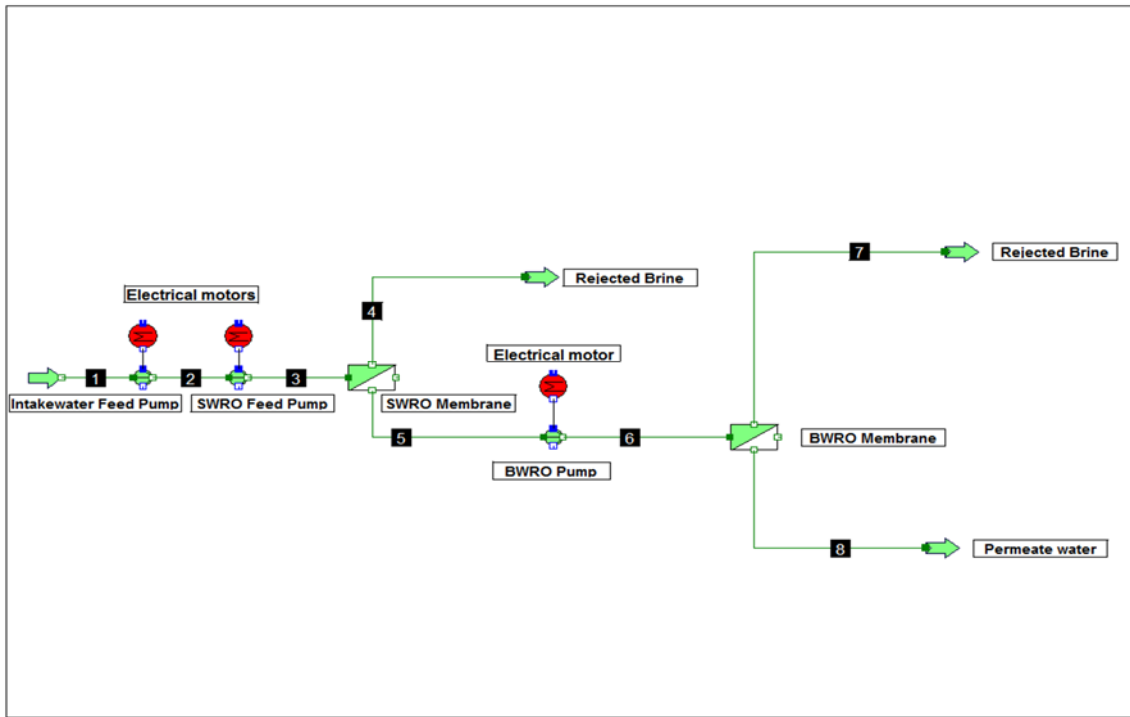
Figure 4-6: Two-pass RO desalination standalone

Table 4-17: Set/ Calculated values in RO model

Stream NO:	Composition	Flow	Temperature	Pressure	Enthalpy	Entropy	Specific volume
1	Seawater	Set	Set	Set	Cal	Cal	Cal
2	Seawater	Cal	Cal	Set	Cal	Cal	Cal
3	Seawater	Cal	Cal	Set	Cal	Cal	Cal
4	Rejected brine	Cal	Cal	Cal	Cal	Cal	Cal
5	Brackish water	Cal	Cal	Set	Cal	Cal	Cal
6	Brackish water	Cal	Cal	Set	Cal	Cal	Cal
7	Rejected brine	Cal	Cal	Set	Cal	Cal	Cal
8	Permeate water	Cal	Cal	Set	Cal	Cal	Cal

Table 4-18: Seawater RO validation (SWRO)

SWRO membrane				
Parameters		Vendor	Model	Differences (%)
Design flow	t/h	327.6	327	-0.18%
Permeate flow	t/h	147.4	147.10	-0.20%
Permeate salinity	g/kg	less than 500	0.486	-
Rejected flow	t/h	180.20	179.8	-0.22%
Rejected salinity	g/kg	65.10	65.06	-0.06%

For a model sensitivity study the input conditions of the RO were operational (recovery ratio, feed pressure) or environmental (feed temperature and salinity) changed ±5% to determine the sensitivity of the model calculation (Table 4-19). The results are sensitive to uncertainties in feed water salinity and pressure as well as recovery ratio. The greatest sensitivity is to feed pressure for salt passage and hence permeate salinity and thus the related minimum separation work and exergy efficiency because this pressure drives the flow through the membrane. Permeate salinity and hence water flux and salt passage are sensitive to feed water salinity, as would be expected. However, recovery ratio affects more parameters than other three, though with a lesser impact than those affected by feed salinity or pressure. These results suggested that for the RO model, a sensitivity analysis as discussed here is not a measure of reliability, despite the good performance shown in table 4-19.

Table 4-19: Summary of RO sensitivity

Parameter	Change of recovery ratio (±5 %)	Change of feed water Temperature (±5%)	Change of feed water salinity (±**5**%)	Change of feed pressure (±5%)
Osmatic pressure	±0.010	±0.001	±5.008	±0.010
Salt rejection	±0.106	±0.002	±0.109	±0.222
Salt passage	±8.003	±0.002	±8.232	±16.692
Water flux	±4.976	±0.013	±9.250	±14.657
Permeate flow	±4.995	±0.014	±0.005	±0.005
Permeate salinity	±7.943	±0.699	±12.822	±16.659
Rejected salinity	±4.183	±0.572	±4.954	±0.099
Minimum separation work	±6.698	±0.051	±4.559	±10.981
Exergy Efficiency	±6.118	±0.604	±4.522	±14.894
Exergy destruction total	±0.846	±0.016	±0.985	±6.660
Specific power consumption	±4.762	±0.000	±0.136	±5.079

4.7 Summary

Prior to using IPSEpro software in this study for plant simulation, it was necessary to validate all these models against manufacturer's operating data. This chapter covers the validation of five different models which were used in this study and simulated using IPSEpro software:

1. The first model that was built and validated was for an existing CCPP located at Zawya City in Libya. The results showed good agreement between the vendor's and model data, with a maximum relative differences of about 1.9%. A sensitivity study was also carried out by changing by a number of parameters ±5% and the results indicate that the pressure ratio is the most important parameter that could affect CCPP performance.

2. The second model to be built and validated was that of an adsorption chiller (AC). This was intended to improve the performance of the CCPP and avoid any fluctuation in its output power and efficiency due to changes in ambient temperature. This would also reduce specific CO_2 emissions. A LiBr-H_2O single-effect AC was proposed to be added to the CCPP. The model of the AC was built by IPSEpro and validated against an existing unit and the results showed good agreement with a maximum relative difference of 3.3%.

3. Thirdly, an SED unit model was built. This was based on a unit that exists at Waddan City, Libya. The results also proved that the model has good agreement compared with the actual operating data, with a maximum difference of 3.7%.

4. The fourth model was of a MED-TVC. This model was also built using the IPSEpro software package desalination library and it was validated with actual data. The difference between the model and actual data was found to be very small.

5. The fifth model was a two-pass RO desalination unit. This model was based on an existing plant in Oman. It was found that this model also was in good agreement with the operational data.

Based on the validated results of the simulations models, it was considered possible to move forward to carry out the analysis whose aims are outlined in the introductions to chapters 5 and 6.

CHAPTER 5. DESALINATION

5.1 Introduction

This chapter considers two proposed desalination plants, modelled by IPSEpro software. The results of two main analyses are discussed:

Seawater (Section 5.2): A comparison is conducted of the two different types of desalination technologies: MED-TVC as a thermal desalination process and two-pass RO as a membrane desalination process. Data from the Libyan environment is used, with average seawater salinity 37g/kg and temperature 20°C [176].

Brackish water desalination (Section 5.3): A comparison is performed between Single Effect Desalination (SED) and Single-pass Reverse Osmosis (SRO), with geothermal water used as a feed water with salinity 1.96 g/kg and average temperature after cooling down in open tank is 25°C (Figure 5-25), where geothermal water temperature is 73 °C which is used to power SED system [12].

5.2 Seawater Desalination

5.2.1 *Multi-effect desalination with thermal vapour compression (MED-TVC)*

5.2.1.1 Plant process description

The desalination plant used in the present study consists of four blocks, each containing seven effects. Figure 5.1 shows a schematic diagram of a single block. Each block produces 6000 m^3/day of potable water and is powered by low pressure steam extracted from an existing Combined Cycle Power Plant (CCPP), where the steam pressure is 3.78 bar. Each block receives 12 kg/s of steam from the CCPP and the total steam extracted for the four blocks to produce 24000m^3/day of potable water is 48 kg/s.

In the present study the total seawater flow (M) at stream number 1 (Figure 5-1) enters the condenser for two purposes, to cool the distillate water and to increase the seawater feed temperature. Then it leaves the condenser at point 3 and is divided into two streams. Stream M-F goes back to the tank and stream F is directed to the effects and split into seven parts (F_1 to F_7) .

The extracted motive steam (S_m) goes directly to the steam ejector (Thermo-Compressor) and is mixed in the ejector or TVC with entrained steam (D_r) which was split from the steam generated from the last effect (D_7), where the other part (D_f) entered the condenser and then combined with the other steam condensate flow from the other effects.

The vapour generated from the first effect is passed through demisters and enters effect number two and so on into the next effect and the brine remaining in the feed water of the first effect is passed to the second effect as raw water B_1 [89]. Meanwhile the condensate steam from the first effect in the four blocks is split into two streams: S (in stream number 12) returns back to the CCPP while D_r passes to the product line. The vapour formed outside the tubes in the first effect is passed to the second effect and so on to the other effects (D_1 to D_7), each time to heat the next effect feed water. In doing so it, then condenses as distillate water with all streams collected in the product line.

Stream D_7 from the last effect is split (as noted above) with the portion not going to the thermo-compressor passing through the condenser (D_f) before joining the product line. A similar process occurs in the remaining effects up to the last effect. The brine streams (B_1 to B_7) as shown in figure 5-1 started from the first effect then passed to the second effect which has lower pressure decreasing gradually until effect number 7 from which it is extracted by the brine pump.
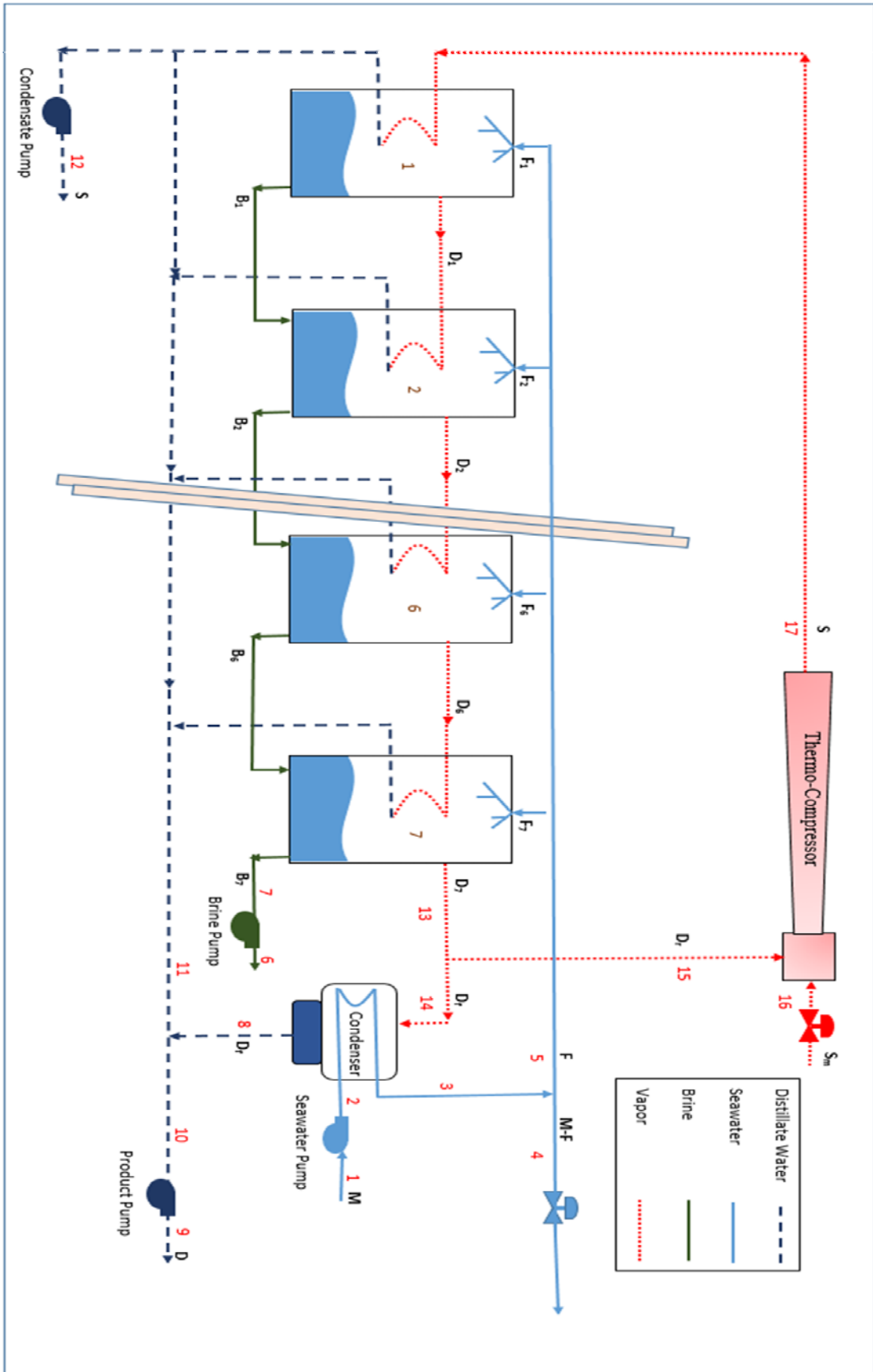
Figure 5-1: A schematic diagram of seven effect MED-TVC

To determine the optimum operating conditions the temperature differences between the effects are assumed to be equal [75, 182].

$$\Delta T = \frac{T_s - T_f}{N + 1}$$

(5-1)

where T_s is the motive steam temperature, T_f is the feed temperature and N is the number of effects.

The temperature difference between the effects depends only on the surface area available in the effects. Increasing the surface area leads to a decrease in the temperature difference between the effects, but this can not be lower than 2.5°C because of the pressure drop between the effects. The feed water temperature is related to the cooling water temperature and surface area of the condenser.

5.2.1.2 Energy and Exergy Analyses

After validating the model and confirming that it is working properly (Section 4.4), it was then scaled up to produce 24000 m³/day and Libyan environmental data were used for this study. When scaling the MED-TVC, it is assumed that there is a linear relationship in the following equipment of the parameters: condenser area, effects area, seawater flow, rejected seawater flow, steam flow, motive steam, brine rejected flow. The other parameters, including Gain Output Ratio (GOR), concentration factor, salinity per effect, seawater temperature and condenser pinch point temperature difference, are considered to be fixed. Energy and exergy analyses have been discussed in the literature [68, 73, 75, 81, 94], but no detailed exergy analysis for MED-TVC has been published, especially including the chemical exergy of the seawater and brine. This study covers many possible influences on the MED-TVC desalination plant, such as seawater salinity and seawater temperature.

Table 5.1 shows the calculated thermodynamic properties of all of the MED-TVC numbered streams shown in figure 4.6. For the purposes of exergy analysis, the selection of the dead state (exergy datum) varies according to the research objectives [139, 142]. In the present study, the dead state has been selected as the average Libyan environmental conditions, as discussed in chapter 3, defined as follows: P_0 = 1.013 bar, $w_{s,0}$ = 37 g/kg, and T_0 = 20°C [176]. These values represent the average seawater data in the Libyan environment. The enthalpy (h_0) and entropy (s_0) for water and seawater at the dead state were 80.976 (kJ/kg) and 0.286 (kJ/(kg.K)) respectively. Physical and chemical exergy values are negative in table 5.1 when the stream

conditions are lower than in the dead state. Streams number 4-A, 6-A, 9-A, 12-A in table 5-1 represent the residual exergy when they move to the dead state at (p_0, T_0) to calculate the minimum separation work (w_{min}) as explained in section 3.3.

Table 5-1: Thermodynamic properties of the streams indicated

Stream No.	T (°C)	Pressure P (kPa)	Mass flow m (kg/s)	Salinity w_s (g/kg)	Enthalpy h (kJ/kg)	Entropy s kJ/kg.K)	Specific physical exergy e_{ph} (kJ/kg)	Specific chemical exergy e_{ch} (kJ/kg)	Total specific exergy e $_{total}$ (kJ/kg)	Total exergy E $_{total}$ (MW)
1	20.00	101.3	1950.7	0.000	80.976	0.286	0.000	0.000	0.000	0.000
2	20.01	150.0	1950.7	37.000	81.044	0.286	0.047	0.000	0.047	0.092
3	24.00	150.0	1950.7	37.000	95.534	0.335	0.109	0.000	0.109	0.213
4	24.00	150.0	1026.0	37.000	95.534	0.335	0.109	0.000	0.109	0.112
5	24.00	150.0	924.7	37.000	95.534	0.335	0.109	0.000	0.109	0.101
6	45.56	200.0	646.7	53.000	177.678	0.596	5.596	-1.296	4.301	2.781
7	45.53	9.6	646.7	53.000	177.394	0.596	5.404	-1.296	4.108	2.656
8	44.92	9.6	11.8	0.000	188.089	0.638	3.836	2.997	6.832	0.081
9	59.18	200.0	278.0	0.000	247.863	0.821	9.817	2.997	12.813	3.562
10	59.15	30.0	278.0	0.000	247.590	0.821	9.632	2.997	12.629	3.511
11	59.78	30.0	266.2	0.000	250.228	0.828	9.942	2.997	12.938	3.444
12	71.15	32.8	52.7	0.000	297.785	0.969	16.259	2.997	19.255	1.015
4-A	20.00	101.3	1026.0	37.000	80.976	0.286	0.000	0.000	0.000	0.000
6-A	20.00	101.3	646.7	53.000	78.909	0.273	1.568	-1.288	0.280	0.181
9-A	20.00	101.3	278.0	0.000	85.466	0.301	-0.138	2.997	2.859	0.795
12-A	20.00	101.3	52.7	0.000	85.466	0.301	-0.138	2.997	2.859	0.151
13	45.52	9.6	31.8	0.000	2583.470	8.168	189.037	5.871	194.908	6.203
14	45.52	9.6	11.8	0.000	2583.472	8.168	189.039	5.871	194.910	2.305
15	45.52	9.6	20.0	0.000	2583.472	8.168	189.039	5.871	194.910	3.898
16	142.43	387.0	52.7	0.000	2645.175	6.687	685.415	5.871	691.287	36.433
17	71.23	32.9	72.7	0.000	2628.201	7.736	360.560	5.871	366.431	26.641

Table 5-2 summarizes the exergy analysis of all of the numbered total exergies E_{in} in the calculation referring to the number in figure 4-6, where equation 3.23 is used to calculate the overall exergy efficiency of the MED-TVC. The sum of the pump work and heating steam exergy is the input exergy to the unit, where pump efficiency is assumed to be typically 75% [100, 101, 139]. The sum of discharged distillate water and brine exergies relative to the exergy of the cooling water entering the unit is known

as the minimum separation work. The difference between the inputs and outputs of the exergies of individual components is called exergy destruction. Based on the previous results, the exergy destruction ratios of the MED-TVC components are shown in figure 5-2. The exergy efficiency of the MED-TVC studied was only 3.4%, due to the low seawater temperature. The greatest amount of the exergy destruction occurs in the ejector with its typical irreversible process giving high exergy destruction (mixing processes) and in the effects (phase change), followed by product, brine disposal (not a component), and condenser, whereas the level of exergy destruction in the pumps was only 0.25%.

Table 5-2: Summary of the exergy analysis used for the study of the MED-TVC plant for four blocks

Equipment	Calculation Method	Resu	Unit
Seawater pump exergy in	$E_2 - E_1$	0.102	MW
Brine pump exergy in	$E_6 - E_7$	0.112	MW
Distillate pump exergy in	$E_9 - E_{10}$	0.0522	MW
Pumps input exergy in	$= (1/0.75)\text{X}\left(\sum\left((E_{2-}E_1)+(E_6-E_7)+(E_9-E_{10})\right)\right)$	0.355	MW
Heating system exergy in	E_{16}	33.64	MW
Exergy in	Heating system exergy in + pump input exergy in	33.99	MW
Minimum separation work	$= E_{6-A} + E_{4-A} + E_{12-A}$	1.162	MW
Exergy efficiency	$\eta_{II} = \dfrac{W_{min}}{E_{16} + E_{pp}}$	3.420	%
Total exergy destruction	Exergy in – minimum separation work	32.83	MW
Exergy destroyed in pumps	$E_{d,pp} = (1 - 0.75)XE_{pp}$	0.089	MW
Exergy destroyed in	$E_2 + E_{14} - E_3 - E_8$	2.573	MW
Exergy destroyed in ejector	$E_{15} + E_{16} - E_{17}$	12.83	MW
Exergy destroyed in effects	$E_5 + E_{17} - E_7 - E_{13} - E_{12} - E_{11}$	11.96	MW
Exergy destroyed in	$E_9 - E_{9-A}$	2.490	MW
Exergy destroyed in brine	$E_6 - E_{6-A}$	2.010	MW
Exergy destroyed in	$E_2 + E_{14} + -E_3 - E_8$	0.798	MW
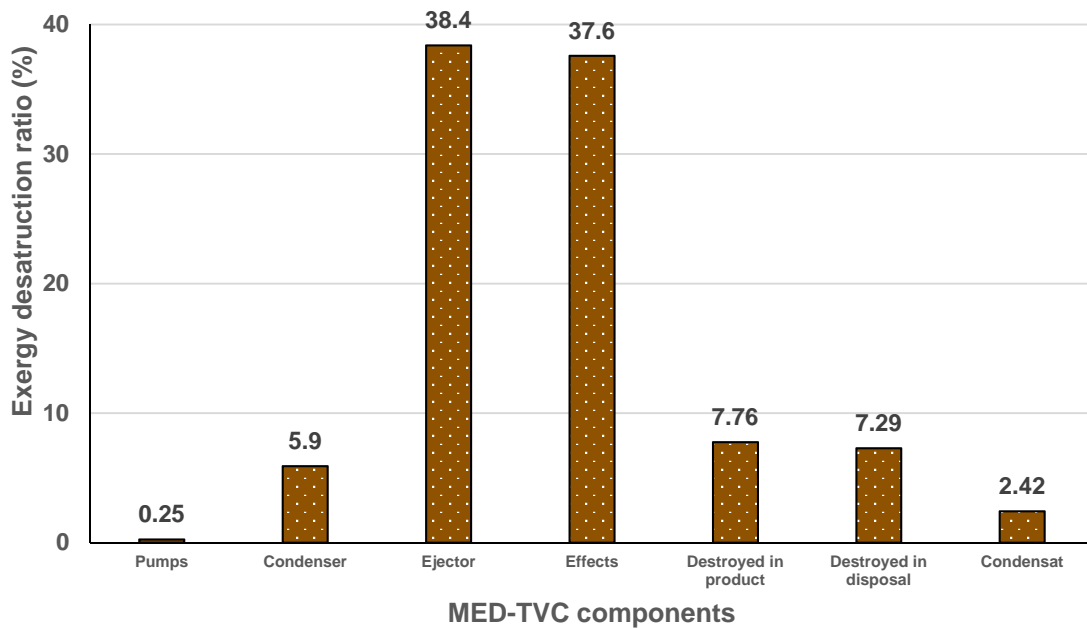
Figure 5-2: Exergy destruction ratio in MED-TVC desalination plant

Figure 5-3 shows that the first effect represented about 30% of the total exergy destruction of all the effects. This because it is close to the heat source and the temperature difference between the steam and feed water is high, whereas the last effect had the lowest exergy destruction ratio due to the low temperature difference between the steam and the feed.
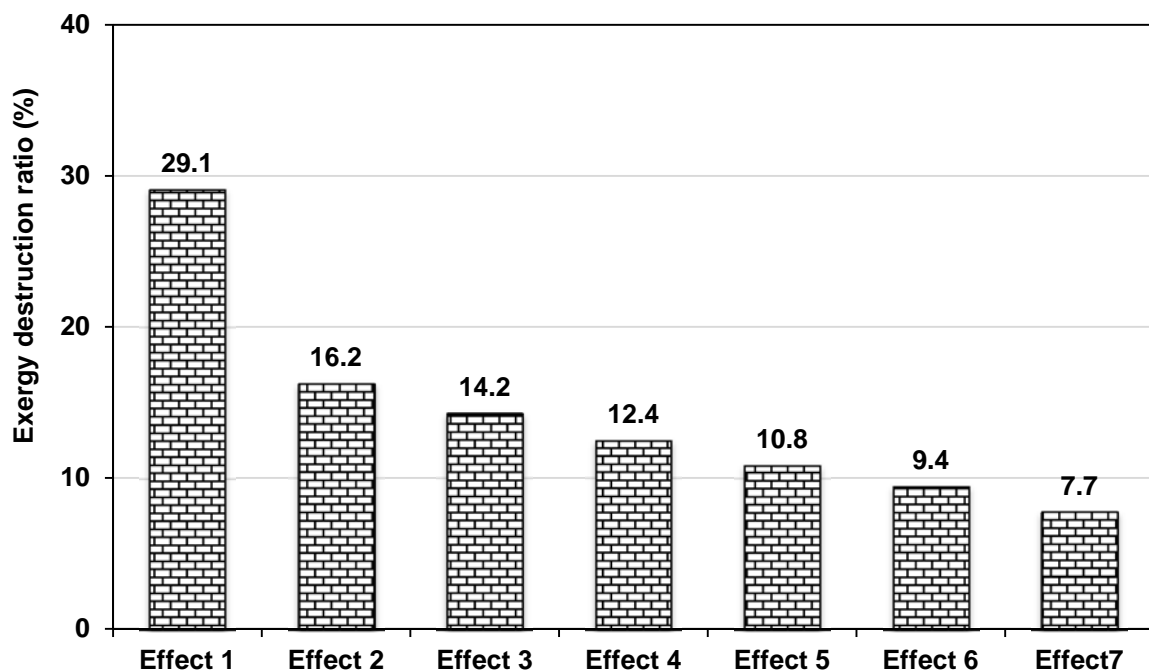
Figure 5-3: Exergy destruction ratio in each effect of MED-TVC

5.2.1.3 **Parametric Study**

Parametric studies assess the impact of variations around the design conditions of (a) Feed water salinity, (b) Feed water temperature, (c) Number of effects, (d) Ratio of entrained steam flow and (e) Part load operation.

a) Effect of seawater feed salinity on MED-TVC

The effect of seawater salinity was investigated using a wide range of salinity ranging between 20-40 g/kg at constant plant capacity (100%) and an average seawater temperature of 20°C. However, the range of Zawya city seawater salinity is only from 34.6 to 38.6 g/kg [176]. The GOR is defined as the ratio of the distillate product to steam supplied to the desalination. Figure 5-4 shows that the exergy efficiency and GOR of the unit increase as seawater salinity increases as a result of its increased enthalpy (and also increase in waste brine water), which agrees with the results of previous studies [28, 61, 75]. However, this is only a small change in GOR which would only be noticeable over a long period.
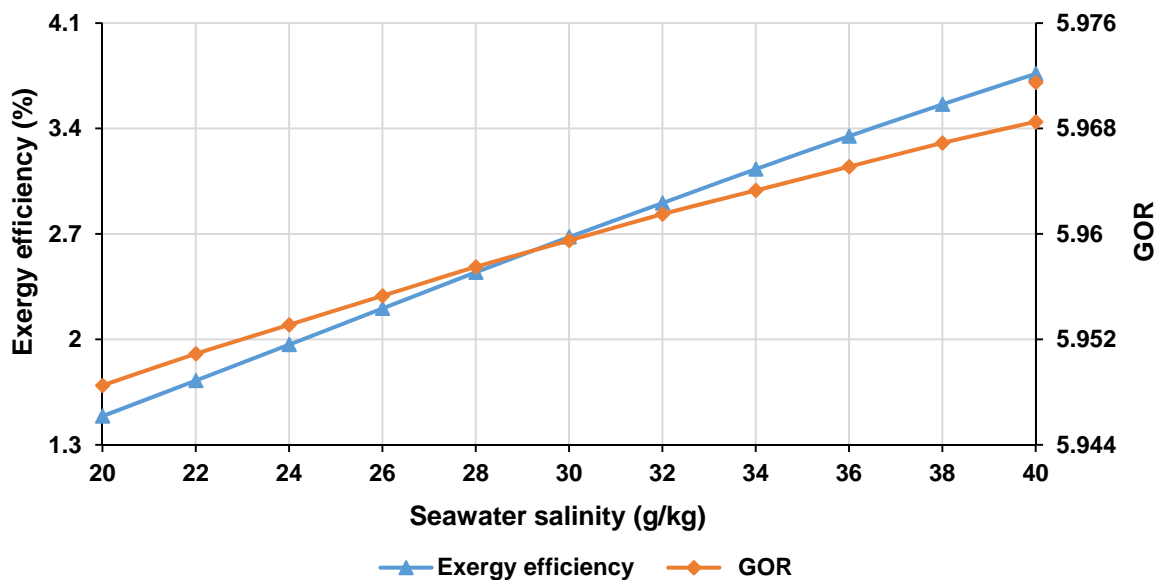
Figure 5-4: Effect of seawater salinity on GOR and exergy efficiency

Both exergy destruction and specific heat capacity decrease as seawater salinity increases (Figure 5-5). This enhances the exergy efficiency and reduces steam consumption. The required cooling feed water flow and heat transfer conductance (UA) increase as feed water salinity increases (Figure 5-6) because more distillate water is produced. This will required more power for cooling and distillate water as shown in figure 5-7.
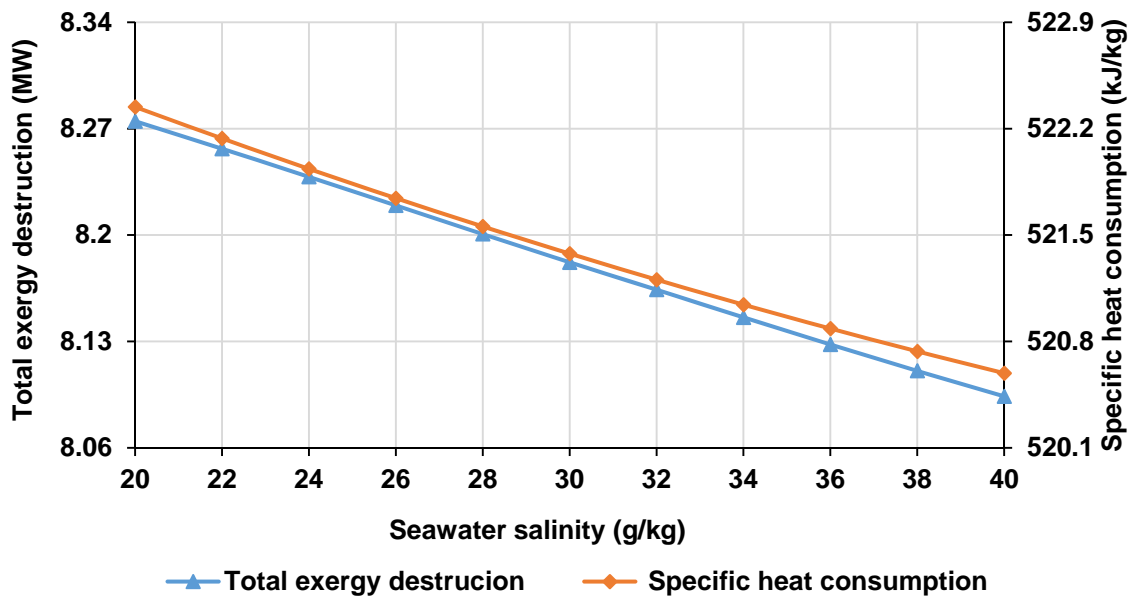
Figure 5-5: Effect of seawater salinity on total exergy destruction and specific heat consumption
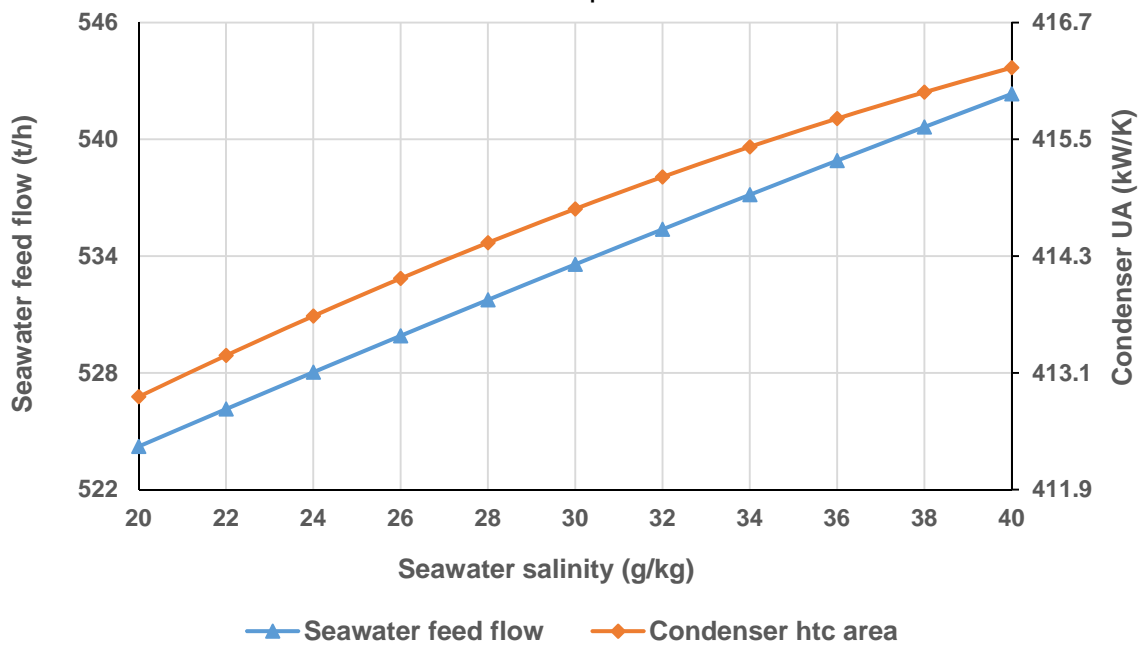
Figure 5-6: Effect of seawater salinity on cooling feed water flow and condenser UA
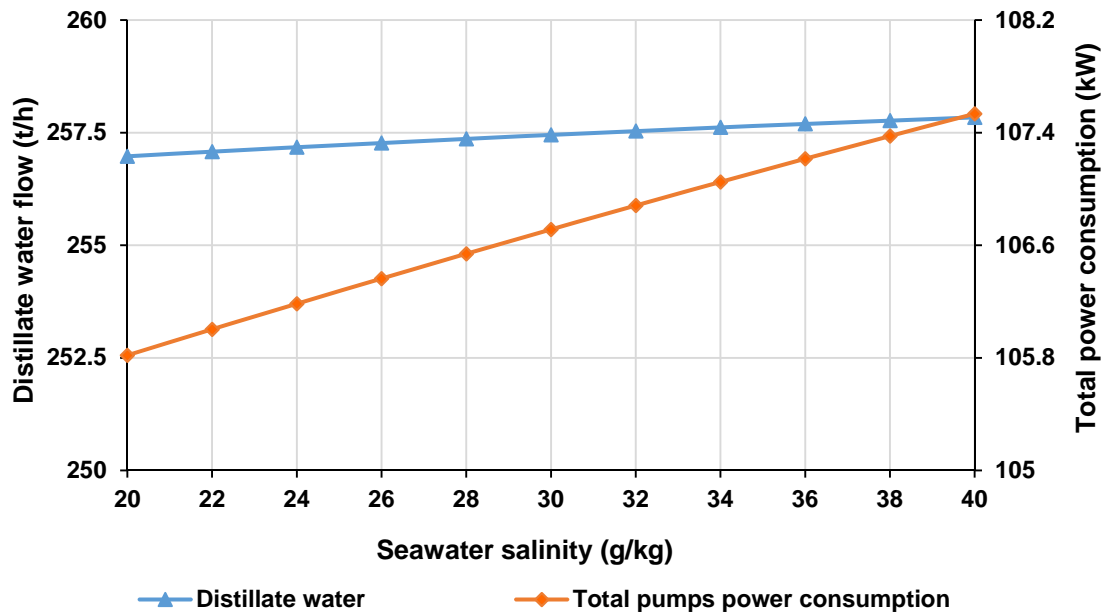
Figure 5-7: Effect of seawater salinity on distillate water flow and total power consumption

b) Effect of cooling water temperature on the MED-TVC system

The influence of the cooling water inlet temperature was investigated at constant feed seawater salinity 37 g/kg and constant output product of 24000 m³/d. It is known that seawater temperature changes during the year over the range 14 -30°C [176].

Figure 5-8 shows the effect of variation in seawater temperature on the performance of the MED-TVC unit. As the cooling seawater temperature increases the exergy efficiency and GOR increase by about 5.0% and 3.0%, respectively, for every 2°C increase. The reason for this is clear from the fall in exergy destruction at higher seawater temperatures from 8.57MW at 14°C to 6.83MW at 30°C as seen in figure 5-9. Moreover, because of the increase in the minimum separation work (W_{min}) more distillate water is produced and this result agrees with previous findings [75, 88, 94].

The specific heat consumption declines by about 176 kJ/kg for every 2°C increase (Figure 5-10). The reason behind this is that the feed seawater at high temperature needs less heat in preheating [77]. In contrast the total power consumption increases with cooling water temperature by about 118 kW when the feed temperature rises from 14°C to 30°C as shown in figure 5.10 due to water flow rate increase.
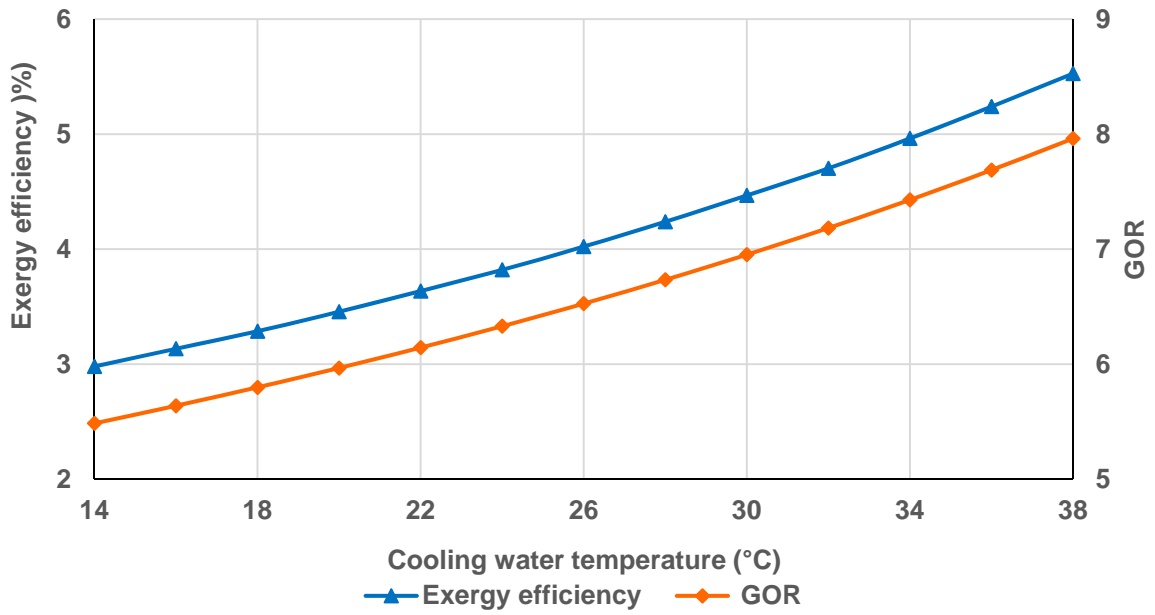
Figure 5-8: Effect of seawater temperature on exergy efficiency and GOR
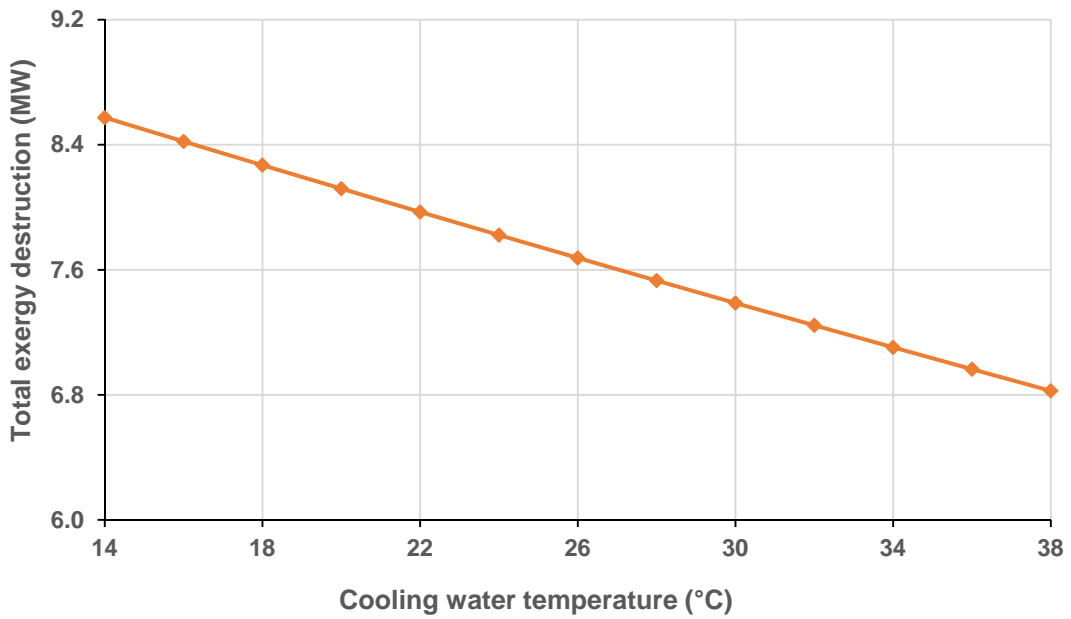
Figure 5-9: Effect of seawater temperature on total exergy destruction
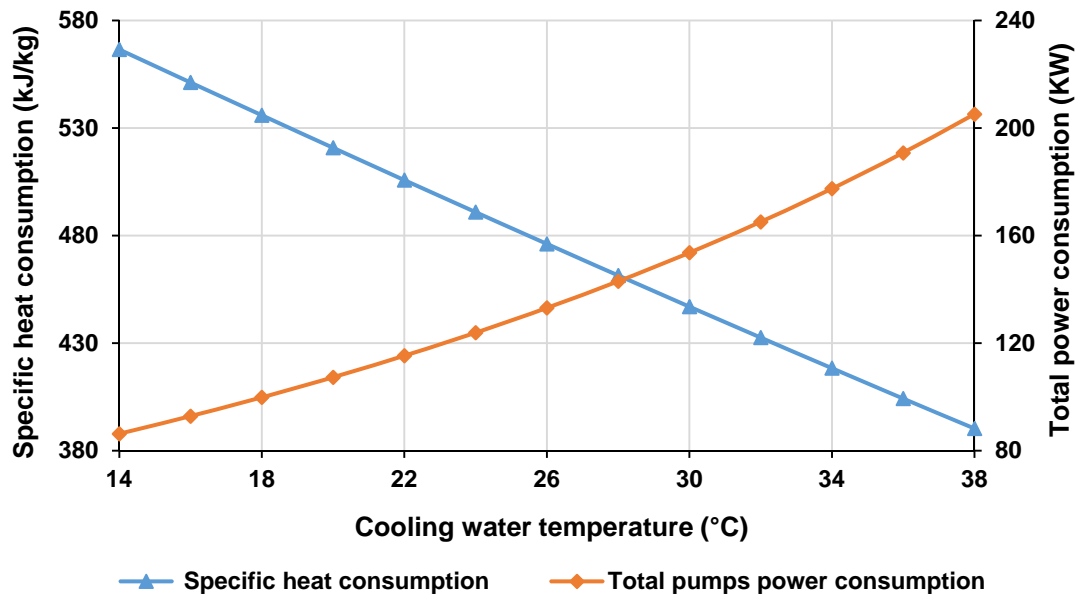
Figure 5-10: Effect of seawater temperature on specific heat consumption and total power consumption

c) Effect of number of effects

The number of effects in thermal desalination systems significantly affects plant performance and output capacity [28]. Therefore, the influence of number of effects was investigated by keeping the MED-TVC input parameters constant with only the number of effects in the unit varied from one to ten effects. It was found that ten effects gives the highest GOR value and lowest specific heat consumption [25]. However the current study required only seven effects to produce the required fresh water. Figure 5-11 illustrates the exergy efficiency and exergy destruction versus the number of effects. As can be seen, when the number of effects increases from one to ten, the exergy efficiency increases from 0.924% to 4.4% because of an increase in minimum separation work and decrease in exergy destruction. The reduction in exergy destruction at high numbers of effects is also explained as a result of the utilization of more exergy [94, 119], while the value of GOR increases with number of effects from 1.16 to 7.90, due to the distillate water rate increasing from about 50 t/h to 340 t/h, as shown in figure 5-12 [28, 75, 88, 91].
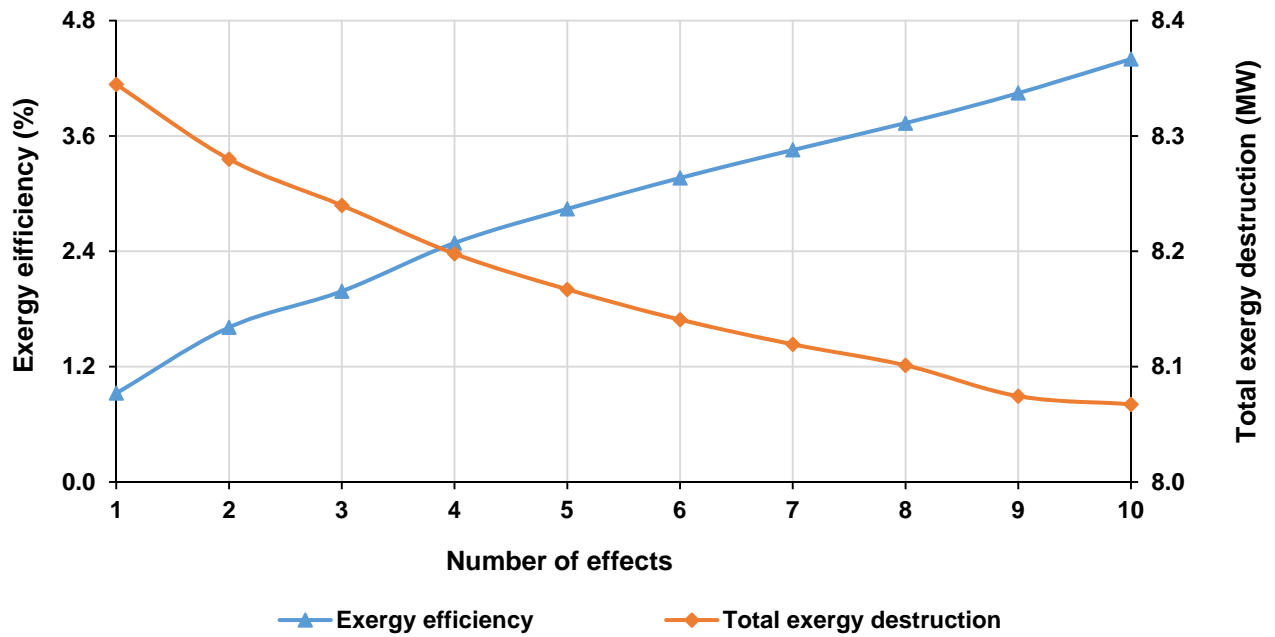
Figure 5-11: Effect of number of effects on exergy efficiency and total exergy destruction
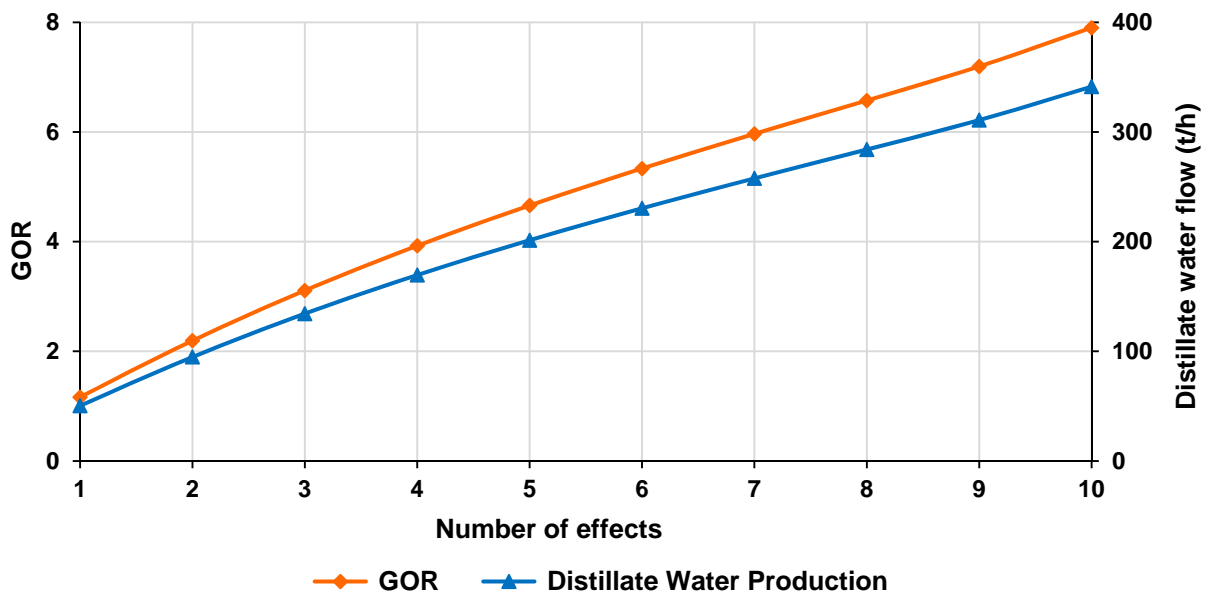
Figure 5-12: Effect of number of effects on GOR and distillate water flow

Another benefit of increasing the number of effects is the reduction of the seawater cooling flow by about 16% for each further effect added as shown in figure 5-13. This drop in seawater cooling flow is because of the decline in water production from the last effect, due to reduced distillate water produced from the last effect.
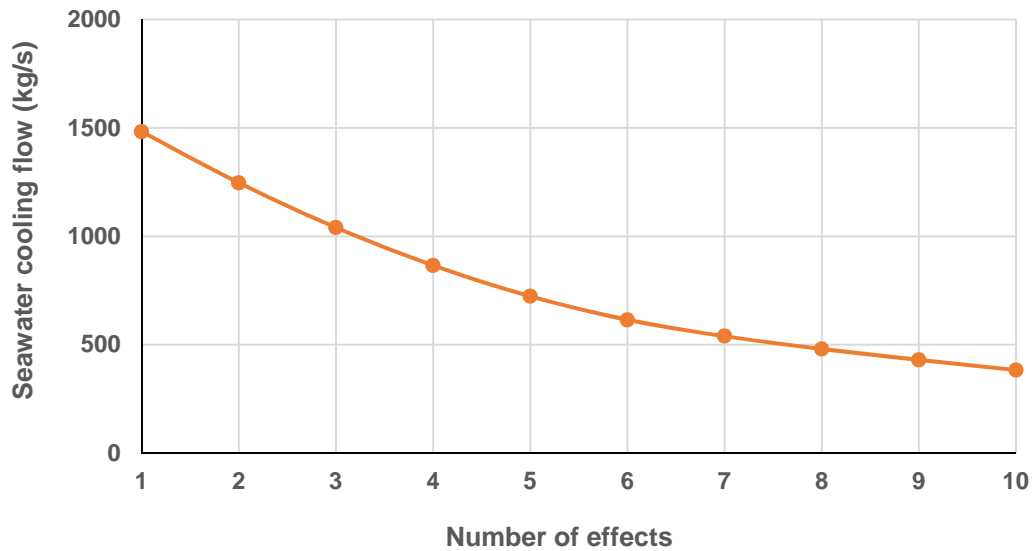
Figure 5-13: Effect of number of effects on seawater cooling flow

Figure 5-14 shows the exergy destruction for each component at ten different configurations of the MED-TVC. It can be seen that the ejector records the highest exergy destruction followed by the effects and condenser and the exergy destruction decreases with increasing number of effects.
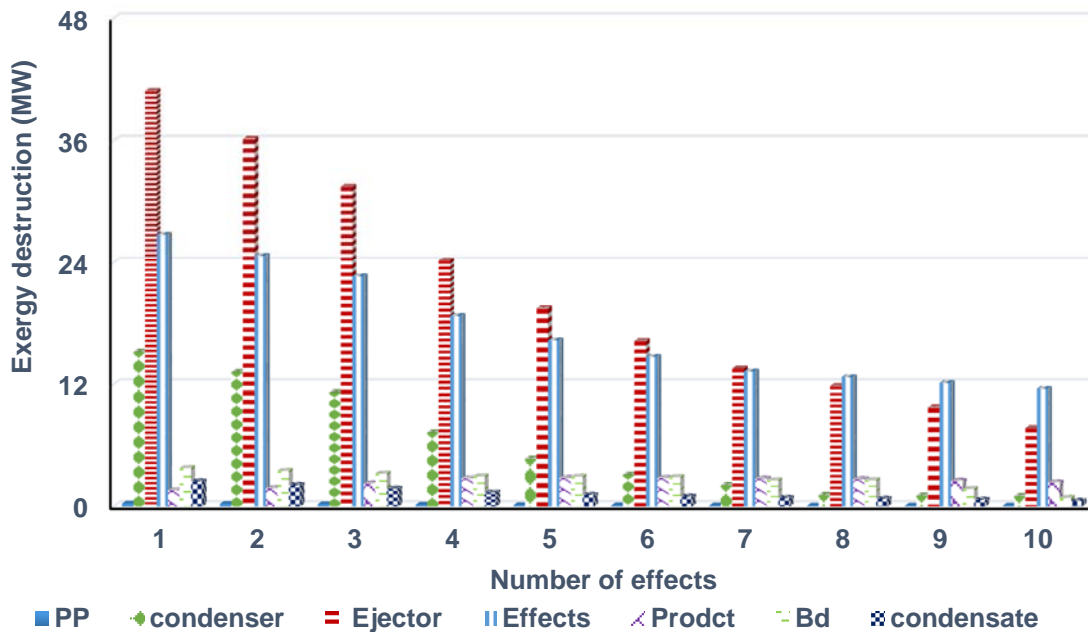
Figure 5-14: Effect of number of effects on exergy efficiency destruction in each effect component

d) Effect of entrained steam flow

With Thermal Vapour Compression (TVC), the entrained steam flow ratio is defined as the ratio of the motive steam mass to the mass of entrained vapour. This could be considered the most important parameter which can affect the performance of the desalination unit, because it controls the energy consumed and the heat exergy in the condenser.

The effect of entrained steam was investigated and the results show that, as the entrained steam mass increases, it means less vapour enters the condenser so there is less exergy destruction and cooling water flow required. As a consequence the exergy efficiency and GOR increase whereas the cooling seawater flow and motive steam flow decrease as shown in figures 5-15 and 5-16, respectively. Consequently the total power consumption and total exergy destruction decline (figure 5-17).
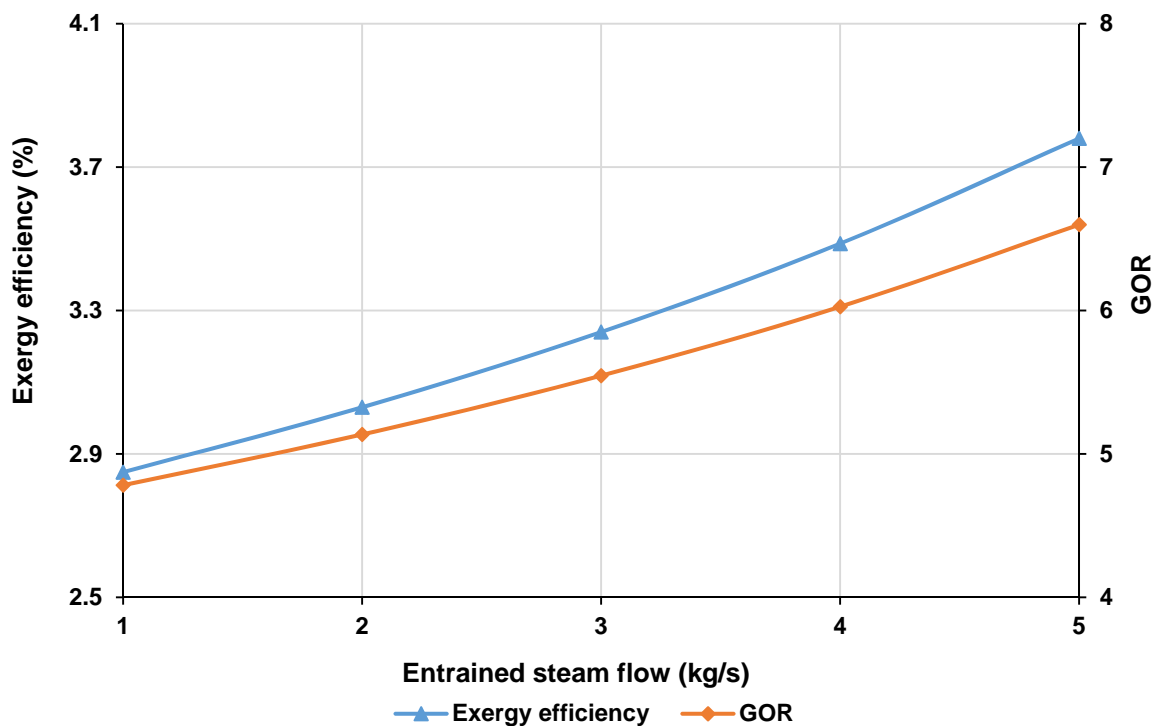
Figure 5-15: Effect of entrained steam flow on exergy efficiency and GOR
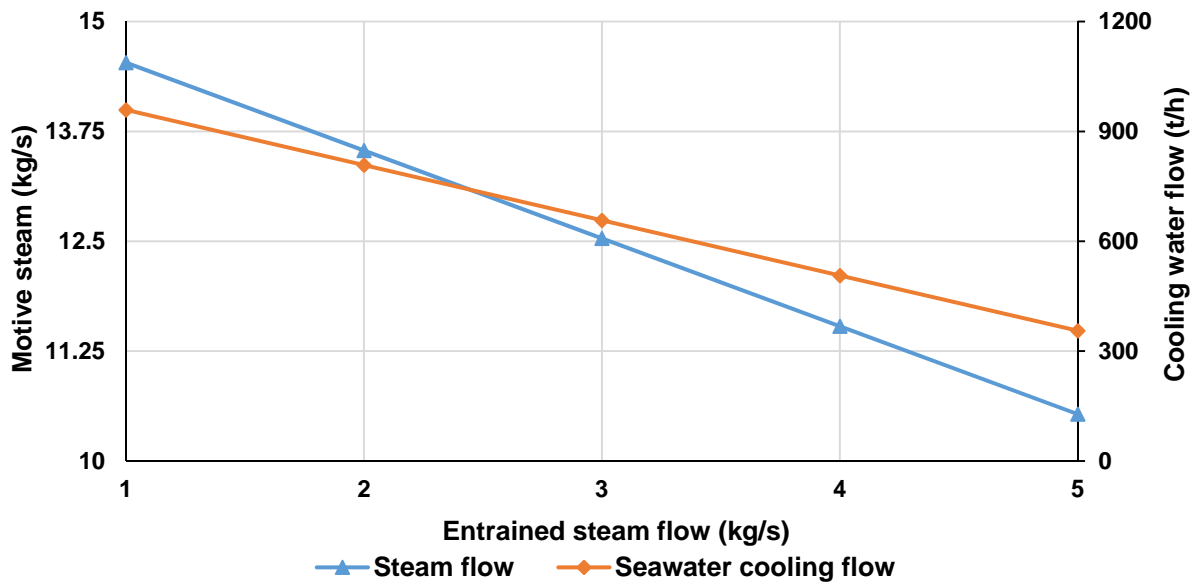
Figure 5-16: Effect of entrained steam flow on motive steam and cooling water flow
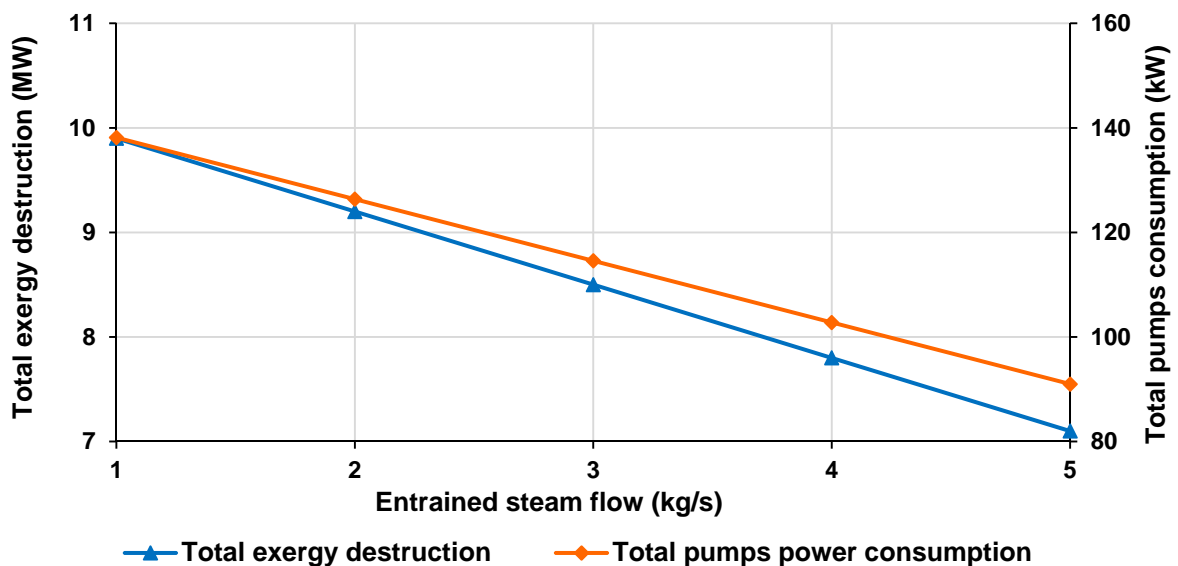
Figure 5-17: Effect of entrained steam flow on total exergy destruction and total power consumption

e) Effect of plant partial load

Figure 5-18 shows the influence of plant capacity change from 25% load to 100%, from the total plant capacity by operate one block for 25% then 2 blocks, 3 blocks and at 100% four blocks. With each block operation at design this gives an increase from 12 kg/s to 48kg/s in motive steam flow and in cooling water flow from 506 kg/s to 2025 kg/s. This results that more steam flow is required to produce more distillate water and more cooling water required to cool the vapour entering the condenser.

This will lead to increases in power consumption, exergy destruction and minimum separation work as shown in figures 5-19 and 5-20.
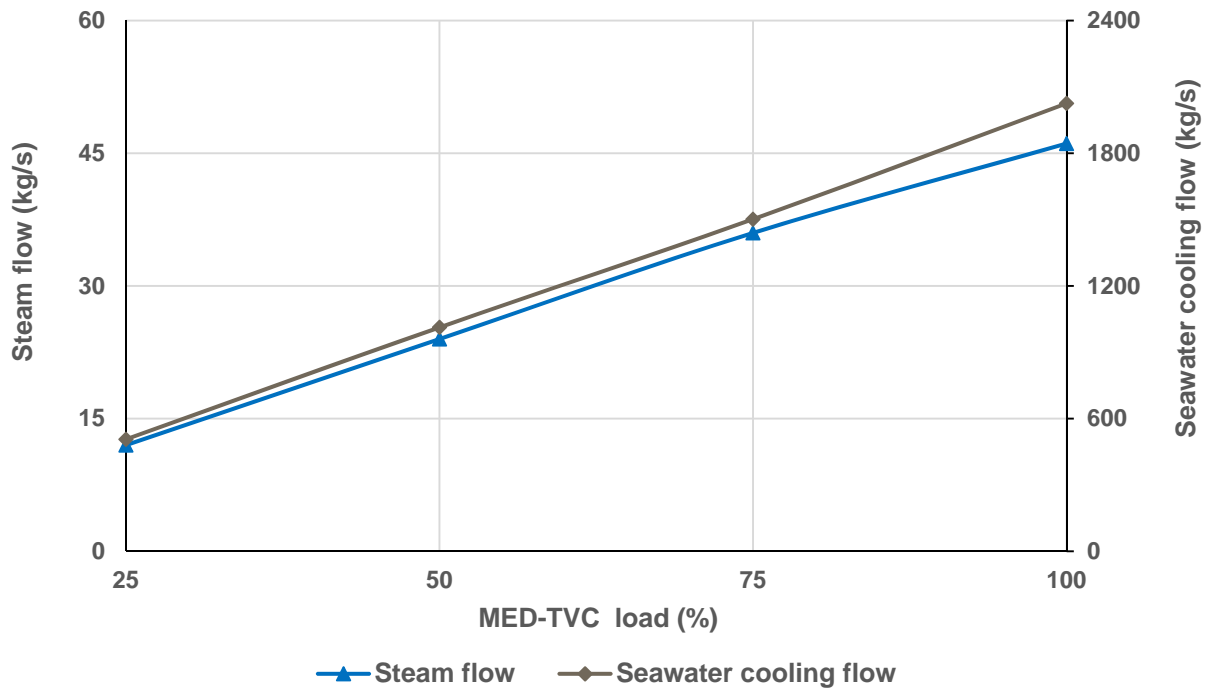
Figure 5-18: Effect of plant load on steam flow and seawater cooling flow
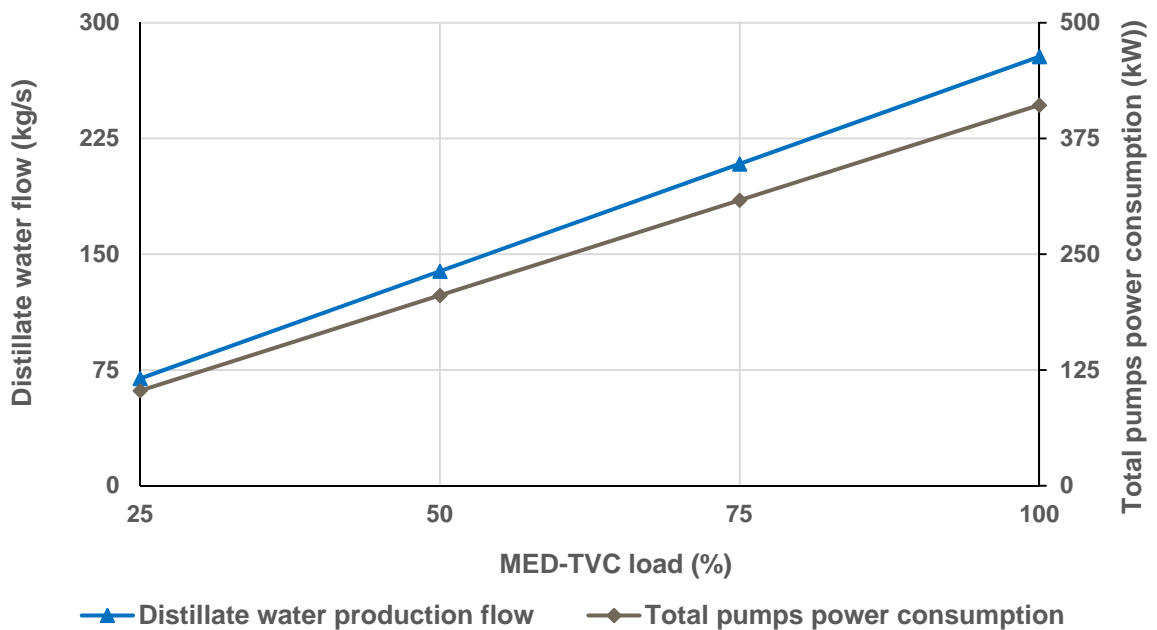
Figure 5-19: Effect of plant load on distillate water flow and total power consumption
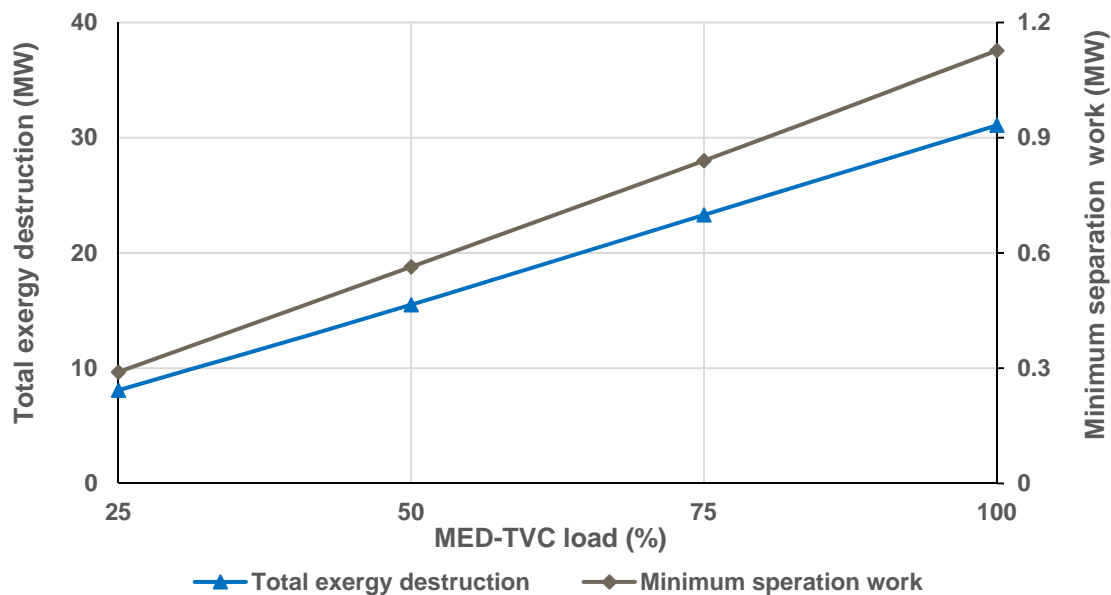
Figure 5-20: Effect of plant load on total exergy destruction and minimum separation work

5.2.1.4 A comparison of the system with and without a preheater

As discussed earlier in section 5.2.1.3 (b), increasing the seawater feed temperature will enhance the performance of MED-TVC desalination. As can be seen in figure 5-8 the exergy efficiency and GOR increase with cooling water temperature and it can be possible to raise the feed temperature using recovery of heat from the hot distillate water using the simplest configuration of a heat exchanger as preheater. Figure 5-21 shows the MED-TVC desalination plant with a preheater heat exchanger.
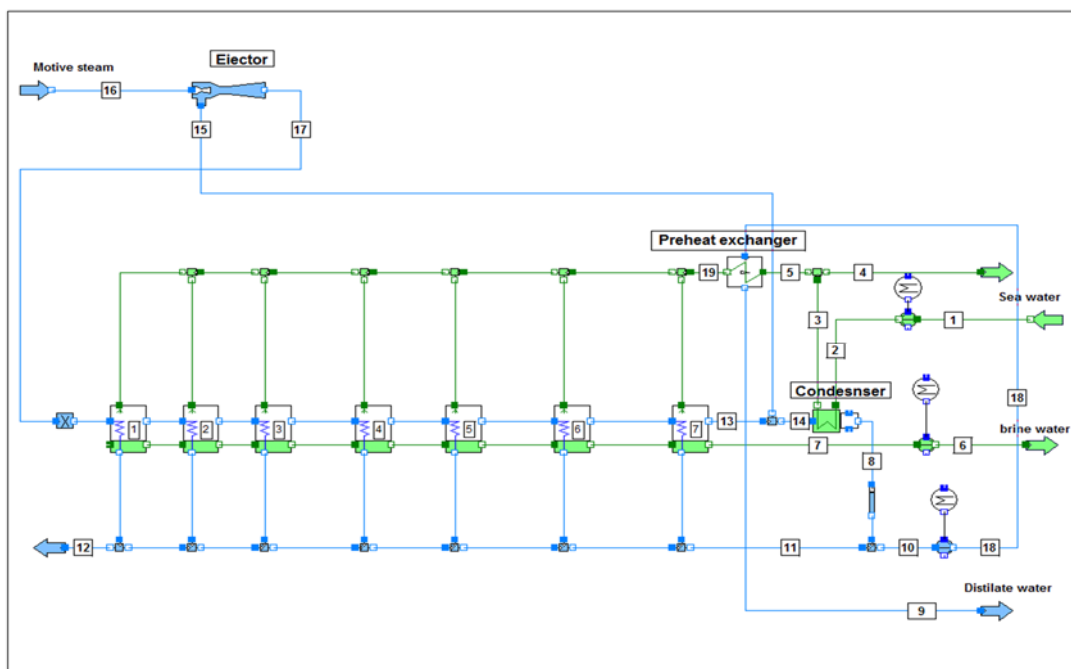
Figure 5-21: MED-TVC model with heat exchanger

Figure 5-22 shows a comparison between the GOR performance versus seawater temperature in the MED-TVC systems with and without the heat exchanger (preheater). As can be seen, the GOR of MED-TVC with the heat exchanger improved by an average about 9% compared with MED-TVC without the preheater exchanger (PHE). Also increases in exergy efficiency and distillate water resulted, of an average 8% and 5.5%, respectively, as shown in figures 5-23 and 5-24, and the specific heat consumption was reduced by an average of 5% as seen in figure 5-25.
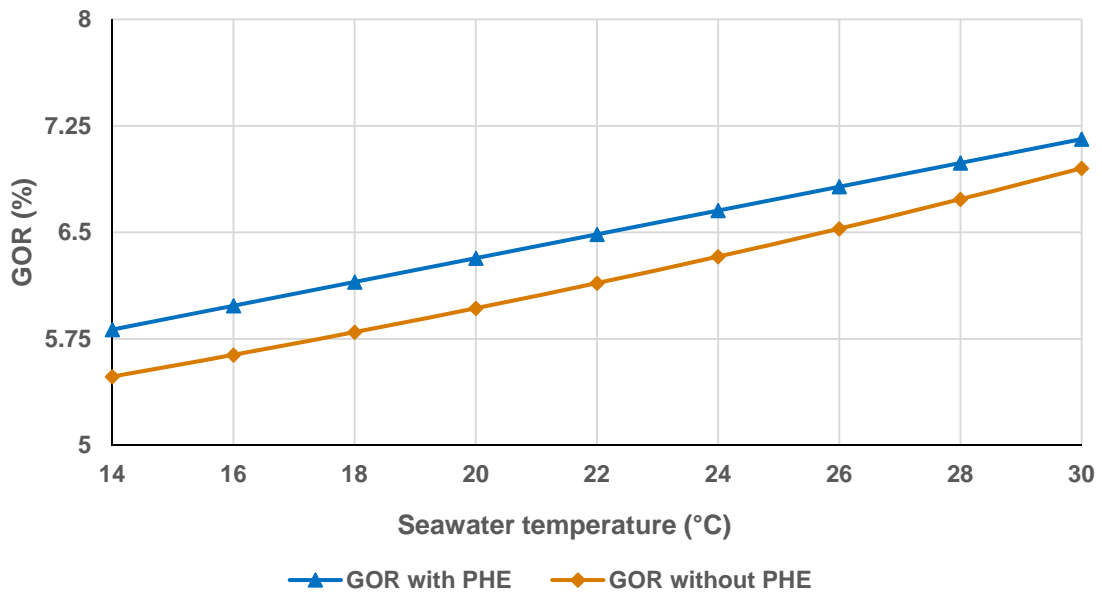
Figure 5-22: Effect of seawater temperature on GOR
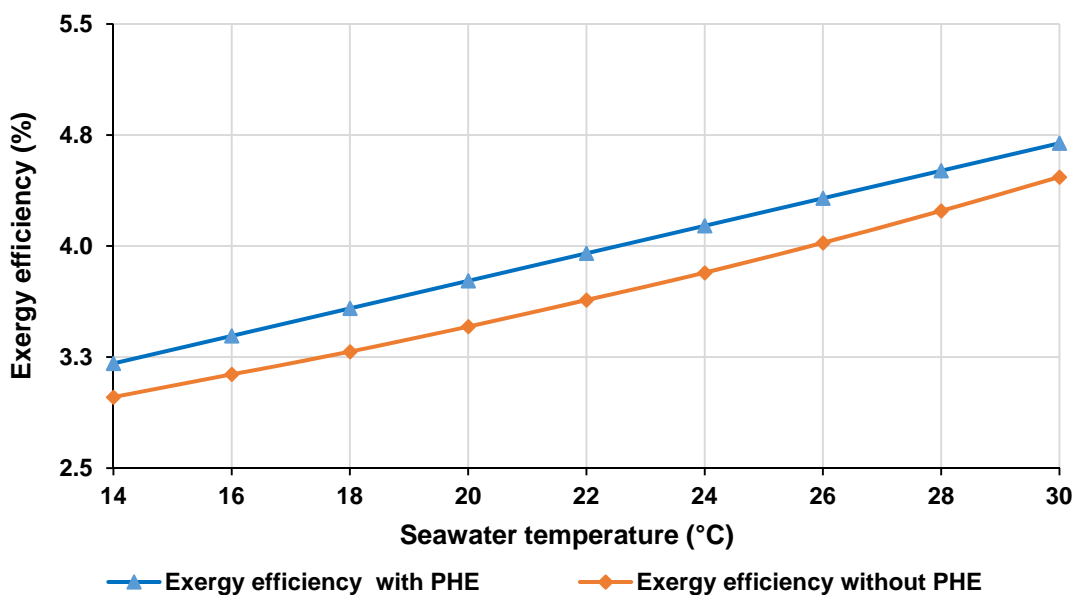
Figure 5-23: Effect of seawater temperature on exergy efficiency
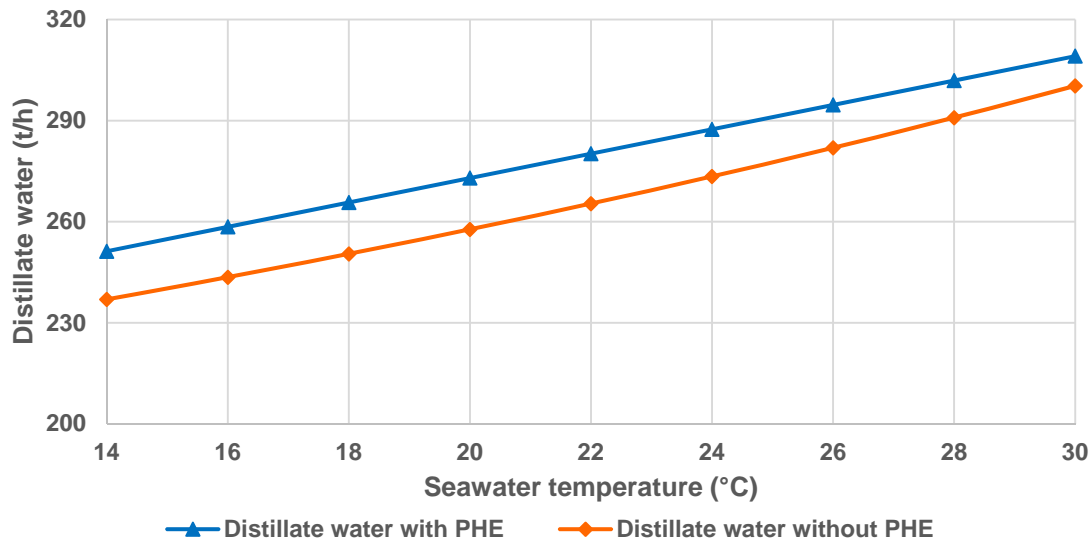
Figure 5-24: Effect of seawater temperature on distillate water flow
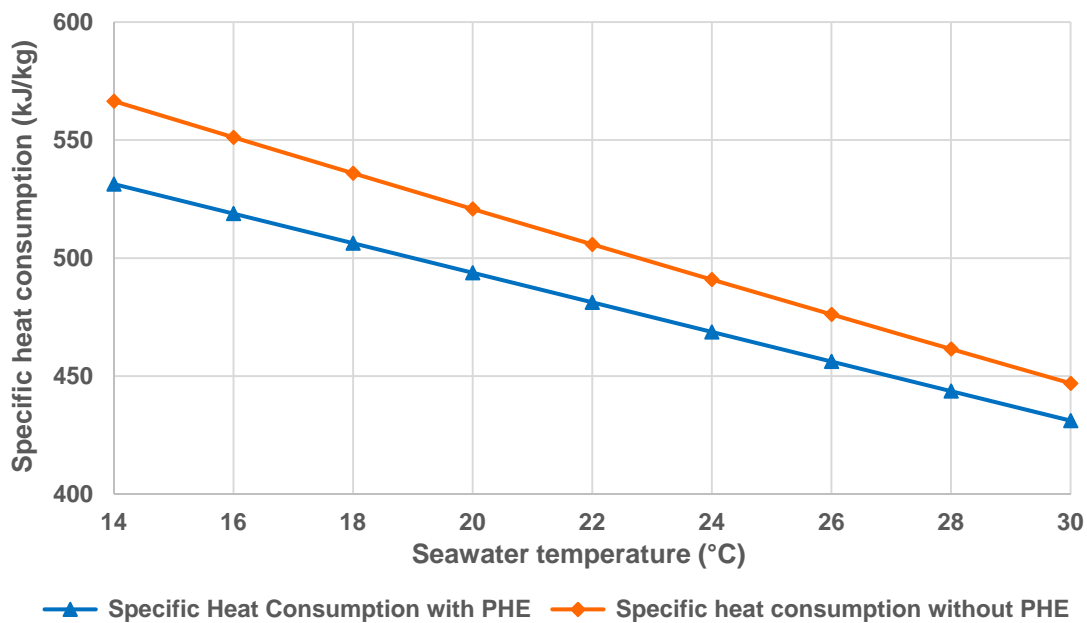
Figure 5-25: Effect of seawater temperature on specific heat consumption

5.2.2 *Two-pass Reverse Osmosis (RO)*

The working principle of RO desalination depends on separating the solvent (pure water) from the solute (sea and brackish water) by exploiting pressure to make the solvent flow in the opposite direction to osmosis, leaving the solute on the high pressure side of the semi-permeable membrane. Unlike in thermal desalination techniques, RO feed seawater should be passed through a pre-filtration system to

remove suspended solids before it reaches the membrane, which does not have mechanical filtration capabilities. A high pressure pump is used to increase the pressure of the filtered seawater up to 65 bar in order to facilitate the separation of salts from the seawater [1, 38, 48]. The RO desalination of seawater can be classified based on purpose, obtaining either better water quality or higher product flow. For better product quality, a two-pass RO is used, where the product from the first stage Sea Water RO (SWRO) is filtered again in a second stage Brackish Water RO (BWRO), with the stream permeate from the first stage SWRO is directed to the second stage in order to further decrease the salinity of the product.

The literature review (Section 2.1.3) showed RO performance can be improved and costs reduced by introducing energy recovery devices across the membranes. A comparison of five different two-pass RO configurations is therefore conducted, namely standard RO without energy recovery, with first stage Energy Recovery Turbine (ERT) or Pressure exchanger (PX) and with PX + ERT or PX + PX at both stages. Previous studies [10, 38] suggested that PX is better than ERT (Section 2.1.3). However, these studies modelled the seawater as an ideal mixture, whereas the present study will use the latest published data for seawater as a real mixture [38, 68, 100]. Also this comparison is extended to using these devices at the second stage as well. All the models were built using IPSEpro software and figures 5-26 to 5-30 show schematic illustrations of these models. The standard RO model was validated against operational data as discussed in section 4.5.
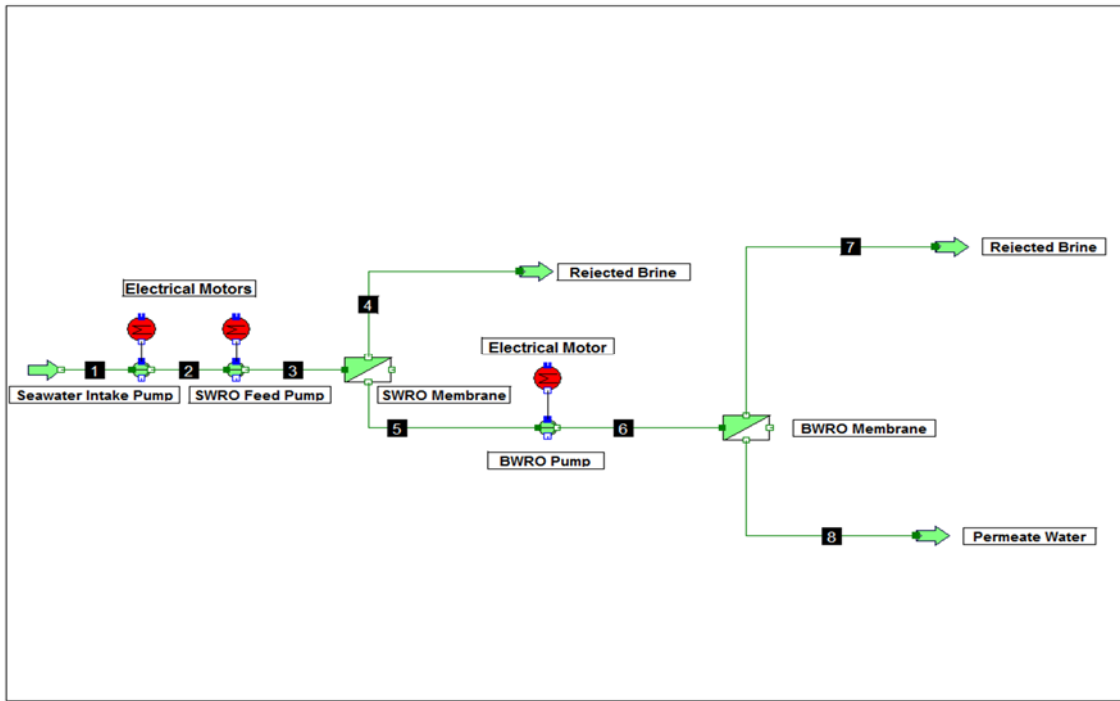
Figure 5-26: IPSEpro model for standard two-pass
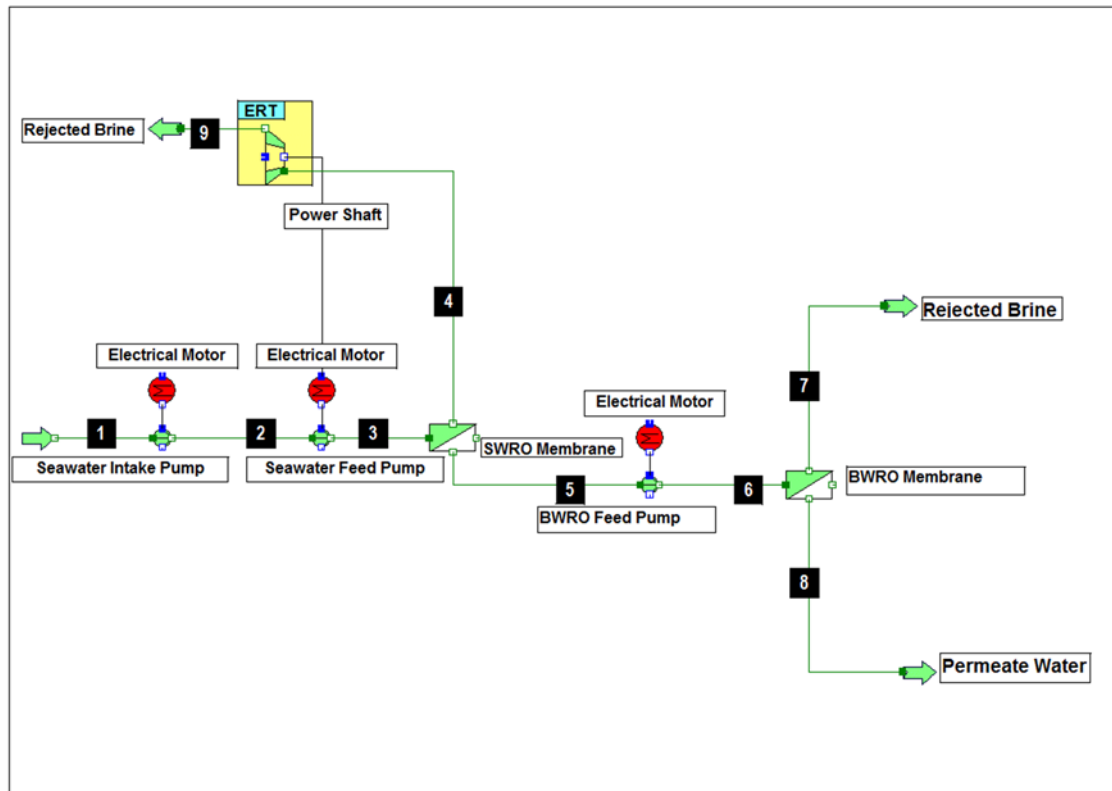
Figure 5-27: IPSEpro model for two-pass RO with ERT on first stage
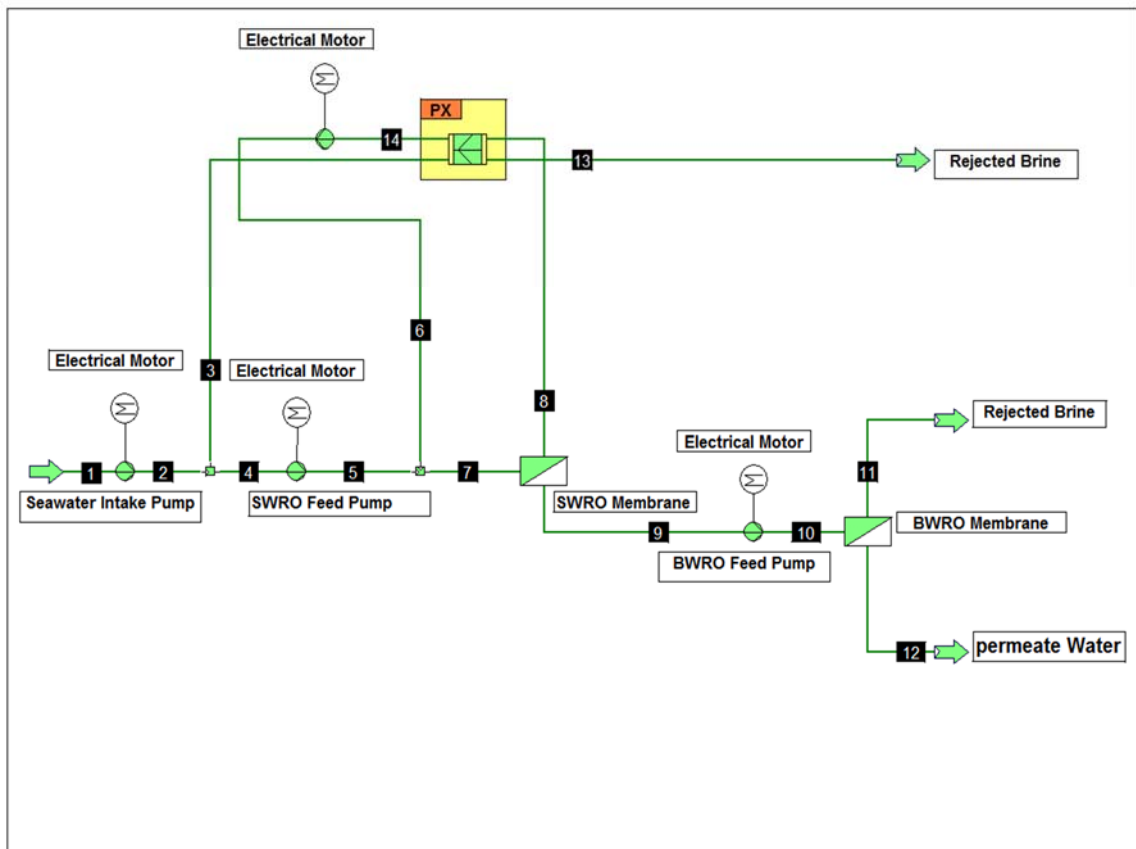
Figure 5-28: IPSEpro model for two-pass RO with PX on the first stage
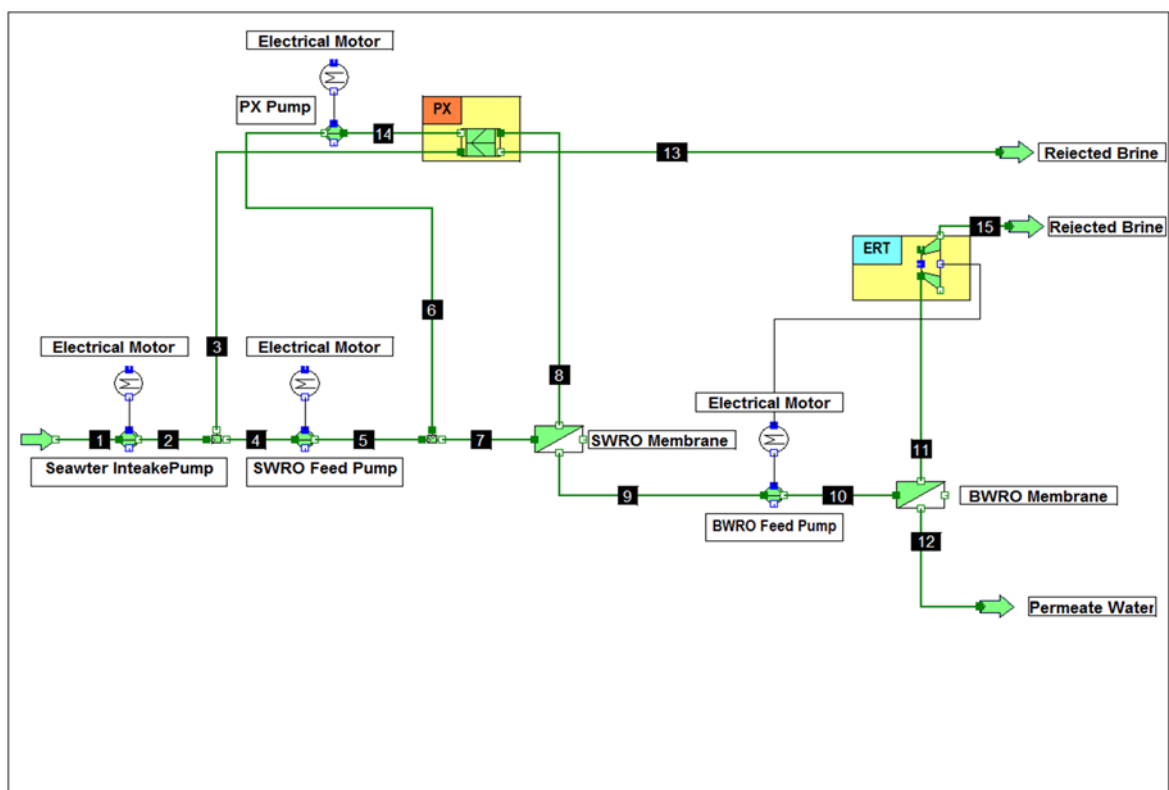
Figure 5-29: IPSEpro model for two-pass RO with PX (1st. stage) + ERT (2nd. Stage)

Figure 5-30: IPSEpro model for two-pass RO with PX (1st. stage) + PX (2nd. Stage)

5.2.2.1 Comparison of RO energy recovery options

Using the model validated (Section 4.6) 8 parallel trains were used to produce 24000 t/day of fresh water for a local community. Tables 5-3 to 5-7 show the calculated thermodynamic properties for all of the numbered streams in Figures 5-26 to 5-30 respectively. It is worth mentioning that the exergy rates for all streams for RO models are positive since they are above the dead state condition as in the findings of Sharqawy et al [100]. In the current exergy analysis, the dead state has been selected at values of $P_0 = 101.3$kPa, $w_{s,0} = 37$ g/kg, and $T_0 = 20°C$, which matches the seawater intake parameters [176]. On other the hand, these values could end with negative values even though they are above the dead state values if the seawater is assumed to be an ideal mixture [62, 101]. Tables 5-8 to 5-12 were used to calculate the exergy efficiency and exergy destruction for each component in the system and for the whole system using equations 3.22 and 3.23.

The input exergy to the system is the pump work input, where pump efficiency is assumed to be typically 80% [36, 100]. The output minimum separation work (for the exergy efficiency) is the sum of the discharge distillate and rejected brine relative to the exergy of the sea water feed entering the unit. The last three streams (4-A, 7-A, 8-A in table 5.3; 7-A, 8-A, 9-A in table 5.4; and 11-A, 12-A, 13.A in table 5.5, 12-A, 13-A,

15-A in table 5-6 and 18-A, 19-A, 20-A in table 5-7) represent the residual exergy when they move to the dead state at (P_0, T_0) to calculate the minimum separation work (W_{min}).

Initially, the study focuses on improving the performance of RO desalination by reducing the power consumption of the first stage of the SWRO membrane by energy recovery (PX or ERT, figures 5-27 and 5-28). The simulation results show that the total power consumption of the standard SWRO desalination is reduced from 8420 kW to 5930 kW and 5250 kW respectively, with ERT and PX (Table 5-3). As a result of using ERT and PX in the first stage of RO desalination system the improvements in the specific power consumption of the SWRO per m^3 water are reductions from 7.2 kWh/m^3 to 5.1 kWh/m^3 and 3.6 kWh/m^3 respectively as shown in figure 5-32. These results are in agreement with those of previously published studies [41, 183, 184].

Table 5-3 Power consumption (kW)

RO technology with and without ERDs	Power consumption (kW)	
	SWRO	BWRO
Standard RO	8420	974
RO with ERT at the first stage	5930	974
RO with PX at the first stage	5250	974
RO with Px at the first stage and ERT at second stage	5250	773
RO with Px at the first and second stages	5250	637

However, the values of BWRO power consumption of the first three configurations remain at the same value of 974 kW as shown in table 5-3. Subsequently, in the fourth configuration PX was used in the first stage so the SWRO power consumption remains at 5250 kW, with ERT added at the second stage (figure 5-29) and in configuration five PX is used in both stages (figure 5-30). The results show that the power consumption of the second stage declines from 974 kW to 773 and 637 kW when ERT and PX, respectively, are used at the second stage. Using ERT or PX in the second stage for rejected brine reduces the specific consumption of BWRO from 1.01 kWh/m^3 to 0.80 and 0.66 kWh/m^3, respectively, as shown in figures 5-31 and 5-32. However this

thermodynamic improvement must be taken into account with the additional cost related to using ERT and PX in the unit to get the complete picture in section 7.5.
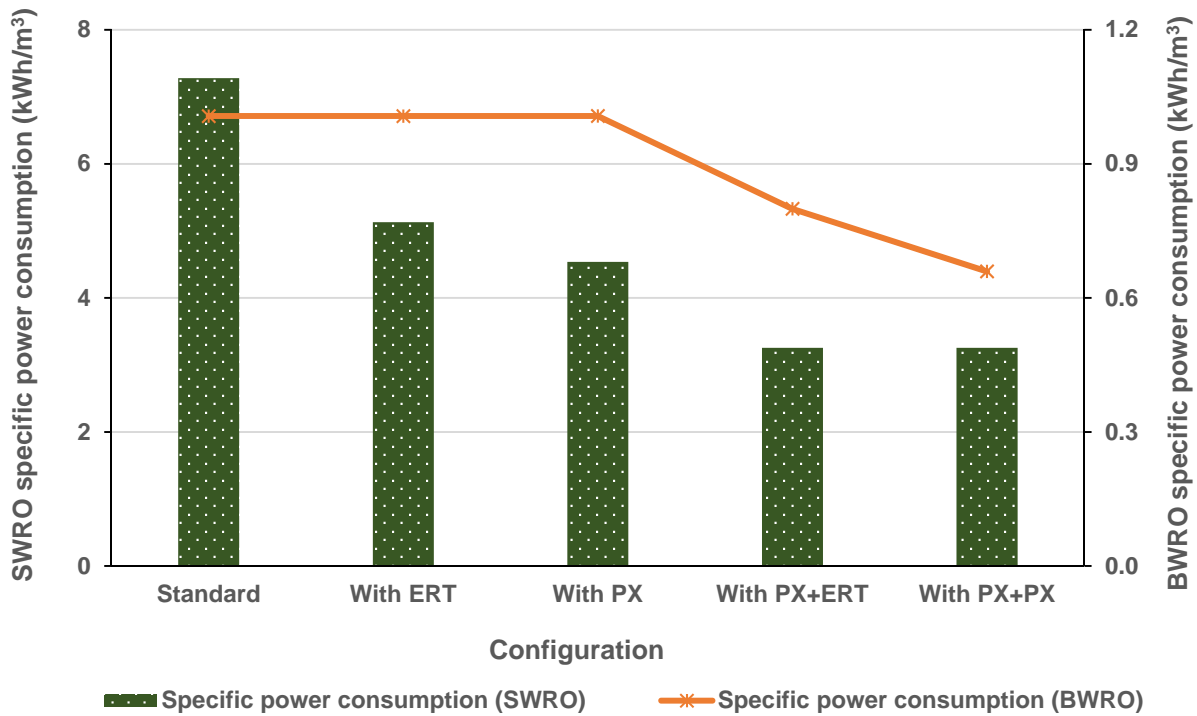
Figure 5-31: Specific power consumption for SWRO and BWRO with energy recovery options

Figure 5-32 shows the total specific power consumption SWRO and BWRO of the five configurations, which was reduced from 8.2 kWh/m^3 in the standard configuration to 4.5 kWh/m^3 with PX at both stages, because the pump power was reduced.
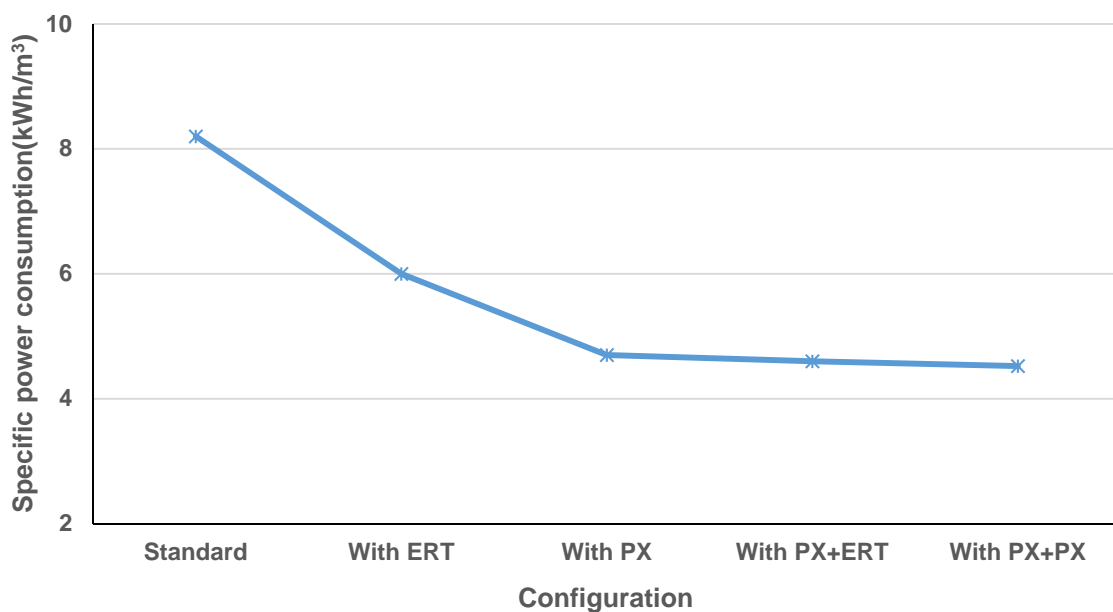
Figure 5-32 Total specific power consumption for SWRO and BWRO membrane

Figure 5-33 shows the exergy efficiency and exergy destruction of the five different RO configurations, where the exergy efficiency is calculated from the stream exergy values in tables 5-4 to 5-8. The results show that significant increases in exergy efficiency and declines in exergy destruction occur when ERT and PX are used in the first stage of SWRO, because the rejected pressure at the first stage is high at 62 bar which can be converted to power by ERT or the feed pressure increased by PX. This improvement is only slightly increased when ERT or PX is used in the second stage BWRO as can been seen in figure 5-33 because the rejected pressure of BWRO is lower at only 17 bar.
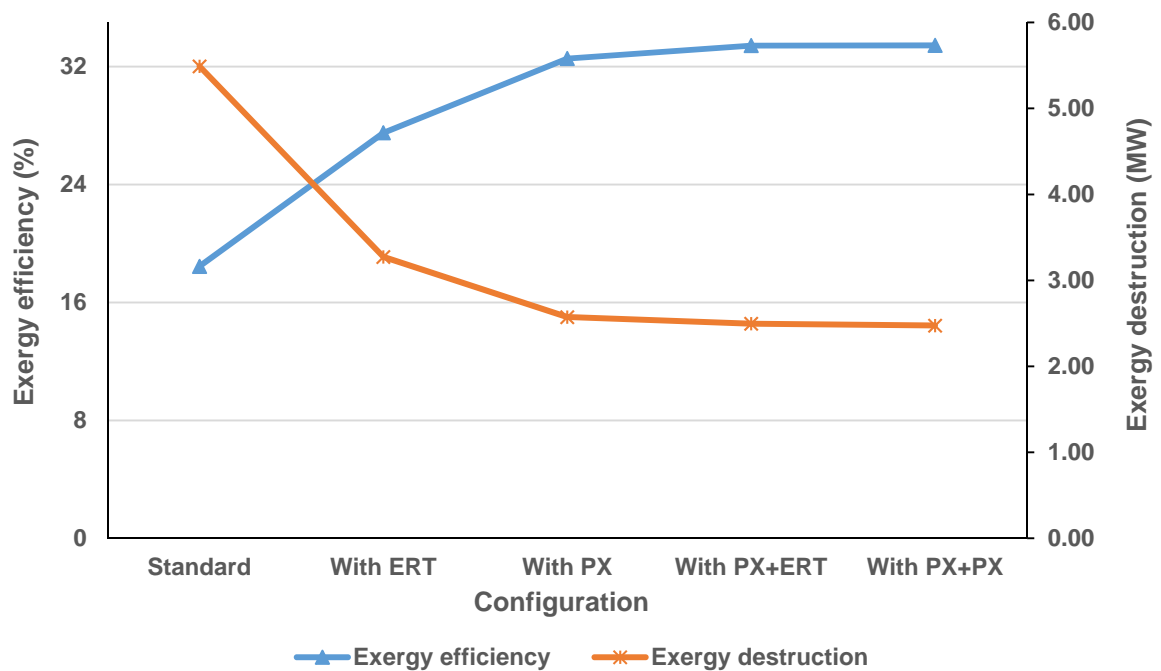
Figure 5-33: Exergy efficiency and exergy destruction for two-pass RO at different configurations

Table 5-4: Simulation results for the thermodynamic properties of the streams indicated in Figure 5.26 for standard RO desalination

Stream No.	Mass flow $\dot{m}$ (kg/s)	Temperature T (°C)	Pressure P (kPa)	Salinity w_s (g/kg)	Specific exergy e_T (kJ/kg)	Total exergy $\dot{E}_T$ (MW)
1	726.2	20.0	101.3	37	0.105	0.076
2	726.2	20.0	150.0	37	0.050	0.036
3	726.2	20.5	6500.0	37	6.234	4.527
4	399.4	20.5	6200.0	67	6.649	2.656
5	326.8	20.5	200.0	0.000	2.874	0.939
6	326.8	20.6	1800.0	0.000	4.477	1.463
7	49.0	20.6	1700.0	3	3.908	0.192
8	277.8	20.6	150.0	0.000	2.913	0.809
4-A	399.4	20.0	101.3	67	0.841	0.336
7-A	49.0	20.0	101.3	3	2.308	0.113
8-A	277.8	20.0	101.3	0.000	2.862	0.795

Table 5-5: Simulation results for the thermodynamic properties of the streams indicated in Figure 5.27 for RO desalination with ERT

Stream No.	Mass flow $\dot{m}$ (kg/s)	Temperature T (°C)	Pressure P (kPa)	Salinity w_s (g/kg)	Specific exergy e_T (kJ/kg)	Total exergy $\dot{E}_T$ (MW
1	726.2	20	101.3	37.0	0.000	0.000
2	726.2	20.0	150	37.0	0.047	0.034
3	726.2	20.5	6500	37.0	6.232	4.526
4	399.4	20.5	6200	66.8	6.652	2.657
5	326.8	20.5	200	0.485	2.865	0.936
6	326.8	20.6	1800	0.485	4.469	1.460
7	49.0	20.6	1700	3.18	3.899	0.191
8	277.8	20.6	150	0.01	2.904	0.807
9	399.4	20.5	150	66.8	0.886	0.354
7-A	49.0	20.0	101.3	3.18	2.299	0.113
8-A	277.8	20.0	101.3	0.01	2.853	0.792
9-A	399.4	20	101.3	66.9	0.845	0.337

Table 5-6: Simulation results for the thermodynamic properties of the streams indicated in figure 5.28 for RO desalination with PX

Stream No.	Mass flow $\dot{m}$ (kg/s)	Temperature T (°C)	Pressure P (kPa)	Salinity w_s (g/kg)	Specific exergy e_T (kJ/kg)	Total exergy $\dot{E}_T$ (MW)
1	725.2	20.0	101.3	37.0	0.0	0.0
2	725.2	20.0	150.0	37.0	0.0	0.0
3	389.8	20.0	150.0	37.0	0.0	0.0
4	335.5	20.0	150.0	37.0	0.0	0.0
5	335.5	20.5	6500.0	37.0	6.2	2.1
6	390.7	20.1	6500.0	37.0	6.2	2.4
7	726.2	20.3	6500.0	37.0	6.2	4.5
8	399.4	20.3	6200.0	66.9	6.7	2.7
9	326.8	20.3	200.0	0.5	2.9	0.9
10	326.8	20.4	1800.0	0.5	4.5	1.5
11	49.0	20.4	1700.0	3.2	3.9	0.2
12	277.8	20.4	150.0	0.0	2.9	0.8
13	398.4	20.3	147.4	66.9	0.9	0.4
14	390.7	20.1	5900.0	37.0	5.6	2.2
11-A	49.0	20.4	150.0	3.2	2.3	0.1
12-A	277.8	20.0	101.3	0.0	2.9	0.8
13-A	398.4	20.0	101.3	66.9	0.8	0.3

Table 5-7: Simulation results for the thermodynamic properties of the streams indicated in Figure 5.29 for RO desalination with PX + ERT

Stream No.	Mass flow $\dot{m}$ (kg/s)	Temperature T (°C)	Pressure P (kPa)	Salinity w_s (g/kg)	Specific exergy e_T (kJ/kg)	Total exergy $\dot{E}_T$ (MW)
1	725.2	20.0	101.3	0.0	0.0	0.0
2	725.2	20.0	150.0	0.0	0.0	0.0
3	389.8	20.0	150.0	0.0	0.0	0.0
4	335.5	20.0	150.0	0.0	0.0	0.0
5	335.5	20.5	6500.0	0.0	6.2	2.1
6	390.7	20.1	6500.0	0.0	6.2	2.4
7	726.2	20.3	6500.0	0.0	6.2	4.5
8	399.4	20.3	6200.0	0.1	6.7	2.7
9	326.8	20.3	200.0	0.0	2.9	0.9
10	326.8	20.4	1800.0	0.0	4.5	1.5
11	49.0	20.4	1700.0	0.0	3.9	0.2
12	277.8	20.4	150.0	0.0	2.9	0.8
13	398.4	20.3	147.4	0.1	0.9	0.4
14	390.7	20.1	5900.0	0.0	5.6	2.2
15	49.0	20.4	150.0	0.0	2.3	0.1
12-A	277.8	20.0	101.3	0.0	2.9	0.8
13-A	398.4	20.0	101.3	0.1	0.8	0.3
15-A	49.0	20.0	101.3	0.0	2.3	0.1

Table 5-8: Simulation results for the thermodynamic properties of the streams indicated in Figure 5.30 for RO desalination with PX + PX

Stream No.	Mass flow $\dot{m}$ (kg/s)	Temperature T (°C)	Pressure P (kPa)	Salinity w_s (g/kg)	Specific exergy e_T (kJ/kg)	Total exergy $\dot{E}_T$ (MW)
1	725.1	20.0	101.3	37.00	0.000	0.000
2	725.1	20.0	150.0	37.00	0.047	0.034
3	389.7	20.0	150.0	37.00	0.047	0.018
4	390.7	20.1	5900.0	37.00	5.649	2.207
5	335.4	20.5	150.0	37.00	0.045	0.015
6	335.4	20.5	6500.0	37.00	6.232	2.090
7	390.7	20.1	6500.0	37.00	6.233	2.435
8	726.1	20.3	6500.0	37.00	6.232	4.526
9	399.4	20.3	6200.0	66.88	6.654	2.657
10	326.8	20.3	150.0	0.47	2.817	0.920
11	277.9	20.3	150.0	0.47	2.817	0.783
12	48.9	20.3	150.0	0.47	2.817	0.138
13	48.9	20.3	1650.0	0.47	4.319	0.211
14	48.9	20.3	1800.0	0.47	4.470	0.219
15	277.9	20.4	1800.0	0.47	4.470	1.242
16	326.8	20.4	1800.0	0.47	4.470	1.461
17	49.0	20.4	1700.0	3.11	3.909	0.192
18	277.8	20.4	150.0	0.01	2.903	0.806
19	49.0	20.4	121.1	3.11	2.331	0.114
20	398.4	20.3	147.4	66.96	0.889	0.354
18-A	277.8	20.0	101.3	0.01	2.853	0.792
19-A	49.0	20.0	101.3	3.11	2.310	0.113
20-A	398.4	20.0	101.3	66.96	0.849	0.338

Table 5-9: Standard RO desalination standard exergy analysis results

Equipment	Calculation method	Result	unit
Seawater pump exergy in	$E_2 - E_1$	0.034	MW
SWRO feed pump exergy in	$E_3 - E_2$	4.488	MW
BWRO feed pump exergy in	$E_6 - E_5$	0.524	MW
Pumps input exergy in	$E_{pp} = (1/0.75) \times (\sum((E_2 - E_1) + (E_3 - E_2) + (E_6 - E_5)))$	5.046	MW
Minimum separation work	$W_{min} = E_{(4-A)} + E_{(7-A)} + E_{(8-A)}$	1.274	MW
Exergy efficiency	$\eta = \dfrac{W_{min}}{\dot{E}_{input}}$	18.450	%
Total exergy destruction	$E_d = E_{input} - E_{output}$	5.490	MW
Exergy destroyed in pumps	$E_{d,pp} = (1-0.75) \times E_{pp}$	1.683	MW
Exergy destroyed in SWRO membrane	$E_{d,SWRO} = E_3.E_4-E_5$	0.900	MW
Exergy destroyed in BWRO membrane	$E_{d,BWRO} = E_6 - E_7 - E_8$	0.462	MW
Rejected seawater disposal	$E_{d,RSWD} = (E_4-(E_{4-A}))$	2.316	MW
Rejected brackish water disposal	$E_{d,RBWD} = (E_7 - (E_{7-A}))$	0.078	MW
Product water disposal	$E_{d,PWD} = (E_8- (E_{8-A}))$	0.014	MW

Table 5-10: RO desalination with ERT exergy analysis results

Equipment	Calculation method	Result	unit
Seawater pump exergy in	$E_2 - E_1$	0.034	MW
SWRO RO feed pump	$E_3 - E_2$	4.492	MW
BWRO feed pump	$E_6 - E_5$	0.524	MW
Pump input exergy	$E_{PP} = \left(1/0.75\right) X \left(\Sigma\left((E_2 - E_1) + (E_3 - E_2) + (E_6 - E_5)\right)\right)$	5.049	MW
Exergy input from ERT	$E_{ERT} = W_{ERT}$	2.055	MW
Total exergy input	$E_{PP} - E_{ERT}$	6.733	MW
Minimum separation work	$W_{min} = E_{(7-A)} + E_{(8-A)} + E_{(9-A)}$	1.243	MW
Exergy efficiency	$\eta = \dfrac{W_{min}}{\dot{E}_{input}}$	27.514	%
Total exergy destruction	$E_d = E_{input} - E_{output}$	3.273	MW
Exergy destroyed in ERT	$E_{d,ERT} = E_4 - E_9 - W_{ERT}$	0.248	MW
Exergy destroyed in pumps	$E_{d,pp} = (1-0.75) \times E_{pp}$	1.683	MW
Exergy destroyed in SWRO membrane	$E_{d,SWRO} = E_3.E_4 - E_5$	0.932	MW
Exergy destroyed in BWRO membrane	$E_{d,BWRO} = E_6 - E_7 - E_8$	0.463	MW
Rejected seawater disposal	$E_{d,RSWD} = (E_9 - (E_{9-A}))$	0.017	MW
Rejected brackish water disposal	$E_{d,RBWD} = (E_7 - (E_{7-A}))$	0.078	MW
Product water disposal	$E_{d,PWD} = (E_8 - (E_{8-A}))$	0.0142	MW

Table 5-11: RO desalination with PX exergy analysis results

Equipment	Calculation method	Result	unit
Seawater pump exergy in	$E_2 - E_1$	0.034	MW
SWRO RO feed pump	$E_3 - E_2$	2.074	MW
BWRO feed pump	$E_6 - E_5$	0.524	MW
Pump input exergy	$E_{PP} = \left(1/0.75\right) X \left(\Sigma\left((E_2 - E_1) + (E_3 - E_2) + (E_6 - E_5)\right)\right)$	2.861	MW
Exergy input from PX	$E_{PX} = E_{PX}$		MW
Total exergy input	$E_{PP} - E_{PX}$		MW
Minimum separation work	$W_{min} = E_{(11-A)} + E_{(12-A)} + E_{(13.A)}$	1.241	kW
Exergy efficiency	$\eta = \dfrac{W_{min}}{\dot{E}_{input}}$	32.552	%
Total exergy destruction	$E_d = E_{input} - E_{output}$	2.573	MW
Exergy destroyed in PX	$E_{d,PX} = E_8 - E_{14} - E_{13} - W_{PX}$	0.116	MW
Exergy destroyed in pumps	$E_{d,PP} = (1 - 0.75) \times E_{pp}$	0.954	MW
Exergy destroyed in SWRO membrane	$E_{d,SWRO} = (E_7 - E_8 - E_9)$	0.932	kW
Exergy destroyed in BWRO membrane	$E_{d,BWRO} = E_{10} - E_{11} - E_{12}$	0.463	MW
Rejected seawater disposal	$E_{d,RSWD} = (E_{13} - (E_{13.A}))$	0.018	MW
Rejected brackish water	$E_{d,RBWD} = (E_{11} - (E_{11-A}))$	0.078	MW
Product water disposal	$E_{d,PWD} = (E_{12} - (E_{12-A})$	0.014	MW

Table 5-12: RO desalination with PX + ERT exergy analysis results

Equipment	Calculation method	Result	unit
Seawater pump exergy in	$E_2 - E_1$	0.034	MW
SWRO RO feed pump	$E_3 - E_2$	2.074	MW
BWRO feed pump	$E_6 - E_5$	0.524	MW
Pump input exergy	$E_{PP} = \left(1/0.75\right) X \left(\sum\left((E_2 - E_1) + (E_3 - E_2) + (E_6 - E_5)\right)\right)$	2.861	MW
Minimum separation work	$W_{min} = E_{(11-A)} + E_{(12-A)} + E_{(13.A)}$	1.241	kW
Exergy efficiency	$\eta = \dfrac{W_{min}}{\dot{E}_{input}}$	33.429	%
Total exergy destruction	$E_d = E_{input} - E_{output}$	2.496	MW
Exergy destroyed in PX	$E_{d, PX} = E_8 - E_{14} - E_{13} - W_{PX}$	0.116	MW
Exergy destroyed in pumps	$E_{d,PP} = (1 - 0.75) \times E_{pp}$	0.954	MW
Exergy destroyed in SWRO membrane	$E_{d,SWRO} = (E_7 - E_8 - E_9)$	0.932	kW
Exergy destroyed in BWRO membrane	$E_{d,BWRO} = E_{10} - E_{11} - E_{12}$	0.463	MW
Rejected seawater disposal	$E_{d,RSWD} = (E_{13} - (E_{13.A}))$	0.018	MW
Rejected brackish water	$E_{d,RBWD} = (E_{11} - (E_{11-A}))$	0.078	MW
Product water disposal	$E_{d, PWD} = (E_{12} - (E_{12-A})$	0.014	MW

Table 5-13: RO desalination with PX + PX exergy analysis results

Equipment	Calculation method	Result	unit
Seawater pump exergy in	$= E_2 - E_1$	0.034	MW
SWRO RO feed pump	$= E_3 - E_2$	2.074	MW
BWRO feed pump	$= E_6 - E_5$	0.445	MW
Total exergy input	E_{pp}	2.788	MW
Minimum separation work	$W_{min} = E_{(7-A)} + E_{(8-A)} + E_{(9-A)}$	1.243	MW
Exergy efficiency	$\eta = \dfrac{W_{min}}{\dot{E}_{input}}$	33.442	MW
Total exergy destruction	$= E_{input} - E_{output}$	2.474	MW
Exergy destroyed in PX1	$E_d = E_3 + E_9 - E_4 - E_{20}$	0.115	MW
Exergy destroyed in PX2	$E_d = E_{12} + E_{17} - E_{13} - E_{19}$	0.004	
Exergy destroyed in pumps	$E_{d,pp} = (1-0.75) \times E_{pp}$	0.929	MW
Exergy destroyed in SWRO membrane	$E_{d,SWRO} = E_3.E_4 - E_5$	0.932	MW
Exergy destroyed in BWRO membrane	$E_{d,BWRO} = E_6 - E_7 - E_8$	0.463	MW
Rejected seawater disposal	$E_{d,RSWD} = (E_9 - (E_{9-A}))$	0.016	MW
Rejected brackish water disposal	$E_{d,RBWD} = (E_7 - (E_{7-A}))$	0.001	MW
Distillate water	$E_{d,PWD} = (E_8 - (E_{8-A}))$	0.014	MW

5.2.2.2 Parametric study

The parametric studies investigate the influence of a number of parameters varied around the design conditions: a) feed water salinity, b) feed water temperature and c) recovery ratio d) SWRO high pressure pump feed pressure and e) pump efficiency. The main purpose of this section to find how RO is affected by these parameters.

Effects of environmental, (a) feed water salinity and (b) temperature

The effect of increases in feed water salinity on exergy efficiency (Table 5-14) and specific power consumption (Figure 5-34) with a recovery ratio of 45% and a feed water temperature of 20°C for different configurations shows an increase in power consumption but also improvements in exergy efficiency [61]. This, however, does not encourage the use of high seawater salinity due to higher corrosion in RO plant pipes and membranes. The impact on the specific power consumption/m^3 showed that, as sea water salinity increases, the specific power consumption increases by about 3.0% for each 2 g/kg due to the increase in osmotic pressure which requires more power.

Table 5-14: Effect of feed water salinity on exergy efficiency for different RO configurations at 45% and 20°C

Feed water salinity (g/kg)	30	32	34	36	38	40
Exergy efficiency	(%)					
Standard	14.7	15.9	16.9	18.0	19.0	20.0
With ERT	21.9	23.6	25.2	27.0	28.3	30.0
With PX	26.1	28.1	30.0	31.8	33.4	35.0
With PX + ERT	26.6	28.6	31.0	32.4	34.1	35.6
With PX + PX	27.2	29.3	31.3	33.2	35.1	36.7
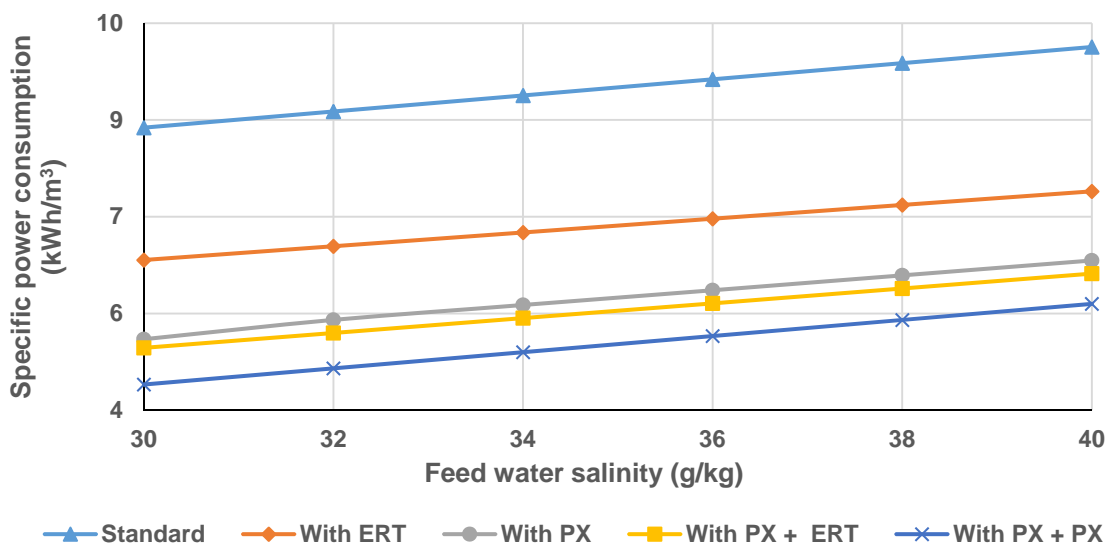
Figure 5-34: Effect of seawater salinity on specific power consumption at a recovery ratio of 45% and 20°C in different configurations

Feed water temperature is the most noticeable environmental condition affecting the performance of RO systems. The effect of seawater feed temperature on exergy efficiency, specific power consumption/m³ and recovery ratio was investigated. The results showed that, as feed water temperature increases mechanisms such as water viscosity decline and the structure of the membrane changes due to increases in pore diameter, leading to water passing more easily through the membrane. This leads to an increase in recovery ratio. So the exergy efficiency increases and specific power consumption reduces due to decreasing exergy destruction and increased minimum separation work, as confirmed in figures 5-35 to 5-37.
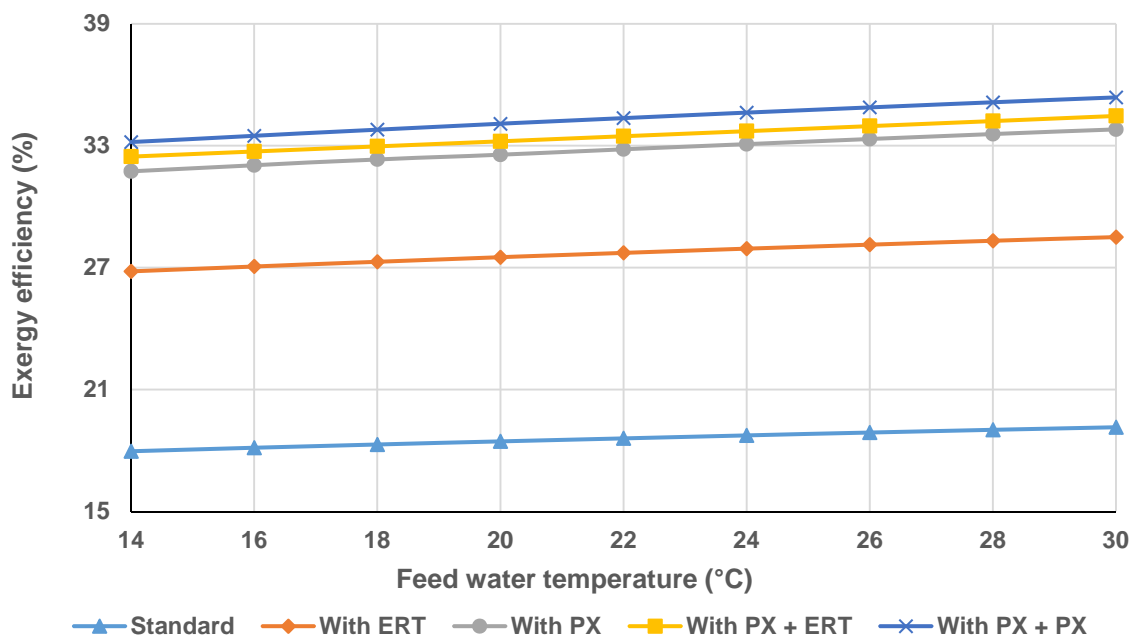
Figure 5-35: Effect of seawater temperature on exergy efficiency at five different configurations for 37g/kg salinity
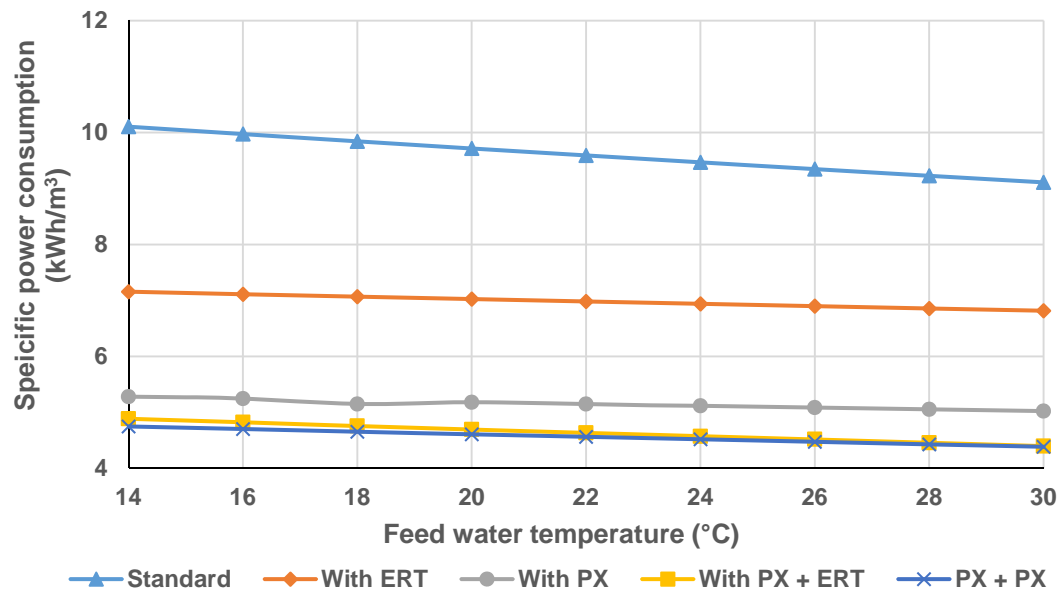
Figure 5-36: Effect of sea water temperature on specific power consumption at different configurations for 37 g/kg salinity
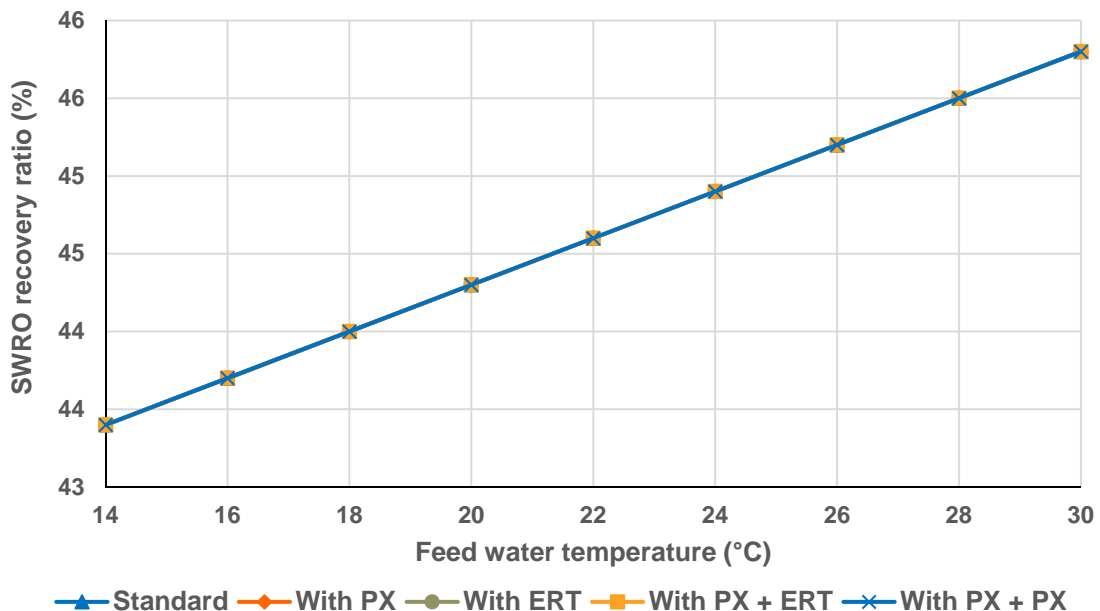
Figure 5-37: Effect of feed temperature on SWRO recovery ratio for different configurations

Figure 5-38 shows that, as feed water temperature increases, so does permeate flow, but also permeate salinity. This is reflected by salt passage rise with increasing seawater temperature, but salt rejection decline as shown in figure 5.39. This is because of the changes in the membrane pores and a decline in water viscosity and these results agree with those of other publications [10, 64, 185, 186].
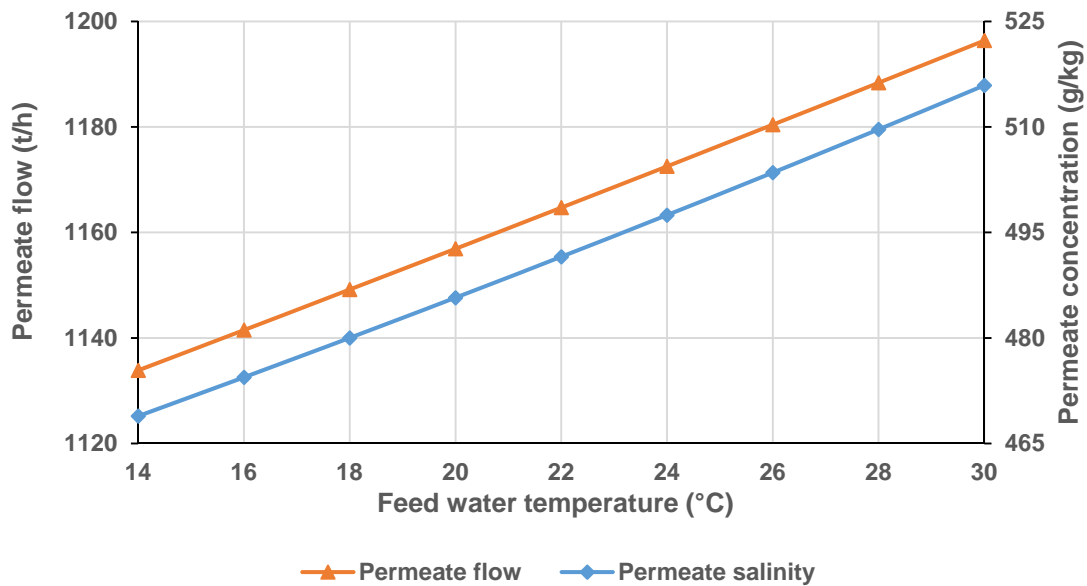
Figure 5-38: Effect of feed water temperature on permeate flow and concentration on SWRO for 20°C and 45% recovery ratio
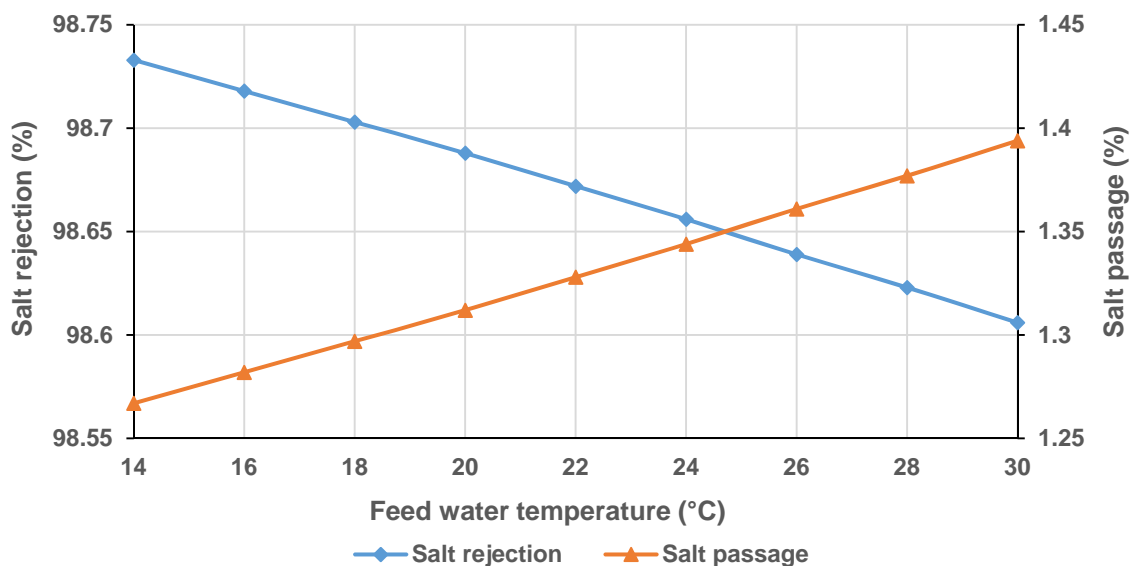
Figure 5-39: Impact of feed seawater temperature on SWRO salt passage and rejection

5.2.3 *Effect of plant design SWRO (a) recovery ratio (b) high pressure pump feed pressure and (c) efficiency*

The recovery ratio is defined as the percentage of membrane system feed water that emerges from the system as product water or permeate. Membrane system design is based on expected feed water quality and recovery is fixed through the initial adjustment of the valves on the concentrate stream. The influence of recovery ratio

varying from 40% to 60% on exergy efficiency for the five configurations is that the exergy efficiency relative increases by about 11% for every 5% increase in recovery ratio (Figure 5-40) due to the decrease in exergy destruction (Figure 5-41). Exergy efficiency is improved with all the energy recovery configurations compared to the standard RO. Although the highest value is for PX + PX, this is not significantly better than with PX alone see (Figures 5-42 and 5-43. Consequently, the total power consumption (SWRO + BWRO) declined from 9.6 kWh/m^3 with the standard plant to 7.1, 6.4, 4.7 and 4.5 kWh/m^3 with ERT, PX, PX + ERT and PX + PX, respectively, at a recovery ratio of 45%, as shown in figure 5-42 and this result agrees with those of previous studies [10, 37].

It's clear from these results that as the recovery ratio is increased all the options are better.
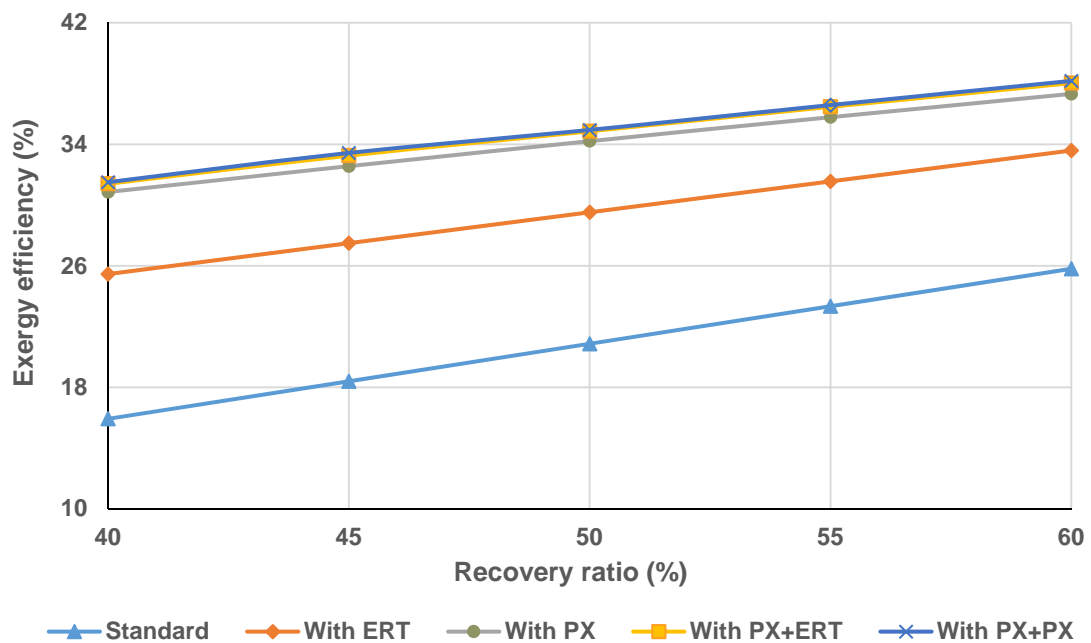
Figure 5-40: Effect of the recovery ratio on exergy efficiency at five different configurations for 37 g/kg and 20°C
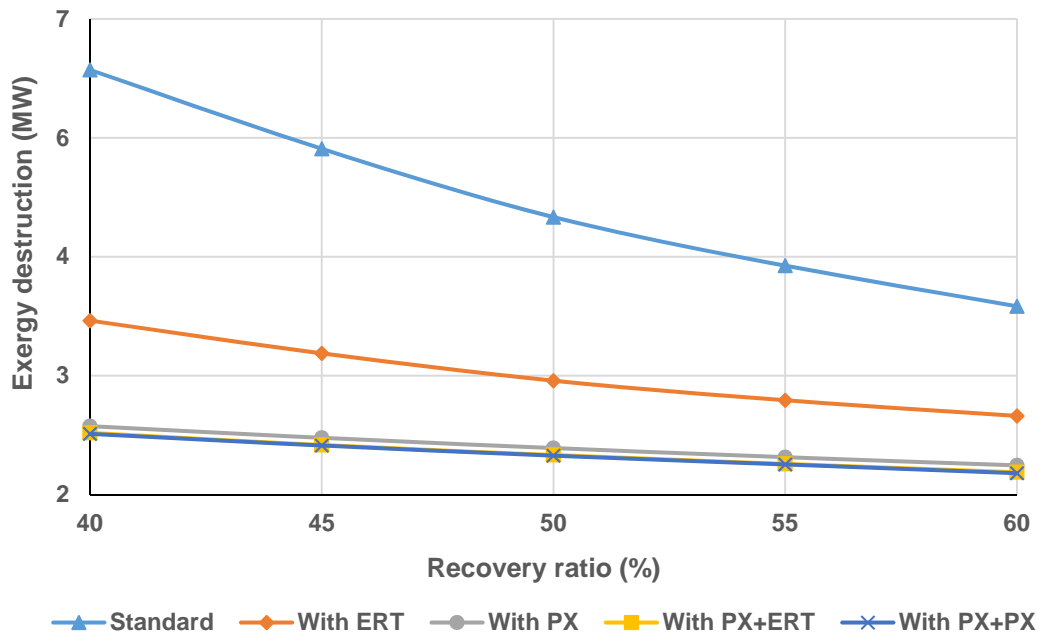
Figure 5-41: Effect of the recovery ratio on exergy destruction at five different configurations for 37 g/kg and 20°C
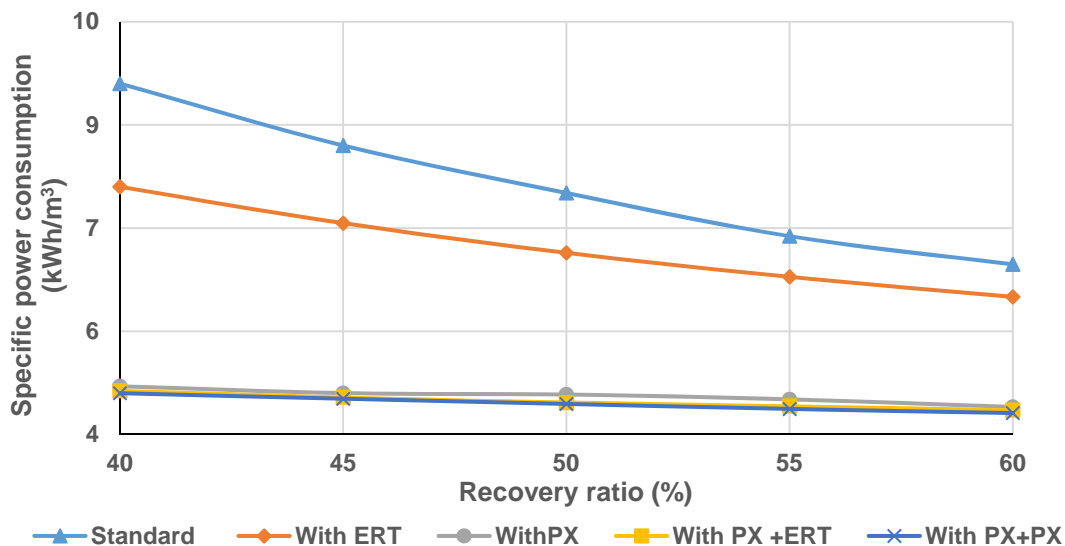
Figure 5-42: Effect of recovery ratio on power consumption at five different configurations for 37 g/kg and 20°C

The applied pressure is one of the parameters which affects RO membrane performance. Figure 5-43 illustrates the relationship between first stage feed pressure and the specific power consumption at constant temperature and salinity (20°C and 37g/kg), where the pressure at the second stage remains constant at 18 bar. As would be expected, as the feed pressure increases the specific power consumption increases by an average 7% with every 5 bar of pressure increase. Also the permeate flux increases from 3.1 to 12.9 (l/m^2/h) when the feed pressure change from 50 bar to 75 bar, as seen in figure 5-44. In addition, figure 5-45 shows that the salt rejection

increases non-linearly from 96.4% to 99.1% when the feed pressure increases from 50 bar to 75 bar. These results are in agreement with previous findings [10, 154, 185].
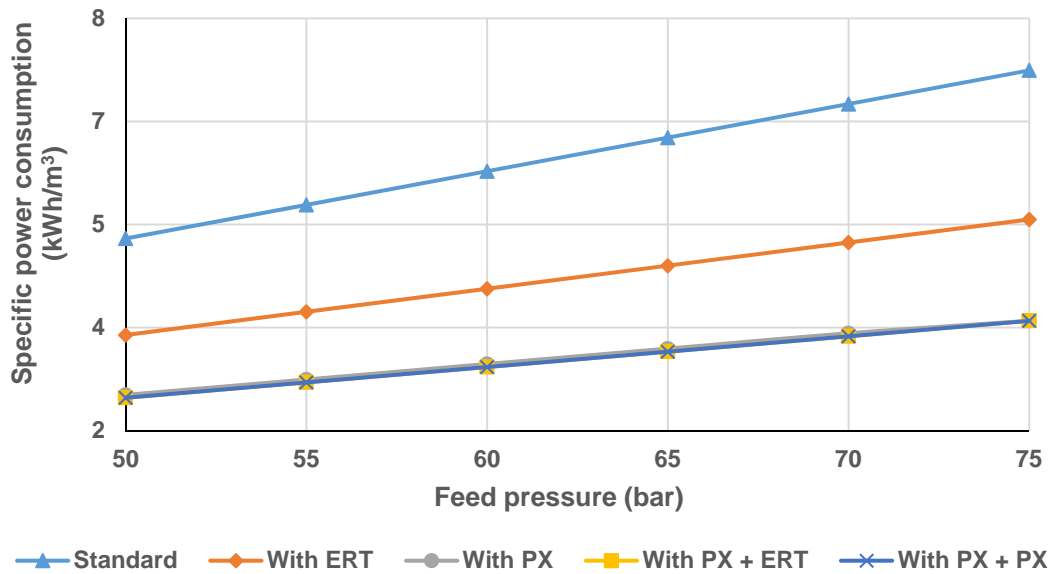
Figure 5-43: Effect of SWRO pump feed pressure on specific power consumption at different configurations for 37 g/kg salinity and 20°C
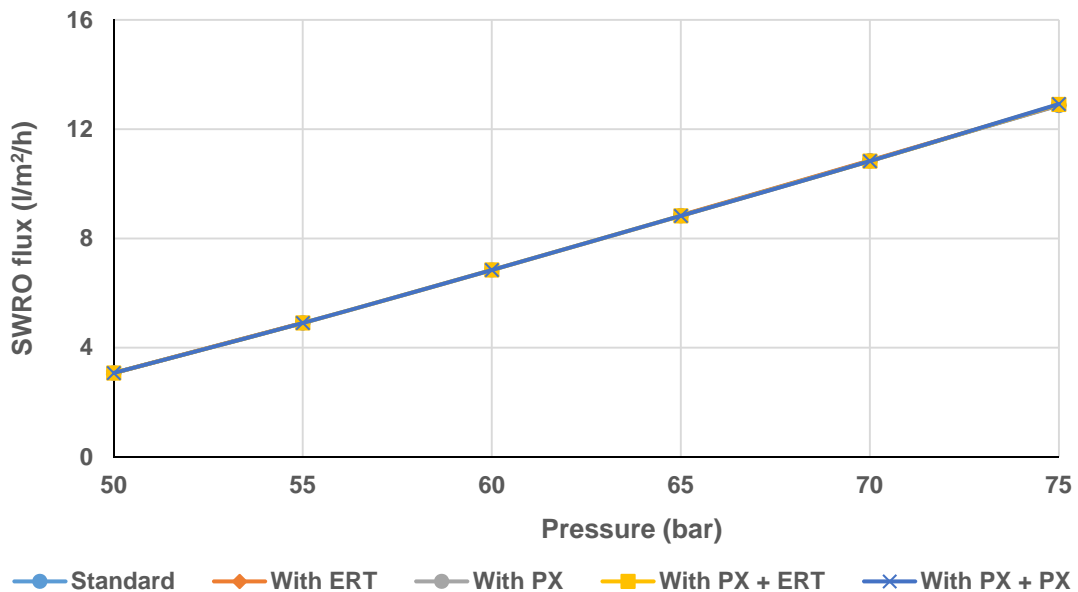
Figure 5-44: Effect of SWRO pump feed pressure on SWRO flux at different configurations for 37 g/kg salinity and 20°C
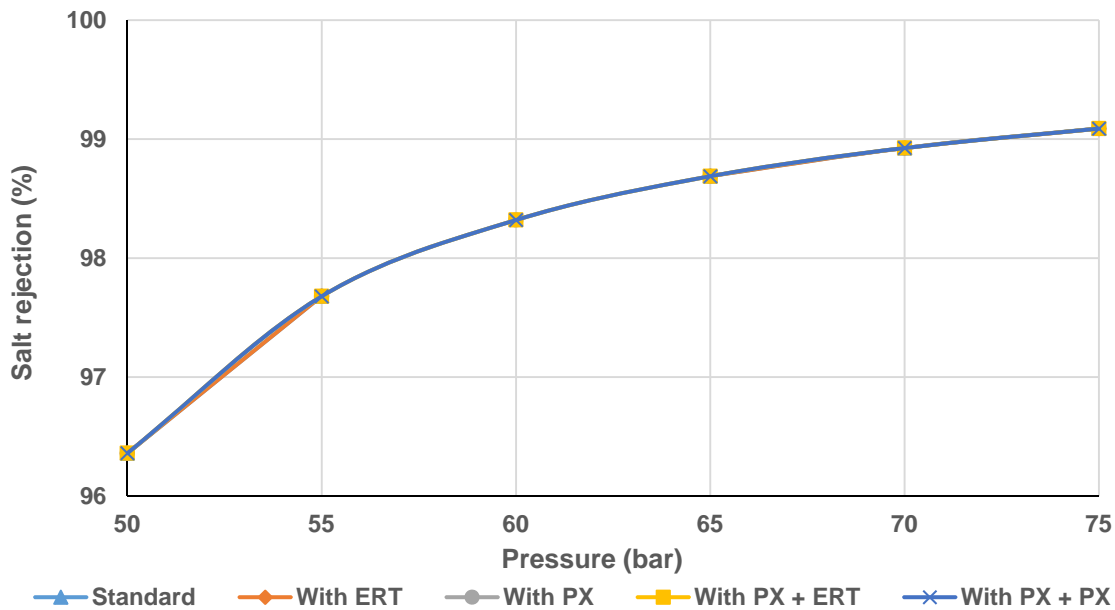
Figure 5-45: Effect of SWRO pump feed pressure on salt rejection at different configurations for 37 g/kg salinity and 20°C

On the other hand the exergy efficiency reduces by an average of about 5% for every 5 bar pressure increase as seen in figure 5-46. This is due to more pump exergy input to the system. Also the required membrane area (Figure 5-47) and solute concentration (Figure 5-48) decline non-linearly with feed pressure increase.
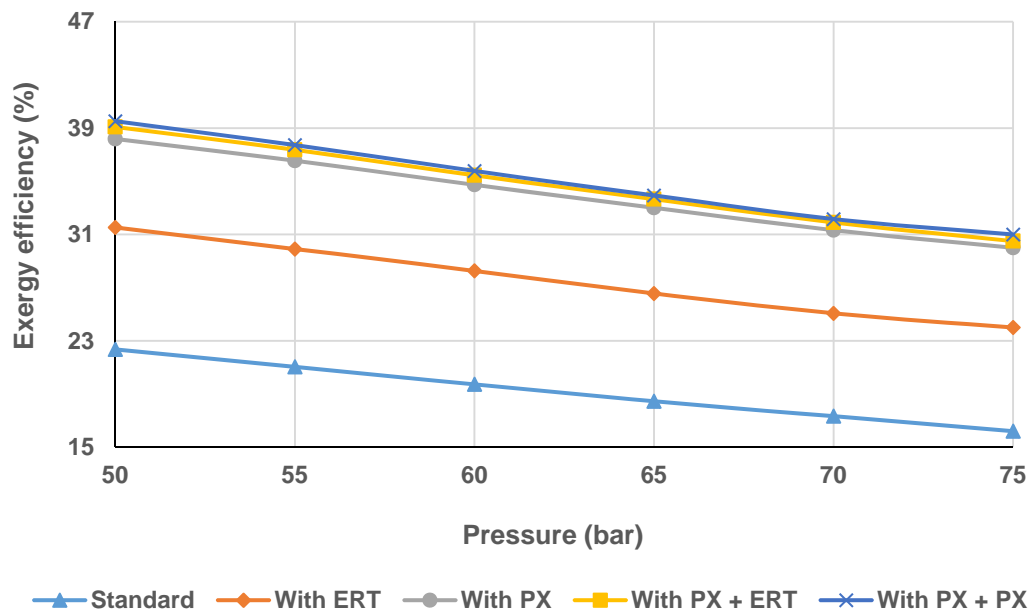
Figure 5-46: Effect of SWRO pump feed pressure on exergy efficiency at different configurations at 37 g/kg salinity and 20°C
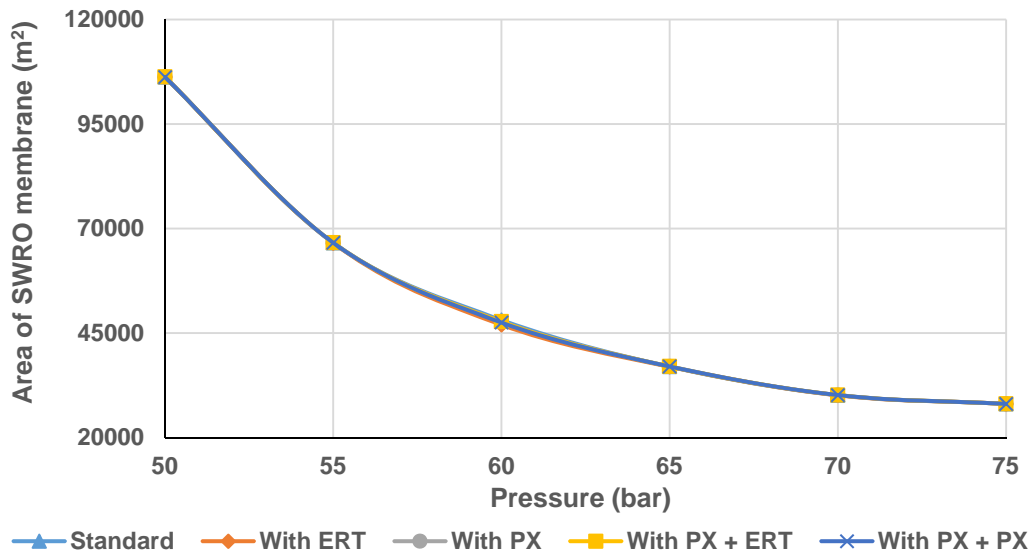
Figure 5-47: Effect of SWRO pump feed pressure on required SWRO membrane area at different configurations at 37 g/kg salinity and 20°C
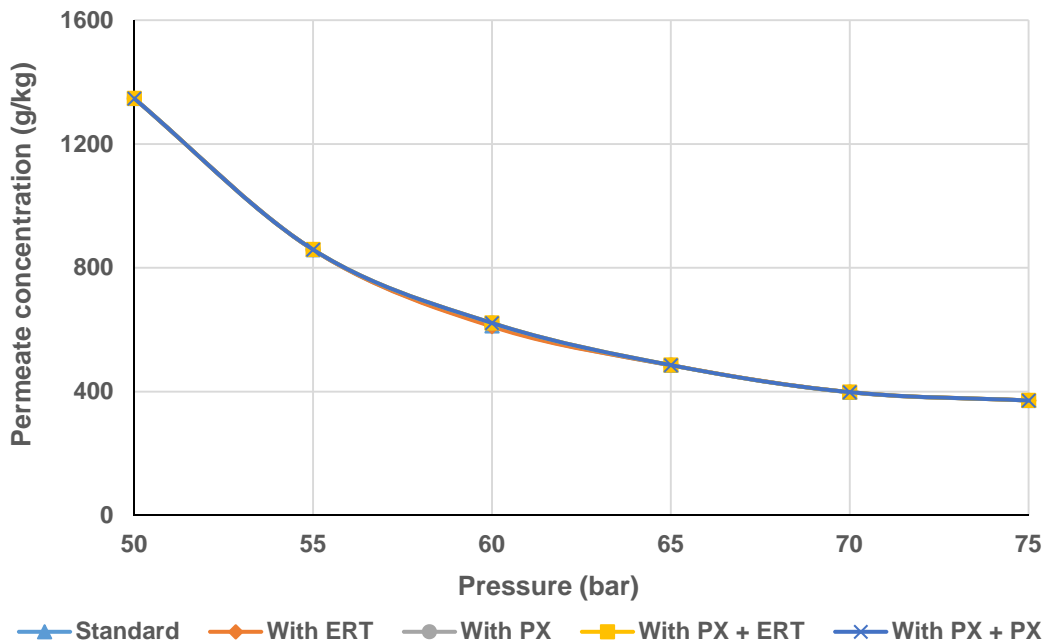
Figure 5-48: Effect of SWRO pump feed pressure on permeate concentration at different configurations for 37 g/kg salinity and 20°C

Figure 5-49 shows that, by raising the high pressure pump (SWRO pump) efficiency, the specific power consumption is greatly reduced because the high pressure pump has high energy consumption [40]. However, the exergy efficiency remains steady, because as the exergy increases so also the minimum work separation increases (Figure 5-50).
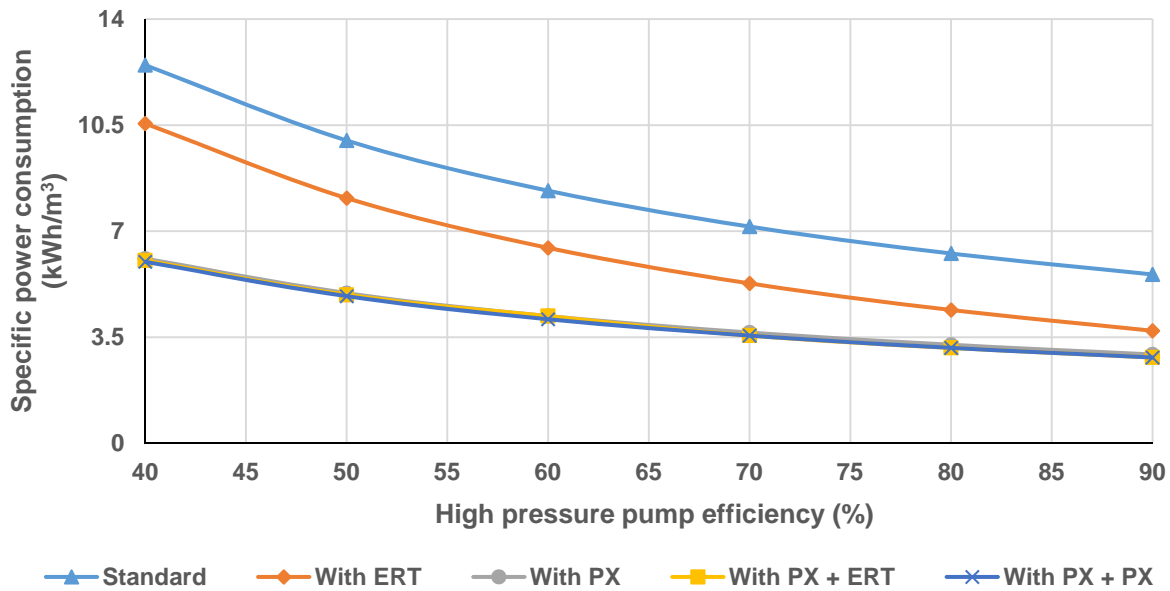
Figure 5-49: Effect of SWRO pump efficiency on SWRO specific power consumption at different configurations for 37 g/kg salinity and 20°C
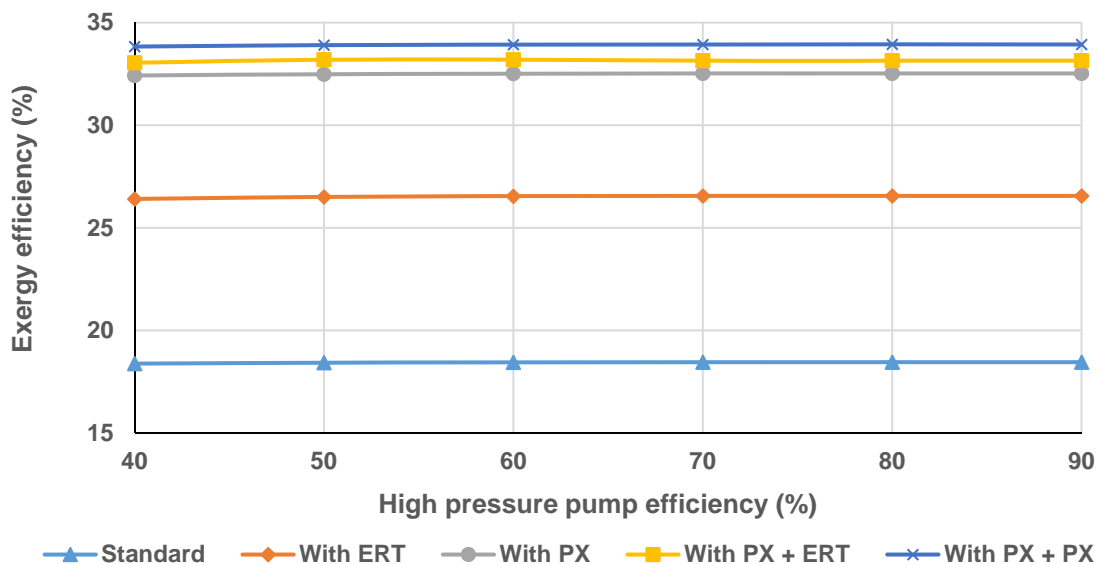
Figure 5-50: Effect of SWRO pump efficiency on SWRO exergy efficiency at different configurations for 37 g/kg salinity and 20°C

5.2.3.1 Comparison between MED-TVC and RO

Table 5-15 shows the comparison between Multi Effect Desalination with Thermal Vapour Compression (MED-TVC) and two-pass Reverse Osmosis (RO) plants, producing 24,000 m³/day fresh water from seawater with average seawater temperature and salinity of 20°C and 37 g/kg respectively. Parameters which can be used for thermodynamic comparison are exergy efficiency, exergy destruction and power consumption. However, the main inputs differ as electricity and thermal steam

whereas the outputs of fresh water are the same in both cases. The MED-TVC consumed about 48 kg/s steam flow which is produced by a separate boiler or extracted from power plant as in the present study. This will reduce the power plant electrical output by about 22.5MW plus about 430kW for the pumps, whereas the two-pass RO consumed only electricity with a maximum 9.4MW in the standard configuration.

The results show that the exergy efficiency of the two-pass RO is improved from 18.45% at the standard configuration to 33.4% with PX + PX in both stages. This represents an increase of about 81% and also power consumption and exergy destruction were reduced by 46% and 55%, respectively. On the other hand, the exergy efficiency of MED-TVC is only 3.5% because thermal desalination has low exergy efficiency with high exergy destruction at 32.4MW. These results agree with those of previous studies [68, 100]. The performance of MED-TVC can be improved by about 10% by adding the Preheater Heat Exchanger (PHE) but exergy efficiency remains low and power consumption high.

It can be concluded that the RO is more efficient and requires less power consumption than MED-TVC. This will be confirmed economically at chapter seven.

Table 5-15: Comparison between MED-TVC desalination and two-pass RO desalination systems at temperature 20°C and salinity 37g/kg.

	MED-TVC standalone	MED-TVC with PHE	Standard RO	RO with ERT	RO With PX	With PX+ERT	With PX+PX
Steam consumption (kg/s)	48	47.28	-	-	-	-	-
Electrical power consumption (MW)	0.430	0.468	9.4	6	4.7	4.6	4.5
Distillate water quality (ppm)	<20	<20	<20	<20	<20	<20	<20
CCPP power reduction (MW)	22.50	22	-	-	-	-	
Exergy efficiency (%)	3.42	3.77	18.45	27.50	32.55	33.43	33.44
Exergy destruction (MW)	32.40	32.40	5.49	3.434	2.574	2.51	2.47

5.3 Brackish Water Desalination (Waddan City– Libya)

In this study Waddan City in Libya is chosen as a case study where a source of geothermal brackish water is available (as opposed to seawater). Two different desalination technologies were compared: Single Effect Desalination (SED) (Figure 4.4) and Single-pass Reverse Osmosis.

The main purposes of this study are:

a) Free heat source can be used to power SED to produce distillate water from brackish water.

b) Find the best optimal selection desalination system to provide distillate water to this City which suffers from lack of drinking water.

c) Fill the research gap in such conditions.

The comparison is based on producing the same quantity of distillate water as required in Waddan City and will focus on exergy efficiency and power consumption with subsequent economic analysis (Section 7.8) to find the appropriate desalination technique for this location. SED is a thermally driven desalination process, separating salt from water by a process of evaporation and condensation powered by hot geothermal water to evaporate the brackish water. However, the heat is free but power is still required for pumping the hot water to the effect. Single-pass Reverse Osmosis (SRO) is an electrically driven membrane process in which the water diffuses through a semi-permeable membrane against the osmotic pressure. The geothermal brackish water is cooling down to about 25°C in an open collection tank (Figure 5-51)

Figure 5-51: Picture of brackish water tank Waddan City [187]

5.3.1 *Parametric study*

After the validation of the model (Section 4.4), the parametric study was carried out to investigate the influence of environmental data (salinity and temperature) on SED desalination plant. The SED is powered by geothermal hot water which is driven by electrical pumps.

The effect of feed water temperature shows that as the feed of the brackish water in the tank cannot be controlled, it necessary to study the effect of this variation on the system's performance. Figures 5-52 and 5-53 show the effect of feed water temperature on exergy efficiency and specific power consumption for SRO and SED. The exergy efficiency increased with feed water temperature for both techniques (membrane pore size increased and the feed water passes more easily for SRO, whereas for SED exergy destruction decreases and evaporated steam increases the minimum separation work). The exergy efficiency of SED is very low because all the thermal desalination plant efficiencies are low compared with membrane systems. The specific power consumption declined by about 1.7% for SRO and only 1% for SED with every 5°C temperature increase. SRO specific power consumption is lower than SED by about 50%.
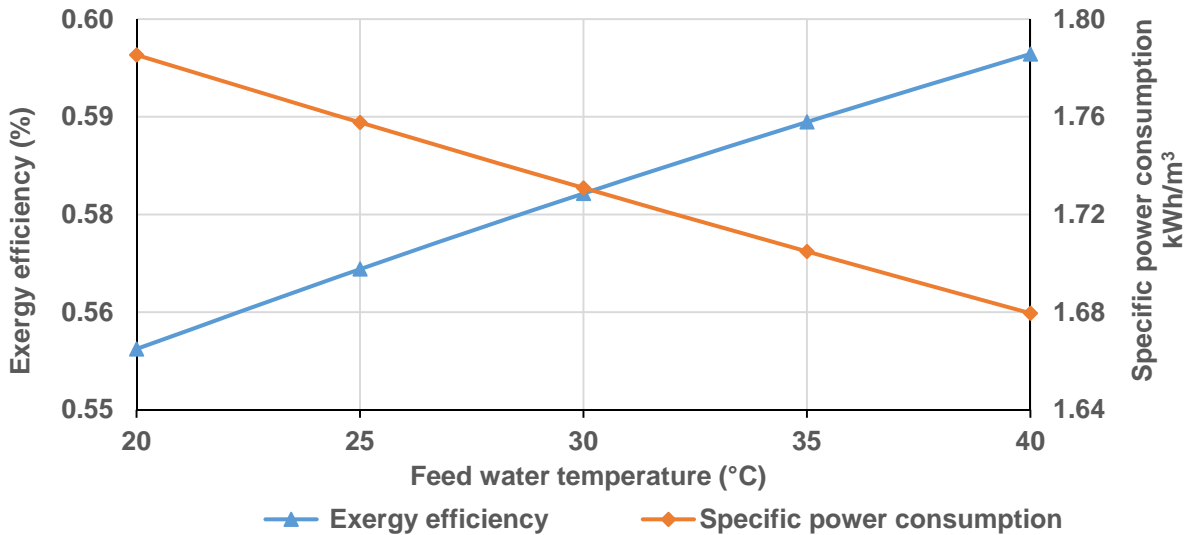
Figure 5-52: Effect of feed temperature on exergy efficiency and specific power consumption for SRO at salinity 1.96 g/kg
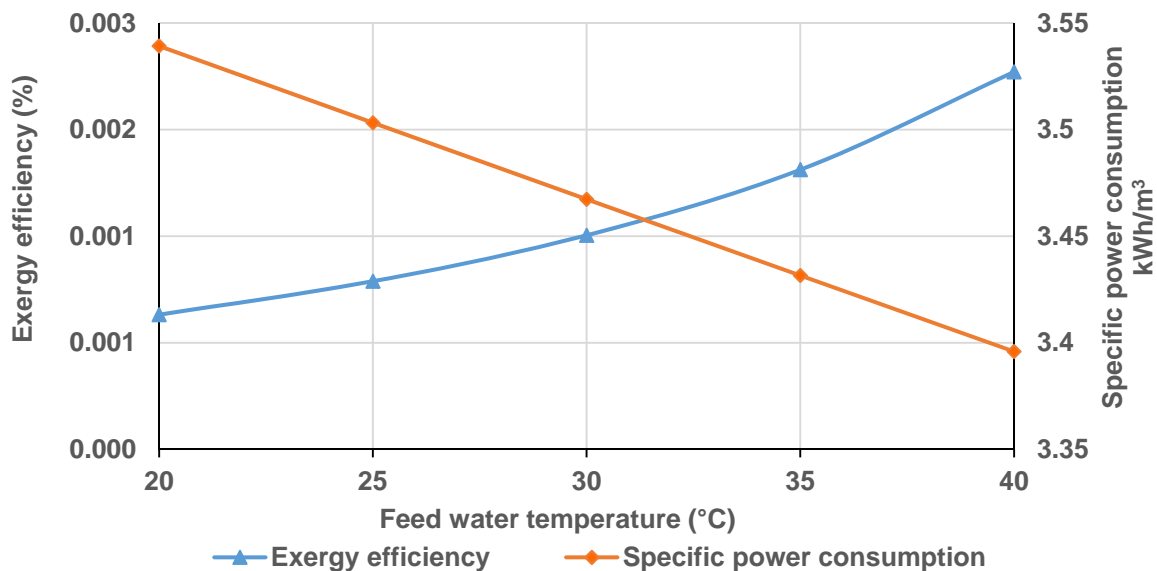
Figure 5-53: Effect of feed temperature on exergy efficiency and specific power consumption for SED at salinity 1.96 g/kg

Raising the feed water salinity increases exergy efficiency for SRO (Figures 5-54) due to increase in the inlet enthalpy [28], where the specific power consumption increased. Also in SED both the exergy efficiency and specific power consumption increase (Figure 5-55) due to osmotic pressure increase. The exergy efficiency of SED is lower than exergy efficiency of SRO because of high electricity in to the SED for the high flow requires. However this does not mean highly saline water is favoured because corrosion will affect the membrane and pipes at SRO desalination plants. The exergy efficiency and specific power consumption are almost constant with plant load changes as seen in Figures 5-56 and 5-57 for both techniques.
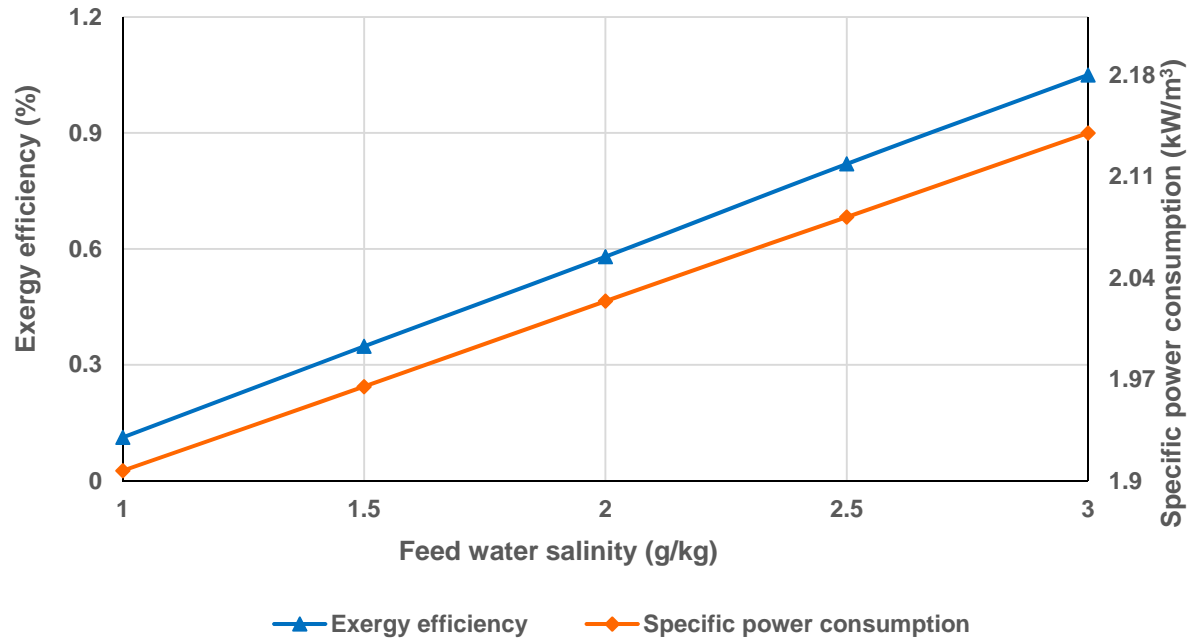
Figure 5-54: Effect of feed water salinity on exergy efficiency and specific power consumption for SRO at 25°C
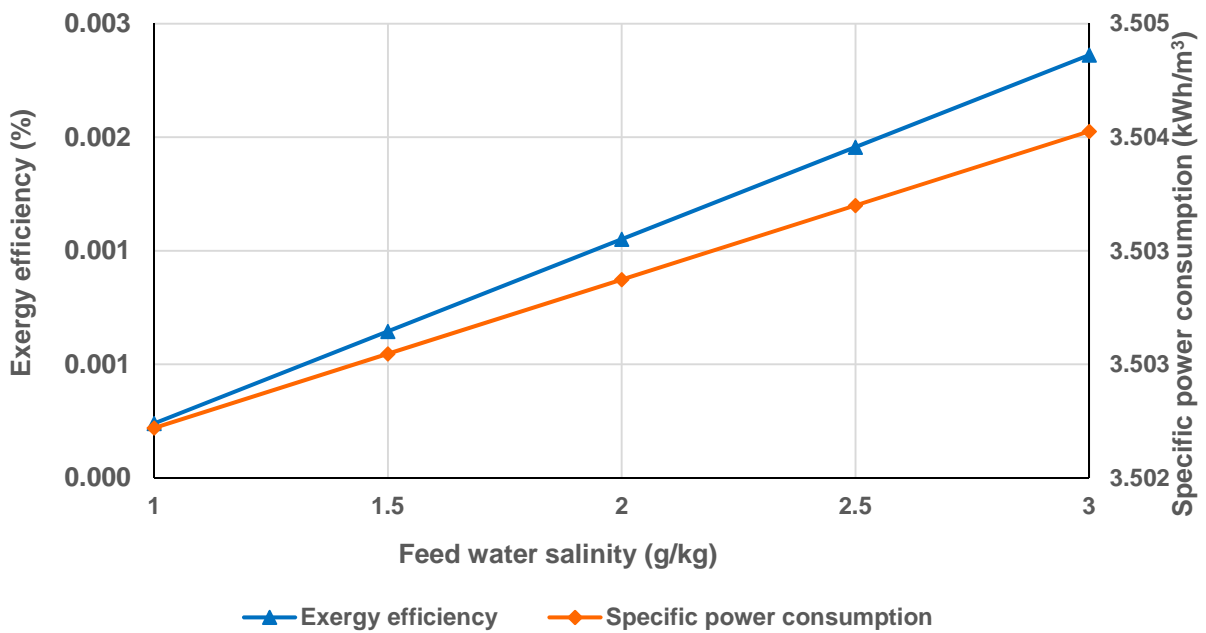
Figure 5-55: Effect of feed water salinity on exergy efficiency and specific power consumption for SED at 25°C
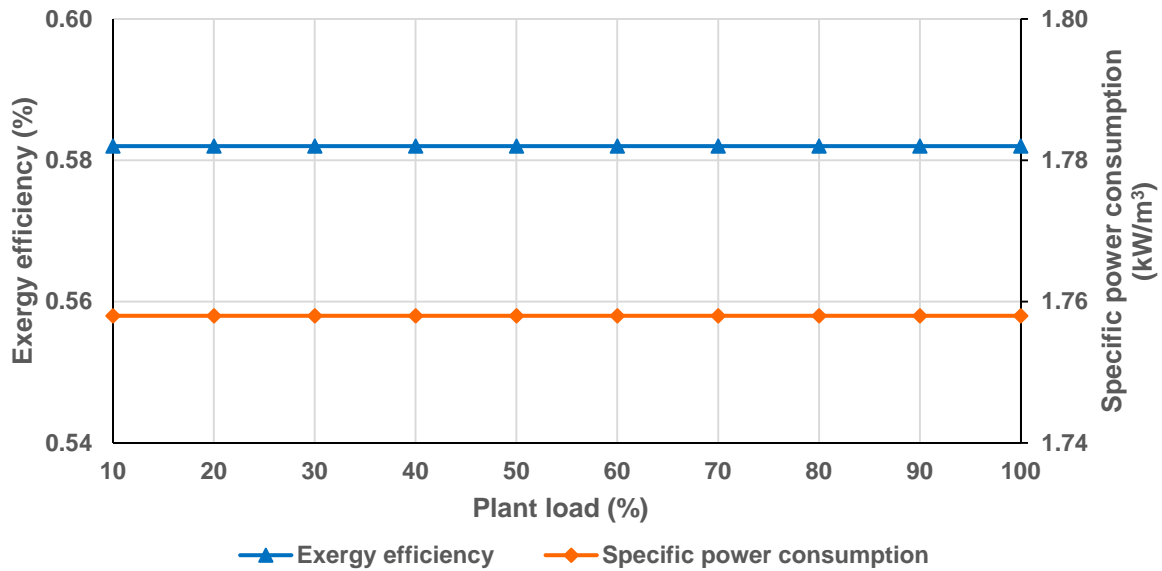
Figure 5-56: Effect of plant load on exergy efficiency and specific power consumption for SRO at feed water salinity 1.96g/kg and 25°C
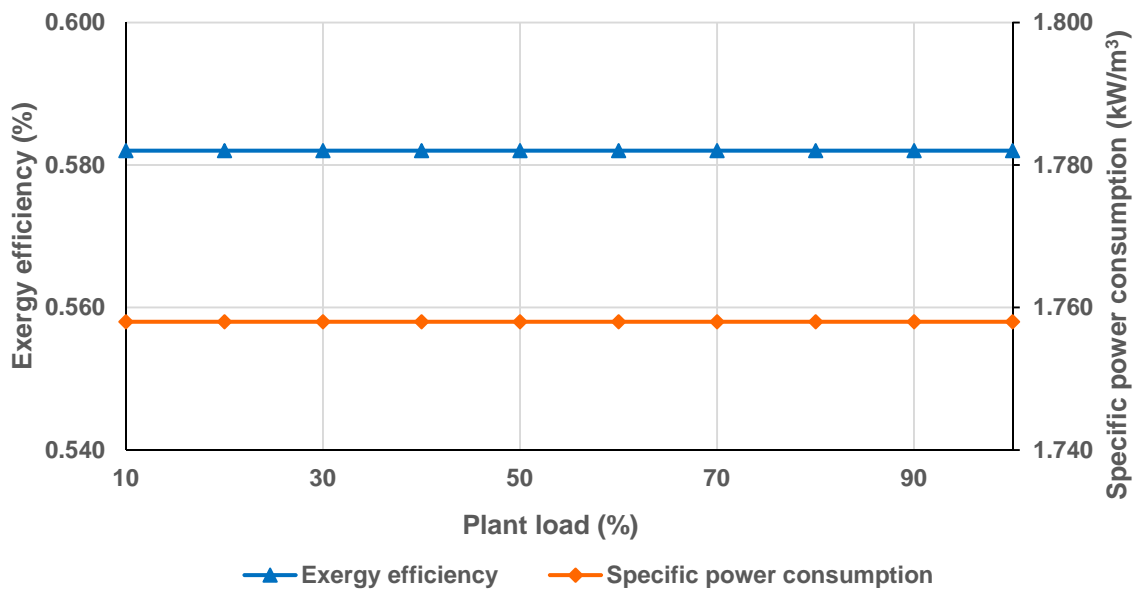
Figure 5-57: Effect of plant load on exergy efficiency and specific power consumption for SED at feed water salinity 1.96g/kg and 25°C

Table 5-16 compares SRO and SED at feed water temperature 25°C. The feed mass flow rate and rejected mass flow of SRO are less than for SED, because SRO is a membrane process with no brine rejected. Consequently the exergy efficiency of SED is very significantly lower than with SRO.

It can be concluded that as the feed water temperature increased the exergy efficiency increased and specific power consumption reduced for SRO and for SED.

The effect of feed water salinity on specific power consumption showed that as the feed salinity increased the specific power consumption for both SRO and SED rose. The exergy efficiency and specific power consumption almost remain constant with plants capacity change.

Table 5-16:A comparison between SRO and SED plants at feed water temperature 25 °C for 306 m³/h product

	SRO	SED
Feed mass flow rate (m³/h)	680	6960
Power consumption (kW)	538	1070
Reject mass flow (m³/h)	373	6620
Brine mass flow (m³/h)	-	283
Exergy efficiency (%)	0.570	0.001

5.4 Summary

The models and simulation results for four different proposed plants have been investigated in this chapter. These include two thermal desalination technologies, SED and MED-TVC, as well as a single-pass RO and a two-pass RO desalination technologies. All of these models were studied using Libyan environmental data for seawater and brackish water. The first part of this chapter discussed the MED-TVC and two-pass RO which were configured to produce 24000m³/day from seawater for a local community at Zawya City in Libya. These two technologies were powered by an existing combined cycle power plant (CCPP) either using electricity for RO or extracted steam to power MED-TVC. A thermodynamic analysis was carried out for each technology. The results showed that the two-pass RO desalination plant was more efficient than the MED-TVC with high exergy efficiency and low power consumption from the CCPP. Moreover, this was the first time the use of a preheating exchanger to improve MED-TVC performance has been examined. In addition, energy recovery devices (ERDs) at both the stages of the two-pass RO were considered and the latest information about the thermodynamic properties of seawater was utilised.

The second part of this chapter described a comparison between SRO and SED using brackish water at Waddan City, Libya. These two technologies were studied to produce about 7344m³/day for the local community. The same performance criteria as in the first part were applied in the thermodynamic analysis. The results indicated that the

SRO was also much better thermodynamically than SED, even when using the brackish water.

It can be concluded that reverse osmosis technologies are much more efficient than thermal processes, especially after adding the energy recovery devices.

CHAPTER 6. COGENERATION PLANT PARAMETRIC STUDY AND ABSORPTION CHILLER SYSTEM

6.1 Introduction

This chapter discusses the existing standalone power plant in Zawya, Libya [8], with proposed absorption chiller and proposed desalination plants. IPSEpro software was used to model the power plant, absorption chiller and desalination plants. These models were validated against the manufacturer or actual data (chapter four), then the simulation results utilized for a detailed thermal evaluation using energy and exergy (chapter three). The aims of this analysis are as follows:

- Firstly, to evaluate the effect of ambient temperature, humidity, and load for the standalone Combined Cycle Power Plant (CCPP) and with MED-TVC + PHE and two pass RO with PX in both stages desalination plants. Energy and exergy analyses are used to determine efficiencies and overall performance of the system and exergy destruction in all of the components to understand the thermal status of the system and the equipment which has most impact on performance.

- Secondly, to calculate the effect of thermal MED-TVC+PHE desalination and membrane desalination RO+PX at both stages on CCPP output power, energy and exergy efficiencies.

- Thirdly, to study the effect of Absorption Chiller (AC) on CCPP performance and also the effect of cooling and chilled water temperature on the absorption chiller exergy efficiency, COP and evaporator heat transfer.

6.2 Power Plant Operation Scenario for Energy and Exergy Analysis

To evaluate the performance of the power plant at three different scenarios, energy and exergy analyses were used. The values for energy and exergy were calculated at the plant full load using 1.013 bar pressure and average Libyan ambient temperature of 21°C and relative humidity of 66%. Three scenarios are used, scenario I (CCPP standalone), scenario II (CCPP+MED-TVC) and scenario III (CCPP+RO). The

thermodynamic properties of scenarios I, II and III are shown in Table 6-1 a, b and c. The numbered streams in figure 4-1 were used in tables 6-1 to 6-3 and to calculate values of exergy efficiency and destruction (Table 6-4).

Table 6-1: Simulated results of the cycle streams thermodynamic properties for CCPP standalone (Scenario I, figure 4.1)

Stream number (Figure 4.1)	Mass flow $\dot{m}$ (kg/s)	Pressure p (bar)	Temperature T (°C)	Enthalpy h (kJ/kg)	Entropy s (kJ/kgK)	Physical exergy E_{ph} (MW)	Chemical exergy E_{ch} (MW)	Total exergy E_T (MW)
1, 22	508	1	21	21	7	0	0	0
2, 21	10	24	15	31	10	5	522	527
3, 23	518	1	534	586	8	130	2	132
4, 24	518	1	116	122	7	8	2	10
5, 25	63	92	496	3375	7	92	0	92
6, 37	63	93	306	2738	6	70	0	70
7, 18	14	9	306	3068	7	14	0	14
8	28	9	306	3068	7	28	0	28
9	150	4	130	548	2	12	0	12
10	4	4	142	2727	7	3	0	3
11	63	4	142	599	2	3	0	3
12, 40	63	94	144	611	2	7	0	7
13	14	10	142	600	2	1	0	1
14	63	4	142	599	2	6	0	0
15	4	4	142	599	2	1	0	1
16	138	4	28	119	0	0	0	1
17	4	4	142	2727	7	3	0	3
19	0	4	84	352	1	0	0	0
26	126	92	496	3375	7	184	0	184
27	28	9	306	3068	7	28	0	28
28	154	9	217	2876	7	139	0	139
29	126	9	199	2833	7	111	0	112
30	154	4	142	2727	7	115	0	115
31	150	4	142	2727	7	112	0	112
32	149	0	33	2155	7	19	0	20
33	9600	1	25	105	0	7	24	31
34	9600	1	33	137	0	20	24	45
35	150	0	28	118	0	0	0	1
36	150	4	28	119	0	0	0	1
37	63	93	306	2738	6	70	0	70
38	4	4	142	2727	7	0	0	0
39	0	4	142	2727	7	0	0	0
40	63	94	144	611	2	7	0	7
41	28	4	142	599	2	3	0	3

Table 6-2: Simulated results of the cycle streams thermodynamic properties for CCPP + MED-TVC (Scenario II appendix 6-A)

Stream number (Figure 4.1).	$\dot{m}$ Mass flow rate (kg/s)	Pressure p (bar)	Temperature T (°C)	Enthalpy h (kJ/kg)	Entropy s (kJ/kgK)	Physical exergy E_{ph} (MW)	Chemical exergy E_{ch} (MW)	Total exergy E_T (MW)
1, 22	508	1	21	21	7	0	0	0
2, 21	10	24	15	31	10	5	522	527
3, 23	518	1	534	586	8	130	2	132
4, 24	518	1	116	122	7	8	2	10
5, 25	63	92	496	3375	7	92	0	92
6, 37	63	93	306	2738	6	70	0	70
7, 18	14	9	306	3068	7	14	0	14
8	28	9	306	3068	7	28	0	28
9	153	4	141	593	2	14	0	14
10	0	4	142	2727	7	3	0	3
11	63	4	142	599	2	3	0	3
12, 40	63	94	144	611	2	7	0	7
13	14	10	142	600	2	1	0	1
14	63	4	142	599	2	6	0	0
15	4	4	142	599	2	1	0	1
16	138	4	28	119	0	0	0	1
17	4	4	142	2727	7	3	0	3
19	48	4	111	564	1	1	0	1
26	126	92	496	3375	7	184	0	184
27	28	9	306	3068	7	28	0	28
28	154	9	217	2876	7	139	0	139
29	126	9	199	2833	7	111	0	112
30	154	4	142	2727	7	115	0	115
31	105	4	142	2727	7	79	0	79
32	105	0	34	2155	7	14	0	14
33	9600	1	25	105	0	7	24	31
34	9600	1	34	127	0	16	24	40
35	105	0	30	118	0	0	0	0
36	105	4	28	119	0	0	0	0
37	63	93	306	2738	6	70	0	70
38	4	4	142	2727	7	36	0	36
39	48	4	142	2727	7	0	0	0
40	63	94	144	611	2	7	0	7
41	28	4	142	599	2	3	0	3

Table 6-3: Simulated results of the cycle streams thermodynamic properties for CCPP + RO (Scenario III)

Stream Number (Figure 4.1).	Mass flow rate $\dot{m}$ (kg/s)	Pressure P (bar)	Temperature T (°C)	Enthalpy h (kJ/kg)	Entropy s (kJ/kgK)	Physical exergy E_{ph} (MW)	Chemical exergy E_{ch} (MW)	Total exergy E_T (MW)
1, 22	508	1	21	21	7	0	0	0
2, 21	10	24	15	31	10	5	522	527
3, 23	518	1	534	586	8	130	2	132
4, 24	518	1	116	122	7	8	2	10
5, 25	63	92	496	3375	7	92	0	92
6, 37	63	93	306	2738	6	70	0	70
7, 18	14	9	306	3068	7	14	0	14
8	28	9	306	3068	7	28	0	28
9	150	4	130	548	2	12	0	12
10	4	4	142	2727	7	3	0	3
11	63	4	142	599	2	3	0	3
12, 40	63	94	144	611	2	7	0	7
13	14	10	142	600	2	1	0	1
14	63	4	142	599	2	6	0	0
15	4	4	142	599	2	1	0	1
16	138	4	28	119	0	0	0	1
17	4	4	142	2727	7	3	0	3
19	0	4	84	352	1	0	0	0
26	126	92	496	3375	7	184	0	184
27	28	9	306	3068	7	28	0	28
28	154	9	217	2876	7	139	0	139
29	126	9	199	2833	7	111	0	112
30	154	4	142	2727	7	115	0	115
31	150	4	142	2727	7	112	0	112
32	149	0	33	2155	7	19	0	20
33	9600	1	25	105	0	7	24	31
34	9600	1	33	137	0	20	24	45
35	150	0	28	118	0	0	0	1
36	150	4	28	119	0	0	0	1
37	63	93	306	2738	6	70	0	70
38	4	4	142	2727	7	0	0	0
39	0	4	142	2727	7	0	0	0
40	63	94	144	611	2	7	0	7
41	28	4	142	599	2	3	0	3

Table 6-4: Summary of the exergy analysis used for studying the combined cycle power plant at Zawya Libya

Equipment	Exergy Efficiency (%)	Exergy destruction (MW)
GT1	$\dfrac{W_{out}}{[((E_1 + E_2) - E_3)]}$	$[(E_1 + E_2 - E_3 - W_{out})]$
GT2	$\dfrac{W_{out}}{[((E_{21} + E_{22}) - E_{23})]}$	$[E_{21} + E_{22} - E_{23} - W_{out}]$
HPT	$\dfrac{W_{out}}{[E_{26} - E_{29}]}$	$[E_{26} - E_{29} - W_{out}]$
MPT	$\dfrac{W_{out}}{[E_{28} - E_{30}]}$	$[E_{28} - E_{30} - W_{out}]$
LPT	$\dfrac{W_{out}}{[E_{31} - E_{32}]}$	$[(E_{31} - E_{32} - W_{out})]$
HRSG1	$\dfrac{[(E_5 + E_7) - (E_{13} + E_{14})]}{(E_3 + E_4)}$	$E_{12} + E_{13} + E_3 - E_4 - E_5 - E_7$
HRSG2	$\dfrac{[(E_{25} + E_{18}) - (E_{20} + E_{40})]}{(E_{23} - E_{24})}$	$E_{20} + E_{40} + E_{24} - E_{18} - E_{25} - E_{24}$
Condenser	$\dfrac{[(E_{33} - E_{24}) - ccp]}{(E_{32} - E_{36})}$	$E_{33} + E_{32} - E_{34} - E_{35}$
Deaerator	$\dfrac{(E_{11} + E_{14})}{(E_9 - E_{10})}$	$E_9 + E_{10} - E_{11} - E_{14}$
Stack for 2	---	$E_4 + E_{24}$
MED-TVC	$\eta = \dfrac{W_{min}}{E_{.}}$	$(1 - \eta_{TVC}) X E_{19} - E_{39}$
RO	$\eta = \dfrac{W_{min}}{E_{in}}$	$E_{in} - W_{min}$

6.2.1 *Power plant energy analysis*

Energy analysis results for the performance of the three different scenarios are shown in table 6-5. The effect of these scenarios on CO_2 emission is calculated from correlations (eq. 3.73 to 3.75) based on using energy and exergy analysis. The gas turbine output power 156.9MW x 2, GT efficiency 35.1%, power consumption 4.4MW, Heat Recovery Steam Generator (HRSG) efficiency 65.6%, product steam 553.3 t/h and gas consumption 20.3 kg/s the same at all three scenarios.

Table 6-5: Power plant energy performance at three different scenarios

Performance Indicator		Scenario		
		I	II	III
MED-TVC load	%	0	100.0	0
RO load	%	0	0	100.0
ST power	MW	153.9	131.5	149.1
Net power	MW	463.3	440.8	458.6
Cycle efficiency	%	52.4	49.9	51.9
Heat Utilization Factor (HUF)	%	52.4	62.6	51.9
CO_2 emission (energy base)	g/kWh	494	411	500

The highest output power is generated from scenario I, because both gas turbines and steam turbines are running at full load, whereas at scenario II the MED-TVC desalination plant is coupled with the power plant and part of the steam generated is extracted from low pressure steam. The steam turbine output power is reduced by 22.5MW. At scenario III with two-pass RO desalination plant in service instead of MED-TVC, the total output power is decreased by about 4.5 to 9.4MW depending on the configuration of the two-pass RO, ie standard or using an energy recovery device (Section 5.2). Both GT and HRSG efficiencies remain the same for the three scenarios because they are at the same operating condition.

Scenario I has the highest cycle power plant efficiency (52.4%) followed by scenario III (51.9%) and scenario II (49.9%). This result matches with other studies [28, 122], with the consideration that the plant outputs in this study are allocated for two different products (power and water). Scenario II power plant efficiency is the lowest, because energy used to power the LP steam turbine was extracted to power the MED-TVC desalination instead. From an energy analysis aspect, the overall cogeneration plant (power and MED-TVC desalination) performance can be judged using the Heat Utilization Factor (HUF) since this combines the energy outputs as power produced from the power plant and heat used to power the MED-TVC desalination plant [149]. At full load, the steam turbine produces 153.9MW when the MED-TVC is not in use, whereas the MED-TVC desalination plant consumed about 22.5MW heat. Therefore, scenario II has the highest HUF since 15% of the produced steam is used in the MED-TVC desalination plant. Although HUF can be used to evaluate cogeneration plant performance, it is an indicator for the heat usage more than for overall plant performance evaluation. This challenge is raised because the MED-TVC desalination output is not in the form of energy, but simply the amount of distillate water produced [146]. In scenario III only electricity was used to drive the RO feed pumps.

6.2.2 *CCPP + desalination parametric study*

In the following sections the CCPP has been combined with an absorption chiller (AC) to stabilise the performance of the CCPP against changes in ambient temperature. The CCPP is then operating at its nominal design point condition. The stream properties required to perform exergy analysis were extracted from the simulated model data presented in table 6.1 for scenario I but with the inlet temperatures (1 and 22 in figure 4.1) held constant at 288K. The exergy efficiencies and exergy destruction

for the combined cycle power plant components are calculated as in table 6-4 and shown in figures 6-1 and 6-2. Although the exergy efficiency is defined as the utilization percentage of the output from the exergy, the amount of exergy destruction is necessary in thermal system enhancement and improvement. A good example of that is that the exergy efficiency of the MED-TVC is low at 3.5% which represents a low use of the input exergy. However, improvement and optimization cannot be made unless the location of exergy destruction is known. Therefore (Figure 6-1) describes the exergy efficiency of plant components at the three different scenarios. It can be seen that the exergy efficiency of most components remains the same across the scenarios, except the high pressure steam turbine (HPT), condenser and deaerator values, due to the heat and electrical power used to power the desalination system, where the power required for RO with PX in both stages is only 4.5MW.
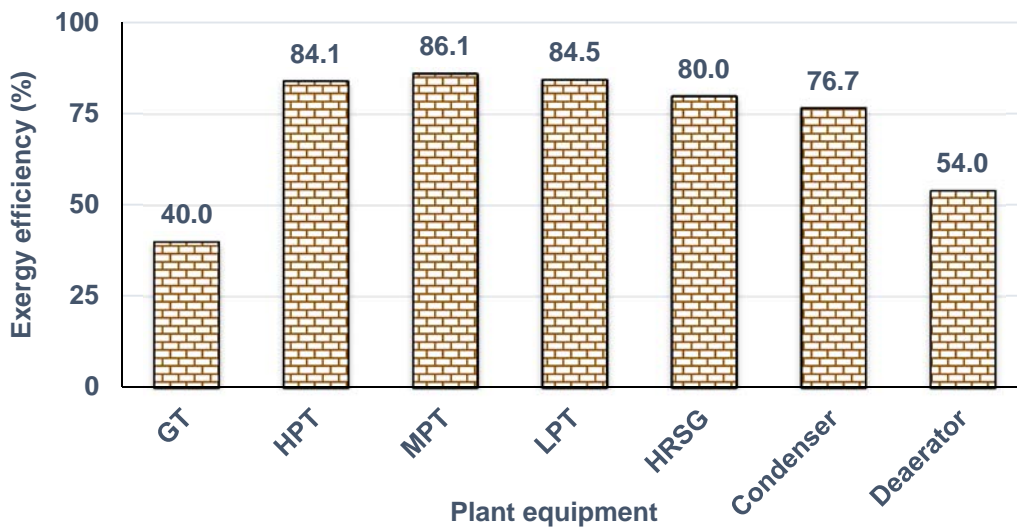
Figure 6-1: (a) Exergy efficiency of the power plant equipment standalone (Scenario I)
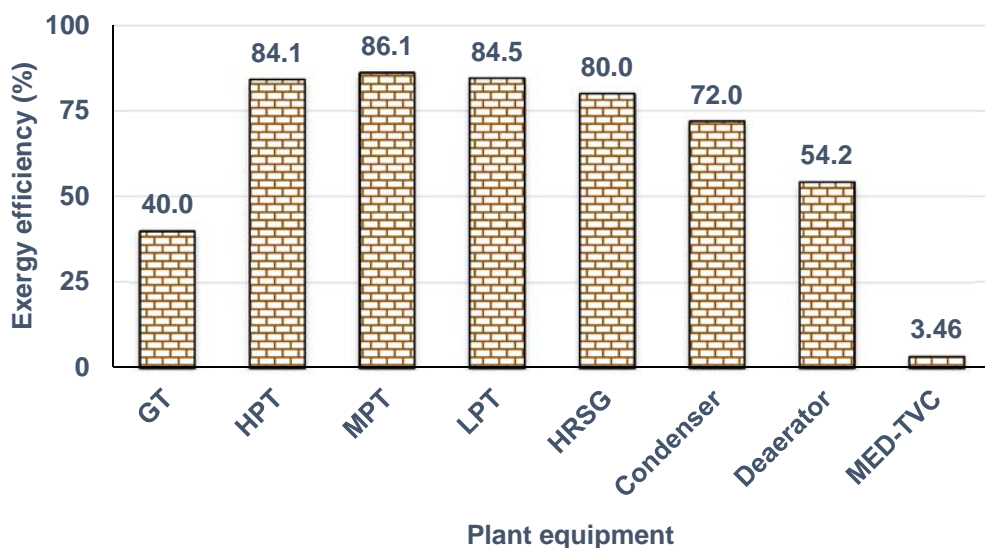
Figure 6-1 (b): Exergy efficiency of the power plant equipment coupled with MED-TVC (scenario II)
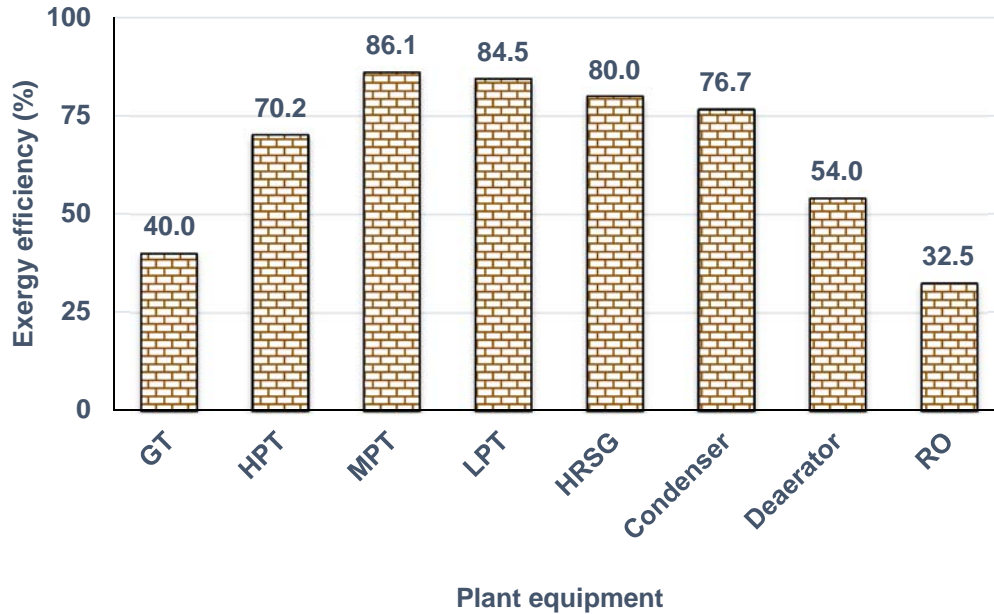
Figure 6-1 (c): Exergy efficiency of the power plant equipment coupled with RO (scenario III)

Figure 6-2 shows the exergy destruction with respect to the fuel input (the input fuel exergy is 1054MW for all three scenarios). The exergy efficiency is the highest for scenario I at 43.9%, whereas it is 41.9% and 43.3% for scenarios II and III, respectively. The benefits of the exergy methods can be seen clearly by explaining the reasons behind the lower exergy efficiencies. At scenario II, where the steam is extracted from the low steam pressure to power MED-TVC, the steam turbine output power is reduced to 131.5MW by 22.5MW (equivalent electrical power), as compared with scenario III where the power plant lost only 4.5 - 9.4MW depending on the reverse osmosis desalination configurations.

For all three scenarios the GTs were the dominant exergy destruction component (about 45% exergy destruction). This agrees with published research in this field relating to high exergy destruction in fuel burning at the combustion chamber [28, 120, 122, 188]. In contrast this study shows that the HRSGs and stack each consume about 2% from the input exergy. The MED-TVC and RO destroy about 3% and less than 0.5%, respectively, reflecting the heat transfer processes in the thermal MED-TVC process.
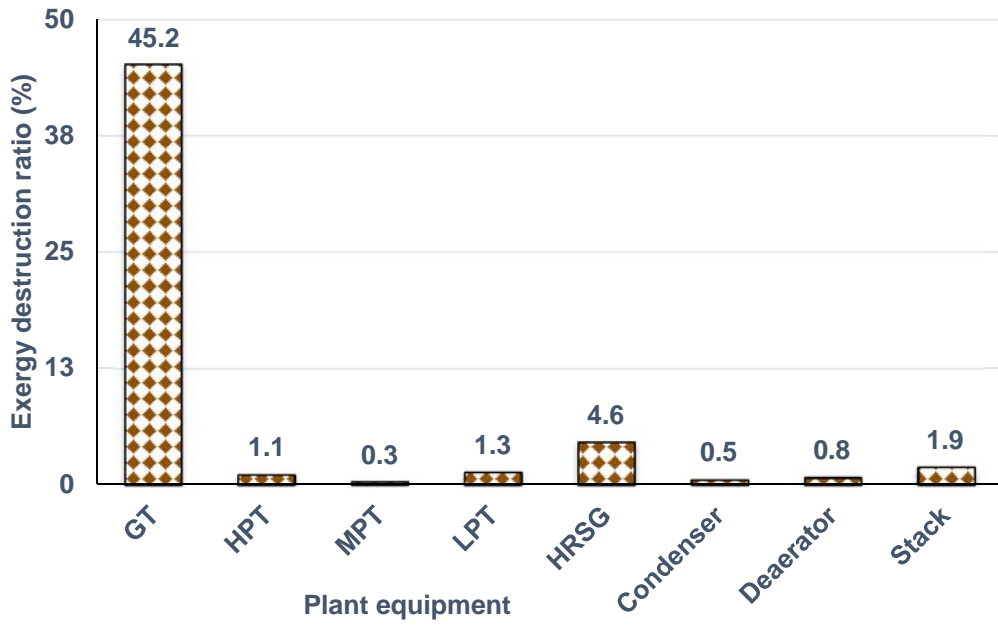
Figure 6-2: (a): Exergy destruction ratio for combined cycle power plant standalone (scenario I) input exergy = 1054MW and exergy efficiency = 43.9%
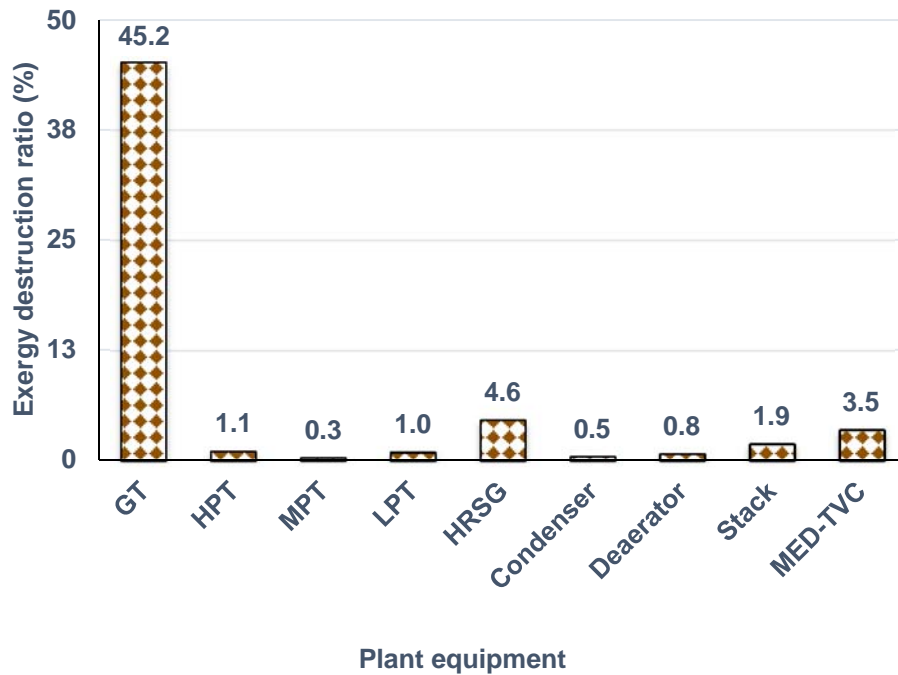
Figure 6-2 (b): Exergy destruction ratio for combined cycle power plant with MED-TVC (scenario II) input exergy = 1054MW and exergy efficiency = 41.9%
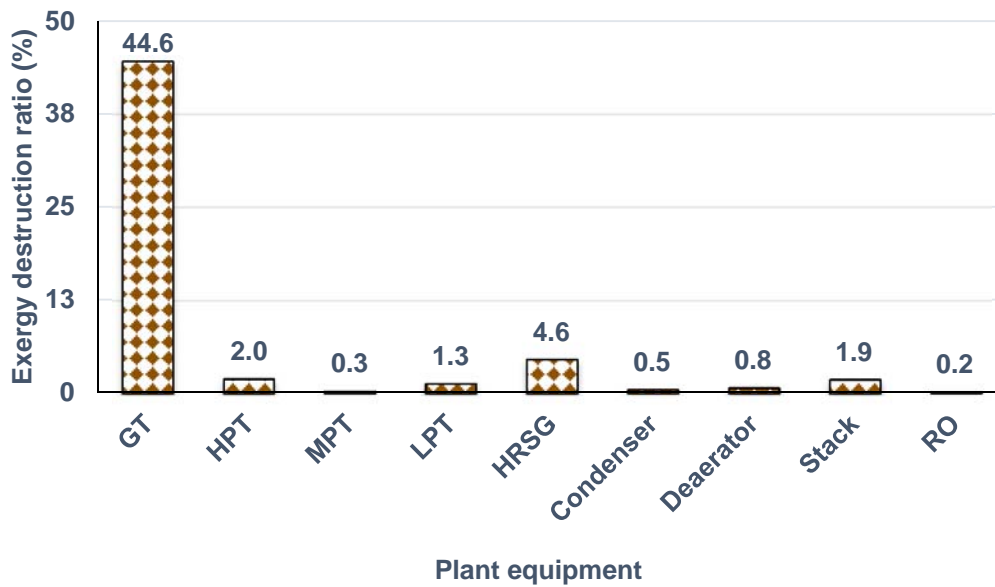
Figure 6-2 (c): Exergy destruction ratio for combined cycle power plant with RO (scenario III) input exergy = 1054MW and exergy efficiency = 43.3%

The heat utilization factor (HUF) is improved by coupling the combined cycle power plant with reverse osmosis RO or MED-TVC desalination plants, as can be seen in figure 6-3. The HUF for CCPP + MED-TVC is improved more than CCPP + RO. Coupling MED-TVC with CCPP CO_2 emission reduced by 16%, where only it only 0.07% when CCPP coupled with RO.
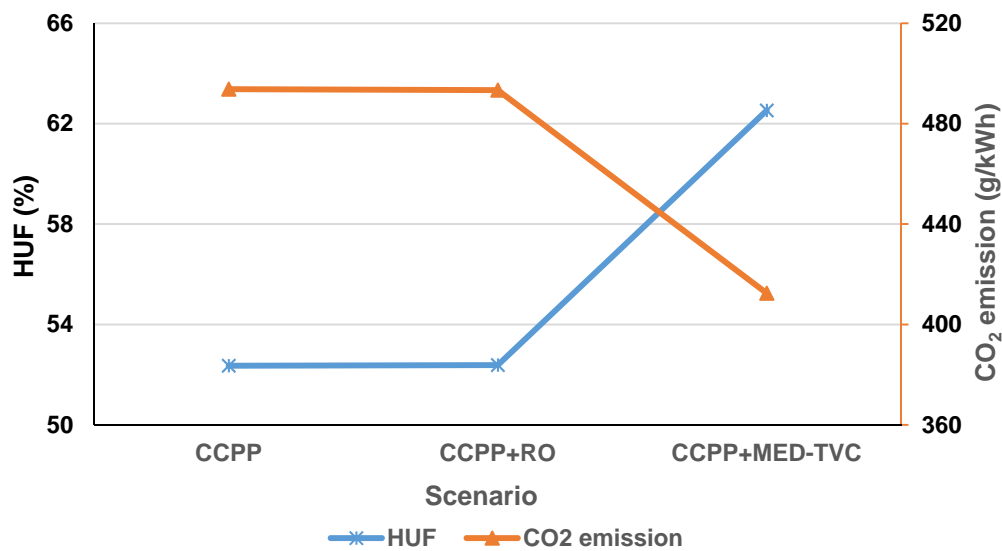
Figure 6-3: Power plant parametric study

During power plant operation, the two main environmental factors that can affect the combined cycle power plant (CCPP) are changes in ambient temperature and the affect of relative humidity, where the affect of relative humidity is very small it is

assumed negligble. Operationally, the desalination load for either MED-TVC or RO with PX in both stages will impact total power production and steam turbine power.

6.3 Parametric study

6.3.1 *Effect of ambient temperature*

Figure 6-4 shows the impact of changing the ambient temperature over the range from 10°C to 50°C on the power plant gross power at full load for the three different scenarios. As can be seen, the gross power is reduced by an average of 5.3% for every 10°C ambient temperature rise for all the three scenarios. This is in agreement with the findings of previous research [116, 139, 189-191]. CCPP gross power with MED-TVC and with two-pass RO drop by about 5% and 1.2%, respectively, due to steam or electrical power extracted from the power plant.
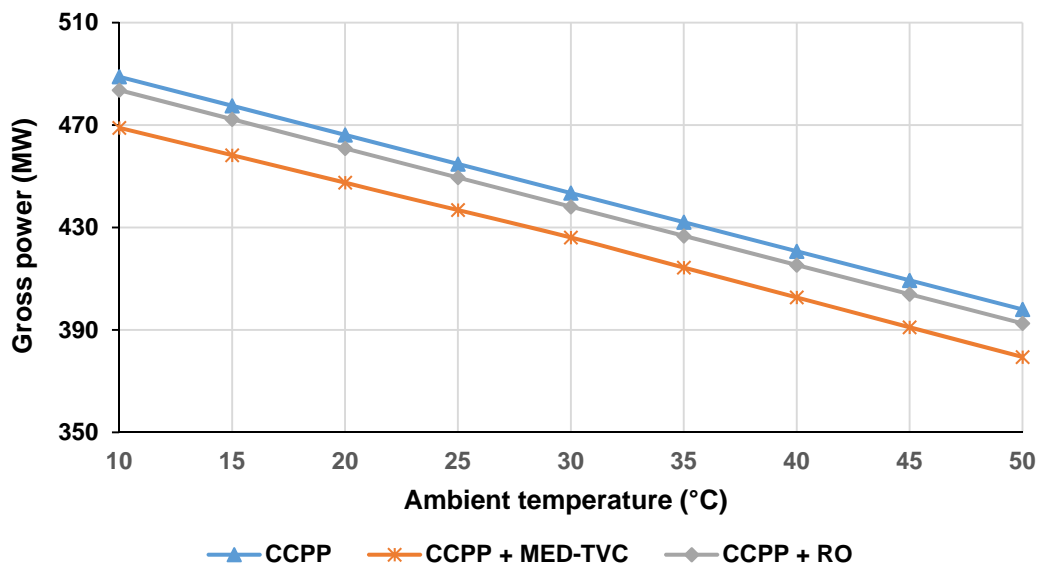
Figure 6-4: Effect of ambient temperature on CCPP gross power

Correspondingly, figure 6-5 shows a decrease in plant thermal efficiency by about 2.4% and 0.0.5% when the CCPP is coupled with MED-TVC or with RO, respectively. These also declined with every 10°C rise in ambient temperature by about 0.2% for standalone and with RO and 0.3% when MED-TVC is in use. These are due to the GT compressor consuming more power as ambient inlet air temperature increases [139]. In contrast, figure 6-6 shows an increase in heat utilization factor when the CCPP is coupled with MED-TVC as the ambient temperature rises, whereas it decreases for

CCPP standalone or with RO. This is because the large quantity of extracted heat for MED-TVC is assumed to be used effectively.
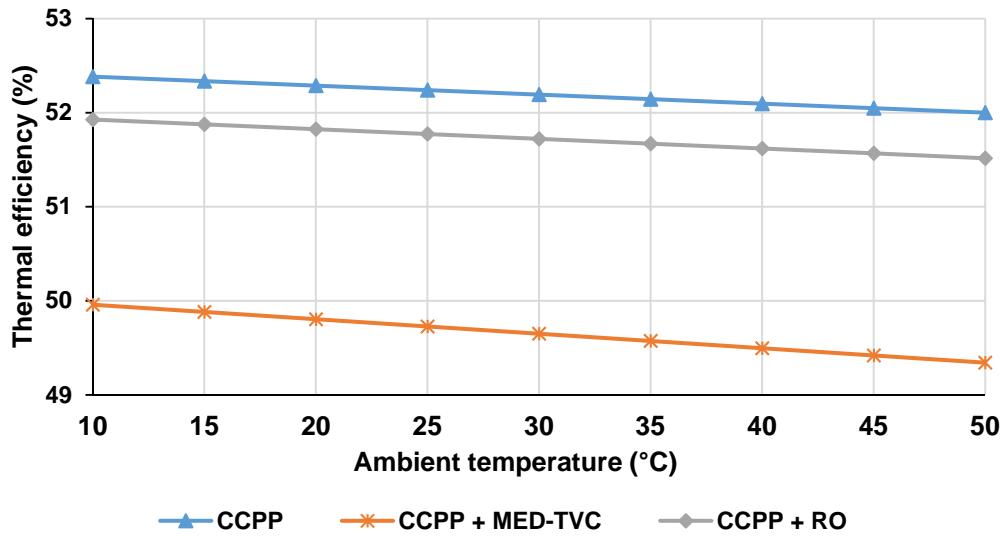
Figure 6-5: Effect of ambient temperature on plant thermal efficiency
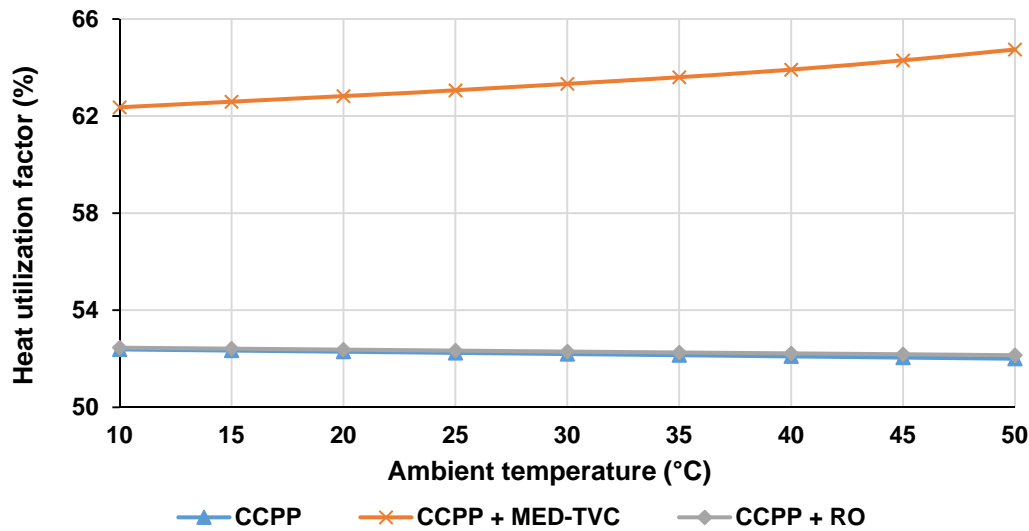
Figure 6-6: Effect of ambient temperature on power plant heat utilization factor

Similarly figure 6-7 shows that as the ambient temperature increased the exergy efficiency decreased, due to more power consumed by the compressor to compress air with low density, also coupling the power plant with MED-TVC and two-pass RO also decreases the overall exergy efficiency, reflecting that the exergy destruction at thermal desalination is higher than the electrical power used for reverse osmosis.
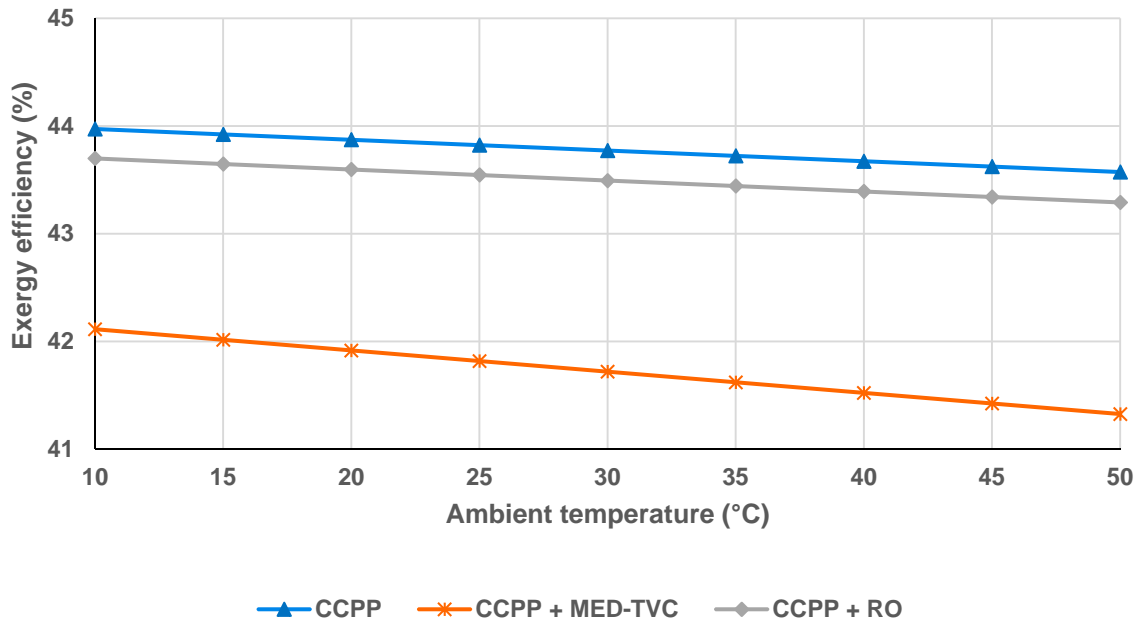
Figure 6-7: Effect of ambient temperature on plant exergy efficiency

Figure 6-8 shows that the CO_2 emissions (exergy base) increase by about 0.36% for every 10°C raise in ambient temperature when the CCPP is coupled with MED-TVC desalination unit and by 0.24% with the RO system. The minor effect for both desalination systems shows that the power side impact is predominant due to high fuel and product exergy relative to water side. In the three scenarios exergy bases CO_2 intensity vary with ambient temperature and the CCPP-RO is to be shown the worse scenario while the CCPP standalone produces low emission levels. Figure 6-9 shows that the effect of ambient temperature onto CO_2 emission energy base at different scenarios, it showed the CCPP+MED-TVC was the worst scenario.
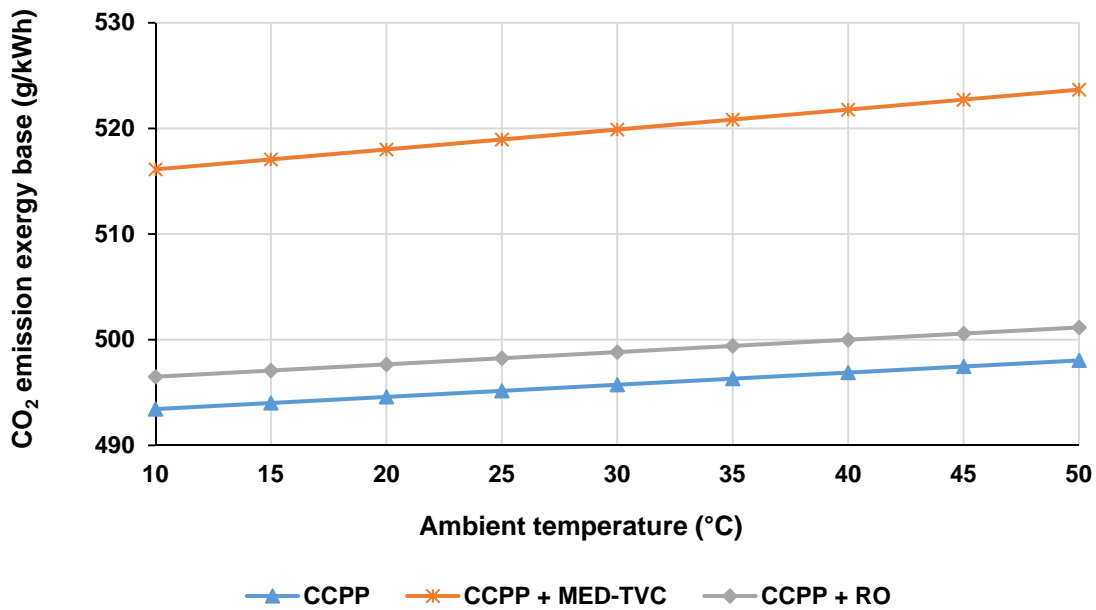
Figure 6-8: Effect of ambient temperature on CCPP CO_2 emission exergy base
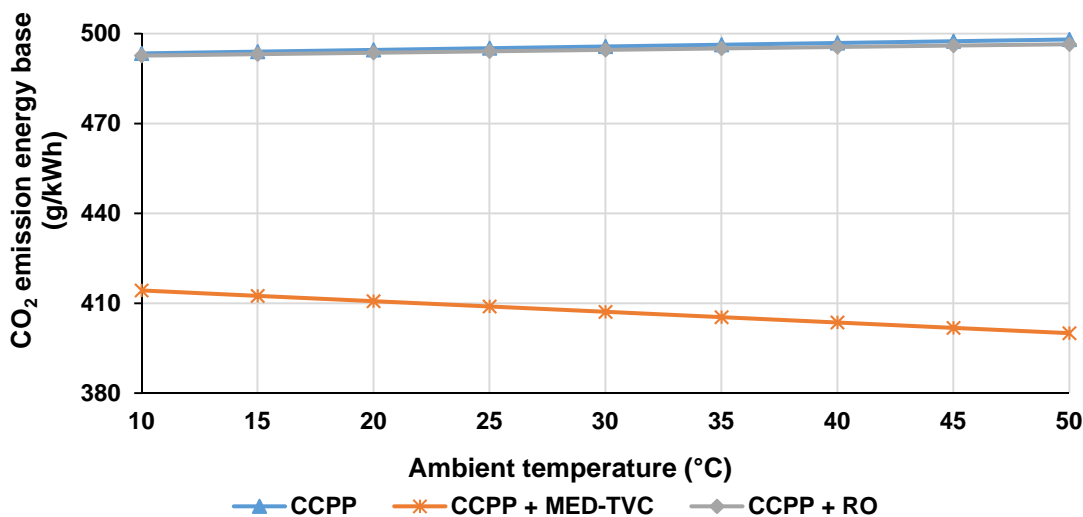
Figure 6-9: Effect of ambient temperature on CCPP CO_2 emission (energy base)

6.3.2 *Effect of relative humidity*

Libya is one of those countries characterized by a high variation of relative humidity (Section 3.12.1). The influence of relative humidity changes on CCPP performance is investigated by varying it from 10% to 100% to cover any change on the relative humidity at full load for the standalone CCPP and 21°C ambient temperature. As can be seen in figure 6-10, the gross power and steam turbine power with same natural gas consumption increased slightly by only about 0.04% for every 10% change in relative humidity, due to the GT exhaust density increase [27]. This will cause the

steam produced by HRSG to increase with consequently more electrical power from the steam turbine. This result is in agreement with previous studies [28, 116, 122].

Plant thermal and exergy efficiencies increase by 0.045% for every 10% rise in relative humidity as shown in figures 6-11. This can be explained by the enhancement of the steam turbine power, whereas the fuel feed exergy remains the same.
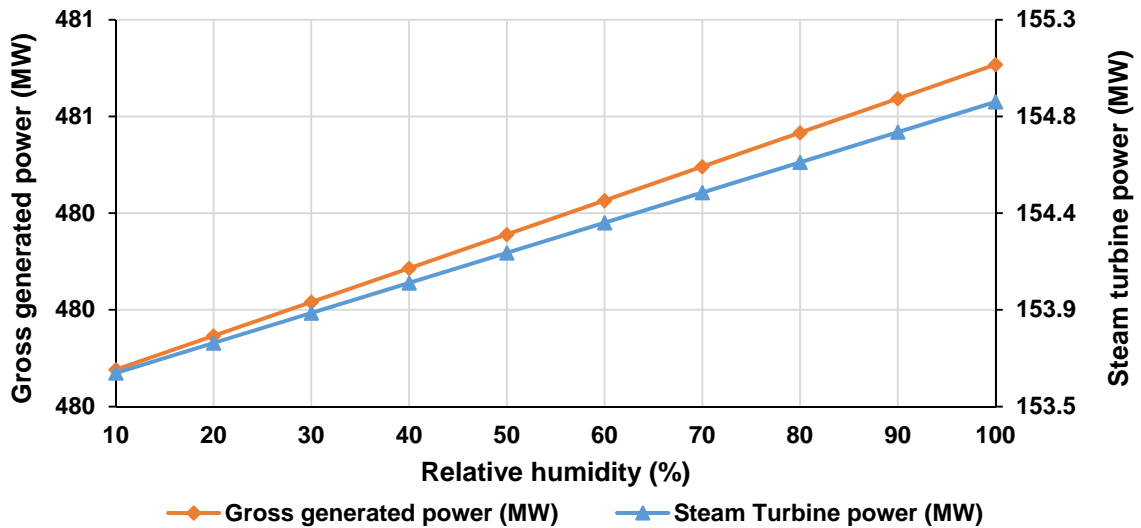
Figure 6-10: Effect of relative humidity on CCPP gross power
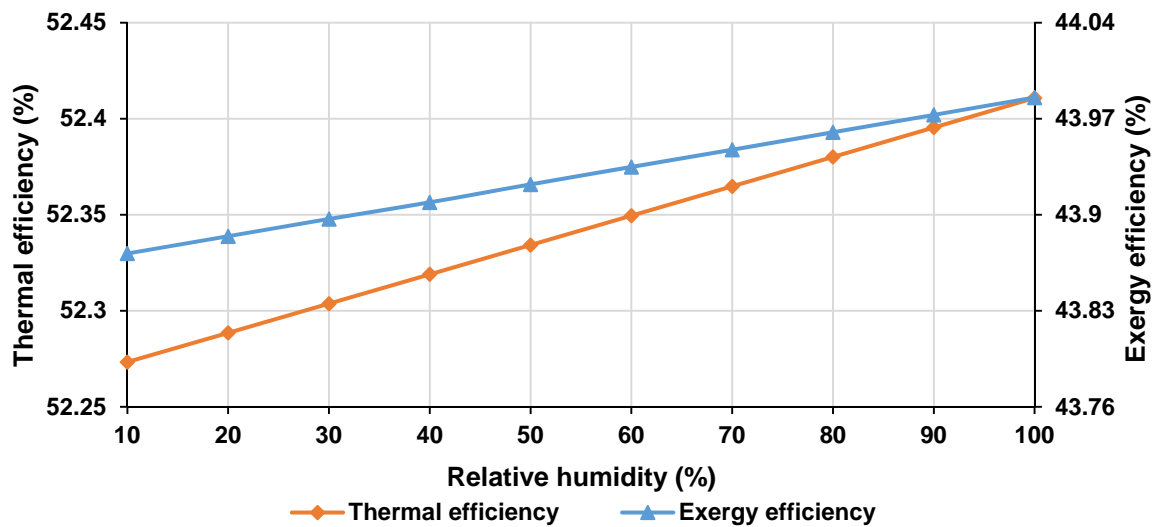
Figure 6-11: Effect of relative humidity on CCPP thermal and exergy efficiencies

Figure 6-12 shows the effect of relative humidity on the CO_2 g/kWh emission (energy base). As can be seen, the CO_2 emission declines by 0.043% when relative humidity rises by 10% and although this is a small effect it will become cumulatively significant

during the year. This can be explained by the increase in steam turbine power for the same fuel consumption.
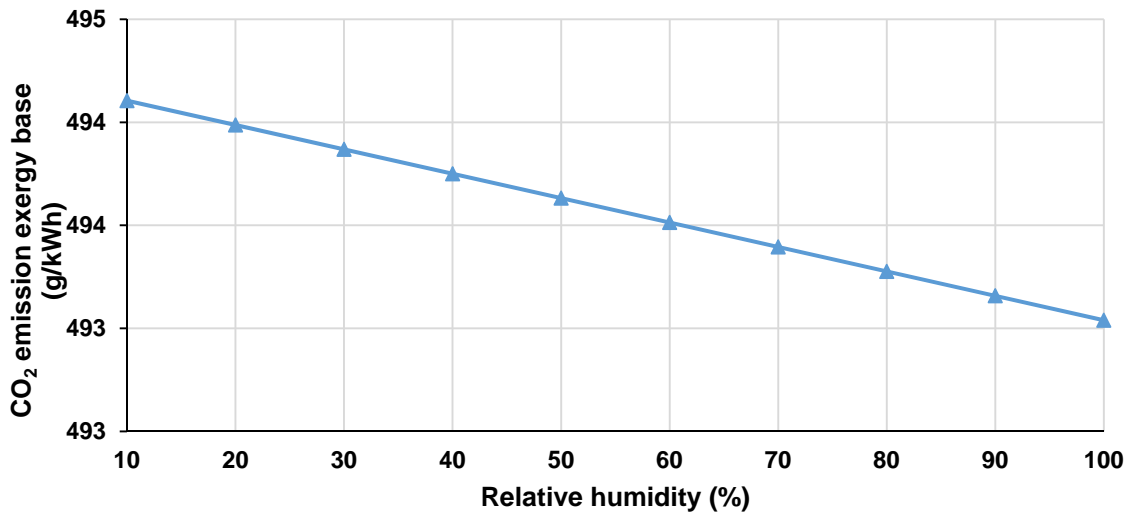
Figure 6-12: Effect of relative humidity on CCPP CO_2 emission (exergy base)

6.3.3 *Effect of MED-TVC load on CCPP*

The MED-TVC desalination system load can be varied from 10% to 100% load as it changes from CCPP standalone to CCPP + MED-TVC. The total output power declines linearly by about 0.27% for every 10% increase in MED-TVC load, as a result of reduction of the steam turbine power generation by about 1.4% as shown in figure 6-13. This is because a part of the LP steam normally used to produce power from the LP steam turbine is extracted to power the MED-TVC. Consequently, the power plant thermal efficiency also dropped with increase in MED-TVC load. On the other hand, Heat Utilization Factor (HUF) increases from 53% standalone power plant to 62% for MED-TVC desalination full load as shown in figure 6-14.
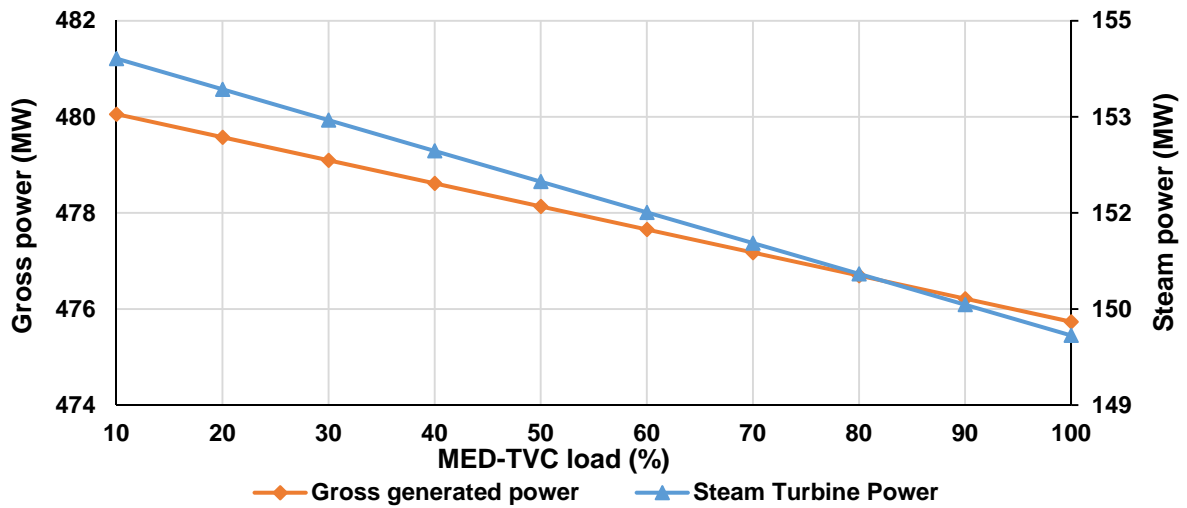
Figure 6-13: Effect of MED-TVC load on CCPP gross and steam turbine power
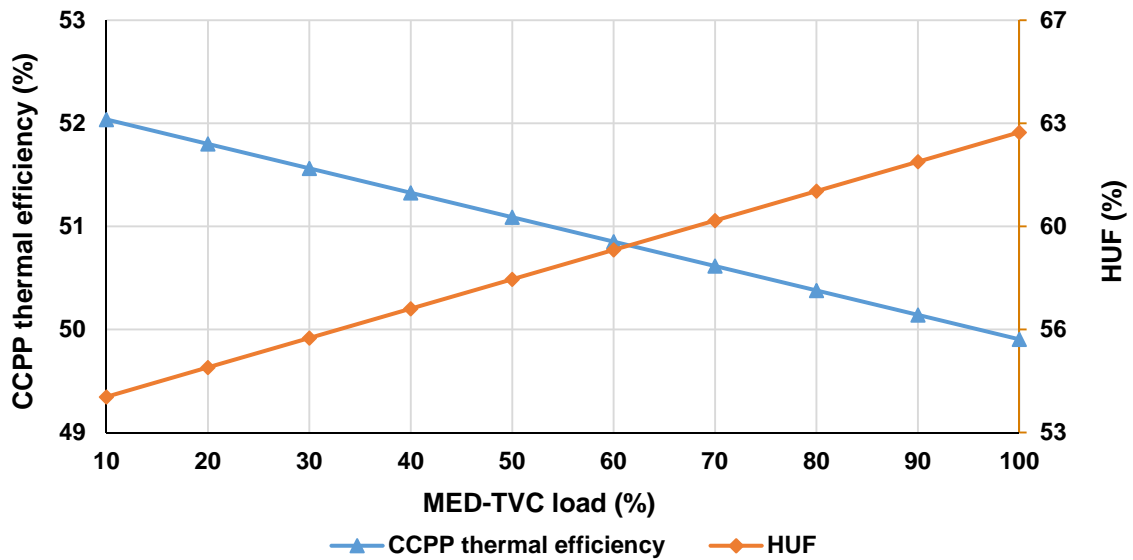
Figure 6-14: Effect of MED-TVC load on CCPP thermal efficiency and HUF

As with thermal efficiency (Figure 6.14) there is a decrease in exergy efficiency with increase of MED-TVC load by about 0.27% for every 10% raise in MED-TVC load (Figure 6-15), because more exergy is used to power the MED-TVC with more exergy destruction. There is no impact of MED-TVC load change on the power plant equipment which is running at full load, (except for the LPT steam turbine) due to extract part of the steam to power MED-TVC.

CO_2 emission appears to increase by 0.45% with every 10% MED-TVC load increase (Figure 6-16) because more heat is apparently utilized to power MED-TVC and net output power decreases.
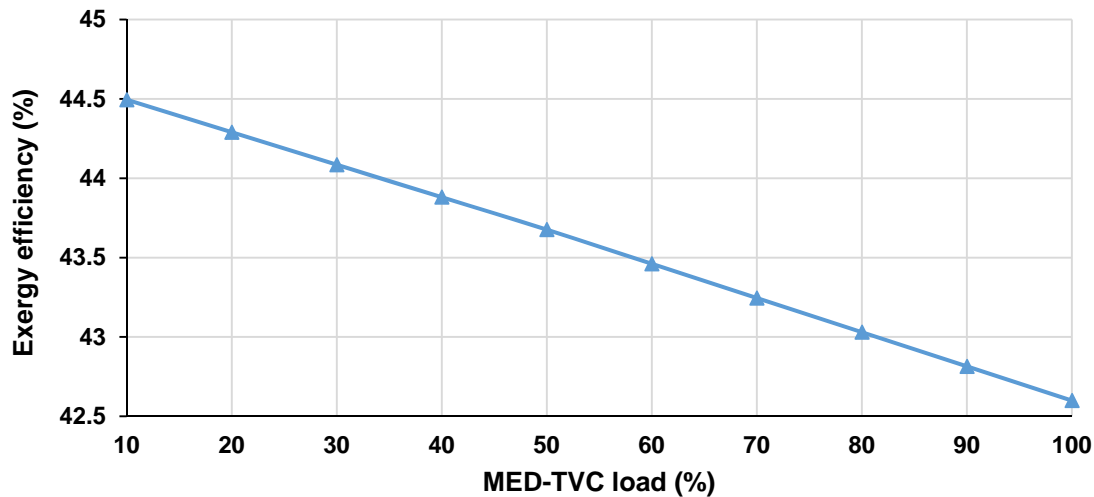
Figure 6-15: Effect of MED-TVC load on CCPP exergy efficiency
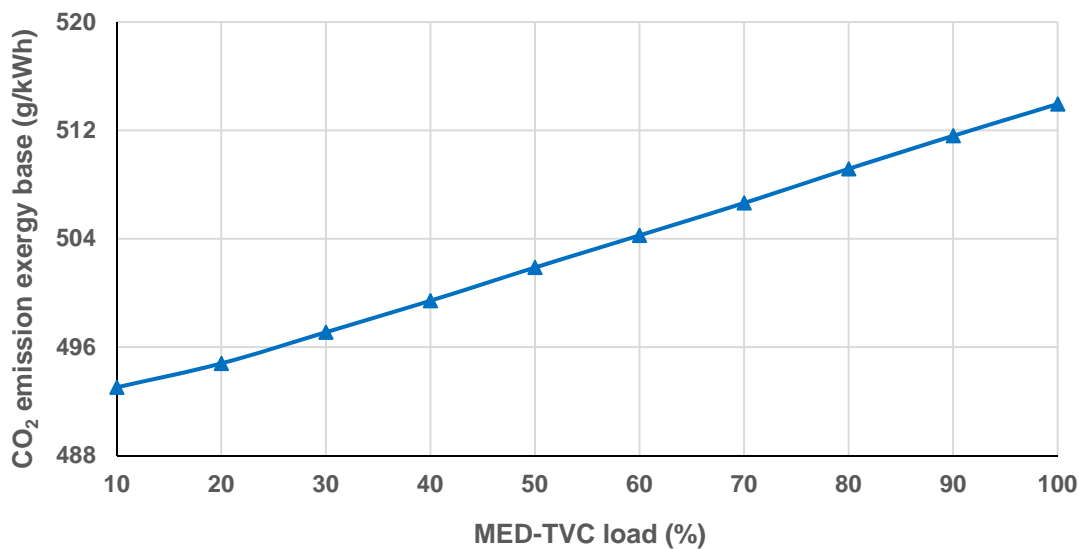
Figure 6-16: Effect of MED-TVC load on CO_2 emission (exergy base)

6.3.4 *Effect of two-pass RO load on CCPP*

The two-pass RO also can be varied from 10% to 100% load as change from scenario I combined cycle power plant standalone to (CCPP + RO), to investigate the effect of the combined power plant with membrane desalination. Both thermal and exergy efficiency of the power plant were reduced by about 0.1% and 0.07% (Figure 6-17), respectively. The gross output power drops linearly with RO load increase by about 0.19% when RO without PX (or 0.1% with PX) for every 10% increase in RO load increase (Figure 6-18), as a result of extracting electrical power to drive the membrane desalination pumps required for feed pressure.

Figure 6-19 shows the increase CO_2 emission with reverse osmosis load increase by about 1% every 10% increase in reverse osmosis load raise, due to decrease in net output power.
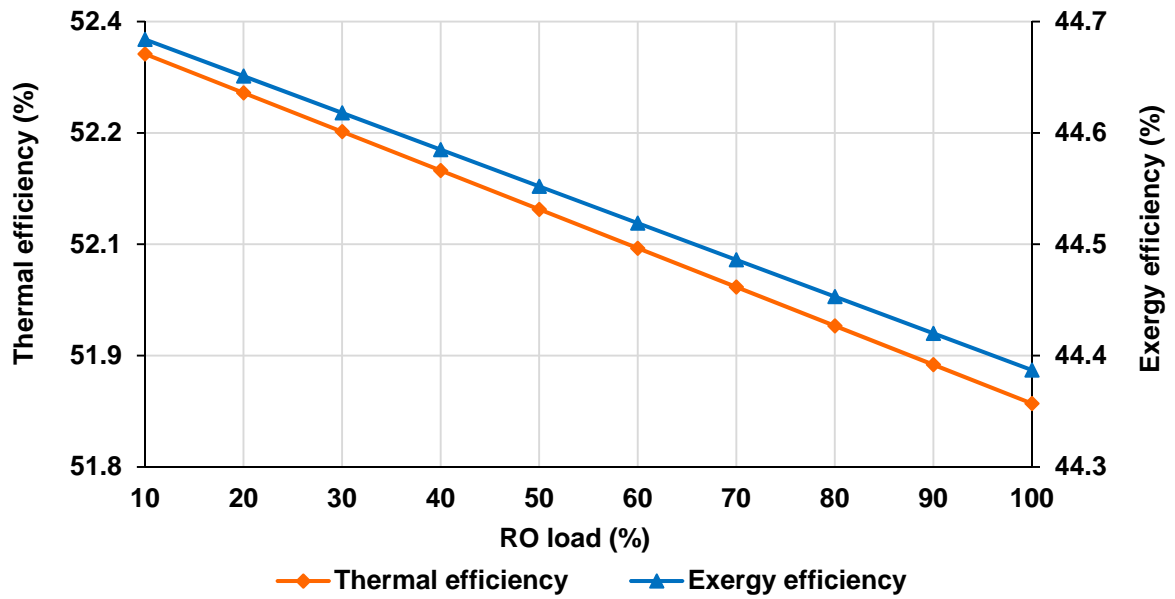
Figure 6-17: Effect of RO load on CCPP thermal and exergy efficiency
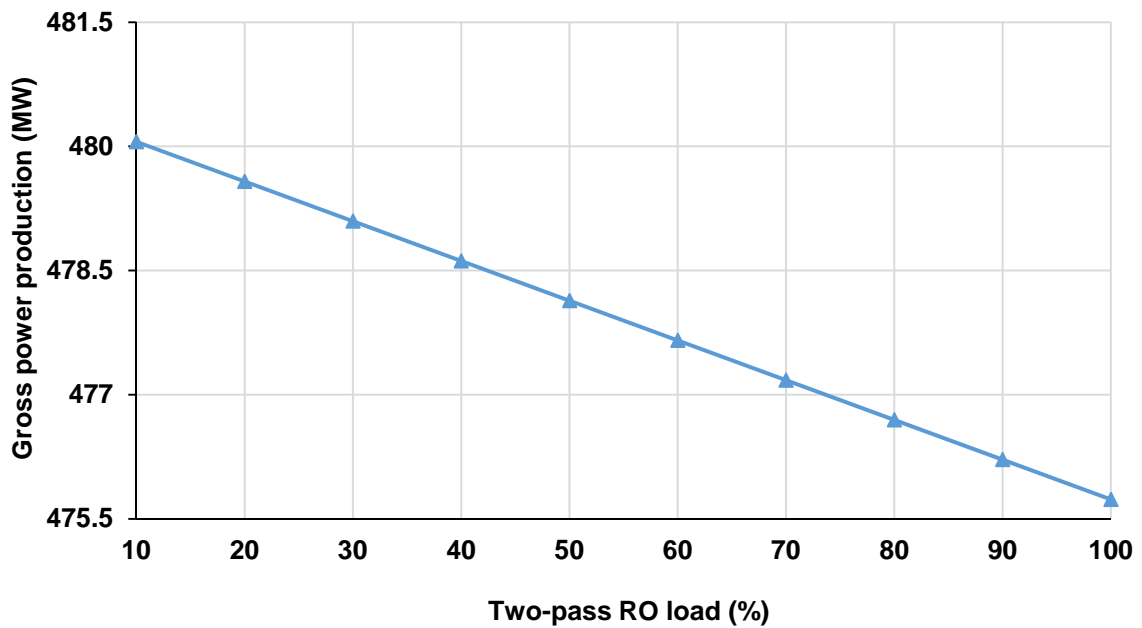
Figure 6-18: Effect of RO load on CCPP gross power
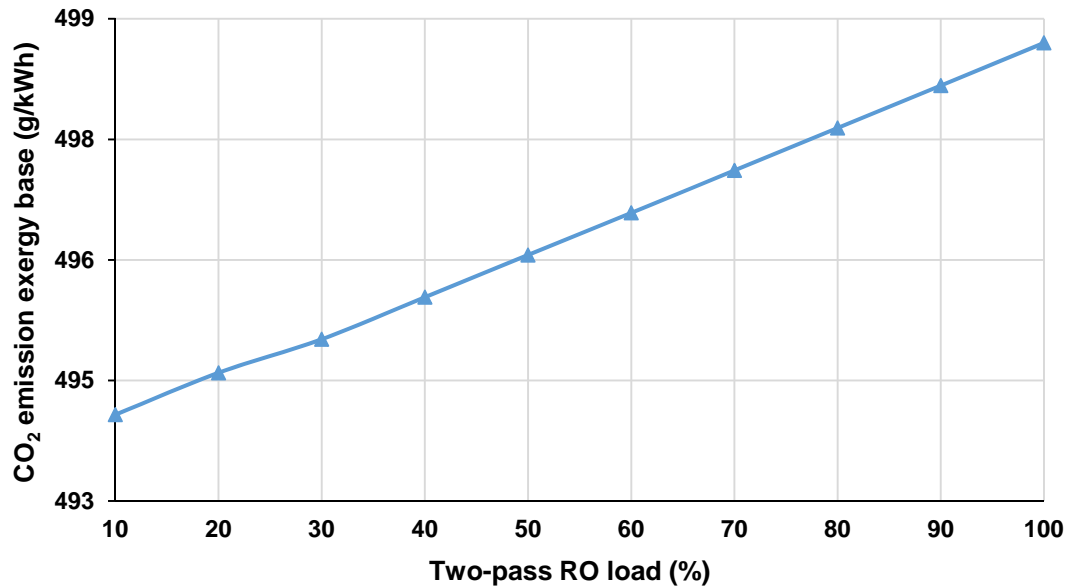
Figure 6-19: Effect of RO load on CO_2 emission (exergy base)

6.4 Absorption Chiller

The climate condition is a big issue for power plant performance and CO_2 emission, especially variation in ambient temperature. As the ambient temperature increases the output power decreases. As mentioned in section 4.3, a Lithium-Bromide-water solution single effect absorption chiller powered by waste heat energy from the plant exhaust gases after leaving HRSG is used in this study. The ability to utilize waste heat energy to operate the absorption refrigeration machine is attractive from the perspective of environmental impact.

6.4.1 *Absorption chiller cycle*

The principles of the absorption chiller were discovered in the nineteenth century and since the 1960s a number of improvements have been made [192]. Figure 4-2 shows a schematic diagram for the working principle of absorption chillers. This principle is similar to that of normal refrigerators, where both cycles evaporate the refrigerant at relatively low pressure to create the cooling effect, then condense the refrigerant at high pressure to reject its heat. The difference between the two cycles is the mechanism by which it reaches the high pressure level. Absorption chillers are powered by a thermal source; this is usually delivered to the chillers via steam, hot water, or combustion. Water is used as the refrigerant of the single effect absorption unit and lithium bromide (salt) as the absorbent. There exist strong attractions between these two fluids which makes the cycle work. The entire process occurs in almost a

complete vacuum [193]. There are five main components in an absorption chiller: solution pump, desorber, condenser, evaporator and absorber.

a) Solution pump

The weak solution of lithium bromide is collected at the bottom of the absorber vessel. From here an airtight solution pump moves the solution through a shell and tube heat exchanger for preheating.

b) Desorber

After exiting the preheater, the dilute solution is collected into the upper shell of the desorber. The solution is surrounded by a pack of coils, which carry either steam or hot water. The steam or hot water transfers heat into the pool of dilute lithium bromide solution. The solution boils leading to the vaporisation of refrigerant. Consequently, the refrigerant escapes to the condenser leaving behind strong lithium bromide. The strong lithium bromide solution exits to the heat exchanger and is subsequently chilled by the dilute solution moving up to the desorber.

c) Condenser

The refrigerant vapour migrates through mist eliminators to the condenser tube bundle. The refrigerant vapour is cooled down on the tubes by rejecting heat to the cooling water and the refrigerant is subsequently gathered at the bottom of the condenser.

d) Evaporator

The refrigerant liquid proceeds to the evaporator at lowered vacuum pressure [6mm Hg (0.8 kPa)] where it gains heat from the fluid being chilled and boils at approximately 3.9°C, creating the refrigerant effect.

e) Absorber

The refrigerant is vapourised in the evaporator and then proceeds to the absorber where Lithium Bromide (LiBr) solution coming from the desorber is sprayed over it. Due to the affinity of the two fluids, water molecules are absorbed by the concentrated solution of LiBr leading to the creation of vacuum in the evaporator. Heat is generated during the absorption process which is rejected to the cooling water. Consequently, a weak solution of LiBr is produced which is pumped back to the desorber and the cycle starts again.

6.4.2 *Absorption chiller exergy analysis*

The exergy analysis of the single effect absorption chiller is carried out at the cooling water dead state T_0 of 20°C and pressure p_0 at 101.3 kPa. Table 6-6 presents the exergy destruction and efficiency calculations for the absorption chiller components.

Table 6-6: Exergy efficiency and destruction calculation of single effect AC components

Equipment	Exergy efficiency (%)	Exergy destruction (MW)
Desorber	$\dfrac{\dot{E}_4 + \dot{E}_7 + \dot{E}_{12}}{\left(\dot{E}_{11} + \dot{E}_3\right)}$	$\dot{E}_{11} + \dot{E}_3 - \dot{E}_4 - \dot{E}_7 - \dot{E}_{12}$
Condenser	$\dfrac{\dot{E}_8 + \dot{E}_{15}}{\left(\dot{E}_7 + \dot{E}_{14}\right)}$	$\dot{E}_7 + \dot{E}_{14} - \dot{E}_8 - \dot{E}_{15}$
Evaporator	$\dfrac{\dot{E}_{10} + \dot{E}_{17}}{\left(\dot{E}_9 + \dot{E}_{16}\right)}$	$\dot{E}_9 + \dot{E}_{16} - \dot{E}_{10} - \dot{E}_1 - \dot{E}_{17}$
Absorber	$\dfrac{\dot{E}_{13} + \dot{E}_1 + \dot{E}_{14}}{\left(\dot{E}_6 + \dot{E}_{10}\right)}$	$\dot{E}_6 + \dot{E}_{10} + \dot{E}_{13} - \dot{E}_1 - \dot{E}_{14}$
Expansion valves	$\dfrac{\dot{E}_9}{\dot{E}_8}$	$\dot{E}_8 - \dot{E}_9$
Heat exchanger	$\dfrac{\dot{E}_3 + \dot{E}_5}{\left(\dot{E}_2 + \dot{E}_4\right)}$	$\dot{E}_2 + \dot{E}_4 - \dot{E}_3 - \dot{E}_5$

It is necessary to calculate the chemical exergy for all the AC cycle as well as the physical exergy. The chemical exergy destruction, caused by dissolving LiBr, is added to the standard chemical exergy of pure LiBr, which is estimated experimentally [164]. Most previous studies neglected the chemical exergy of pure LiBr [14, 25, 129, 194] because in the difficulty of estimating it for the LiBr solution. This might lead to incorrect answers for the values of exergy efficiency and destruction of the absorption chiller.

Figure 6-20 shows the exergy efficiencies of the absorption chiller components. The results show that the internal heat exchanger has the highest exergy efficiency followed by the condenser, whereas the expansion valve has the lowest value as expected. The desorber has high exergy destruction because of the temperature difference between the exhaust gases and absorbent (LiBr and water), as shown in figure 6-21.
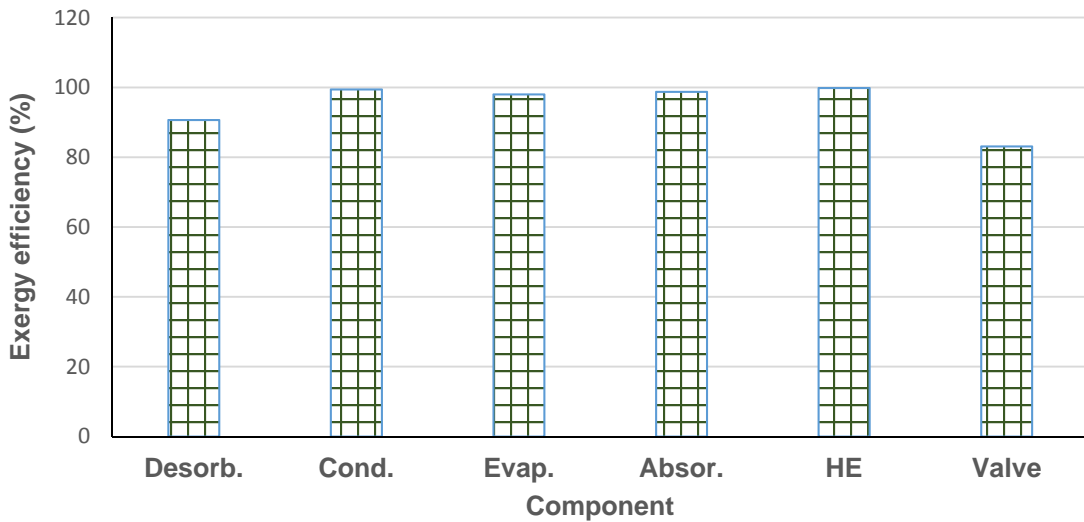
Figure 6-20: Exergy efficiency of absorption chiller components
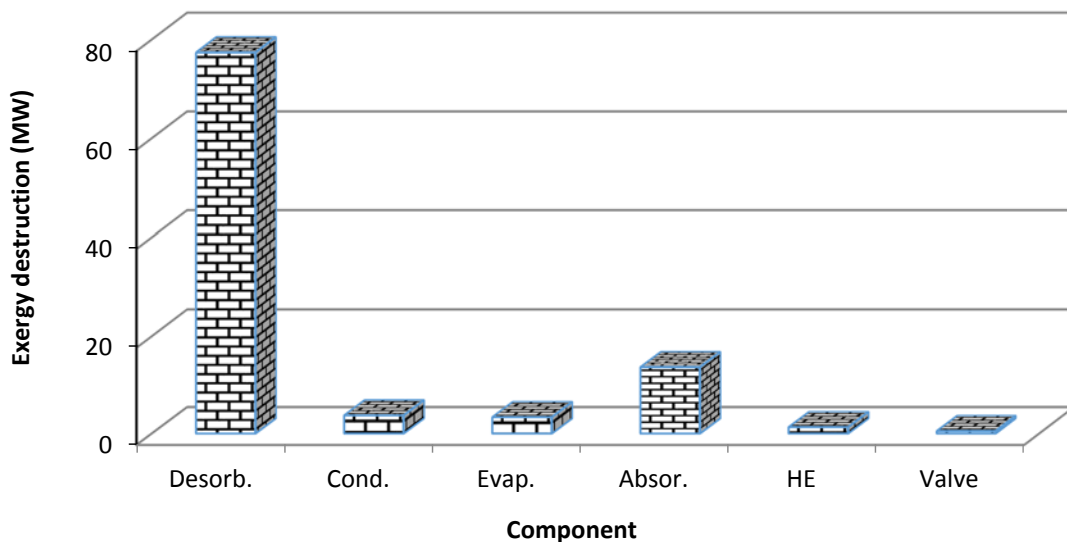
Figure 6-21: Exergy destruction of AC components

Figure 6-22 shows the effect of change in ambient temperature on the CCPP output power at every month. As can be seen the output power declines with ambient temperature rise. July and August are the peak of temperature and thus record the lowest output power. This real issue can be solved by using an absorption chiller powered by the exhaust gas, where the AC cooling is delivered to the GT inlet air, which leads to power saving and avoids degradation in output power. In addition the AC also reduces CO_2 emissions by mitigating the impact of increased temperature.
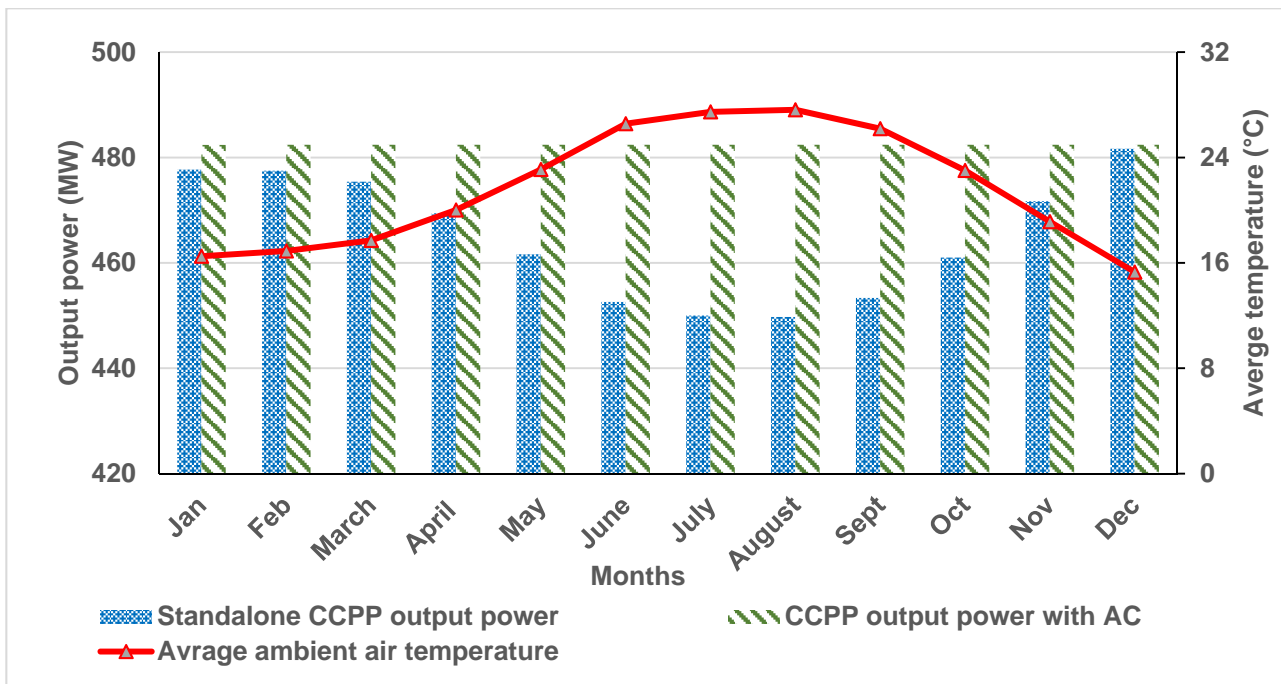
Figure 6-22: Average temperature and corresponding CCPP output power for each month over the year

6.5 Summary

After the model was validated against vendor data it was deemed credible to move forward to the performance analysis with the aims outlined in chapter 1. A number of parametric studies were carried out in this chapter for three different scenarios (standalone CCPP, CCPP + MED-TVC desalination unit and CCPP + two-pass RO desalination unit). The results can be summarized as follows:

Firstly, there is a clear impact of inlet air ambient temperature on the efficiency and output power of the power plant, both of which declined by about 0.2% and 5.4% respectively for every 10°C rise in ambient temperature.

This is due to a combination of different effects. The first is the reduction in the air density, which reduces the compressor mass flow and thus the power output. Also on the compressor T-S diagram, the lines of constant pressure diverge with increased pressure and so more work is done by the compressor in compressing hot gas over a specified pressure ratio compared with cold gas. Finally the mass flow function of the compressor is fixed if the turbine nozzles are choked, which reduces the compressor ratio if the ambient temperature increases and the mass flow is constant. The general results then, are that the specific fuel consumption (SFC) increases and the power

output decreases by 1% for each 1% increase in ambient temperature above the design condition. One impact of increased SFC is an increase in the specific CO_2 emissions, but this is ameliorated to some extent by the presence of the steam turbine which is less sensitive to ambient temperature changes.

The problem of the degradation of output power was solved by adding an absorption chiller powered by exhaust gas to cool the inlet air to the design condition. This increase in performance and efficiency added 145 GW to the power output and reduced the specific CO_2 emissions.

Secondly, the exergy efficiency in scenario I (CCPP standalone) was the highest whereas for scenario II (CCPP+MED-TVC) it was the lowest due to the utilisation of waste heat energy to produce water, which reduced the CCPP's output power by about 22.5MW.

Thirdly, when the CCPP was coupled with RO the output power was reduced by about 4.5 – 9.4MW depending on the RO energy recovery device used and the load, whereas the extraction of steam required to power the MED-TVC reduced the output power by about 22.5MW.

It can be concluded that the parametric study has revealed that the power plant was highly affected by ambient temperature in terms of power output and efficiency. Relative humidity had little impact on performance. In addition, coupling the CCPP with two ROs has less effect on CCPP performance compared with coupling it to the MED-TVC. To confirm these results, an economic analysis is carried out in the next chapter.

CHAPTER 7. ECONOMIC ANALYSIS

7.1 Introduction

Any new project requires an economic feasibility study, even if this project has a high efficiency. The main purpose of economic analysis is to design and select an acceptable project that contributes to the region or country. Using economic analysis at early stage of the project can help the decision maker to proceed or not with the project. There are many factors to be taken into account during economic analysis [195]. In order to assess the viability and profitability of the proposals it is possible to ascertain a range of economic indicators such as Pay Back Period (PBP), Average Rate of Return (ARR), Net Present Value (NPV) and Profitability Index (PI).

The purpose of this chapter is to assess economically four scenarios:

Scenario I: the combined cycle power plant (CCPP) standalone. The CCPP is an existing power plant in Libya (which is the source of the electricity and steam required to power the RO and MED-TVC), where the AC as proposed is a single effect refrigeration system used to provide cool inlet air to the CCPP.

- ➤ Scenario II: MED-TVC and RO desalination improvements. The MED-TVC and RO models are proposed desalination plants to produce about 7.5 million m^3/year distillate water from seawater and powered by CCPP. The capacity factor for the present study is considered to be 85% with the usual power plant capacity factor [142].
- ➤ Scenario III: cogeneration systems comparing CCPP + AC + MED-TVC with CCPP + AC + RO.
- ➤ Scenario IV: comparison of single effect desalination (SED) and single pass reverse osmosis (SRO) desalination systems. The SRO is powered by electricity and SED is powered by ground geothermal water. Both models would provide 2.5 million m^3/year from the brackish ground water to provide distillate water for local communities.

7.2 Initial Cost Estimates

The proposed plant models have been built and investigated in the previous chapters. The capital cost of each system was initially obtained from official sources or previous

studies. Then the profitability of each plant is calculated by totalling the expenses (O&M) and calculating net profit after selling the electricity or water product. This study is carried out for different scenarios with the CCPP and desalination systems at full load with an average seawater temperature and salinity 20°C and 37g/kg, respectively. The lifetime of the project is assumed to be 20 years with 5% interest and the system running for 85% hours per year.

The initial cost of equipment to be purchased can be taken directly from the vendor or from past studies or alternatively by using the extensive cost database maintained by the engineering company. The initial cost for each model was obtained to give comprehensive information about the economic feasibility of the proposals by finding the total cost of the AC, RO, MED-TVC, SED and SRO plants. According to Bejan and Moran [142], contingency factors, which represent for example sudden changes in price and transportation difficulties, were added as an extra 5% to the Equipment Purchase Cost (EPC), while the equipment installation cost added 33% of EPC to the capital equipment cost. Electrical equipment and material added 13% and finally instrumentation and controls added 12% to the total equipment cost for all systems.

7.3 Heat Exchanger Cost Estimation

The existing model of the CCPP was combined with a single-effect absorption chiller containing cooling heat exchangers and it was very difficult to obtain a direct quotation for their initial cost from the supplier company and this was also true for the MED-TVC. Heat exchangers are used in most of the proposed models, although their size depends on the absorbed heat. The cost of the heat exchangers are estimated using the ESDU 92013 method [169] because it is difficult to obtain direct quotations. ESDU has gained a good reputation among British heat exchanger manufacturers, [168], the major UK vendor of heat exchangers, IMI Marston, uses ESDU to provide the C-values required in calculating the cost of heat exchangers. This method depends on the estimation of heat exchanger NTU (equation 3.68) with available data for cold/hot stream inlet/outlet temperatures. The heat exchanger material is assumed to be 316L stainless steel. The final cost of the heat exchanger is calculated in a Microsoft Excel spreadsheet by inserting the required data from the ESDU tables, eg. Figure 7.1.

The required data for both hot and cold streams includes the hot and cold side temperatures which can be determined using IPSEpro simulation software. The initial

and outlet hot and cold temperatures (T_h, T_c) for each stream are used as input data to calculate the mean temperature difference in the following equation:

$$\Delta T_m = \Delta T_{lm} = \frac{[(T_{h,in} - T_{c,out}) - (T_{h,out} - T_{c,in})]}{\log_e[(T_{h,in} - T_{c,out})/(T_{h,out} - T_{c,in})]} \tag{7.1}$$

The value of $\dot{Q}/\Delta T_{lm}$ is calculated to find the values of C_1 and C_2 by reading directly from the ESDU tables [169]. As the value of $\dot{Q}/\Delta T_{lm}$ is found between two scales as shown in figure 7.1 for double pipe heat exchangers [169], the C-value is then calculated by logarithmic interpolation as follows:

$$C = \exp\left\{\log_e C_1 + \frac{\log_e(C_1/C_2)\log_e[(\dot{Q}/\Delta T_m)/(\dot{Q}/\Delta T_m)_1]}{\log_e(\dot{Q}/\Delta T_m)_1/(\dot{Q}/\Delta T_m)_2}\right\} \tag{7.2}$$

where:

C_1 is estimated cost at $\dot{Q}/\Delta T_{m1}$ (£/W/K)

C_2 is estimated cost at $\dot{Q}/\Delta T_{m2}$ (£/W/K)

Multiplying the C-value by $\dot{Q}/T_m$ will give the final cost of the heat exchanger. Figure 7-1 shows a heat exchanger calculation.

Heat exchanger calculator			
	Heat Exchanger Costing		
Hot side			
	temperature In	52	°C
	Temperature Out	25.4	°C
Cold side			
	temperature In	24	°C
	Temperature Out	33	°C
Heat load Q		9130	W
Mean Temp. Difference (Eq. 7.1)		6.7485523	°C
$(Q/\Delta T_m)$		1353	W/°C
	C1	2.8	
	C2	1.4	
	$(Q/\Delta Tm)_1$	10000	
	$(Q/\Delta Tm)_2$	1000000	
C-value (Eq. 7.2)		5.32	$/W/°C
Heat Exchanger final cost		11083.898	$

Figure 7-1: Example of heat exchanger cost calculation

The operation and maintenance (O&M) cost for the heat exchanger varies but is assumed as 5% of the purchased cost [28]. The installation and piping costs are assumed to be 30% of equipment purchased cost, the supervision and construction are costed 30% [142].

7.4 Annual Cash Outflow and Inflow

The annual cash outflow covers the money spent for operation and maintenance (O&M). It has been calculated as a function of plant capacity per year. All proposed systems are assumed to operate at 85% per year [142]. For the combined cycle power plant referring to the Libyan Electrical Company the operating fuel is natural gas and the cost is estimated to be $0.16/kg [196] but the natural gas price is subsidised in Libya for industrial and petrochemical use. In this study the real cost of $0.16/kg is used. The O&M costs are evaluated for each separate system. The CCPP O&M is calculated by as a fixed value 13.17$/kW/year [89], whereas the absorption chiller O&M is calculated according to Boonnasa and Namprakai [197] and the MED-TVC O&M cost is estimated to be $0.39/m³ [89], RO operation and maintenance costs are $0.126/m³ [105].

Revenue or sales income profit is represented by the annual cash flow balance of O&M costs against revenue income. In this study, the products sold are electrical power and potable water. According to the Libya Electricity Company, the electricity selling tariff in Libya is $0.07/kWh [89], which is highly subsidised [198]. The potable water selling tariff is $2.5/m^3 for domestic consumers [89]. The revenue for each model was calculated according to Libyan prices and in order to compare the effect of different sales prices on annual revenue, to find at what selling price the project is not economic a variations in the prices of electricity and potable water will be considered from $0.04/kWh to $0.09/kWh and $1.25/m^3 to $ 2.75/m^3, respectively.

7.5 Plant Costs

a) *Combined cycle power plant estimation cost*

The combined cycle power plant (CCPP) purchase cost is based on a specific cost in $/kW obtained from Libyan General Electrical Company [177]. The estimated cost for CCPP is £228.8/kW which is equivalent to $352.4/kW (the rate of exchange is assumed at £1=$1.54 corresponding to the date of ascertaining the information [10]. The equipment purchase cost of this study's CCPP, which produces 487MW at ISO conditions [8], is $172000 million.

b) *Absorption chiller*

In this study two absorption chillers are proposed for cooling the CCPP inlet air. Their costs were obtained from a recently published study [197] and for a capacity of 8188 kW a specific cost of £78.21 /kW equivalent to $120.44 /kW is obtained. Applying this to each absorption chiller with a capacity of 8188 kW, this gives the total cost $986,000.

c) *Multi effect desalination with thermal vapour compression*

The MED-TVC desalination plant purchase costs were obtained from the previous study by Hanafi el al [89]. The specific cost was $1524/m^3, where operation and maintenance costs are fixed at $0.39/m^3. The estimated investment cost of the MED-TVC desalination plant with a capacity of 24,000 m^3/day is $37,000,000.

d) *Two-pass RO desalination*

There are five different two-pass RO configurations which are thermodynamically investigated in Chapter 5. The purchase costs of these configurations are estimated using the previous study by Ghaffour et al [16].   The estimated total investment cost

of the RO desalination plant with a capacity of 24,000 m^3/day is $33,000,000. The costs of ERT and PX are calculated using equation 3.80, then the cost is added to the RO cost.

e) Single effect desalination

The initial cost of the single effect desalination is estimated according to the literature [199] based on the annual volume of water produced. This system is proposed to provide 8208 m^3/day of potable water from brackish water. The initial cost of SED is $6740000 [28], with the operation and maintenance costs estimated at $105m^3/day).

f) Single-pass RO

The cost of the proposed single-pass unit with PX to produce 8208 m^3/day of potable water from brackish water is estimated [16] as $2.5 million. whereas the operation and maintenance costs are $0.126/m^3 [105].

7.6 Profitability Evaluation

Economic assessment is performed for each proposed system to find its profitability.

a) Scenario I stand-alone CCPP

The stand-alone CCPP produces 487MW of electricity at ISO conditions. However, there are fluctuations in output power during the year due to variations in inlet ambient temperature around Zawya City average temperature 20°C (Section 3.12.1). This could be solved by adding a single-effect absorption chiller to reduce the ambient inlet air temperature to ISO condition 15°C. The output power at 20°C is 464MW with plant load factor 85% and the economic/project life time of 20 years was assumed to be the reasonable estimated length of time for the proposed systems [12], which is less than the usual lifetime which could be 30 years. Table 7-2 shows the PBP, NPV, ARR and PI.

Table 7-1: Economic analysis for stand-alone CCPP

	At average temperature 20°C	At ISO temperature 15°C
Life time (year)	20	20
PBP (year)	4.6	4.2
NPV $ million	891	999
ARR (%)	29.5	31.6
PI	1.9	2.1

For the CCPP without AC, the project total capital investment would be paid back within 4.6 year (this agrees with [25]) and with ARR 29.5% and PI 1.9, where the NPV is $891Million for 20 years of plant operation. The PBP could be reduced to 4.2 years with increase in NPV, ARR and PI ($999 million, 31.6% and 2.1, respectively), by adding AC to the CCPP to operate the plant at inlet air temperature 15°C. Despite additional capital expenditure of $2,000,000, addition of the absorption chiller to CCPP significantly improves all the economic indicators while still leaving waste heat at a temperature of 97°C which can be used for desalination.

b) Scenario II desalination systems

Different desalination technologies and configurations will be evaluated economically as shown in table 7.1.

Table 7-2: The desalination systems

Number	Mode	Configuration
1	Thermal desalination	MED-TVC
2	Thermal desalination	MED-TVC+PHE
3	Two-pass reverse osmosis	Standard RO
4	Two-pass reverse osmosis	RO + ERT
5	Two-pass reverse osmosis	RO + PX
6	Two-pass reverse osmosis	RO + PX + ERT
7	Two-pass reverse osmosis	RO + PX + PX
8	Single effect desalination	SED
9	Single-pass reverse osmosis	SRO

The MED-TVC and RO desalination plants are powered by energy that comes from a CCPP and each plant produces 24000m^3/day of potable water. The lifetime of the proposed desalination plants is assumed to be 20 years. Figure 7-2 shows the PBP (equation 3.76), of these 7 proposed desalination systems which are used to produce distillate water from seawater. As can be seen in figure 7.2 the MED-TVC system stand-alone has the highest PBP of about 4.5 years compared with the other systems. This period could increase at low potable water selling price. On the other hand this period could be reduced to 2.93 years by adding the preheater to raise feed water temperature. This result agrees with thermodynamic analysis (Section 5.2.1.4) which showed that the GOR and exergy efficiency improved with the preheater.

Meanwhile the standard two-pass RO PBP is about 2.9 years, Despite additional expenditure for adding PX to the RO there is significant improvement on all economic aspects, because of reduced power consumption. The PBP could be reduced to 2.1 years when PX added to both the first and second stages, which is the lowest PBP compared with the other scenarios. This result is confirmed by thermodynamic analysis that the exergy efficiency of RO is higher than MED-TVC (Section 5.2.3.1) because the energy consumed by MED-TVC is higher than for the RO system. Where the MED-TVC consumes steam which could generate 22.5MW, standard RO consumed only 9.4MW and only 4.5MW with PX in both stages.
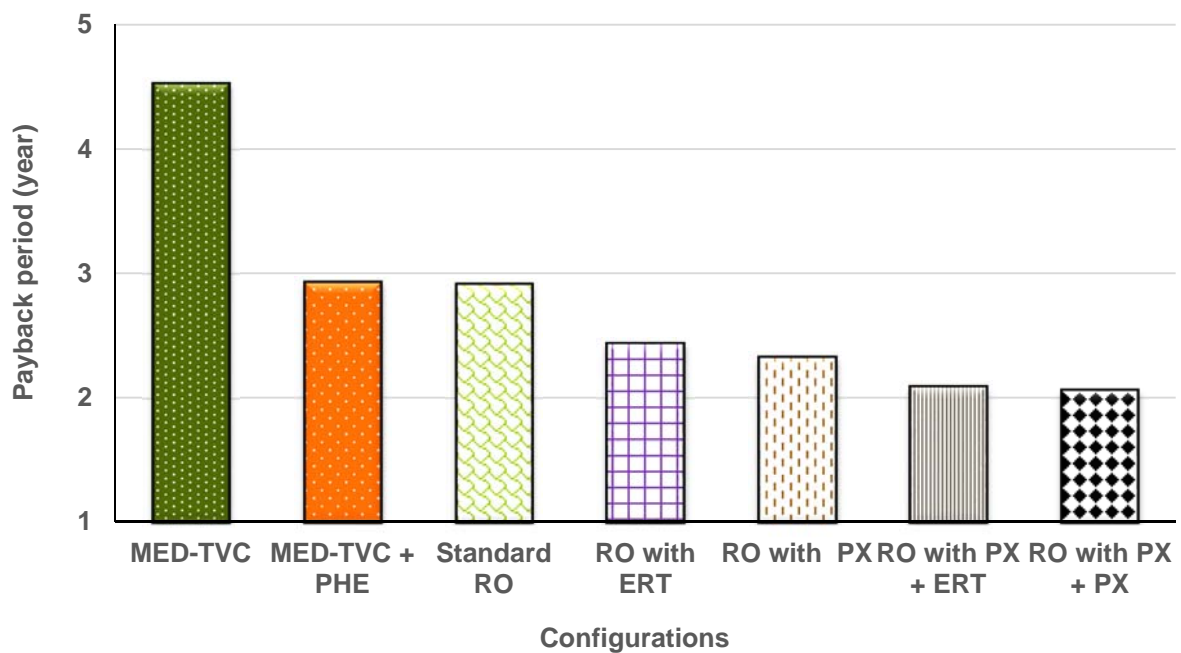
Figure 7-2: PBP for different desalination systems

Figure 7-3 to 7-5 illustrate the NPV, ARR and PI for these different desalination systems (equations 3.77 to 3.79). As can be seen MED-TVC has the lowest NPV at $71 million, because it consumed more energy, whereas RO with PX at both stages has the highest value with about $118 million as a result of consuming less power compared with the other configurations. However, the PBP of MED-TVC with PHE is almost the same as standard RO but it has higher NPV, because it produces more high revenue water over the remaining lifetime after PBP. Whereas ARR and PI, figures 7-4 and 7-5 (Equations 3.78 and 3.79), agree with PBP. From these results it can be concluded that MED-TVC + PHE is the best choice of thermal desalination whereas RO with PX at both stages is the best choice for RO membrane desalination. The subsequent sensitivity study will focus on these two systems.

	MED-TVC	MED-TVC + PHE	Standard RO	RO with ERT	RO with PX	RO with PX + ERT	RO with PX + PX
☐NPV	71	104	93	106	109	117	118

Configurations
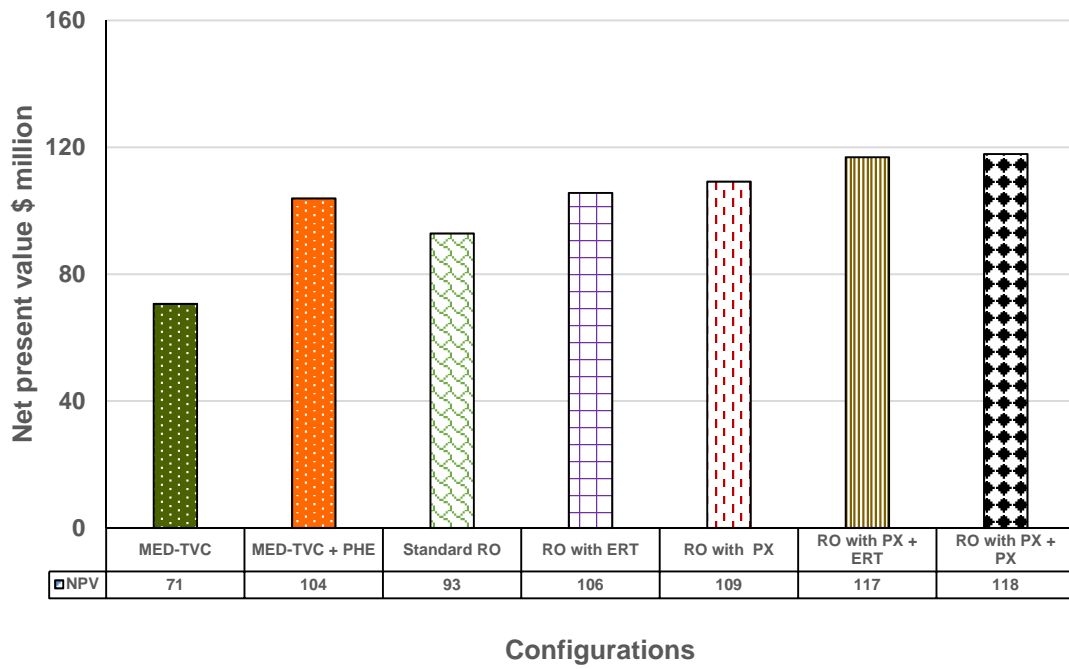
Figure 7-3: NPV for different desalination systems

	MED-TVC	MED-TVC + PHE	Standard RO	RO with ERT	RO with PX	RO with PX + ERT	RO with PX + PX
☐ARR	29.9	39.1	39.2	43.2	44.3	46.7	47.0
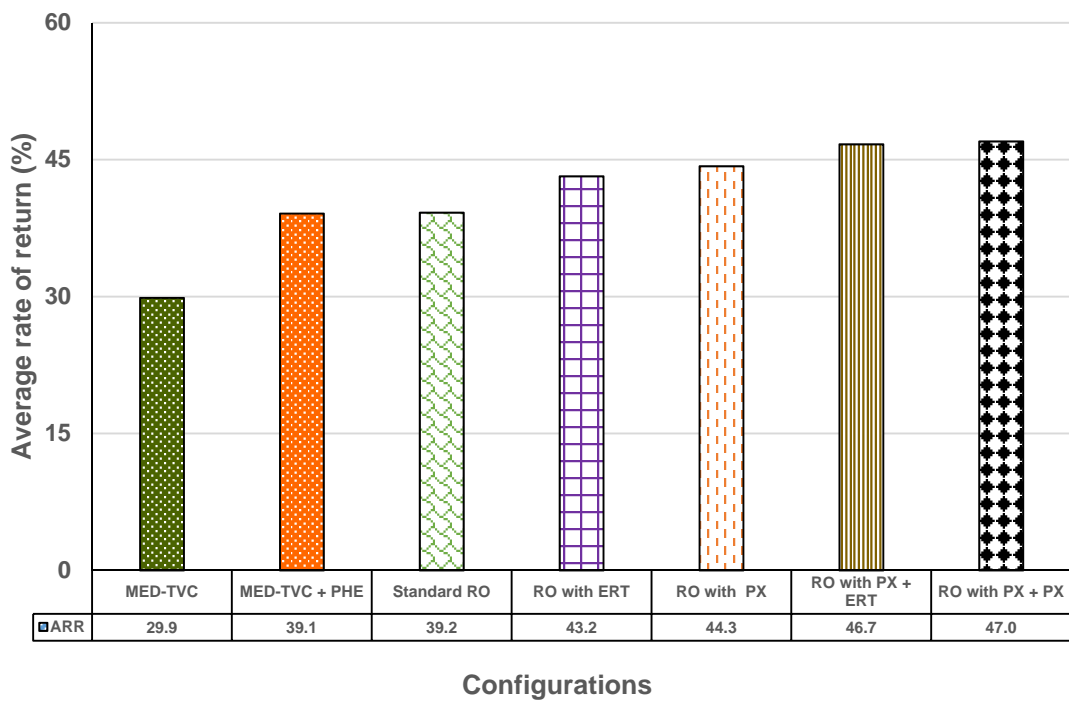
Configurations

Figure 7-4: ARR for different desalination systems

	MED-TVC	MED-TVC + PHE	Standard RO	RO with ERT	RO with PX	RO with PX + ERT	RO with PX + PX
▪PI	1.9	2.1	2.8	3.2	3.3	3.6	3.6
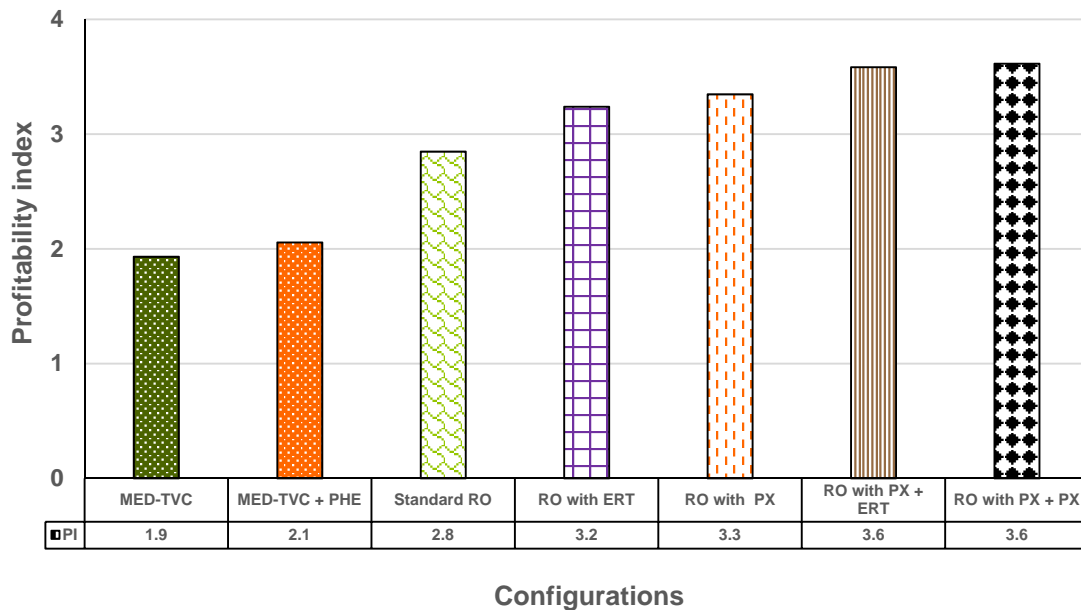
Configurations

Figure 7-5: PI for different desalination systems

c)   Scenario III cogeneration systems

In this scenario the CCPP is coupled with the different desalination configurations. Figure 7-6 shows the PBP for 7 different configurations.

- ➢ Columns two shows the BPB reduced by adding AC to confirm previous results (a) and provide a benchmark for the following cogeneration cases.
- ➢ Columns 3 to 5 show that the PBP of CCPP + MED-TVC is higher than CCPP standalone, because the thermal desalination has low efficiency (Section 5.2.1.3) and when the CCPP is coupled with MED-TVC the plant efficiency decreases (Section 6.2.2.1).
- ➢ Columns 6 and 7 show CCPP with RO is always better than CCPP alone, even with AC, and the PBP drops to 4.2 and 3.9 years. This result agrees with energy and exergy efficiency when the CCPP is coupled with RO desalination, because the RO desalination efficiencies are high and low energy is consumed (Section 5.2.2.2).

The previous results confirmed that CCPP + AC + RO is the most preferred project as it has greatest NPV, greatest ARR (Figures 7-7 and 7-8).

	CCPP	CCPP+AC	CCPP+MED-TVC	CCPP+AC+MED-TVC	CCPP+AC+MED-TVC+PHE	CCPP+RO	CCPP+AC+RO
PBP	4.3	4.1	4.6	4.4	4.1	4.2	3.9
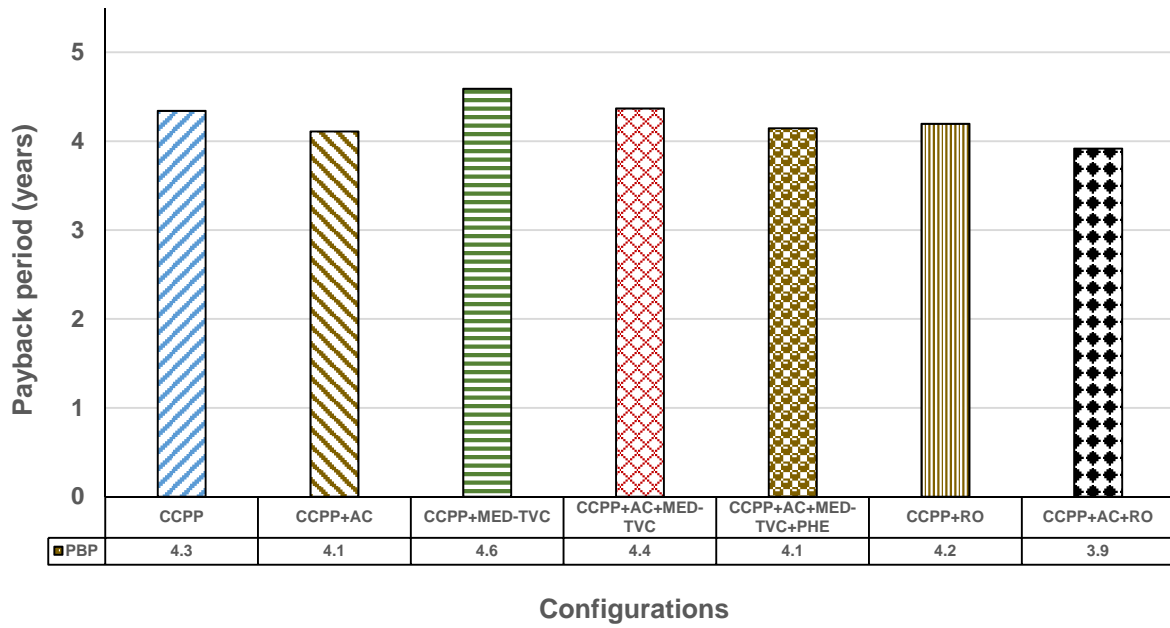
Configurations

Figure 7-6: PBP for different configurations

	CCPP standalone	CCPP+AC	CCPP+MED-TVC	CCPP+AC+MED-TVC	CCPP+AC+MED-TVC+PHE	CCPP+RO	CCPP+AC+RO
NPV	948	1009	966	1020	1078	1048	1128
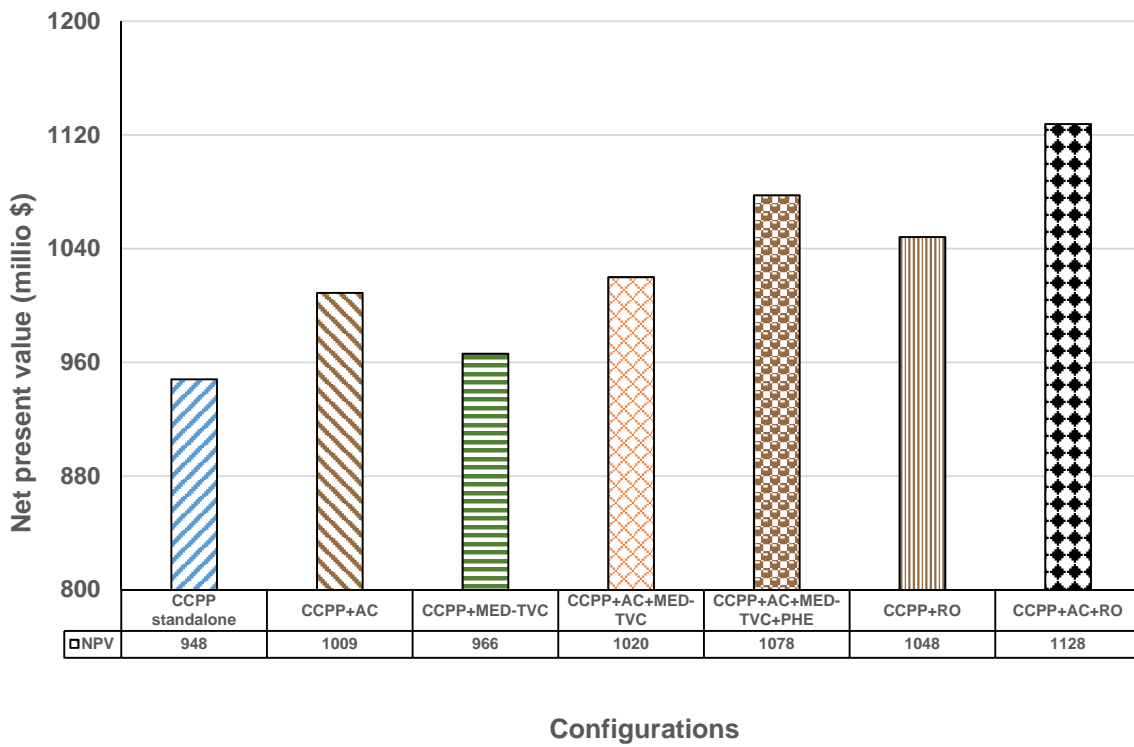
Configurations

Figure 7-7: NPV for different configurations
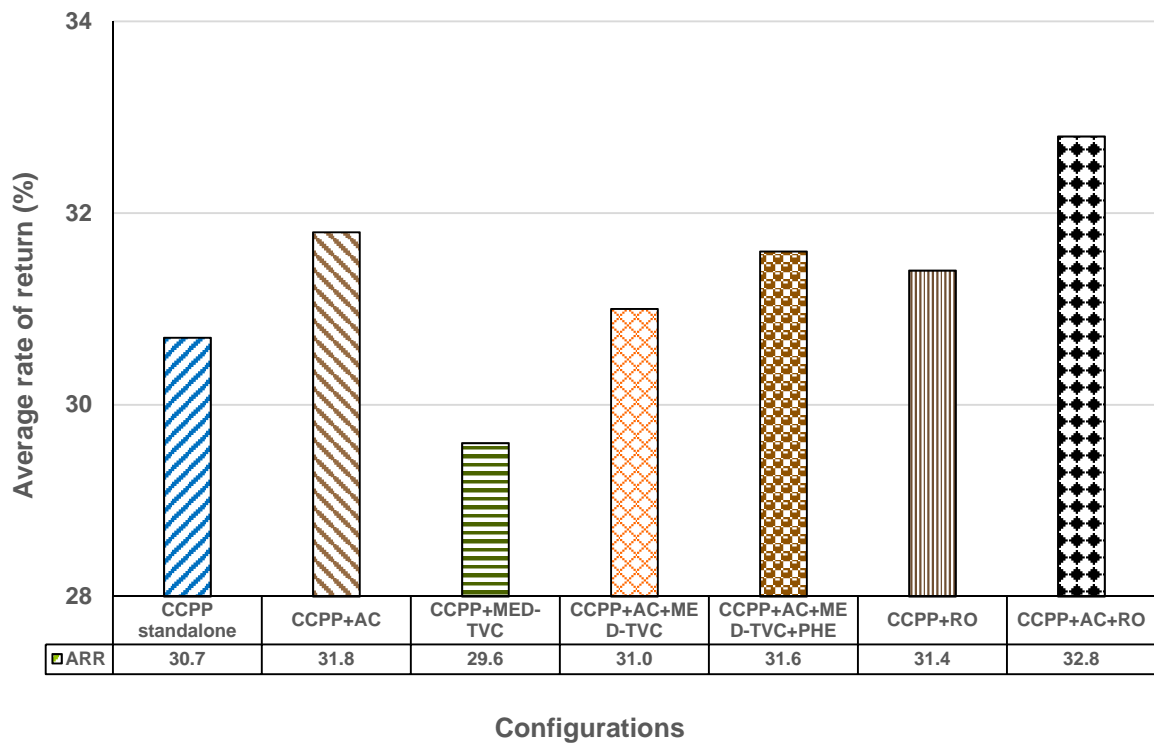
Figure 7-8: ARR for different configurations

	CCPP standalone	CCPP+AC	CCPP+MED-TVC	CCPP+AC+MED-TVC	CCPP+AC+MED-TVC+PHE	CCPP+RO	CCPP+AC+RO
ARR	30.7	31.8	29.6	31.0	31.6	31.4	32.8
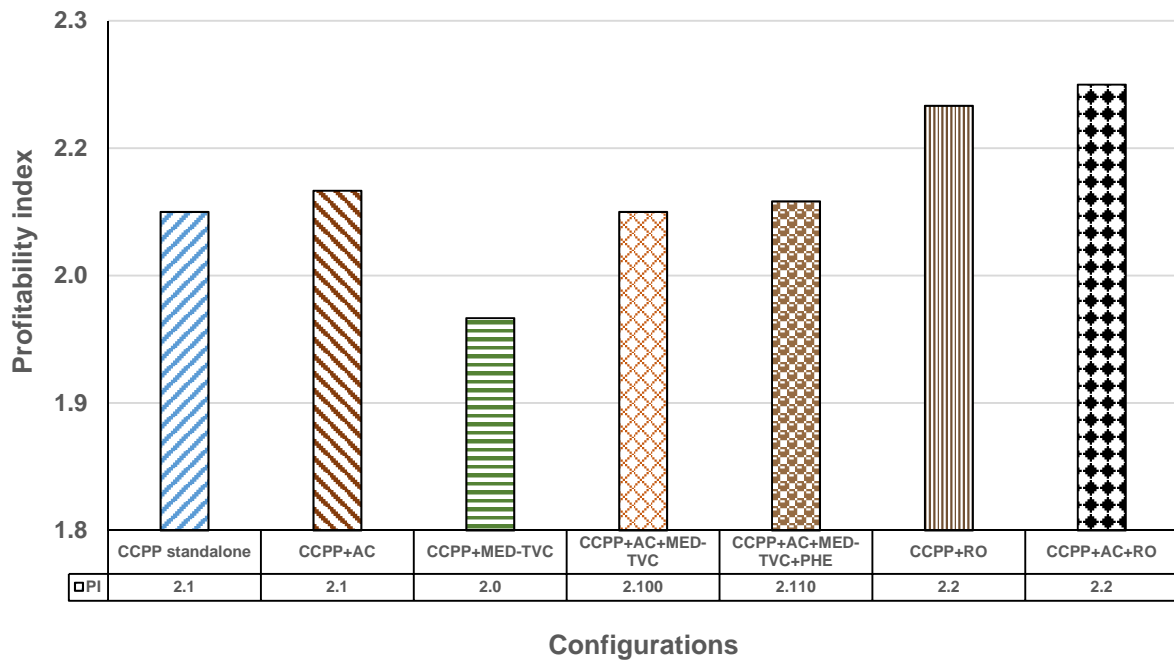
Configurations

Figure 7-9: PI for different configurations

	CCPP standalone	CCPP+AC	CCPP+MED-TVC	CCPP+AC+MED-TVC	CCPP+AC+MED-TVC+PHE	CCPP+RO	CCPP+AC+RO
PI	2.1	2.1	2.0	2.100	2.110	2.2	2.2

Configurations

d) *Scenario IV SED and SRO systems*

The SED and SRO are chosen to produce distillate water from brackish water, where the SED is powered by geothermal water at a temperature of 73°C and the SRO plant by electricity to produce 8208 m³/day. Table 7-3 shows the comparison between SED plant and SRO plant. The PBP of SRO is lower than SED by 0.6 year also the net

present value of SRO is higher than SED by about $17 million. Similarly SRO outperformance SED with respect to ARR and PI. While, the heat required to evaporate the brackish water with SED is free, electricity is still required to pump the geothermal water and feed water to the effect.

Table 7-3: Comparison between SED and SRO desalination systems

	SED	SRO
Lifetime (year)	20	20
Total capital cost (million)	6.6	2.5
PBP (year)	1.1	0.5
NPV $ million	33	50
ARR (%)	61	230
PI	5	20

7.7 Sensitivity Study

The sensitivity of the economic analysis was investigated in terms of the effect of electricity, fuel and potable water prices because the most common factors affect the economic analysis. A number of studies were conducted where three of the proposed models were assumed to operate at full load in ISO conditions with seawater temperature set at 20°C with 85% capacity factor.

7.7.1 *Electricity selling prices*

The electricity prices were chosen to be in the line with those in Libya, However, electricity prices in Libya are subsidized heavily by the government [200], but in this study the real selling prices are used. The main purpose of performing this sensitivity study with different electricity prices was to determine at what minimum price each model can become economically viable and also to show how increases in this price could affect the use of the selected economic evaluation methods. Variations in electricity price were created in steps of $0.01/kWh, from $0.04/kWh to $0.09/kWh this range was chosen to find at what price the project will not preferable. Meanwhile the fuel and potable water prices for the systems are fixed at the real rate $2.5/m^3 and $0.16/kg respectively. The previous operating assumptions were also used so that all models operated at full load in Libyan environmental conditions and with an average seawater temperature of 20°C and 37g/kg salinity, while the desalination systems produced potable water at full capacity as shown in figures 7-6 to 7-9. Moreover, the lifetime of this project was again considered to be 20 years.

The effect of the variation in electricity prices on payback period is illustrated in figure 7.10. At an electricity price of below \$0.04/kWh, the standalone CCPP model was found to be non-viable due to exceeding the 20 year life time of the project, indicating recovering capital costs could not be achieved within the project's lifetime at \$0.04/kWh. Whereas, the PBP could be reduced to 2 years if the electricity price increased to \$0.09/kWh. The CCPP standalone at \$ 0.04/kWh has a negative NPN due to high initial and O&M costs. There is a clear influence of electricity selling price increase for PBP, NPV, ARR and PI. The CCPP PBP could reduce from 25 years to 15 years when coupled with AC and RO at the lowest electricity price \$0.04/kWh. However, the cogeneration plants of CCPP+AC+RO and CCPP+AC+MED-TVC+PHE were found not feasible with the PBP more than 20 years at electricity selling price \$0.036/kWh and \$0.037/kWh.

Coupling CCPP with AC and two-pass RO is the best alternative cogeneration system, since it has a lower PBP and higher NPV, ARR and PI, as shown in figure 7-11 and figure 7-12 and 7-13. In addition, as the electricity price increases the PBP for all scenarios dramatically decline, due to increase of product revenue from electricity and water. An increase in electricity price to \$0.09/kWh decreased the length of the payback period to a range of less than 2.5 years for all of the models, while the lowest value was obtained for CCPP + AC + RO. This is because it generated the higher levels of electric energy sold for \$0.09/kWh to set against its initial capital costs.
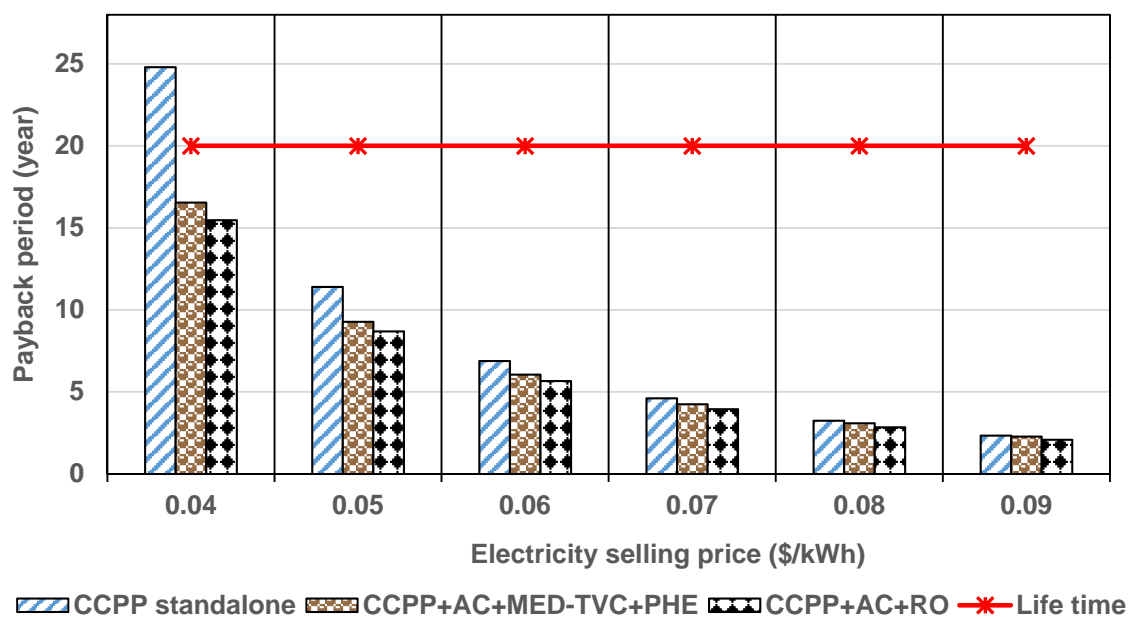
Figure 7-10: Payback period against electricity price for different configurations
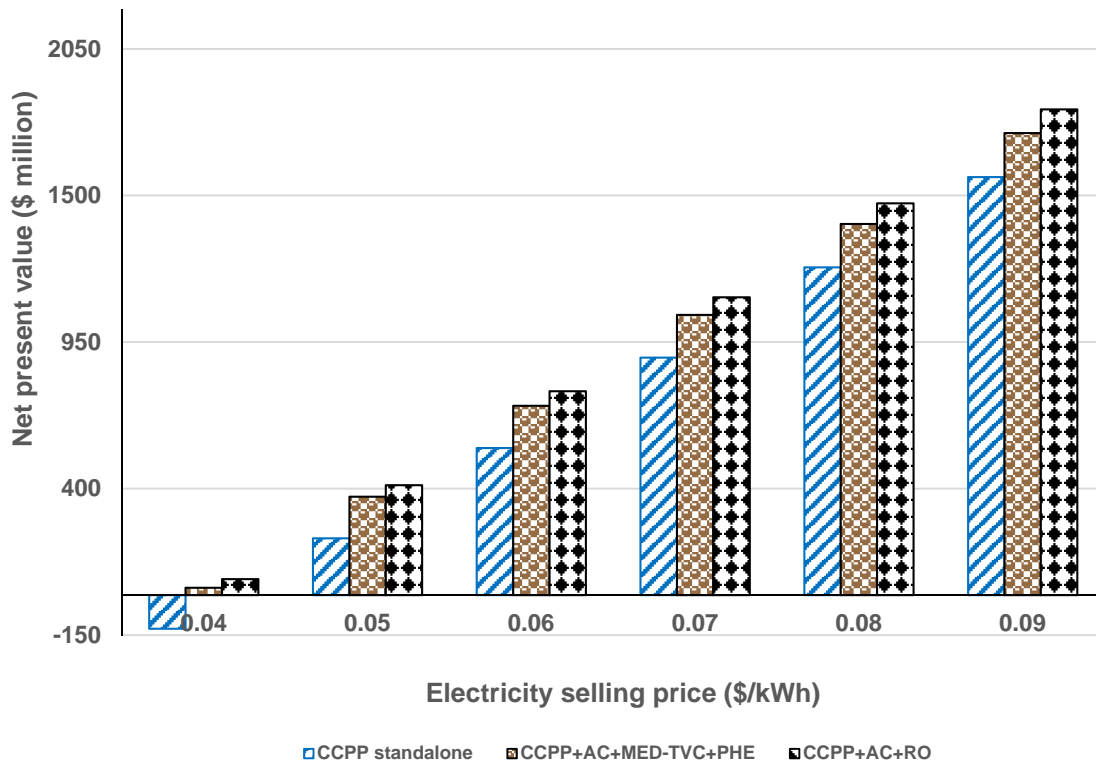
Figure 7-11: Net present value against the selling electricity prices variation
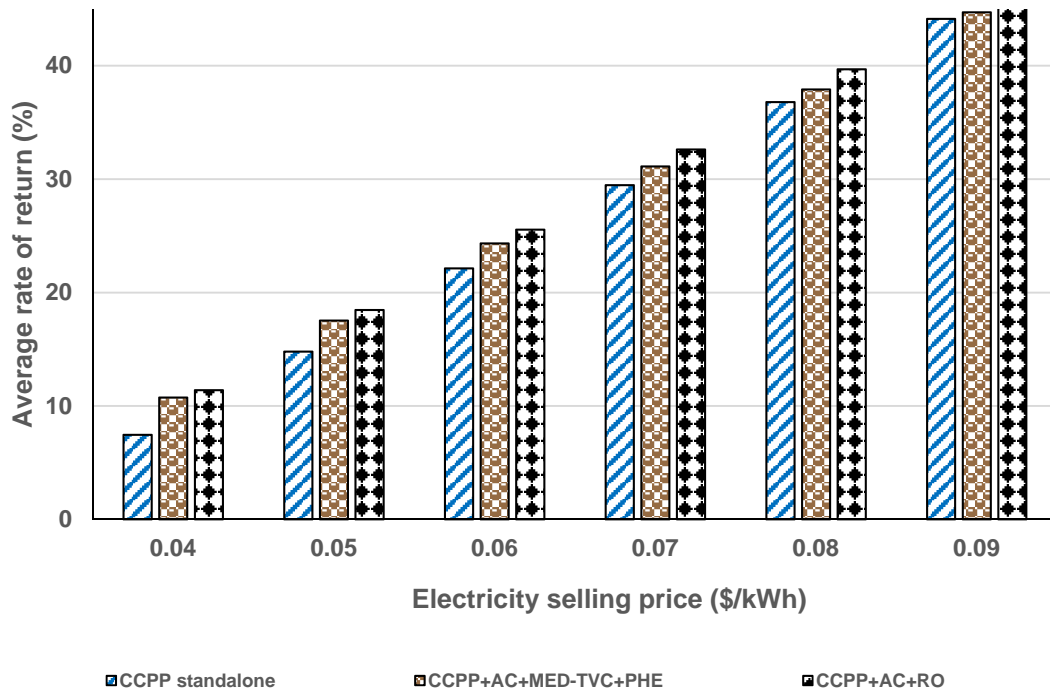
Figure 7-12: Average rate of return against the electricity price variation
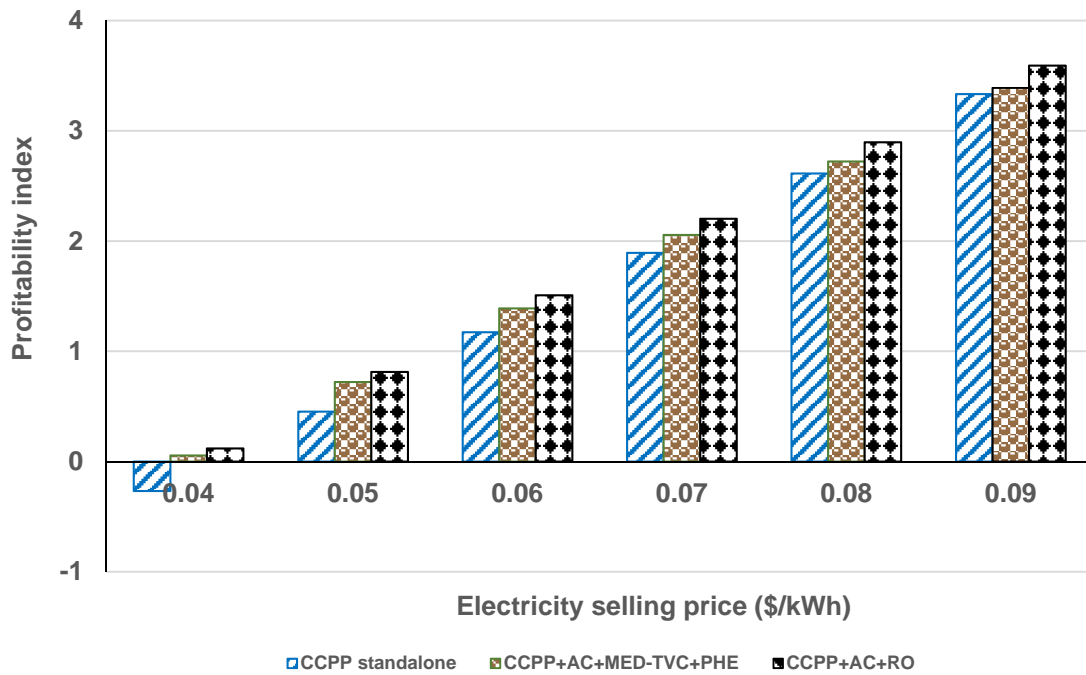
Figure 7-13: Profitability index against the electricity price variation

7.7.2 *Fuel Prices*

The fuel price has a major influence on economic performance because it represents about 80% of the recurrent cash outflow. In order to investigate the effect of fuel prices the price was varied from $0.12/kg to $0.36/kg with steps of $0.04/kg. Figure 7-14 shows that as the fuel price increases the PBP increases from 3.5 years to 24.9 years for stand-alone CCPP and from 3.5 years to 19.7 years for CCPP+AC+MED-TVC+PHE and from 3.2 years to 16.5 year for CCPP+AC+RO which is the lowest PBP configuration and the best option between the cogeneration systems. In addition, all the configurations are not feasible when the fuel price rises above $0.36/kg. This value is high because the fuel out cash flow is higher than the in cash flow. Meanwhile the NPV decreases with increase of fuel price from $1347 million to $30 million for CCPP+AC+RO (Figure 7-15). Figures 7-16 shows the ARR of the three configurations, which shows the same trend as for the NPV. Figure 7-17 shows that if the fuel cost reaches $0.36/kg the CCPP standalone and CCPP+AC+MED-TVC PI dropped to below zero, whereas CCPP+AC+RO is drops below zero at $0.365/kg fuel selling price. This means all the configurations will not be valuable at high fuel prices and this should be taken into consideration before starting the project, where the electricity selling price and water selling price are assumed fixed at $0.07kWh and $2.5/m^3 respectively.
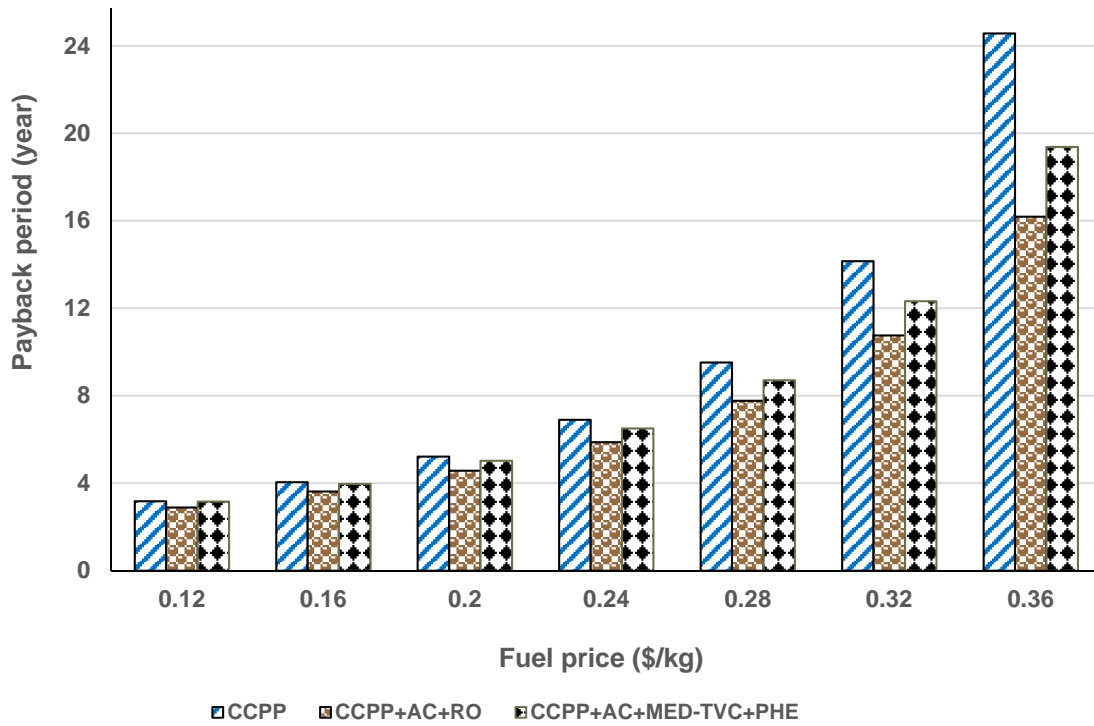
Figure 7-14: Influence of fuel price on the PBP for different configurations
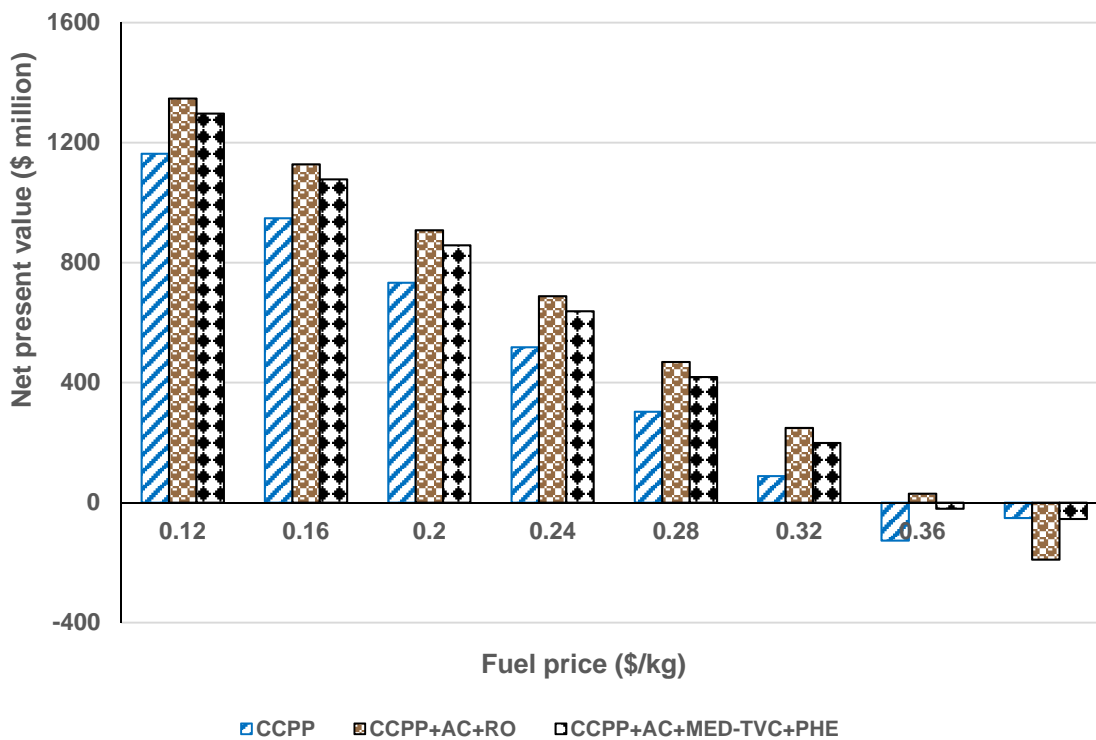
Figure 7-15: Influence of fuel price on the NPV for different configurations
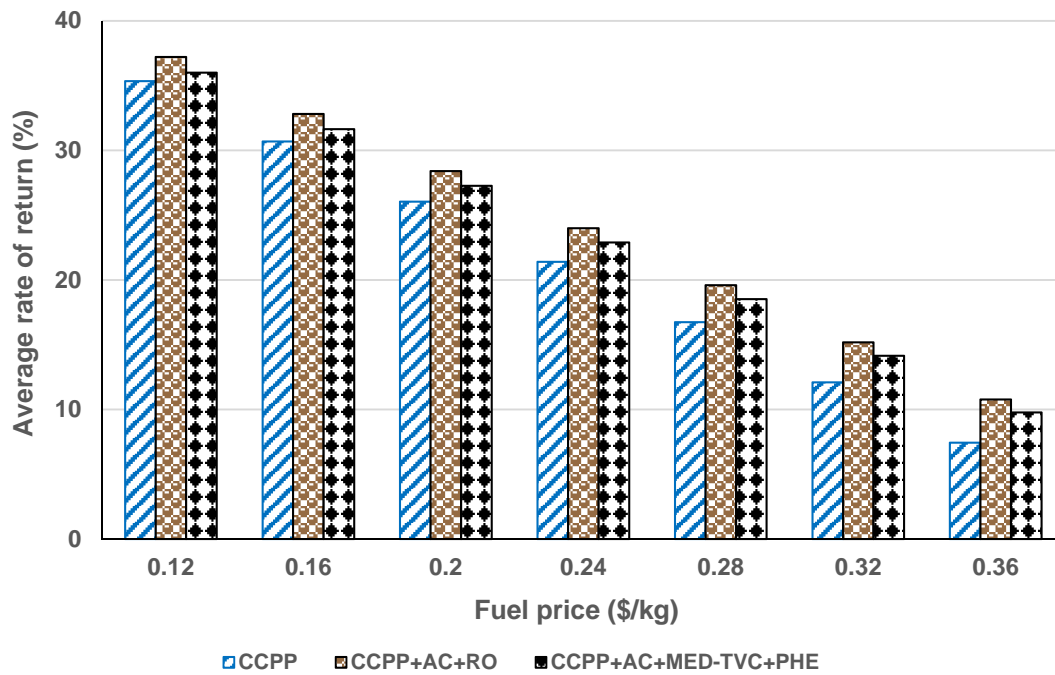
Figure 7-16: Influence of fuel price on the ARR for different scenarios
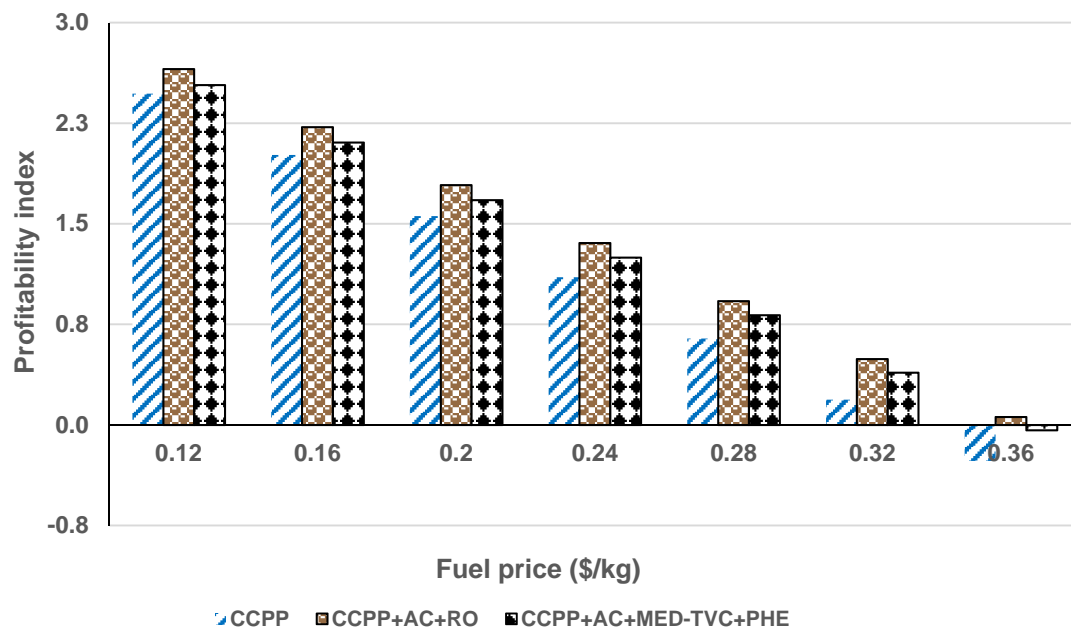
Figure 7-17: Influence of fuel price on the PI for different scenarios

7.7.3 *Potable Water Selling Price*

The influence of the price of potable water was examined by varying price from $1.25/m^3 to $ 2.75/m^3 with steps of $0.25/m^3 to find at which price the project is not preferred. This analysis is carried out at only two configurations, because CCPP standalone produces only electricity. The study is performed using the same assumptions concerning condition and availability. Figure 7-18 shows that the CCPP+AC+MED-TVC+PHE configuration has PBP higher than CCPP+AC+RO at 4.7

years with potable water prices of $ 1.25/m^3, whereas it is only 4.3 years for CCPP+AC+RO at the same selling price. The PBP of all configurations decreased by 2% every $0.25/m^3 price step (Figure 7-18). As can be seen there is only a small effect of the potable selling price, because the cogeneration plant produce two products (electricity and water) and the electricity revenue is much higher than potable water revenue (about 28 times). Even when the selling price dropped to $1.25/m^3 the PBP is still less than 5 years for both configurations.

Figure 7-19 shows the effect of potable water selling price against NPV. The CCPP+AC+RO configuration has the highest value, because the RO desalination system has less total capital cost and did not consume steam, however, it is consumed higher electricity than MED-TVC with the same water production compared with the MED-TVC desalination system. Raising the selling price increases the NPV, ARR and PI for the two configurations (Figure 7-19 to 7-21) as a result of receiving more cash flow from selling water, but not to a large extent.
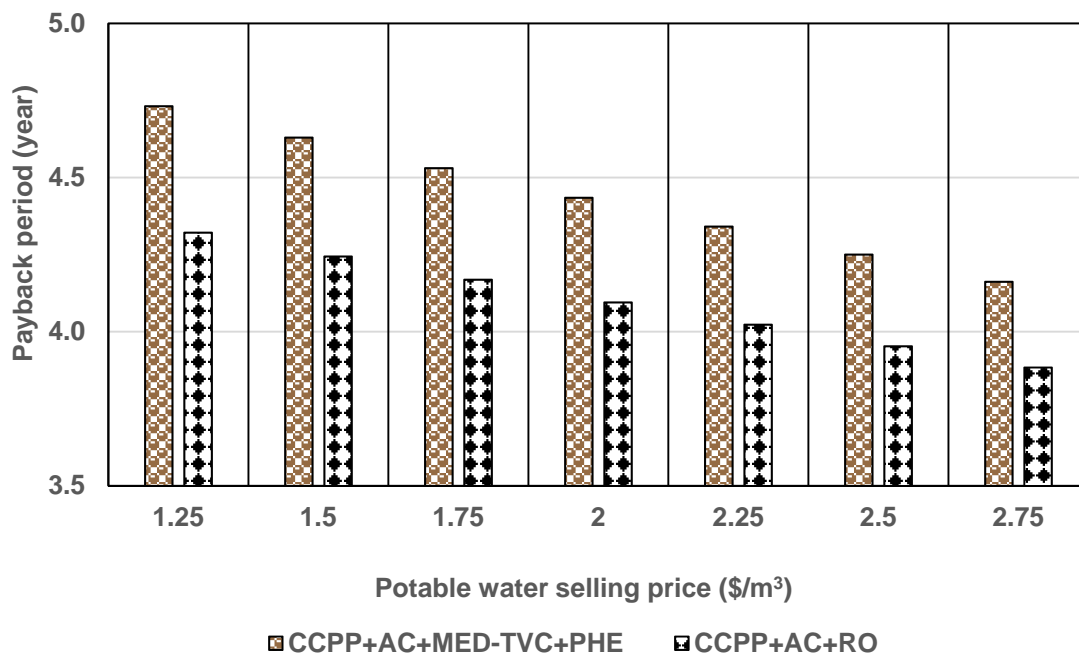
Figure 7-18: Payback period against the price of water for different configurations
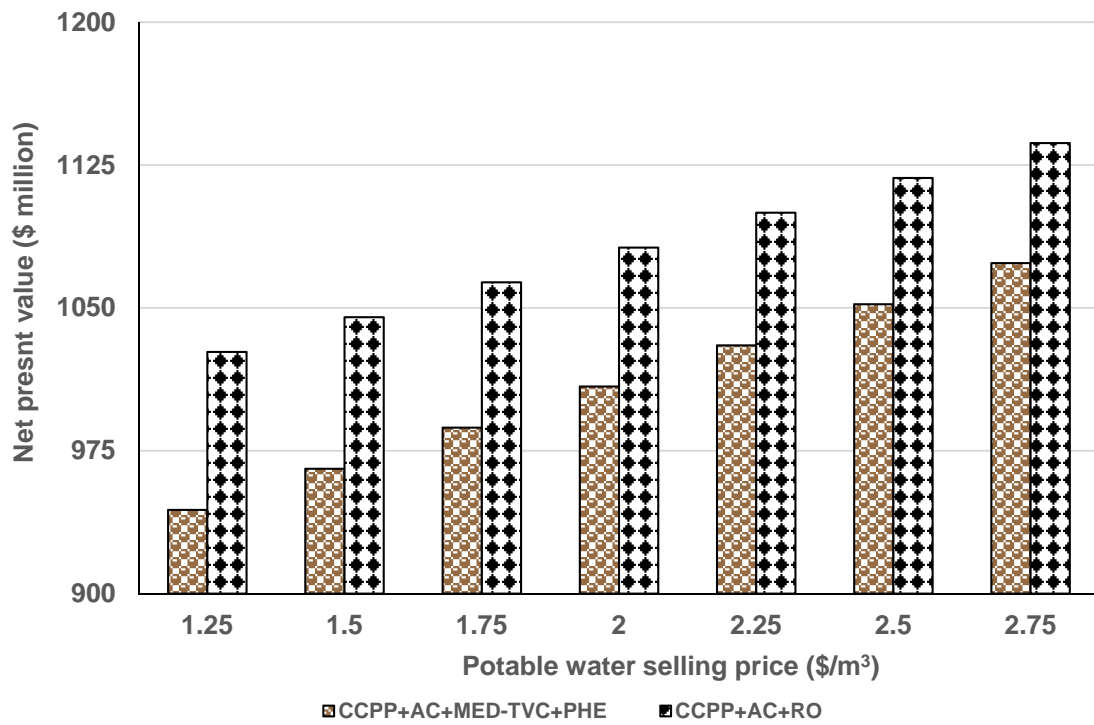
Figure 7-19: Net present value against the price of water for different configurations
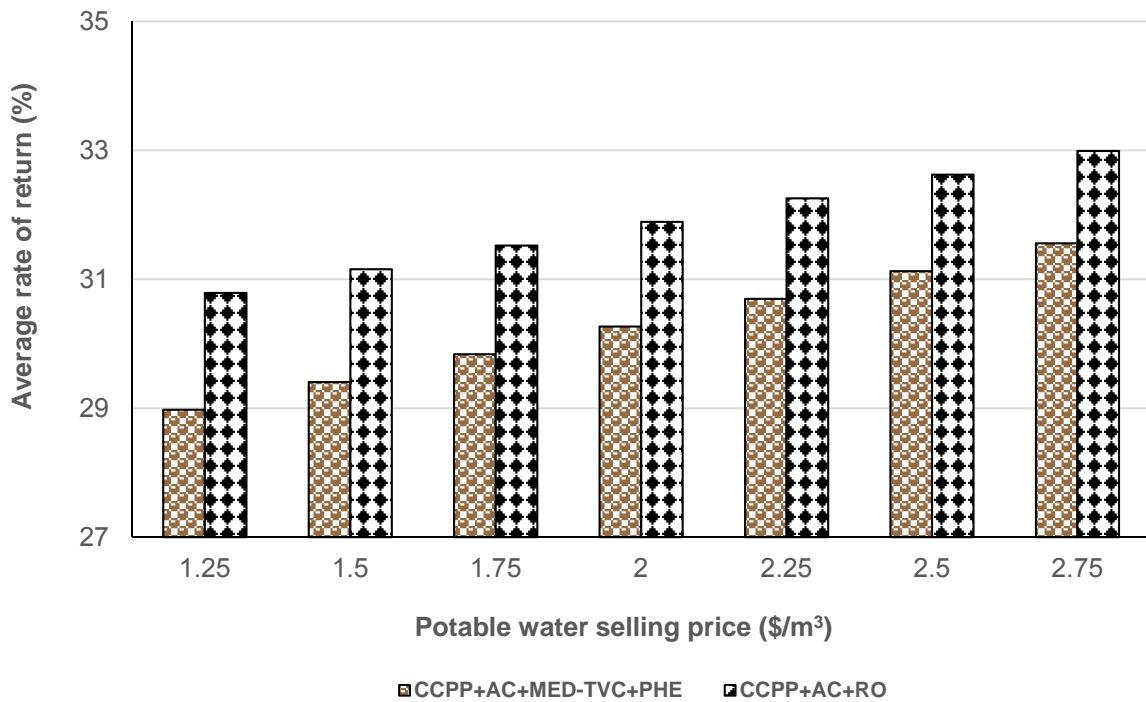
Figure 7-20: Average rate of return against the price of water for different configurations
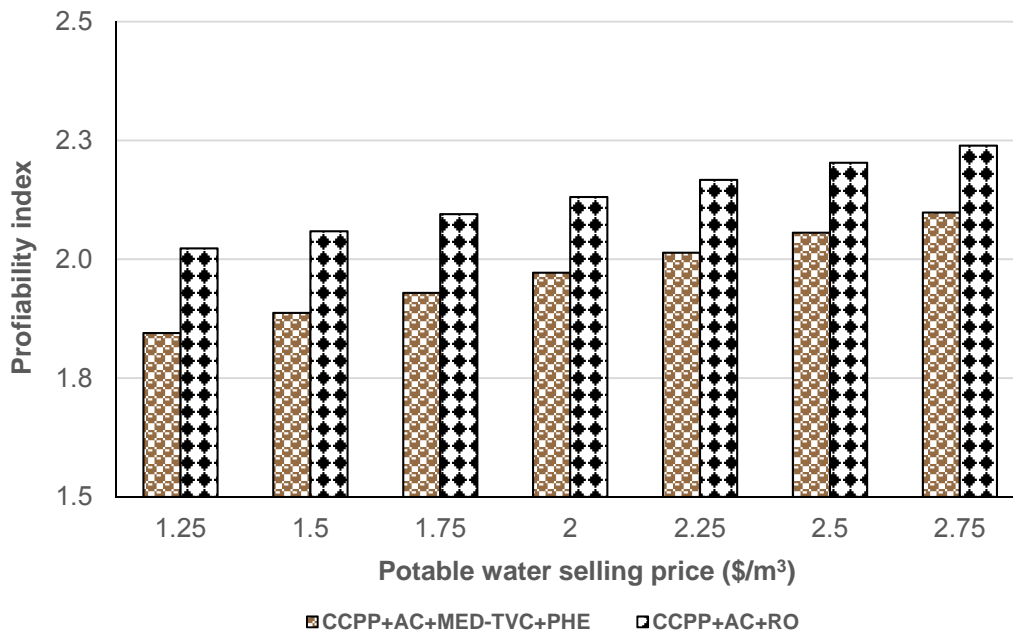
Figure 7-21: Profitability index against the price of water for different scenarios

7.8 Sensitivity Study for SED and SRO Comparison

The sensitivity analysis of SED and SRO was performed to find which is the optimal selection to produce distillate water from brackish water geothermal water. The same purchasing price and criteria as in section 7.6 are used. In this section there are only two parameters could affect the desalination system economically, electricity purchasing price and potable water selling price.

7.8.1 Effect of electricity price

Figure 7.22 shows that the PBP of SED is 1.3 times higher than SRO at electricity selling price $0.04/kWh and potable water selling price $2.5/m^3$. This difference could be increase to 3 times, when the electricity purchasing price is $0.09/kWh, because the total capital investment and power consumption of SED are both higher than for SRO. These changes in the selling price also affect the NPV, ARR and PI of both models which are reduced with increase in electricity price (Figures 7-23 to 7-25).
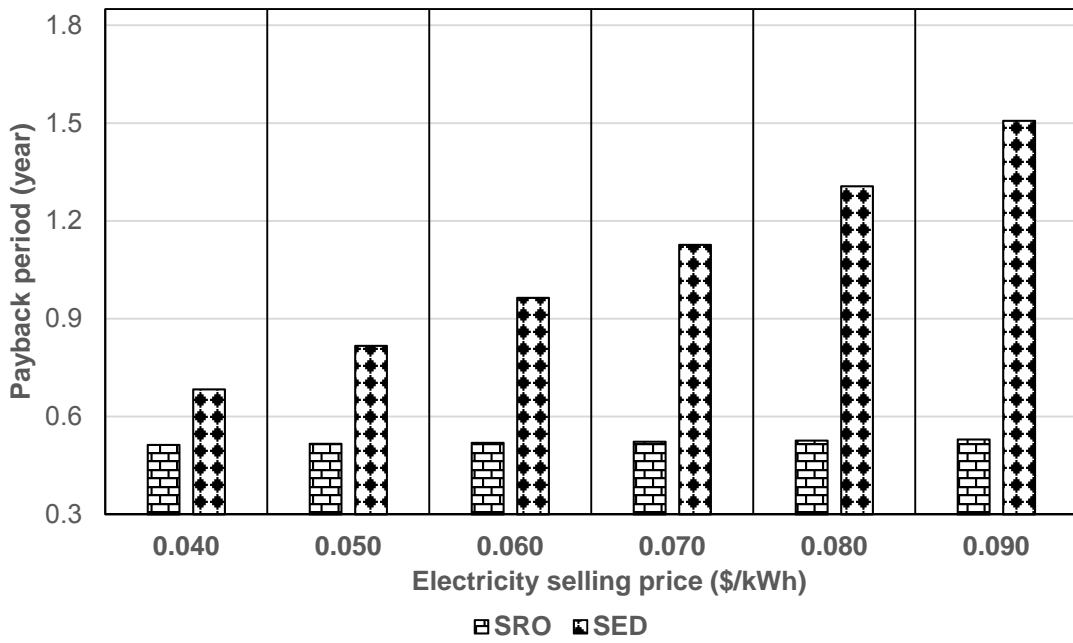
Figure 7-22: Payback period against the selling electricity prices variation
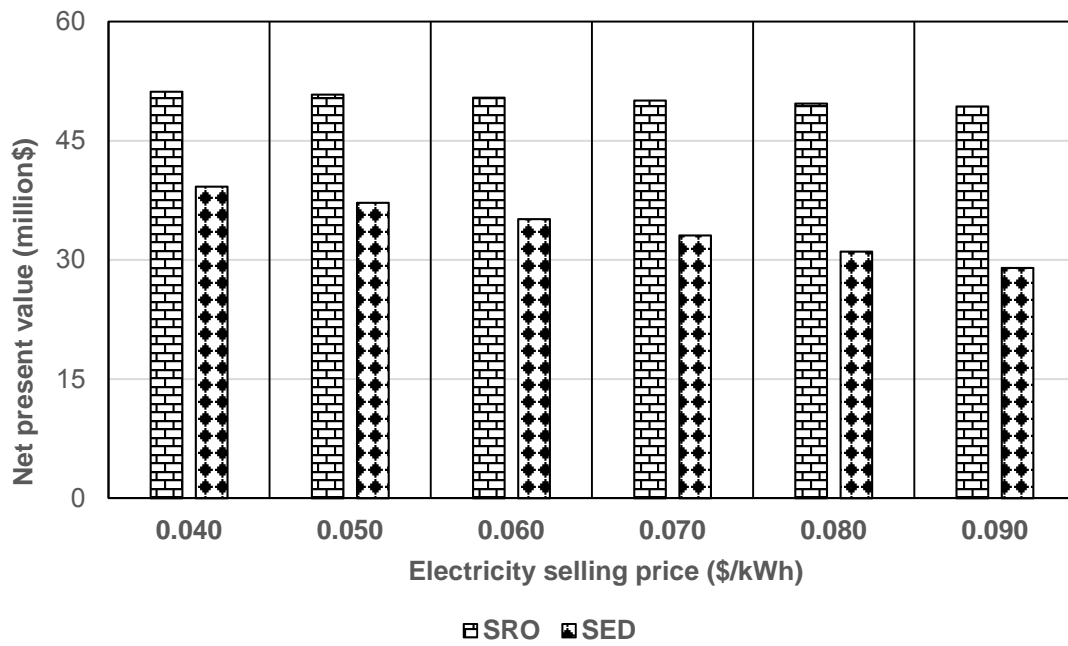
Figure 7-23: Net present value against the selling electricity prices variation
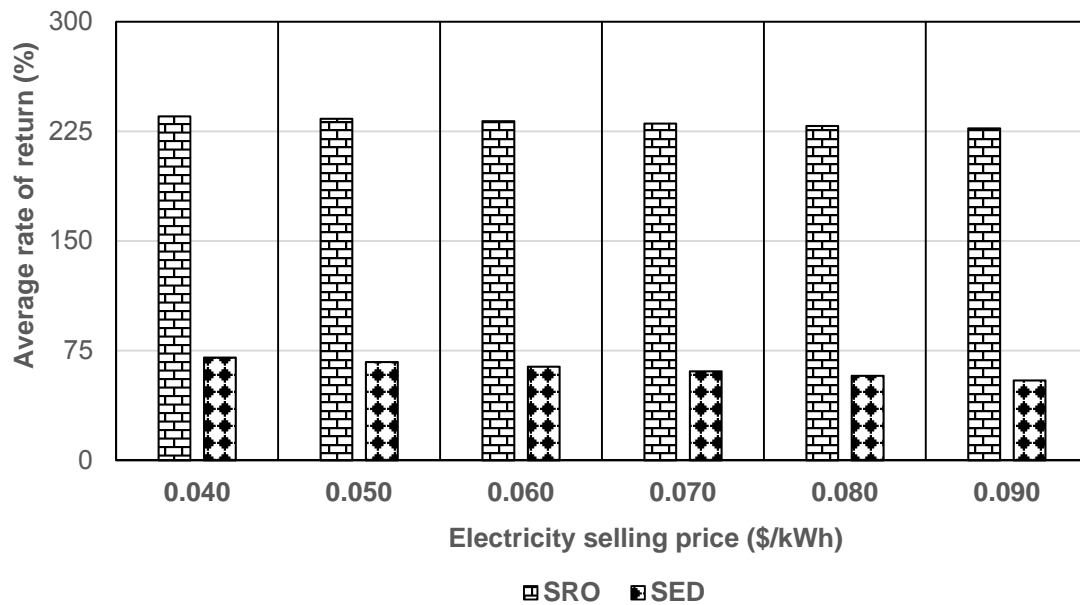
Figure 7-24: Average rate of return against the selling electricity prices variation
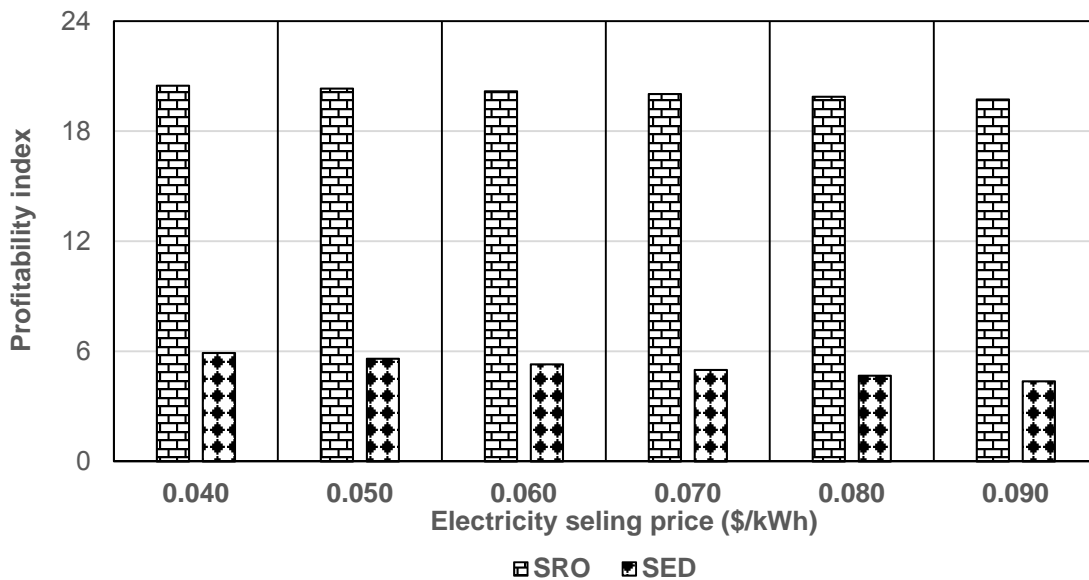
Figure 7-25: Profitability index against the selling electricity prices variation

7.8.2 *Effect of water selling price*

There is also a clear impact of water selling price on these two systems. The PBP of SED is higher than SRO by 13 times at $1.25/m^3 selling price. This is reduced to only 1.3 times at higher selling price $2.75/m^3 (Figure 7-26). Since both produce the same amount of water then at each selling price both have the same income. The change in relative PBP (from 13 times to 1.3 times) must therefore be due to capital invested and electricity cost. The NPV, ARR and PI (Figures 7-27, 7.28 and 7-29), have the same trend, increase with potable water selling price increasing. These results are compatible with thermodynamic analysis (Section 5.3.1).
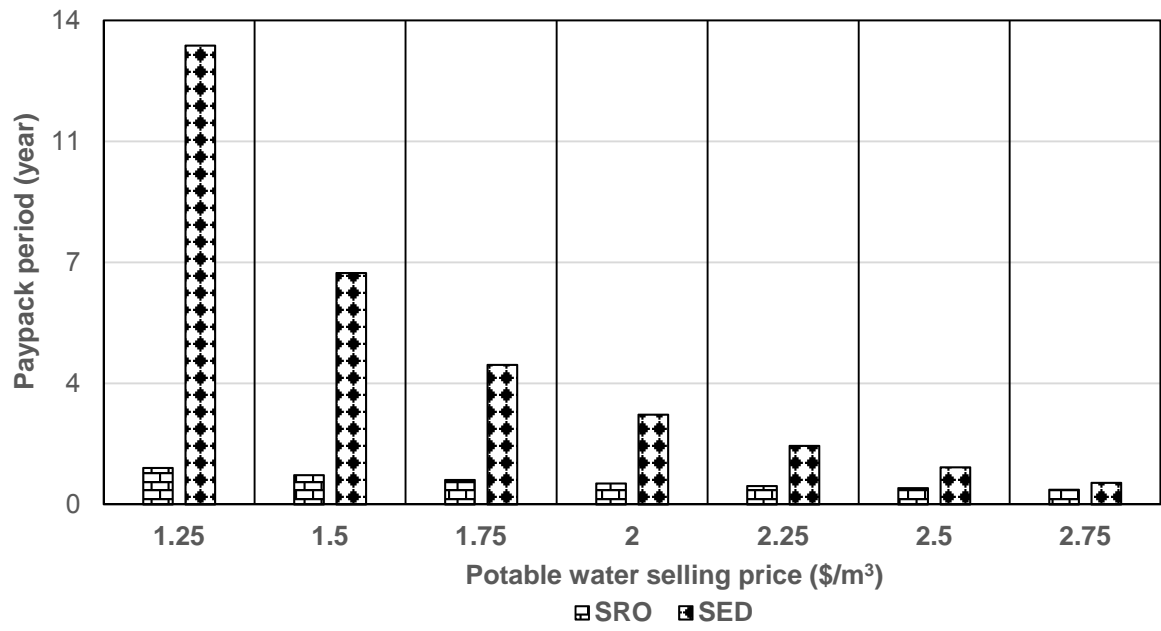
Figure 7-26: Payback period against the selling water selling prices variation
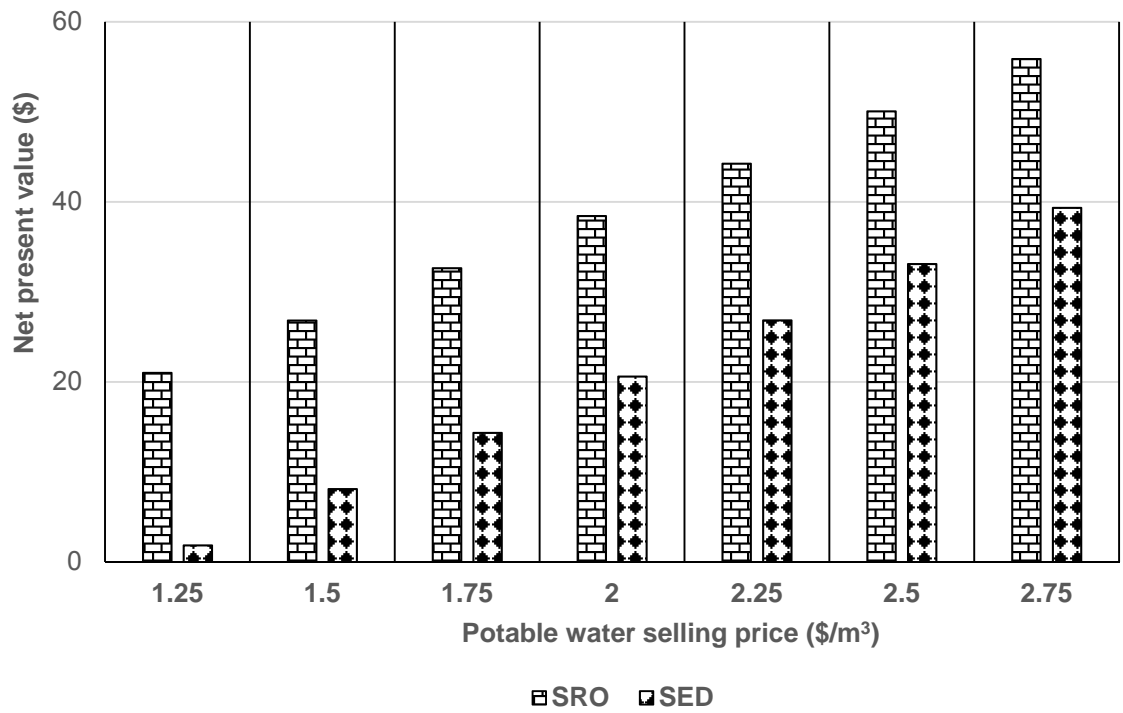
Figure 7-27: Net present value against the selling water selling prices variation
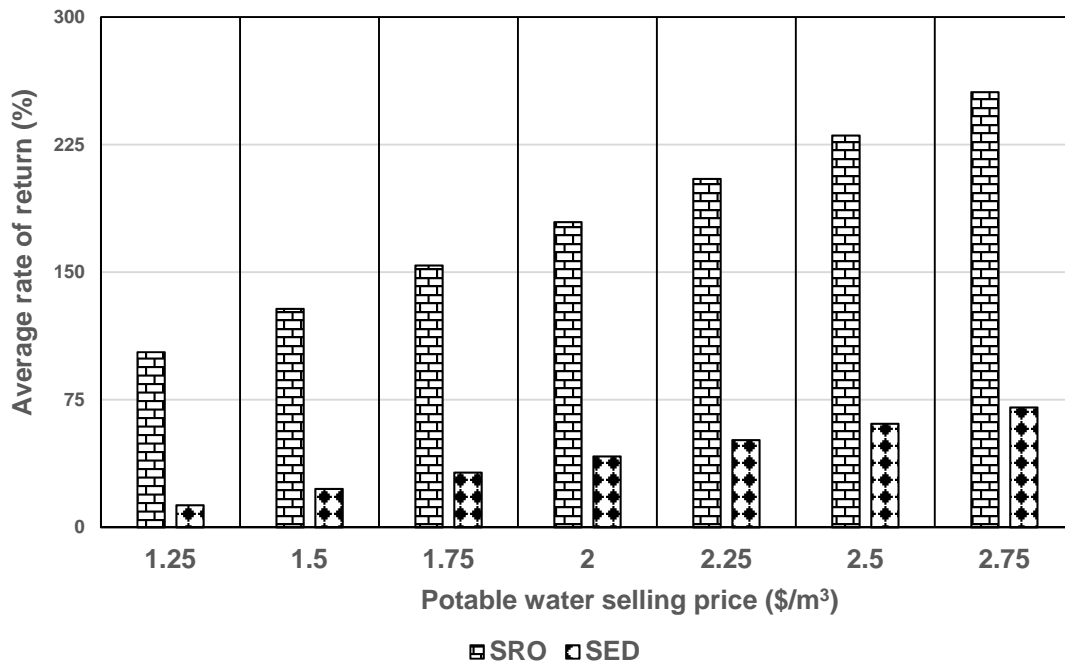
Figure 7-28: Average rate of return against the selling water selling prices variation
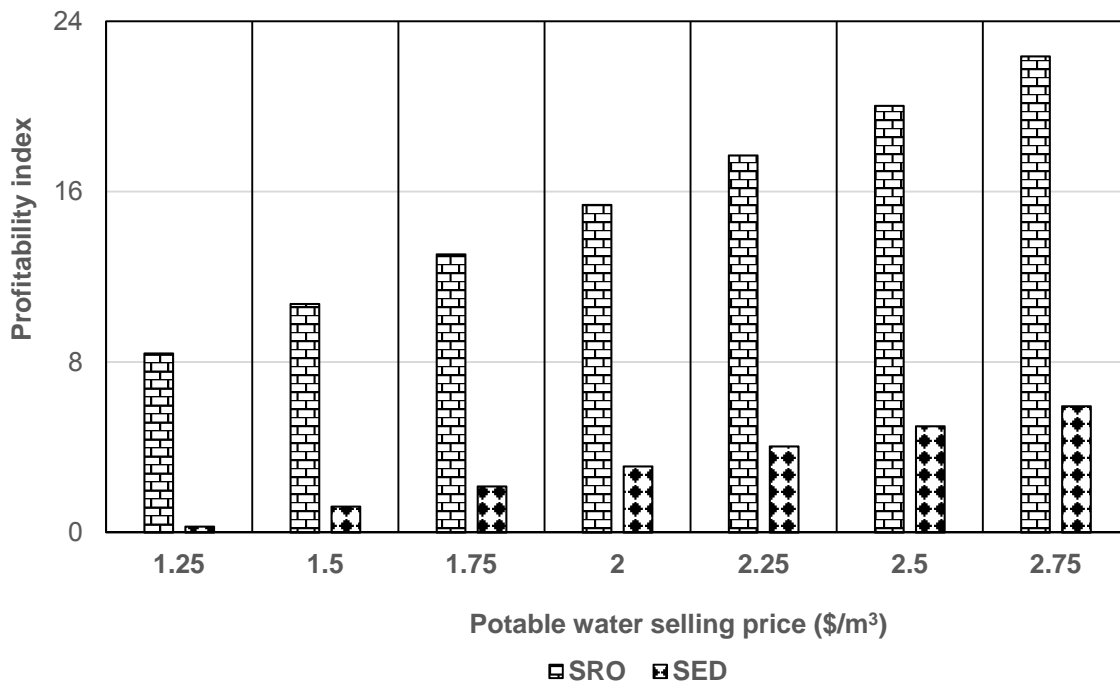
Figure 7-29: Profitability index against the selling water selling prices variation

7.9 Summary

This chapter has presented economic analyses for different scenarios of the combined cycle and desalination units using four economic criteria. The criteria considered were payback period, net present value and average rate of return and profitability index. The purpose of this work was to assess the economic acceptability of the proposed plants. Firstly, the purchase cost for each piece of equipment or sub-plant was presented or calculated using the designed economic MS Excel model and all other capital costs were defined. Secondly, the annual cash out flow was introduced and then used in a second designed economic MS Excel model to automatically calculate annual cash inflows and all the chosen evaluation criteria. Thirdly, a case study was performed in which the plant's economic performance was investigated in more detail in accordance with weather data and in three suggested operating modes. Finally, a number of sensitivity studies were carried out to investigate the impact of certain economic variables for different scenarios, such as electricity selling price, fuel price and potable water selling price.

It was concluded that the electricity selling price for the CCPP standalone could be not less than \$0.05/kWh, and the selling price of potable water from the desalination units should be not less than \$1.5/m^3. When the desalination units are coupled with the CCPP + AC, it was economically acceptable and profitable in all operating modes, with a PBP of less than 4.7 years and an NPV more than \$1000 million. On the other hand, it was found that fuel cost had the greatest effect on the plant economic performance. The potable water selling price was not found to be as important as the hot water selling price and hence could have been discounted without having a great effect on the plant's economic performance.

CHAPTER 8. CONCLUSION

8.1 Introduction

The conclusions are intended to answer the present study's research questions and provide insights according to the key objectives of this thesis presented Section 1.2 which can inform government policymakers, designers and manufacturing engineers about the implications of exergy analysis on the energy and economic aspects of cogeneration and desalination units. To recapitulate the following work has been reported in this thesis:

a) An existing CCPP in Libya was examined as a source of heat or electricity to power a desalination unit in the Libyan context. This included incorporating an absorption refrigeration system to cool the inlet air to avoid power degradation during seasons with high temperature.

b) Existing and further new improvements to both thermal (MED-TVC) and membrane (two-pass RO) desalination systems were examined.

c) The economic as well as thermodynamic and environmental performance of thermal and membrane desalination technologies in two contexts were compared. These were:

i) CCPP thermal or electricity powering in a conventional seawater desalination context.

ii) Geothermal brackish water sources which are not seawater and thus not confined to coastal sites.

The CCPP and AC models have been validated (Sections 4.2 and 4.3) and the correct chemical exergy has been used in the AC model (Section 6.3) to confirm the results of previous research [28], in thermodynamic (Section 6.2) and economic (Section 7.5) aspects.

The main conclusions that can be drawn from this study are outlined in the following subsections.

8.2 CCPP Performance Enhancement

The environmental conditions in Libya (Section 3.12) lead to non-uniform CCPP output during the year due to seasonal temperature variations (Figure 6.22). If a CCPP is

used to power a desalination unit because water demand, unlike power demand, is relatively constant over the year, it is important to add an AC not just for greater efficiency but also to achieve uniform performance across the seasons. This uniformity in output is important where water production is prioritised, as in the Libyan context. The parametric investigation (Section 6.2.2) showed that of the environmental variations in ambient temperature and relative humidity only ambient temperature causes a significant seasonal variation in CCPP output. This can be rectified by the addition of an AC inlet air cooler.

Thermodynamic performance criteria drive environmental performance in terms of CO_2 production per unit of production (Equations 3.73 and 3.74). Improved efficiency gives a more useful product for the same amount of fuel consumed, and hence reduces specific CO_2 production. For cogeneration with two different products (water as well as electricity), the results show that it is important to calculate CO_2 emissions on an exergy rather than energy basis. This is for the same reason that exergy efficiency should be preferred over HUF, which does not reflect the quality of heat energy used (Section 6.2.3).

Electricity prices are subsidised in Libya. The CCPP was found to be non-viable due to the PBP exceeding the 20-year lifetime of the project, an electricity selling price of \$0.04/kWh so that recovering capital costs could not be achieved within the project's lifetime. By contrast, the PBP could be reduced to only 2 years if the electricity price were to be increased to \$0.09/kWh. For this project to be viable, the electricity price received by the generation company should be above \$0.05/kWh.

8.3   Desalination process improvement

The desalination plant IPSEpro models used for comparison have been validated (Sections 4.5 and 4.6) and the latest thermodynamic properties and correct chemical exergy data have been used (Section 3.4).

8.3.1   *Thermal desalination (MED-TVC)*

The present study has confirmed that a greater number of effects on the MED-TVC was shown to improve performance (Section 5.2.1.3 c) and also that as the seawater temperature increased, the MED-TVC performance increased. This study extends this finding to suggest that adding a pre-heater on the main feed stream, which is a low cost improvement, gives a good return on performance both thermodynamically and

thus environmentally (Section 5.2.1.4) and also economically (Section 7.5b). This concept was motivated by parametric studies of MED-TVC performance which showed that, as the seawater temperature (and to a lesser extent salinity) increase, the GOR and exergy efficiency increase (Section 5.2.1.3).

The potable water selling price threshold is 1.5 $/m^3 for the standalone MED-TVC to achieve profitability, and below that price the technology is not feasible. However, in conjunction with CCPP there is only a small effect of the water selling price for a cogeneration system (Section 7.7.3), because of the predominance of electricity sales.

8.3.2 *Membrane desalination (RO)*

This present study (Section 5.1.2.2) confirms that first stage energy recovery improves RO performance (Section 2.1.3) which leads to this study being extended to include recovery at both stages of the two-pass RO.

PX is more expensive as an investment than ERT but gives significantly better returns, both thermodynamically and economically, as does energy recovery at both stages. At the second stage with a lower pressure drop, ERT is cheaper to install but over time PX gives a better return as well as lower PBP, due to its lower power consumption (Figures 5.32, 7.2 and 7.3). This is the first time ERT or PX have been examined for the second stage. Although the rejected pressure before the second stage is only 17 bar nevertheless using an energy recovery device at this second stage does improve the system both thermodynamically and economically (Sections 5.2.2.2 and 7.5 respectively).

RO desalination involves low capital costs compared with MED-TVC, and so it is less sensitive to the water selling price than MED-TVC in terms of feasibility (not less than $0.8/m^3).

8.4 Comparison of thermal and membrane desalination technologies

Economic comparisons depend on context. While this thesis focuses on the Libyan context, within that there are different possibilities. Therefore two different locations have been investigated:

1. Most typical is an existing CCPP at a coastal location which can power seawater desalination on a large scale.

2. By contrast, consideration could also be given to the possibility of smaller scale production from brackish groundwater which need not be restricted to coastal locations.

8.5 Cogeneration plant based on CCPP and desalination technologies

A combined cycle power plant (CCPP) coupled with thermal MED-TVC or membrane two-pass RO desalination plant has been investigated for the same water output. CCPP gross power when coupled with MED-TVC or with two-pass RO drops by about 5% and 1.2% respectively, due to the steam or electrical power extracted from the power plant to power the desalination. The plant's thermal efficiency decreased by about 4.6% and 0.9% respectively (figures 6-1b and 6-1c).

Thermodynamically, RO with or without energy recovery devices is better than MED-TVC, as a result of high irreversibilities at the MED-TVC effects. Coupling CPPP with MED-TVC or two-pass RO generally decreases the overall plant exergy. The exergy destruction in thermal desalination is higher than in RO.

The capital cost of RO is lower than that for MED-TVC, and also RO consumes less power (by about 5MW), whereas MED-TVC consumes steam equivalent to 22.5MW. The payback period of RO is lower than for MED-TVC and its NPV is higher (Section 7.5 b) due to a high cash outflow with MED-TVC and less power consumption with RO for the same amount of revenue from water. These results are in agreement with the thermodynamic results (Section 5.2.3.1). Only in the case of MED-TVC + PHE is the 20-year NPV higher than for standard RO, because MED-TVC + PHE produces 182m^3/h more water than RO over the process lifetime. However, this result changes when an energy recovery device is added to RO.

In the Libyan context where fuel and electricity prices may be subsidized, the influence of fuel purchase price, electricity sale or purchase prices and potable water selling price have strong impacts on economic indicators such as the payback period and net present value (Section 7.7).

8.6 Desalination from brackish geothermal source (SED v SRO)

There is lack of research on the desalination of brackish groundwater. To address this, a study using two different desalination technologies was undertaken to find the optimal technology for producing fresh water from brackish groundwater in Waddan City, Libya. Hot geothermal water can be used to power the single-effect desalination

plant, whereas an electrical power source is required for single-pass reverse osmosis (Section 5.3). Both technologies use electricity to drive the pumps and produce the same quantity of potable water, but the SED consumes more power because it require more feed water to produce the same quantity of potable water (Table 5.15). Although hot geothermal water is used to heat the brackish feed water with SED, it still needs electricity to drive the pumps (Section 5.3.1).

The thermodynamic analysis showed that the performance of SRO is better than that of SED. An economic analysis showed that the total capital investment of SED is 2.5 times higher than for the SRO and the PBP of the SED is higher than that of the SRO by about 2.2 times. This is because the electricity consumption of the SED is higher SRO. The NPV is about 60% when the electricity purchase price is raised to $0.09/kWh. These results indicate that the SRO has the lowest payback period and higher net present value, average rate of return and profitability index (Section 7.8). These results agree with those of the thermodynamic analysis (Section 5.3). Based on this, SRO should be the optimal system in such an area.

8.7   Recommendations for future work

The following recommendations based on this study can be made:

1. It has been shown that the performance of the MED-TVC can be improved by the addition of a preheater. This can be further extended by adding more heaters between the desalination effects.

2. This investigation has indicated that, in the Libyan context, water production is more important than electricity generation. Further work can be done to show that a change in current plant operating practices to prioritise the production of potable water rather than power is a sensible way forward in Libya.

3. It has been established that cogeneration plants are the best type of plant for the Libyan context. This study could be further extended to include more cogeneration elements, such as an Organic Rankine Cycle powering a single effect desalination unit. ORCs are a low-temperature technology that can be powered using the temperatures of geothermal water and they can provide sufficient power for both desalination technologies as the level required is not high. Hot geothermal water could act as a source of not just brackish water but also heat for both the ORC and the SED.

4. The overall concept of combined cycles can be extended further by incorporating solar energy into the overall system. Solar energy could be used to preheat the fluid streams to improve the overall efficiency of the desalination units.

REFERENCES

[1]   V. G. Gude, "Energy consumption and recovery in reverse osmosis," *Desalination and water treatment,* vol. 36, pp. 239-260, 2011.

[2]   T. Mezher, H. Fath, Z. Abbas, and A. Khaled, "Techno-economic assessment and environmental impacts of desalination technologies," *Desalination,* vol. 266, pp. 263-273, 2011.

[3]   X. Wang, A. Christ, K. Regenauer-Lieb, K. Hooman, and H. T. Chua, "Low grade heat driven multi-effect distillation technology," *International Journal of Heat and Mass Transfer,* vol. 54, pp. 5497-5503, 2011.

[4]   Khawaji D. Akili, K. K. Ibrahim, and Wie. J. Mihn, "Advances in seawater desalination technologies," *Desalination,* vol. 221, 2008.

[5]   M. Al-Shammiri and M. Safar, "Multi-effect distillation plants: state of the art," *Desalination,* vol. 126, pp. 45-59, 1999.

[6]   K. Zotalis, E. G. Dialynas, N. Mamassis, and A. N. Angelakis, "Desalination technologies: Hellenic experience," *Water,* vol. 6, pp. 1134-1150, 2014.

[7]   M. M. Elabbar and F. A. Elmabrouk, "Environmental impact assessment for desalination plants in Libya. Case study: Benghazi North and Tobrouk desalination plants," *Desalination,* vol. 185, pp. 31-44, 2005.

[8]   G. E. C. o. Libya, "Zawia Combined Cycle Power plant," Apr. 27,2007.

[9]   A. Al-Zahrani, J. Orfi, Z. Al-Suhaibani, B. Salim, and H. Al-Ansary, "Thermodynamic analysis of a reverse osmosis desalination unit with energy recovery system," *Procedia Engineering,* vol. 33, pp. 404-414, 2012.

[10]   M. S. Atab, A. J. Smallbone, and A. P. Roskilly, "An operational and economic study of a reverse osmosis desalination system for potable water and land irrigation," *Desalination,* vol. 397, pp. 174-184, 2016.

[11]   P.-K. Park, S. Lee, J.-S. Cho, and J.-H. Kim, "Full-scale simulation of seawater reverse osmosis desalination processes for boron removal: Effect of membrane fouling," *Water research,* vol. 46, pp. 3796-3804, 2012.

[12]   S. Masheiti and B. Agnew, "Thermodynamic Simulation Modelling of Low-Temperature Geothermal Source Located in Arid-Zone Area North Africa," *JJMIE,* vol. 4, pp. 61-68, 2010.

[13]   Simtech, Ipsepro, "Process Simulation Environment (PSE)," *Manual version,* vol. 4, pp. 1991-2003, 2003.

[14]   S. A. A. Masheiti, "A thermodynamic and economic simulation modelling study of utilizing low-temperature sources to power absorption and organic Rankine cycles," University of Newcastle Upon Tyne, 2011.

[15]   G. W. Intelligence, "Market profile and desalination markets, 2009–2012 yearbooks and GWI website," ed, 2013.

[16]   N. Ghaffour, T. M. Missimer, and G. L. Amy, "Technical review and evaluation of the economics of water desalination: current and future challenges for better water supply sustainability," *Desalination,* vol. 309, pp. 197-207, 2013.

[17]   N. Mehta Parth, N. Mehta, and C. Panchal, "Exergy Analysis of a Cogeneration Plant," *Exergy,* vol. 1, pp. 75-88, 2014.

[18]   I. H. Aljundi, "Second-law analysis of a reverse osmosis plant in Jordan," *Desalination,* vol. 239, pp. 207-215, 2009.

[19]   J. D. Birkett, "A brief illustrated history of desalination: From the bible to 1940," *Desalination,* vol. 50, pp. 17-52, 1984.

[20]   K. Schliephake,P Brown, A. Mason-Jefferies and K. Lockey " Overiew of treatment process for the production of fit for purpose water: Desalination and membrane technolgies. ," *ASIRC report,* vol. R05, pp. R05-2207, (2005).

[21]   United Nation, "Water desalination technologies in the ESCWA member countries. ," *UN report no; 172,* 2001.

[22]   htt:/amaeridia.com/html/elep.html].

[23] Z. Amor, B. Bariou, N. Mameri, M. Taky, S. Nicolas, and A. Elmidaoui, "Fluoride removal from brackish water by electrodialysis," *Desalination,* vol. 133, pp. 215-223, 2001.

[24] J. E. Miller, "Review of water resources and desalination technologies," *Sandia National Labs Unlimited Release Report SAND-2003-0800,* 2003.

[25] K. S. Al-Zahrani, "Operational simulation and an economical modelling study on utilizing waste heat energy in a desalination plant and an absorption chiller," Newcastle University, 2010.

[26] O. Dlask, N. Václavíková, and M. Dolezel, "Insertion of Filtration Membranes into Electrodialysis Stack and Its Impact on Process Performance," *Periodica Polytechnica. Chemical Engineering,* vol. 60, p. 169, 2016.

[27] D. B. Ozkan, O. Kiziler, and D. Bilge, "Exergy Analysis of a Cogeneration Plant," in *Proceedings of World Academy of Science, Engineering and Technology*, pp. 774-778, 2012.

[28] M. A. S. Al-Washahi, "A Thermodynamic and Economic Modelling Study of Recovering Heat from MSF Desalination Cogeneration Plant," University of Newcastle upon Tyne, 2014.

[29] J. G. Wijmans and R. W. Baker, "The solution-diffusion model: a review," *Journal of membrane science,* vol. 107, pp. 1-21, 1995.

[30] *http://www.sidem-desalination.com,* 2020.

[31] X. Shi and D. Che, "Thermodynamic analysis of an LNG fuelled combined cycle power plant with waste heat recovery and utilization system," *International journal of energy research,* vol. 31, pp. 975-998, 2007.

[32] P. Pechtl, M. Dieleman, M. Posch, B. Davari, M. Erbes, and S. Schneeberger, "Integrated Thermal Power and Desalination Plant Optimization," *General Electric Energy Services, Optimization Software. PowerGen Middle East, confernce,* 2003.

[33] R. Kempton, D. Maccioni, S. M. Mrayed, and G. Leslie, "Thermodynamic efficiencies and GHG emissions of alternative desalination processes," Water Science and technology: Water Supply, Vol. 10, pp. 416-427, 2010.

[34] C. Yunus, "Exergy analysis of a reverse osmisis deslalination plant in California," *Desalination,* vol. 142, pp. 257-266, 2002.

[35] V. Romero-Ternero, L. García-Rodríguez, and C. Gómez-Camacho, "Exergy analysis of a seawater reverse osmosis plant," *Desalination,* vol. 175, pp. 197-207, 2005.

[36] N. Kahraman, Y. A. Cengel, B. Wood, and Y. Cerci, "Exergy analysis of a combined RO, NF, and EDR desalination plant," *Desalination,* vol. 171, pp. 217-232, 2005.

[37] R. S. El-Emam and I. Dincer, "Thermodynamic and thermoeconomic analyses of seawater reverse osmosis desalination plant with energy recovery," *Energy,* vol. 64, pp. 154-163, 2014.

[38] N. M. Eshoul, B. Agnew, M. A. Al-Weshahi, and M. S. Atab, "Exergy Analysis of a Two-Pass Reverse Osmosis (RO) Desalination Unit with and without an Energy Recovery Turbine (ERT) and Pressure Exchanger (PX)," *Energies,* vol. 8, pp. 6910-6925, 2015.

[39] N. M. Eshoul and B. Agnew, "A COMPARISON BETWEEN SED AND SINGLE RO DESALINATION PLANTS USING EXERGY AND ECONOMIC ANALYSIS," in *Extended Abstracts*, 2016, p. 23.

[40] M. A. Jamil, B. A. Qureshi, and S. M. Zubair, "Exergo-economic analysis of a seawater reverse osmosis desalination plant with various retrofit options," *Desalination, pp. 88-98,* 2016.

[41] A. Farooque, A. Jamaluddin, A. Al-Reweli, P. Jalaluddin, S. Al-Marwani, A. Al-Mobayed*, et al.*, "Parametric analyses of energy consumption and losses in SWCC SWRO plants utilizing energy recovery devices," *Desalination,* vol. 219, pp. 137-159, 2008.

[42] R. Dashtpour and S. N. Al-Zubaidy, "Energy efficient reverse osmosis desalination process," *International Journal of Environmental Science and Development,* vol. 3, pp. 339-345, 2012.

[43] H. Ludwig, "Energy consumption of reverse osmosis seawater desalination-possibilities for its optimisation in design and operation of SWRO plants," *Desalination and Water Treatment,* vol. 13, pp. 13-25, 2010.

[44]   P. Geisler, F. U. Hahnenstein, W. Krumm, and T. Peters, "Pressure exchange system for energy recovery in reverse osmosis plants," *Desalination,* vol. 118, pp. 91-IN7, 1998.

[45]   J. P. MacHarg, "Retro-fitting existing SWRO systems with a new energy recovery device," *Desalination,* vol. 153, pp. 253-264, 2003.

[46]   B. A. Qureshi and S. M. Zubair, "Energy-exergy analysis of seawater reverse osmosis plants," *Desalination,* vol. 385, pp. 138-147, 2016.

[47]   H. M. Ettouney, H. T. El-Dessouky, R. S. Faibish, and P. J. Gowin, "Evaluating the economics of desalination," *Chemical Engineering Progress,* vol. 98, pp. 32-40, 2002.

[48]   C. Fritzmann, J. Löwenberg, T. Wintgens, and T. Melin, "State-of-the-art of reverse osmosis desalination," *Desalination,* vol. 216, pp. 1-76, 2007.

[49]   R. L. Stover, "Energy recovery devices for seawater reverse osmosis," *Everything about water,* vol. 67, pp. 40-45, 2006.

[50]   N. M. Eshoul, B. Agnew, A. Anderson, and M. S. Atab, "Exergetic and economic analysis of two-pass RO desalination proposed plant for domestic water and irrigation," *Energy, vol. 122, pp. 319-328,* 2017.

[51]   A. Malek, M. N. A. Hawlader, and J. C. Ho, "Design and economics of RO seawater desalination," *Desalination,* vol. 105, pp. 245-261, 1996.

[52]   N. Liu, Z. Liu, Y. Li, and L. Sang, "Development and experimental studies on a fully-rotary valve energy recovery device for SWRO desalination system," *Desalination,* vol. 397, pp. 67-74, 2016.

[53]   M. S. El-Bourawi, Z. Ding, R. Ma, and M. Khayet, "A framework for better understanding membrane distillation separation process," *Journal of Membrane Science,* vol. 285, pp. 4-29, 2006.

[54]   S. Al-Obaidani, E. Curcio, F. Macedonio, G. Di Profio, H. Al-Hinai, and E. Drioli, "Potential of membrane distillation in seawater desalination: thermal efficiency, sensitivity study and cost estimation," *Journal of Membrane Science,* vol. 323, pp. 85-98, 2008.

[55]   T. Y. Cath, V. D. Adams, and A. E. Childress, "Experimental study of desalination using direct contact membrane distillation: a new approach to flux enhancement," *Journal of Membrane Science,* vol. 228, pp. 5-16, 2004.

[56]   A. M. Farooque, A. T. M. Jamaluddin, A. R. Al-Reweli, P. A. M. Jalaluddin, S. M. Al-Marwani, A. A. Al-Mobayed*, et al.*, "Parametric analyses of energy consumption and losses in SWCC SWRO plants utilizing energy recovery devices," *Desalination,* vol. 219, pp. 137-159, 2008.

[57]   R. L. Stover, "Seawater reverse osmosis with isobaric energy recovery devices," *Desalination,* vol. 203, pp. 168-175, 2007.

[58]   A. Al-Karaghouli and L. Kazmerski, "Economic and Technical Analysis of a Reverse-Osmosis Water Desalination Plant Using DEEP-3. 2 Software," *Journal of Environmental Science and Engineering A,* vol. 1, pp. 318-328, 2012.

[59]   Y. G. Lee, A. Gambier, E. Badreddin, S. Lee, D. R. Yang, and J. H. Kim, "Application of hybrid systems techniques for cleaning and replacement of a RO membrane," *Desalination,* vol. 247, pp. 25-32, 2009.

[60]   S. A. Avlonitis, K. Kouroumbas, and N. Vlachakis, "Energy consumption and membrane replacement cost for seawater RO desalination plants," *Desalination,* vol. 157, pp. 151-158, 2003.

[61]   B. A. Qureshi and S. M. Zubair, "Exergetic efficiency of NF, RO and EDR desalination plants," *Desalination,* vol. 378, pp. 92-99, 2016.

[62]   Y. Cerci, "Exergy analysis of a reverse osmosis desalination plant in California," *Desalination,* vol. 142, pp. 257-266, 2002.

[63]   V. Romero-Ternero, L. García-Rodríguez, and C. Gómez-Camacho, "Thermoeconomic analysis of a seawater reverse osmosis plant," *Desalination,* vol. 181, pp. 43-59, 2005.

[64]   M. Wilf and C. Bartels, "Optimization of seawater RO systems design," *Desalination,* vol. 173, pp. 1-12, 2005.

[65]   S. A. Abdul-Wahab, K. V. Reddy, M. A. Al-Weshahi, S. Al-Hatmi, and Y. M. Tajeldin, "Development of a steady-state mathematical model for multistage flash (MSF)

desalination plant," *International Journal of Energy Research,* vol. 36, pp. 710-723, 2012.

[66]   R. Borsani and S. Rebagliati, "Fundamentals and costing of MSF desalination plants and comparison with other technologies," *Desalination,* vol. 182, pp. 29-37, 2005.

[67]   A. Nafey, H. Fath, and A. Mabrouk, "Exergy and thermoeconomic evaluation of MSF process using a new visual package," *Desalination,* vol. 201, pp. 224-240, 2006.

[68]   M. A. Al-Weshahi, A. Anderson, and G. Tian, "Exergy efficiency enhancement of MSF desalination by heat recovery from hot distillate water stages," *Applied Thermal Engineering,* vol. 53, pp. 226-233, 2013.

[69]   A. Al Ghamdi and I. Mustafa, "Exergy analysis of a MSF desalination plant in Yanbu, Saudi Arabia," *Desalination,* vol. 399, pp. 148-158, 2016.

[70]   www.wabag.com/.../me-tvc-multi-effect-with-thermal-vapour-compressi.

[71]   H. El-Dessouky, H. Ettouney, I. Alatiqi, and G. Al-Nuwaibit, "Evaluation of steam jet ejectors," *Chemical Engineering and Processing: Process Intensification,* vol. 41, pp. 551-561, 2002.

[72]   A. Yehia, "Operating and principle of steam jet ejector," *Process engineer, suez oil processing company (SOPC),* 2013.

[73]   N. M. Al-Najem, M. A. Darwish, and F. A. Youssef, "Thermovapor compression desalters: energy and availability—analysis of single-and multi-effect systems," *Desalination,* vol. 110, pp. 223-238, 1997.

[74]   R. Kamali and S. Mohebinia, "Experience of design and optimization of multi-effects desalination systems in Iran," *Desalination,* vol. 222, pp. 639-645, 2008.

[75]   R. K. Kamali, S. A. Abbassi, S. Vanini, and M. S. Avval, "Thermodynamic Design and Parametric Study of MED-TVC," *Desalination,* vol. 222, pp. 596-604, 2008.

[76]   O. A. Hamed, A. M. Zamamiri, S. Aly, and N. Lior, "Thermal performance and exergy analysis of a thermal vapor compression desalination system," *Energy conversion and management,* vol. 37, pp. 379-387, 1996.

[77]   F. N. Alasfour, M. A. Darwish, and A. O. B. Amer, "Thermal analysis of ME—TVC+ MEE desalination systems," *Desalination,* vol. 174, pp. 39-61, 2005.

[78]   A. O. B. Amer, "Development and optimization of ME-TVC desalination system," *Desalination,* vol. 249, pp. 1315-1331, 2009.

[79]   H.-S. Choi, T.-J. Lee, Y.-G. Kim, and S.-L. Song, "Performance improvement of multiple-effect distiller with thermal vapor compression system by exergy analysis," *Desalination,* vol. 182, pp. 239-249, 2005.

[80]   F. Alamolhoda, R. KouhiKamali, and M. Asgari, "Parametric simulation of MED–TVC units in operation," *Desalination and Water Treatment,* pp. 1-14, 2015.

[81]   O. Samaké, N. Galanis, and M. Sorin, "Thermodynamic study of multi-effect thermal vapour-compression desalination systems," *Energy,* vol. 72, pp. 69-79, 2014.

[82]   A. Binamer, "Second law and sensitivity analysis of large ME-TVC desalination units," *Desalination and Water Treatment,* vol. 53, pp. 1234-1245, 2015.

[83]   Y. Yang, S. Shen, S. Zhou, X. Mu, and K. Zhang, "Research for the adjustable performance of the thermal vapor compressor in the MED–TVC system," *Desalination and Water Treatment,* vol. 53, pp. 1725-1734, 2015.

[84]   A. B. Amer, *New trend in the development of ME-TVC desalination system*: INTECH Open Access Publisher, 2011.

[85]   H. Sayyaadi and A. Saffari, "Thermoeconomic optimization of multi effect distillation desalination systems," *Applied Energy,* vol. 87, pp. 1122-1133, 2010.

[86]   F. N. Alasfour and A. O. B. Amer, "The feasibility of integrating ME-TVC+ MEE with azzour south power plant: economic evaluation," *Desalination,* vol. 197, pp. 33-49, 2006.

[87]   I. J. Esfahani, A. Ataei, V. Shetty, T. Oh, J. H. Park, and C. Yoo, "Modeling and genetic algorithm-based multi-objective optimization of the MED-TVC desalination system," *Desalination,* vol. 292, pp. 87-104, 2012.

[88]   N. M. Eshoul, B. Agnew, and A. M. Mnider, "Parametric study of mult-effect desalination with thermal vapour compression plant," in *2016 7th International Renewable Energy Congress (IREC),* 2016, pp. 1-6.

[89]   A. S. Hanafi, G. M. Mostafa, A. Fathy, and A. Waheed, "Thermo-Economic Analysis of Combined Cycle MED-TVC Desalination System," *Energy Procedia,* vol. 75, pp. 1005-1020, 2015.

[90]   J. P. O. C. a. J. M. Haile, *Thermodynamics Fundamentals for applications*, 2005.

[91]   M. Ameri, S. S. Mohammadi, M. Hosseini, and M. Seifi, "Effect of design parameters on multi-effect desalinationsystem specifications," *Desalination,* vol. 245, pp. 266-283, 2009.

[92]   K. H. Mistry, M. A. Antar, and J. H. Lienhard V, "An improved model for multiple effect distillation," *Desalination and Water Treatment,* vol. 51, pp. 807-821, 2013.

[93]   R. K. Kamali, A. Abbassi, and S. A. S. Vanini, "A simulation model and parametric study of MED–TVC process," *Desalination,* vol. 235, pp. 340-351, 2009.

[94]   A. Almutairi, P. Pilidis, N. Al-Mutawa, and M. Al-Weshahi, "Energetic and exergetic analysis of cogeneration power combined cycle and ME-TVC-MED water desalination plant: Part-1 operation and performance," *Applied Thermal Engineering,* vol. 103, pp. 77-91, 2016.

[95]   M. A. Darwish, "Thermal desalination in GCC and possible development," *Desalination and Water Treatment,* vol. 52, pp. 27-47, 2014.

[96]   R. Saidur, E. T. Elcevvadi, S. Mekhilef, A. Safari, and H. A. Mohammed, "An overview of different distillation methods for small scale applications," *Renewable and Sustainable Energy Reviews,* vol. 15, pp. 4756-4764, 2011.

[97]   A. A. Mabrouk, A. Nafey, and H. Fath, "Thermoeconomic analysis of some existing desalination processes," *Desalination,* vol. 205, pp. 354-373, 2007.

[98]   K. H. Mistry, R. K. McGovern, G. P. Thiel, E. K. Summers, S. M. Zubair, and J. H. Lienhard, "Entropy generation analysis of desalination technologies," *Entropy,* vol. 13, pp. 1829-1864, 2011.

[99]   M. H. Sharqawy, J. H. Lienhard, and S. M. Zubair, "Thermophysical properties of seawater: a review of existing correlations and data," *Desalination and Water Treatment,* vol. 16, pp. 354-380, 2010.

[100]   H. M. Sharqawy, J. H. Lienhard V, and M. S. Zubair, "On exergy calcualtion of seawater with application in desalination systems " *International Journal of Thermal Sciences,* vol. 50, 2011.

[101]   N. Kahraman and Y. A. Cengel, "Exergy analysis of a MSF distillation plant," *Energy Conversion and Management,* vol. 46, pp. 2625-2636, 2005.

[102]   Borsani Roberto and Rebagliati Silvio, "Fundamentals and costing of MSF desalination plants and comparison with other technologies," *Desalination,* vol. 182, 2005.

[103]   A. D. Khawaji, I. K. Kutubkhanah, and J.-M. Wie, "Advances in seawater desalination technologies," *Desalination,* vol. 221, pp. 47-69, 2008.

[104]   G. Raluy, L. Serra, and J. Uche, "Life cycle assessment of MSF, MED and RO desalination technologies," *Energy,* vol. 31, pp. 2361-2372, 2006.

[105]   N. M. Wade, "Distillation plant development and cost update," *Desalination,* vol. 136, pp. 3-12, 2001.

[106]   K. V. Reddy and N. Ghaffour, "Overview of the cost of desalinated water and costing methodologies," *Desalination,* vol. 205, pp. 340-353, 2007.

[107]   V. G. Gude, N. Nirmalakhandan, and S. Deng, "Renewable and sustainable approaches for desalination," *Renewable and Sustainable Energy Reviews,* vol. 14, pp. 2641-2654, 2010.

[108]   M. Shatat and S. B. Riffat, "Water desalination technologies utilizing conventional and renewable energy sources," *International Journal of Low-Carbon Technologies,* p. cts025, 2012.

[109]   M. A. Eltawil, Z. Zhengming, and L. Yuan, "A review of renewable energy technologies integrated with desalination systems," *Renewable and Sustainable Energy Reviews,* vol. 13, pp. 2245-2262, 2009.

[110]   I. C. Karagiannis and P. G. Soldatos, "Water desalination cost literature: review and assessment," *Desalination,* vol. 223, pp. 448-456, 2008.

[111]   I. S. Al-Mutaz and A. M. Al-Namlah, "Characteristics of dual purpose MSF desalination plants," *Desalination,* vol. 166, pp. 287-294, 2004.

[112]   Y. A. Cengel and M. A. Boles, "Thermodynamics, " ed: McGraw-Hill, New York, 2002.

[113] E. Al-Katheeri and S. P. Agashichev, "Feasibility of the concept of hybridization of existing co-generative plant with reverse osmosis and aquifer storage," *Desalination,* vol. 222, pp. 87-95, 2008.

[114] O. M. Al-Hawaj and H. Al-Mutairi, "A combined power cycle with absorption air conditioning," *Energy,* vol. 32, pp. 971-982, 2007.

[115] R. Saidur, J. U. Ahamed, and H. H. Masjuki, "Energy, exergy and economic analysis of industrial boilers," *Energy Policy,* vol. 38, pp. 2188-2197, 2010.

[116] M. Ameri, P. Ahmadi, and S. Khanmohammadi, "Exergy analysis of a 420 MW combined cycle power plant," *International Journal of Energy Research,* vol. 32, pp. 175-183, 2008.

[117] A. Rashad and A. E. Maihy, "Energy and Exergy Analysis of a Steam Power Plant in Egypt," in *13th International Conference on Aerospace Sciences & Aviation Technology, ASAT-13*, 2009.

[118] G. M. Fellah , F. A. Mgherbi and S. M. Aboghres, "Exergoeconomic Analysis for Unit GT 14 of Sought Tripoli Gas Turbine Power Plant," *Jordan Journal of Mechanical and industrial Engineering* vol. 4, pp. 507-516, 2010.

[119] A. Almutairi, P. Pilidis, and N. Al-Mutawa, "Exergoeconomic and Sustainability Analysis of Reheat Gas Turbine Engine," *American Journal of Energy Research,* vol. 4, pp. 1-10, 2016.

[120] T. Ganapathy, N. Alagumurthi, R. P. Gakkhar, and K. Murugesan, "Exergy analysis of operating lignite fired thermal power plant," *Journal of Engineering Science and Technology Review,* vol. 2, pp. 123-130, 2009.

[121] M. Ameri and S. H. Hejazi, "The study of capacity enhancement of the Chabahar gas turbine installation using an absorption chiller," *Applied Thermal Engineering,* vol. 24, pp. 59-68, 2004.

[122] A. Khaliq and I. Dincer, "Energetic and exergetic performance analyses of a combined heat and power plant with absorption inlet cooling and evaporative aftercooling," *Energy,* vol. 36, pp. 2662-2670, 2011.

[123] R. Hosseini, A. Beshkani, and M. Soltani, "Performance improvement of gas turbines of Fars (Iran) combined cycle power plant by intake air cooling using a media evaporative cooler," *Energy Conversion and Management,* vol. 48, pp. 1055-1064, 2007.

[124] A. M. El-Nashar, "Optimal design of a cogeneration plant for power and desalination taking equipment reliability into consideration," *Desalination,* vol. 229, 2008.

[125] P. Ahmadi and I. Dincer, "Thermodynamic and exergonevironmental analysis, and multi-objective optimization of a gas turbine power plant " *Applied Thermal Engineering,* vol. 31, pp. 2529-2540, 2011.

[126] M. Farzaneh-Gord and M. Deymi-Dashtebayaz, "Effect of various inlet air cooling methods on gas turbine performance," *Energy,* vol. 36, pp. 1196-1205, 2011.

[127] M. Alhazmy and Y. Najjar, "Augmentation of gas turbine performance using air coolers," *Applied Thermal Engineering,* vol. 24, pp. 415-429, 2004.

[128] S. Boonnasa, P. Namprakai, and T. Muangnapoh, "Performance improvement of the combined cycle power plant by intake air cooling using an absorption chiller," *Energy,* vol. 31, pp. 2036-2046, 2006.

[129] M. Talbi and B. Agnew, "Exergy analysis: an absorption refrigerator using lithium bromide and water as the working fluids," *Applied thermal engineering,* vol. 20, pp. 619-630, 2000.

[130] H. Khaledi, R. Zomorodian, and M. B. Ghofrani, "Effect of inlet air cooling by absorption chiller on gas turbine and combined cycle performance," in *ASME 2005 International Mechanical Engineering Congress and Exposition*, 2005, pp. 507-515.

[131] R. A. a. B. Agnew, "A Study of the Performance of a Vapour Absorption Automotive Air Conditioning System," *IMechE* vol. C496/015, 1995.

[132] H. L. Luo, R. Z. Wang, Y. J. Dai, J. Y. Wu, J. M. Shen, and B. B. Zhang, "An efficient solar-powered adsorption chiller and its application in low-temperature grain storage," *Solar Energy,* vol. 81, pp. 607-613, 2007.

[133] S. C. Kaushik and A. Arora, "Energy and exergy analysis of single effect and series flow double effect water-Lithium bromide absorption refrigration systems," *International Journal of refrigeration* vol. 32, pp. 1248-1257, 2009.

[134] R. Gomari, "Development of international pressure correlation for the half-effect absorption cooling chiller," *Int. J. of Thermal & Environmental Engineering,* vol. 2, pp. 35-40, 2011.

[135] A. I. Shahata, M. M. Aboelazm, and A. F. Elsafty, "Energy and exergy analysis for single and parallel flow double effect water-lithium bromide vapor absorption systems," *Int. J. Sci. Technol,* vol. 2, pp. 85-94, 2012.

[136] S. Popli, P. Rodgers, and V. Eveloy, "Gas turbine efficiency enhancement using waste heat powered absorption chillers in the oil and gas industry," *Applied Thermal Engineering,* vol. 50, pp. 918-931, 2013.

[137] S. Tech, "Simulation Technology, IPSEpro Simulation Desalination process Library Manual,," *Sim Tech, Austria,* 2005.

[138] B. M. Makhdoum and B. Agnew, "An energy and exergy analysis of a microturbine CHP system," *Journal of Environmental Science and Engineering,* vol. 5, pp. 508-518, 2011.

[139] M. A. S. Al-washahi, "A thermodynamic and economic modelling study of recovering heat from MSF desalination cogeneration plant," *Newcastle University,* 2014.

[140] C. K. Ho, "Software and codes for analysis of concentrating solar power technologies," Sandia National Laboratories, 2008.

[141] Sim Tech Simulation Technology, IPSEpro process simulation manual: process simulation environment, second ed. Sim Tech, Austria, 2005.

[142] A. Bejan and M. J. Moran, Thermal design and optimization: John Wiley & Sons, New York, 1996.

[143] T. J. Kotas, "The exergy method of thermal plant analysis", Butterworths, London 1985.

[144] M. Kanoglu, I. Dincer, and M. A. Rosen, "Understanding energy and exergy efficiencies for improved energy management in power plants," Energy Policy, vol. 35, pp. 3967-3978, 2007.

[145] A. Hepbasli, "A key review on exergetic analysis and assessment of renewable energy resources for a sustainable future," Renewable and Sustainable Energy Reviews, vol. 12, pp. 593-661, 2008.

[146] M. A. Rosen and I. Dincer, "Exergy, Energy, Environment and Simulation Development", Oxford University press, 1st. edn., 2007.

[147] ASME., "PTC4.4 gas turbine heat recovery generators. ist. edn. New York", ASME, 1981.

[148] ASME., "PTC4.4 steam turbines. 1st. edn. New York: ASME", 1996.

[149] M. Darwish, N. Al-Najem, and N. Lior, "Towards sustainable seawater desalting in the Gulf area," Desalination, vol. 235, pp. 58-87, 2009.

[150] N. Lior and N. Zhang, "Energy, exergy, and second law performance criteria," Energy, vol. 32, pp. 281-296, 2007.

[151] Y. Junjie, S. Shufeng, W. Jinhua, and L. Jiping, "Improvement of a multi-stage flash seawater desalination system for cogeneration power plants," Desalination, vol. 217, pp. 191-202, 2007.

[152] R. D. Noble and S. A. Stern, "Membrane separations technology: principles and applications", first ed., 1995.

[153] S. Lee and R. M. Lueptow, "Membrane rejection of nitrogen compounds," Environmental science & technology, vol. 35, pp. 3008-3018, 2001.

[154] T. Kaghazchi, M. Mehri, M. T. Ravanchi, and A. Kargari, "A mathematical modeling of two industrial seawater desalination plants in the Persian Gulf region," Desalination, vol. 252, pp. 135-142, 2010.

[155] R. Rautenbach and R. Albrecht, "Membrane separation processes," CRC press 1989.

[156] S. A. Avlonitis, M. Pappas, and K. Moutesidis, "A unified model for the detailed investigation of membrane modules and RO plants performance," Desalination, vol. 203, pp. 218-228, 2007.

[157] K. Jamal, M. A. Khan, and M. Kamil, "Mathematical modeling of reverse osmosis systems," Desalination, vol. 160, pp. 29-42, 2004.

[158] K. E. Herold, R. Radermacher, and S. A. Klein, *Absorption chillers and heat pumps*: CRC press, 1996.

[159] M. Mehrabian and A. Shahbeik, "Thermodynamic modelling of a single-effect LiBr-H2O absorption refrigeration cycle," *Proceedings of the Institution of Mechanical Engineers, Part E: Journal of Process Mechanical Engineering,* vol. 219, pp. 261-273, 2005.

[160] G. Feuerecker, J. Scharfe, I. Greiter, C. Frank, and G. Alefeld, "Measurement of thermophysical properties of aqueous LiBr-solutions at high temperatures and concentrations," in *The International Absorption Heat Pump Conference, New Orleans, LA, USA, 01/19-21/94,* 1994, pp. 493-499.

[161] Y. Kaita, "Thermodynamic properties of lithium bromide–water solutions at high temperatures," *International Journal of Refrigeration,* vol. 24, pp. 374-390, 2001.

[162] R. Rivero and M. Garfias, "Standard chemical exergy of elements updated," *Energy,* vol. 31, pp. 3310-3326, 2006.

[163] T. J. Kotas, "*The exergy method of thermal plant analysis*": Book, Krieger Melbourne, FL, 1995.

[164] J. Szargut, D. R. Morris, and F. R. Steward, "Exergy analysis of thermal, chemical, and metallurgical processes," 1987.

[165] R. Palacios-Bereche, R. Gonzales, and S. A. Nebra, "Exergy calculation of lithium bromide–water solution and its application in the exergetic evaluation of absorption refrigeration systems LiBr-H2O," *International Journal of Energy Research,* vol. 36, pp. 166-181, 2012.

[166] D. Kim and C. Infante Ferreira, "A Gibbs energy equation for LiBr aqueous solutions," *International journal of refrigeration,* vol. 29, pp. 36-46, 2006.

[167] S. Kakac and H. Liu, "Heat exchangers selection, rating and thermal design", ed: Boca Raton, CRC Press, 2002.

[168] W. Kays and A. London, "Compact heat exchangers", 1984," *New York.*

[169] ESDU92013, "Selection and costing of heat exchanger " *1st. edn., Esdu, UK* 1992.

[170] R. Turton, R. C. Bailie, W. B. Whiting, and J. A. Shaeiwitz, *Analysis, synthesis and design of chemical processes*: Pearson Education, 2008.

[171] V. Romero-Ternero, L. García-Rodríguez, and C. Gómez-Camacho, "Thermoeconomic analysis of wind powered seawater reverse osmosis desalination in the Canary Islands," *Desalination,* vol. 186, pp. 291-298, 2005.

[172] E. W. Perz and S. Bergmann, "A simulation environment for the techno-economic performance prediction of water and power cogeneration systems using renewable and fossil energy sources," *Desalination,* vol. 203, pp. 337-345, 2007.

[173] R. a. A.-C. f. E. Amrican Society of heating, "ASHRAE handbook fundamentals. Atlanta.," 1989.

[174] L. meteorological, 2010.

[175] P. Schausberger, G. Rheina-Wolbeck, A. Friedl, M. Harasek, and E. W. Perz, "Enhancement of an object-oriented power plant simulator by seawater desalination topics," *Desalination,* vol. 156, pp. 355-360, 2003.

[176] M. A. Elmelah, M. A. Benamer and A. Abuissa, "Physical and chemical seawater properties of selected locations from the Libyan Coast," Libyan Journal of Marine Science", vol. 11, pp. 37-50, 2006.

[177] Private discussion with the Libyan General Electricity Company, 2008.

[178] S. Dubey and G. Tiwari, "Thermal modeling of a combined system of photovoltaic thermal (PV/T) solar water heater," *Solar Energy,* vol. 82, pp. 602-612, 2008.

[179] M. Aneke, B. Agnew, and C. Underwood, "Performance analysis of the Chena binary geothermal power plant," *Applied Thermal Engineering,* vol. 31, pp. 1825-1832, 2011.

[180] P. Budhiraja and A. A. Fares, "Studies of scale formation and optimization of antiscalant dosing in multi-effect thermal desalination units," *Desalination,* vol. 220, pp. 313-325, 2008.

[181] D. M. AlWashahi, "Desalination manager, Oman," *E-mail,* 2016.

[182] M. A. Darwish and A. A. El-Hadik, "The multi-effect boiling desalting system and its comparison with the multi-stage flash system," *Desalination,* vol. 60, pp. 251-265, 1986.

[183] R. Dashtpour and S. N. Al-Zubaidy, "Energy Efficient Reverse Osmosis Desalination Process", Vol. 3, pp. 339-345, 2012.

[184] H. Ludwig, "Energy consumption of reverse osmosis seawater desalination - possibilities for its optimisation in design and operation of SWRO plants", *Desalination and water treatment,* vol. 13, pp. 13-25, pp. 13-25, 2010.

[185] H.-J. Oh, T.-M. Hwang, and S. Lee, "A simplified simulation model of RO systems for seawater desalination," *Desalination,* vol. 238, pp. 128-139, 2009.

[186] A. Jawor and E. M. V. Hoek, "Effects of feed water temperature on inorganic fouling of brackish water RO membranes," *Desalination,* vol. 235, pp. 44-57, 2009.

[187] http://www.panoramio.com/photo/32510974#, 0974.

[188] Sanjay, "Investigation of effect of variation of cycle parameters on thermodynamic performance of gas-steam combined cycle," *Energy,* vol. 36, pp. 157-167, 2011.

[189] A. A. Alsairafi, "Effects of ambient conditions on the thermodynamic performance of hybrid nuclear-combined cycle power plant," *International Journal of Energy Research,* vol. 37, pp. 211-227, 2013.

[190] M. A. Ehyaei, S. Hakimzadeh, N. Enadi, and P. Ahmadi, "Exergy, economic and environment (3E) analysis of absorption chiller inlet air cooler used in gas turbine power plants," *International Journal of Energy Research,* vol. 36, pp. 486-498, 2012.

[191] A. P. P. dos Santos, C. R. Andrade, and E. L. Zaparoli, "Comparison of Different Gas Turbine Inlet Air Cooling Methods", international journal of Mechanical, Aerospace, Industrial, Mechatronic and Manufacturing Engineering, Vol. 6, No. 1, 2012.

[192] P. Kistler, "Advantages and disavantages of using absorption chillers to lower utility bills", Naval facilities engineering service center poert hueneme *Tech data Sheet,* 1997.

[193] J. A. Abdusamad, *A Theoretical Examination of Retrofitting Inlet Cooling on the Performance of the Benghazi North Gas Turbine Power Plant*: Newcastle University, Newcastle upon Tyne, 2011.

[194] F. PanahiZadeh and N. Bozorgan, "The energy and exergy analysis of single effect absorption chiller," *International Journal of Advanced Design and Manufacturing Technology,* vol. 4, pp. 19-26, 2011.

[195] L. Ocneanu and R. C. Bucsa, "The Importance of Economic Analysis in Investment Projects," *Economy Transdisciplinarity Cognition,* vol. 17, p. 84, 2014.

[196] National Water, "Emerging trends in desalination: A review," *Waterlines report, National Water Commission, Canberra,* 2008.

[197] S. Boonnasa and P. Namprakai, "Sensitivity analysis for the capacity improvement of a combined cycle power plant (100–600MW)," *Applied Thermal Engineering,* vol. 28, pp. 1865-1874, 2008.

[198] S. Al-Hengari, M. El-Bousiffi, and W. El-Moudir, "Libyan Petroleum Institute experience in evaluation ofdesalination plants in the Libyan oil sector," *Desalination,* vol. 206, pp. 633-652, 2007.

[199] Water Treatment Engineering Group, "Desalting for planner. 3rd edn. USA.," (2003).

[200] Y. Aldali and K. Morad, "Numerical simulation of the integrated solar/North Benghazi combined power plant," *Applied Thermal Engineering,* vol. 108, pp. 785-792, 2016.

APPENDICES

Appendix 3-A

- Table 3-A1 Constants used to calculate the enthalpy and entropy of seawater [68, 99, 100]

b_1 =-2.348 x 10^4	b_6 = -4.417 x 10^1	c_1 = -4.231 x 10^2	c_6 = - 1.443 x 10^{-1}
b_2 = 3.152 x 10^5	b_7 = 2.139 x 10^{-1}	c_2 = 1.463 x 10^4	c_7 = 5.879 x 10^{-4}
b_3= 2.803 x 10^6	b_8 = - 1.991 x 10^4	c_3 = -9.880 x 10^4	c_8 = -6.111 x 10^1
b_4 = - 1.446 x 10^7	b_9 = 2.778 x 10^4	c_4 = 3.095 x 10^5	c_9 = 8.041 x 10^1
b_5 = 7.826 x 10^3	b_{10} = 9.728 x 10^1	c_5 = 2.562 x 10^1	c_{10} = 3.035 x 10^{-1}

- Table 3-A2 Feuerecker equation for LiBr enthalpy estimation[160]

n	an	bn	cn	dn
0	-945.8	-0.3293	7.4285E-3	-2.269E-6
1	47.77339E+1	4.076E-2	-1.5144E-4	
2	-1.59235	-1.36E-2	1.3555E-6	
3	2.09422E-2	-7.1366E-6		
4	-7.689E-5			

- Table 3-A3 Kaita correlation constants [161]

I	Bi0	Bi1	Bi2	Bi3
0	5.127558E-	-1.393954E-02	2.924145E-05	9.035697E-07
1	011.226780e-	-9.156820E-05	1.820453E-08	-7.991806E-10
2	-1.364895e-05	1.068904E-07	-1.381109E-09	1.529784E-11
3	1.021501E-08	0	0	0

- Table 3-A4 Constant for osmotic coefficient estimation [165, 166]

	j = 0	j = 1	j = 2
a_{1j}	-2.196316 x 10^1	4.937232 x 10^3	-6.5548406 x 10^5
a_{2j}	-3.810475 x 10^3	2.611535 x 10^6	-3.669991 x 10^8
a_{3j}	1.228085 x 10^5	-7.718792 x 10^7	1.039856 x 10^{10}
a_{4j}	-1.41674 x 10^6	9.195285 x 10^8	-1.189450 x 10^{11}
a_{5j}	7.765821 x 10^6	-4.937567 x 10^9	6.317555 x 10^{11}
a_{6j}	-1.511892 x 10^7	9.839974 x 10^9	-1.27379 x 10^{12}
a_{0j}	-4.417865 x 10^{-5}	3.114900 x 10^{-2}	-4.36112260 x 10^1
a_{1j}	3.07410 x 10^{-4}	-1.86321 x 10^{-1}	2.738714 x 10^1
a_{2j}	-4.080794 x 10^{-4}	2.160810 x 10^{-1}	-2.5175971 x 10^1

Appendix 3-B

- Table 3-B1 Zawya-Libya seawater temperature

Month	Temperature min.	Temperature max.	Average	Annual Average
Jan.	15.85	17.97	16.36	
Feb	14.7	17.3	15.58	
Mar	15.75	18.1	15.56	
Apr	16.4	19.43	18.76	
May	18.25	21.17	20.35	
Jun	19.33	20.3	20.79	20.35 ± 2.88
Jul	21	23.8	22.7	
Agu	21.7	26.2	23.16	
Sep	22	24.17	23.04	
Oct	21.5	24.1	22.94	
Nov.	18.67	21.65	20.16	
Dec	17	18.65	17.13	

- Table 3-B2 Zawya-Libya seawater salinity

Salinity min	Salinity Max.	Average	Annual Average
34.85	37.91	36.67	
34.6	37.95	36.5	
35.5	38.36	36.97	
35.4	38.4	36.43	
35.42	38.45	37.06	
35.6	38.42	37.26	
35.3	38.6	37.27	37.03 ±0.22
35.3	38.5	37.19	
35.55	37.81	37.13	
35.43	38.4	37.14	
35.27	38.53	37.05	
35.1	37.86	36.83	

Appendix 3-C

- **January 2010**

Date	Dry ambient temperature (°C)								
	Time								
	0	3	6	9	12	15	18	21	Average
1	20.0	15.5	14.0	21.5	26.5	23.0	19.5	18.3	19.8
2	17.5	15.0	13.0	17.5	19.0	17.8	13.0	7.8	15.1
3	8.5	7.7	6.2	15.5	20.0	19.0	11.0	8.4	12.0
4	9.0	8.0	7.0	17.5	23.0	23.8	14.4	12.6	14.4
5	11.0	12.5	10.5	21.5	27.0	26.7	21.2	18.5	18.6
6	17.0	15.0	13.5	20.5	25.0	26.2	16.5	13.6	18.4
7	12.2	11.8	14.0	20.5	27.0	24.2	17.5	17.7	18.1
8	16.0	17.0	19.5	23.4	27.0	26.5	24.2	20.7	21.8
9	19.5	13.5	10.5	14.5	16.3	16.5	14.5	12.2	14.7
10	10.8	6.0	6.2	12.8	14.8	13.9	11.2	5.0	10.1
11	4.0	2.4	2.5	13.4	16.0	19.0	8.0	9.2	9.3
12	7.5	8.0	9.2	13.2	17.2	15.6	13.6	9.0	11.7
13	7.5	7.8	9.5	16.6	21.2	20.5	17.5	16.9	14.7
14	13.8	10.6	8.6	16.0	19.0	19.0	15.5	15.0	14.7
15	16.0	13.5	13.5	16.7	18.2	17.2	14.7	13.5	15.4
16	13.2	12.6	14.5	14.5	15.0	15.0	14.8	15.0	14.3
17	14.5	15.0	14.4	14.6	15.0	16.0	14.2	12.0	14.5
18	12.0	12.7	11.5	15.4	19.2	17.2	13.4	12.5	14.2
19	12.8	12.6	12.5	13.6	14.7	15.7	14.0	9.2	13.1
20	8.2	9.0	9.5	15.0	17.5	16.8	11.6	12.2	12.5
21	11.5	10.8	10.2	15.0	17.5	17.5	14.5	15.8	14.1
22	14.7	14.4	13.5	12.5	15.5	15.5	13.5	9.0	13.6
23	7.3	6.6	6.0	14.0	18.0	16.5	10.5	8.0	10.9
24	7.5	7.5	8.0	15.2	19.2	20.5	14.5	13.0	13.2
25	12.0	11.7	11.2	16.5	21.0	20.2	16.6	14.2	15.4
26	13.6	12.8	11.5	14.8	20.0	21.0	17.0	10.8	15.2
27	10.0	9.5	11.8	17.4	19.4	19.6	15.8	13.0	14.6
28	12.0	10.0	8.4	14.2	18.5	16.2	12.0	8.8	12.5
29	8.2	9.6	9.5	11.8	14.0	15.0	12.4	9.2	11.2
30	9.0	10.0	8.5	16.0	19.0	18.6	16.0	13.3	13.8
31	13.8	11.0	10.0	15.0	19.0	19.5	14.5	12.2	14.4
total	3706	3401	3287	4966	5997	5897	4576	3866	446.2
Average	119.5	109.7	106.	160.2	193.5	190.2	147.6	124.7	14.5

Month January   2010

- **February**

Date	Dry ambient temperature (°C)								
	Time								
	0	3	6	9	12	15	18	21	Average
1	11.0	10.6	11.5	18.0	22.7	20.0	16.0	16.3	15.8
2	15.0	13.0	12.0	13.8	15.0	14.0	12.0	11.6	13.3
3	10.8	10.0	9.4	13.5	15.0	15.0	9.3	6.2	11.2
4	6.2	6.5	5.7	15.0	13.0	20.7	13.0	11.4	11.4
5	10.3	10.5	12.5	18.6	21.6	19.0	15.5	9.8	14.7
6	9.2	9.3	8.7	18.6	22.7	19.4	14.4	11.3	14.2
7	11.2	10.8	11.1	17.0	17.8	17.0	13.5	11.0	13.7
8	11.0	9.0	7.6	15.6	15.8	16.5	13.2	13.5	12.8
9	12.8	14.2	13.0	18.8	22.8	23.4	17.3	16.2	17.3
10	16.0	14.5	12.5	16.2	19.3	18.7	16.5	13.3	15.9
11	12.5	11.6	11.6	16.8	21.2	23.0	20.5	17.9	16.9
12	13.9	13.8	13.8	17.5	17.5	15.2	9.5	7.0	13.5
13	4.6	5.2	4.5	15.2	17.5	16.6	14.6	16.0	11.8
14	16.7	17.5	17.0	15.7	18.0	17.0	14.6	8.8	15.7
15	7.0	6.0	5.5	17.5	21.0	18.3	16.0	18.2	13.7
16	17.7	17.5	17.3	27.5	29.0	28.5	25.0	22.3	23.1
17	20.0	18.0	15.2	23.4	28.0	28.8	24.8	21.8	22.5
18	20.3	16.0	16.5	26.0	30.4	27.7	23.0	20.5	22.6
19	19.8	19.0	19.0	30.7	32.8	32.5	27.8	20.0	25.2
20	19.5	23.2	22.6	22.7	20.0	18.1	14.3	11.0	18.9
21	10.2	9.7	10.0	17.3	21.0	18.0	14.0	14.2	14.3
22	14.8	14.6	15.6	20.0	28.5	27.0	18.5	18.2	19.7
23	13.3	13.0	13.5	23.6	29.0	23.0	19.0	17.5	19.0
24	18.5	17.5	16.0	20.2	21.5	21.4	15.3	14.2	18.1
25	15.2	9.7	9.7	19.4	22.2	20.0	14.6	14.6	15.7
26	13.5	12.8	13.4	25.5	30.0	25.8	17.0	17.0	19.4
27	13.6	13.0	12.5	23.5	28.0	24.6	20.3	18.5	19.3
28	17.5	17.2	16.0	28.8	35.7	33.0	25.5	22.0	24.5
Total	382.1	363.7	353.7	556.4	637.0	602.2	475.0	420.3	473.8
Average	13.6	13.0	12.6	19.9	22.8	21.5	17.0	15.0	16.9

- **March**

Date	Dry ambient temperature (°C)								
	Time								
	0	3	6	9	12	15	18	21	Average
1	21.0	22.5	22.0	32.5	22.5	20.5	17.5	13.6	21.5
2	11.4	9.0	9.2	19.6	21.4	20.0	16.4	15.4	15.3
3	15.8	17.2	17.2	26.2	36.1	38.3	27.4	27.8	25.8
4	27.5	19.0	16.0	21.0	24.4	22.0	18.0	14.0	20.2
5	14.5	12.2	9.0	21.5	22.0	22.0	17.0	14.7	16.6
6	15.6	15.2	12.3	21.0	26.5	21.3	18.0	18.2	18.5
7	18.0	17.5	17.2	19.4	24.0	19.7	19.4	23.4	19.8
8	20.7	15.0	15.8	17.7	16.5	17.4	14.8	13.0	16.4
9	12.5	13.5	13.8	22.3	25.0	26.2	21.5	17.8	19.1
10	16.5	16.0	15.3	16.2	15.5	15.8	12.8	10.4	14.8
11	8.4	8.2	8.0	16.0	20.6	18.8	15.2	13.0	13.5
12	11.5	9.5	9.0	21.0	21.8	25.0	18.8	19.3	17.0
13	18.7	16.4	14.3	19.2	19.8	18.0	15.5	15.2	17.1
14	14.5	13.8	13.8	15.0	15.0	16.2	14.0	13.4	14.5
15	13.0	12.7	13.4	13.7	16.0	15.2	13.8	11.2	13.6
16	10.0	7.6	7.8	11.0	14.5	16.2	12.2	8.3	11.0
17	8.0	4.0	6.7	16.5	17.8	16.7	14.0	9.0	11.6
18	8.0	6.5	5.8	18.0	20.0	18.2	14.0	12.5	12.9
19	11.0	9.7	8.2	19.0	22.0	21.4	16.2	13.0	15.1
20	12.0	9.8	9.5	21.0	25.7	23.0	17.0	15.4	16.7
21	14.8	12.5	10.5	24.0	24.7	23.8	18.0	15.5	18.0
22	13.8	13.0	13.0	25.0	30.0	26.2	22.0	19.0	20.3
23	18.8	18.2	17.5	25.8	24.0	21.0	17.8	16.0	19.9
24	13.4	12.2	13.5	19.0	20.5	20.6	17.1	15.9	16.5
25	16.0	16.3	16.5	27.5	32.7	31.3	26.2	23.0	23.7
26	22.0	21.8	22.2	31.0	35.2	33.3	25.7	23.2	26.8
27	20.8	18.0	17.5	20.0	21.5	19.5	17.3	14.7	18.7
28	13.5	12.0	13.8	19.3	21.0	19.3	15.7	14.7	16.2
29	11.5	9.8	10.6	24.5	26.5	29.0	0.0	0.0	14.0
30	20.3	20.0	22.5	33.6	39.2	39.2	21.0	18.2	26.8
31	14.7	15.4	12.2	21.5	22.5	20.3	17.2	16.6	17.6
total	468.2	424.5	414.1	659.0	724.9	695.4	531.5	475.4	549.1
Average	15.1	13.7	13.4	21.3	23.4	22.4	17.1	15.3	17.7

- **April**

Date	Dry ambient temperature (°C)								
	Time								
	0	3	6	9	12	15	18	21	Average
1	15.0	15.4	15.5	22.5	25.7	24.7	19.5	19.0	19.7
2	18.2	17.2	15.2	20.7	21.8	20.4	17.0	15.0	18.2
3	13.6	12.8	13.0	21.8	23.5	24.0	21.0	20.0	18.7
4	18.6	17.8	18.0	27.5	34.0	34.8	30.0	25.8	25.8
5	18.0	18.0	18.0	20.5	19.7	19.2	16.2	13.5	17.9
6	14.0	12.0	11.0	19.3	20.2	19.0	16.5	15.5	15.9
7	15.2	14.0	14.0	25.4	25.0	24.2	27.0	22.2	20.9
8	18.5	17.5	17.4	22.2	26.9	21.9	18.5	17.8	20.1
9	17.2	16.7	17.0	19.7	19.6	19.1	17.2	17.0	17.9
10	16.5	16.5	17.0	18.5	21.2	20.3	16.7	14.5	17.7
11	13.5	11.5	10.5	19.0	22.8	22.0	18.4	15.4	16.6
12	16.0	17.2	16.8	26.4	28.5	25.7	23.2	23.4	22.2
13	21.4	19.5	20.0	25.2	26.6	27.0	20.0	16.5	22.0
14	16.7	15.5	17.3	23.2	25.0	28.0	27.0	26.2	22.4
15	23.0	14.8	18.0	26.8	27.0	27.8	23.0	24.5	23.1
16	24.5	22.0	19.0	23.5	21.7	21.3	19.5	18.7	21.3
17	18.4	18.3	18.6	21.8	24.5	24.2	22.0	22.0	21.2
18	19.0	19.0	20.0	24.0	31.0	27.0	20.8	19.5	22.5
19	18.6	18.2	18.6	20.5	22.5	20.8	18.0	15.0	19.0
20	13.2	12.2	14.0	21.3	22.5	20.5	18.6	16.0	17.3
21	15.2	14.0	16.0	24.7	24.5	24.8	22.0	19.5	20.1
22	20.2	19.5	19.8	30.7	32.6	34.4	30.2	26.5	26.7
23	24.4	28.0	29.0	32.5	24.0	22.2	21.0	16.8	24.7
24	15.5	14.8	16.0	24.1	24.4	23.3	19.5	18.6	19.5
25	17.0	14.2	18.5	23.0	22.5	22.0	18.8	17.8	19.2
26	17.3	18.0	19.0	20.6	21.2	20.7	18.3	16.8	19.0
27	14.3	14.0	14.4	20.8	22.5	21.8	18.7	16.5	17.9
28	16.0	15.0	17.0	21.5	20.0	16.8	17.8	16.2	17.5
29	14.0	14.5	16.0	21.2	22.0	21.0	18.5	14.6	17.7
30	12.7	12.2	14.5	21.3	22.6	22.0	19.0	16.0	17.5
total	515.7	490.3	509.1	690.2	726.0	700.9	613.9	556.8	600.4
Average	17.2	16.3	17.0	23.0	24.2	23.4	20.5	18.6	20.0

- **May**

Date	Dry ambient temperature (°C)								
	Time								
	0	3	6	9	12	15	18	21	Average
1	15.0	13.7	16.0	25.0	27.5	25.2	22.2	15.6	20.0
2	16.6	16.0	18.8	32.4	30.5	30.0	27.5	24.4	24.5
3	25.0	21.5	22.0	31.4	32.6	28.5	26.0	18.8	25.7
4	19.0	21.6	22.0	37.5	36.6	39.0	36.8	34.5	30.9
5	23.8	20.6	20.5	22.0	23.3	22.5	20.0	17.5	21.3
6	16.6	16.0	18.0	25.8	27.0	25.5	22.0	19.5	21.3
7	18.1	20.6	21.2	25.5	31.4	33.1	30.7	26.7	25.9
8	25.0	21.5	21.0	23.2	23.8	22.2	20.0	18.8	21.9
9	15.0	14.0	16.0	25.6	27.2	23.2	19.7	19.0	20.0
10	19.2	18.0	21.6	32.2	36.8	37.2	33.8	29.5	28.5
11	28.0	25.0	26.5	37.4	31.7	25.4	22.5	20.8	27.2
12	20.2	20.0	21.2	24.3	34.8	32.0	23.8	21.5	24.7
13	20.5	20.0	20.5	25.7	24.6	24.0	21.6	21.6	22.3
14	21.0	20.6	22.4	27.2	34.0	29.5	23.8	27.0	25.7
15	25.0	22.0	20.0	23.7	23.0	22.3	20.2	16.2	21.6
16	15.0	13.5	19.0	26.0	26.5	23.0	20.2	18.2	20.2
17	16.4	15.2	18.2	24.5	24.5	23.5	20.0	18.0	20.0
18	15.2	14.2	16.5	22.5	23.3	22.0	19.5	15.5	18.6
19	14.0	13.6	16.5	24.6	25.2	24.0	21.0	18.8	19.7
20	18.6	18.0	20.5	24.2	23.8	21.8	20.5	18.0	20.7
21	18.3	17.8	20.0	21.8	22.6	21.2	19.4	13.6	19.3
22	12.3	10.8	15.5	22.4	23.6	23.0	20.5	17.0	18.1
23	16.0	17.0	18.4	28.5	31.0	24.5	24.5	22.4	22.8
24	21.0	19.6	20.5	25.3	29.3	24.3	21.0	20.2	22.7
25	19.2	18.5	19.8	22.0	23.0	22.3	20.4	18.0	20.4
26	15.8	14.5	17.0	23.5	26.0	27.0	24.5	19.5	21.0
27	19.3	17.8	22.2	32.4	33.0	33.4	29.5	25.7	26.7
28	23.5	21.6	24.6	33.5	38.5	32.5	30.5	28.0	29.1
29	27.0	26.2	28.4	36.6	36.8	26.2	25.7	30.5	29.7
30	25.0	22.0	21.8	24.5	24.3	22.0	21.2	20.5	22.7
31	21.2	20.7	21.0	23.2	24.4	25.5	25.0	21.2	22.8
total	605.8	572.1	627.6	834.4	880.6	815.8	734.0	656.5	715.9
Average	19.5	18.5	20.2	26.9	28.4	26.3	23.7	21.2	23.1

- **June**

Date	Dry ambient temperature (°C)								
	Time								
	0	3	6	9	12	15	18	21	Average
1	19.2	17.2	23.5	28.6	28.0	28.0	25.3	21.0	23.9
2	18.8	17.5	20.5	30.3	32.0	30.0	26.5	23.5	24.9
3	23.5	21.2	25.4	30.0	28.6	25.6	23.8	22.8	25.1
4	21.8	20.0	22.0	27.0	29.3	27.3	22.7	21.0	23.9
5	19.2	16.0	21.5	24.2	24.5	23.5	21.5	17.4	21.0
6	15.3	14.4	19.4	24.0	25.7	25.0	23.0	19.5	20.8
7	17.4	16.5	19.5	30.8	31.0	31.5	30.5	26.0	25.4
8	24.6	24.2	29.0	38.7	39.5	38.8	35.0	28.8	32.3
9	23.3	23.0	25.5	34.2	34.2	39.4	35.5	29.0	30.5
10	29.2	28.0	30.0	40.0	39.5	41.6	38.0	35.2	35.2
11	30.5	38.6	33.7	38.8	37.5	41.0	33.8	34.7	36.1
12	32.3	29.0	29.2	39.0	41.5	41.5	35.0	30.5	34.8
13	25.4	22.7	25.8	35.7	30.3	28.0	28.5	25.5	27.7
14	24.7	24.0	26.0	30.5	30.3	29.7	29.5	27.3	27.8
15	27.5	27.0	28.5	34.0	39.8	33.3	37.5	33.2	32.6
16	33.4	29.4	27.6	30.5	28.6	27.8	26.8	25.2	28.7
17	24.0	23.7	25.2	33.2	35.7	38.2	34.7	25.3	30.0
18	23.5	21.5	26.0	34.0	36.0	41.6	29.7	24.0	29.5
19	23.2	21.3	23.4	26.0	27.0	27.3	24.3	22.7	24.4
20	22.0	19.8	22.5	27.6	27.5	27.0	25.0	22.3	24.2
21	20.1	17.4	24.0	24.8	25.6	24.6	23.0	18.0	22.2
22	17.8	17.4	22.0	26.5	26.8	24.8	22.2	20.0	22.2
23	17.0	15.2	20.5	24.7	24.8	24.8	22.6	18.0	21.0
24	15.5	14.0	19.5	28.0	28.0	28.0	25.5	22.5	22.6
25	21.5	20.2	24.0	31.7	32.3	31.3	27.8	24.0	26.6
26	23.4	23.3	24.8	33.5	28.5	29.8	27.8	25.5	27.1
27	23.8	22.4	24.2	30.0	28.6	26.2	24.0	22.8	25.3
28	21.5	20.4	22.0	28.5	29.0	27.6	24.3	21.6	24.4
29	20.5	19.4	21.0	26.8	27.8	27.0	25.0	21.5	23.6
30	19.0	16.8	19.5	29.0	29.0	28.5	25.5	21.2	23.6
total	678.9	641.5	725.7	920.6	926.9	918.7	834.3	730.0	797.1
Average	22.6	21.4	24.2	30.7	30.9	30.6	27.8	24.3	26.6

- **July**

Date	Dry ambient temperature (°C)								
	Time								
	0	3	6	9	12	15	18	21	Average
1	19.9	17.5	21.5	28.2	29.1	28.5	26.7	22.8	24.3
2	20.0	19.0	24.0	31.0	32.0	31.5	27.0	22.8	25.9
3	22.0	21.0	24.0	33.0	33.3	33.5	31.0	26.3	28.0
4	24.3	22.0	26.0	29.5	32.4	30.7	28.0	22.5	26.9
5	20.0	18.0	22.5	28.5	30.6	30.6	28.0	22.0	25.0
6	20.0	18.2	23.8	30.2	29.4	29.0	27.0	24.5	25.3
7	21.2	21.0	23.0	28.2	29.2	27.6	25.7	21.8	24.7
8	22.0	23.0	24.6	28.3	29.5	28.2	25.5	23.0	25.5
9	18.7	19.4	20.5	28.7	29.2	29.0	26.8	24.0	24.5
10	21.8	22.0	24.5	31.2	30.6	30.7	28.0	25.4	26.8
11	23.8	22.5	24.6	30.6	31.7	31.5	28.6	25.6	27.4
12	23.8	21.8	24.0	32.5	34.0	32.3	29.0	26.0	27.9
13	26.5	23.0	26.0	35.7	33.7	35.5	31.6	27.5	29.9
14	27.0	25.0	27.0	35.5	35.5	35.5	33.5	28.5	30.9
15	27.7	26.5	29.5	39.8	40.0	39.5	36.7	31.0	33.8
16	28.5	25.2	27.6	37.2	36.4	33.5	29.2	25.5	30.4
17	23.0	19.5	21.7	31.8	33.2	32.5	29.0	24.4	26.9
18	22.8	25.0	24.5	32.5	34.0	32.2	27.7	25.0	28.0
19	21.2	20.2	24.0	31.0	31.4	29.8	27.5	24.5	26.2
20	23.5	22.5	25.5	31.0	31.5	30.5	28.5	26.2	27.4
21	24.8	23.2	25.0	34.5	34.4	36.5	31.5	27.0	29.6
22	26.0	22.7	27.2	36.5	39.0	37.5	33.0	29.2	31.4
23	27.8	25.0	27.4	36.5	37.5	36.5	31.0	26.5	31.0
24	24.0	22.3	26.0	34.0	34.5	34.4	29.5	27.0	29.0
25	26.0	26.2	26.5	28.7	29.4	26.8	26.0	22.8	26.6
26	20.7	20.0	23.5	28.8	28.9	28.7	26.7	25.0	25.3
27	21.0	19.6	23.0	30.5	30.8	29.6	27.0	24.0	25.7
28	22.7	19.8	23.0	30.5	30.5	30.5	27.0	24.5	26.1
29	22.8	21.0	23.0	31.6	31.5	31.0	28.0	25.0	26.7
30	24.0	22.0	24.5	31.8	32.2	30.6	27.7	24.8	27.2
31	22.8	22.0	24.8	32.4	31.8	30.2	27.5	25.0	27.1
total	720.3	676.1	762.7	990.2	1007.2	984.4	889.9	780.1	851.4
Average	23.2	21.8	24.6	31.9	32.5	31.8	28.7	25.2	27.5

- **August**

Date	Dry ambient temperature (℃)								
	Time								
	0	3	6	9	12	15	18	21	Average
1	24.0	22.5	25.0	29.4	30.6	29.3	27.2	23.0	26.4
2	20.7	18.2	23.0	31.0	31.6	30.8	27.0	22.5	25.6
3	21.4	19.5	21.5	31.5	33.4	32.4	29.0	27.0	27.0
4	23.8	22.0	25.5	29.7	30.3	29.2	27.0	25.3	26.6
5	23.0	21.0	23.0	28.2	29.2	28.3	26.2	22.9	25.2
6	21.0	20.5	21.5	29.5	30.2	29.2	26.7	22.2	25.1
7	20.5	19.2	23.0	31.5	31.5	32.3	29.0	26.0	26.6
8	24.5	22.0	23.0	31.5	31.0	30.0	26.8	23.7	26.6
9	22.2	20.0	23.0	28.2	29.0	28.4	25.6	21.8	24.8
10	19.5	18.4	20.5	30.0	30.8	30.0	27.0	21.8	24.8
11	19.8	18.4	21.0	29.4	30.6	30.6	28.0	22.5	25.0
12	20.0	18.8	21.2	31.5	32.2	32.5	28.0	26.0	26.3
13	25.2	24.0	26.0	37.7	37.2	37.6	34.6	29.9	31.5
14	28.8	26.0	27.5	38.7	39.8	39.3	35.7	32.8	33.6
15	31.8	29.8	29.0	35.6	40.0	40.7	37.0	33.8	34.7
16	29.0	23.2	25.5	37.0	36.5	35.0	31.0	29.0	30.8
17	25.2	24.5	26.5	33.7	33.4	33.5	30.0	26.0	29.1
18	23.7	24.5	23.5	34.5	36.5	35.4	30.2	28.0	29.5
19	26.6	24.0	26.0	33.8	36.0	33.7	29.3	27.0	29.6
20	24.5	23.3	25.0	31.6	32.4	32.0	29.4	24.8	27.9
21	23.0	21.0	22.0	33.0	35.4	35.4	31.0	27.0	28.5
22	24.0	23.0	25.0	34.0	38.0	31.7	28.4	27.0	28.9
23	25.5	24.5	26.0	30.5	31.4	30.2	28.4	25.4	27.7
24	24.0	22.0	22.6	31.5	31.5	31.8	28.2	24.4	27.0
25	24.0	22.5	23.8	33.0	34.0	33.5	29.2	25.2	28.2
26	23.0	20.8	22.0	30.5	31.8	30.5	27.5	25.0	26.4
27	23.2	21.8	23.5	30.5	32.4	31.0	28.0	25.5	27.0
28	22.0	19.6	22.0	31.2	32.2	32.8	29.9	24.0	26.7
29	21.0	19.2	21.0	32.3	32.5	30.8	27.5	25.0	26.2
30	22.0	21.8	23.7	30.5	31.7	31.0	27.5	26.0	26.8
31	24.6	23.4	24.0	29.8	30.4	29.4	25.7	24.0	26.4
total	731.5	679.4	735.8	990.8	1023.5	998.3	896.0	794.5	856.2
Average	23.6	21.9	23.7	32.0	33.0	32.2	28.9	25.6	27.6

- **September**

Date	Dry ambient temperature (°C)								
	Time								
	0	3	6	9	12	15	18	21	Average
1	21.0	19.0	21.0	29.4	31.5	29.5	27.0	25.5	25.5
2	24.4	24.0	25.0	35.4	38.4	38.5	35.5	29.0	31.3
3	30.0	28.0	28.0	35.0	38.0	33.0	29.0	26.6	31.0
4	27.8	26.8	26.5	29.0	26.0	26.5	26.0	25.0	26.7
5	24.2	22.5	23.0	29.0	30.3	29.5	26.0	23.6	26.0
6	21.3	19.6	22.2	29.5	31.4	30.8	27.8	24.2	25.9
7	24.0	23.0	22.8	32.5	34.2	34.0	31.0	29.0	28.8
8	25.5	24.0	24.5	33.2	35.5	33.8	31.4	29.0	29.6
9	26.8	24.6	24.5	32.0	34.3	33.0	28.0	26.2	28.7
10	26.0	26.0	28.5	28.5	28.0	27.5	25.2	21.0	26.3
11	19.5	21.0	22.5	27.8	28.0	27.5	24.2	19.0	23.7
12	17.3	17.8	17.5	26.2	28.8	28.7	24.3	20.4	22.6
13	18.5	17.7	19.7	27.8	29.2	28.2	25.5	21.3	23.5
14	18.5	18.5	20.2	25.0	29.0	27.5	25.0	22.0	23.2
15	22.6	18.2	20.0	27.5	28.2	27.5	24.0	20.8	23.6
16	20.7	20.2	20.8	26.0	27.0	27.0	23.5	21.0	23.3
17	20.5	20.0	20.5	28.0	29.4	29.4	26.5	24.3	24.8
18	23.4	21.7	21.5	32.0	33.6	32.3	28.0	24.2	27.1
19	23.8	21.6	19.6	31.5	34.0	34.2	28.0	23.5	27.0
20	22.0	20.6	20.0	30.6	30.2	29.5	25.6	23.0	25.2
21	22.0	21.7	22.5	28.5	31.0	27.5	26.0	25.2	25.6
22	23.5	22.8	23.0	32.5	35.2	33.5	29.0	27.0	28.3
23	26.0	25.2	23.0	29.2	29.2	27.7	25.4	22.0	26.0
24	20.5	19.9	20.3	27.0	32.5	31.0	28.3	22.8	25.3
25	21.8	22.4	22.5	28.0	28.2	27.6	24.5	23.0	24.8
26	22.3	20.0	18.8	31.0	31.7	29.2	26.5	26.8	25.8
27	25.5	24.5	24.5	28.5	38.0	32.5	27.5	27.0	28.5
28	26.4	26.0	26.3	29.0	30.0	28.4	26.8	25.5	27.3
29	25.8	25.2	25.0	28.0	28.0	26.0	24.8	24.0	25.9
30	24.0	23.2	23.5	25.7	26.8	25.8	25.8	22.8	24.7
total	695.6	665.7	677.7	883.3	935.6	897.1	806.1	724.7	785.7
Average	23.2	22.2	22.6	29.4	31.2	29.9	26.9	24.2	26.2

- **October**

Date	Dry ambient temperature (°C)								
	Time								
	0	3	6	9	12	15	18	21	Average
1	16.7	17.2	17.2	25.5	27.0	26.2	22.5	17.2	21.2
2	17.4	15.2	16.5	27.5	29.8	29.0	24.0	20.4	22.5
3	19.5	18.0	17.0	29.0	31.0	29.7	24.0	22.5	23.8
4	21.3	18.5	20.0	32.0	34.0	31.5	26.5	24.5	26.0
5	23.5	22.0	20.5	31.0	34.2	35.5	29.8	27.4	28.0
6	25.5	24.5	23.7	34.6	35.2	32.6	27.0	24.6	28.5
7	22.2	21.7	22.2	26.0	29.5	28.0	25.0	21.8	24.6
8	21.5	20.4	20.0	28.0	30.5	29.5	26.5	25.0	25.2
9	24.3	23.0	22.3	25.0	27.3	31.3	25.8	24.5	25.4
10	23.2	21.5	21.5	32.0	35.0	35.7	29.0	26.8	28.1
11	29.5	25.7	25.3	27.8	29.0	29.4	26.2	28.0	27.6
12	29.4	28.0	24.0	34.0	37.0	34.0	29.8	28.0	30.5
13	26.8	24.8	24.2	28.5	33.0	27.5	25.0	23.8	26.7
14	22.0	20.4	22.0	28.4	30.0	26.5	23.7	19.2	24.0
15	19.0	17.0	18.5	27.6	30.9	28.6	22.4	18.4	22.8
16	19.5	18.5	18.8	31.0	29.0	28.3	22.5	19.4	23.4
17	18.0	18.6	18.0	28.6	28.0	21.5	20.4	20.8	21.7
18	19.5	18.2	18.6	23.0	23.0	22.2	20.0	17.2	20.2
19	16.4	15.0	14.7	21.5	22.8	22.0	20.6	18.5	18.9
20	17.5	15.0	14.0	20.4	23.5	22.6	18.0	16.0	18.4
21	14.8	13.8	13.6	23.3	26.0	24.0	21.8	21.0	19.8
22	20.0	18.2	18.0	25.6	26.5	25.0	22.5	21.5	22.2
23	20.0	18.8	17.5	25.5	30.0	26.6	24.7	23.4	23.3
24	21.8	21.2	21.0	24.2	23.6	23.4	21.7	23.0	22.5
25	22.0	21.0	22.0	24.0	23.6	22.5	19.0	17.2	21.4
26	16.8	16.8	16.8	25.7	28.0	23.8	21.0	18.0	20.9
27	16.7	14.2	13.5	19.2	21.2	21.0	20.0	20.0	18.2
28	19.7	19.2	15.8	21.0	23.0	21.0	19.5	18.5	19.7
29	15.8	14.5	13.2	20.4	23.3	22.3	18.0	14.5	17.8
30	13.5	12.8	13.0	22.2	26.6	24.0	19.0	17.4	18.6
31	14.4	14.2	14.0	26.2	30.4	29.6	23.0	22.5	21.8
total	628.2	587.9	577.4	818.7	881.9	834.8	718.9	661.0	713.6
Average	20.3	19.0	18.6	26.4	28.4	26.9	23.2	21.3	23.0

- **November**

Date	Dry ambient temperature (°C)								
	Time								
	0	3	6	9	12	15	18	21	Average
1	21.7	22.0	21.2	28.2	32.0	28.6	22.4	22.5	24.8
2	19.5	16.6	14.6	22.5	25.5	25.0	18.0	13.0	19.3
3	13.5	12.7	12.5	22.2	24.0	22.5	19.0	13.8	17.5
4	12.5	11.4	10.5	22.7	23.2	22.7	20.5	20.0	17.9
5	21.0	19.6	18.7	22.8	27.2	25.5	21.4	20.5	22.1
6	19.8	19.3	18.3	23.5	27.0	28.0	24.5	23.0	22.9
7	22.0	19.0	16.8	22.2	22.8	22.8	20.5	14.8	20.1
8	16.0	15.0	15.3	23.0	25.7	25.5	21.8	19.4	20.2
9	18.5	20.0	20.3	26.0	28.0	28.0	24.4	21.4	23.3
10	19.4	19.4	21.0	24.7	30.3	30.0	22.5	18.0	23.2
11	16.8	16.0	14.5	24.0	26.8	23.0	20.5	19.0	20.1
12	19.0	18.0	18.0	20.0	20.0	19.5	18.5	18.5	18.9
13	16.4	13.7	14.3	14.0	16.8	17.5	17.0	13.0	15.3
14	13.2	11.5	10.5	20.0	23.5	22.0	16.5	14.7	16.5
15	13.8	13.0	13.5	23.2	27.5	24.2	18.8	15.8	18.7
16	14.3	10.8	11.2	20.5	24.5	21.5	19.5	19.4	17.7
17	17.0	16.8	16.0	18.5	22.8	21.8	15.5	13.0	17.7
18	12.7	10.5	9.2	18.0	22.0	22.0	11.0	7.8	14.2
19	7.5	8.5	8.0	16.1	20.5	20.3	12.4	9.4	12.8
20	9.2	9.5	8.0	19.5	24.2	21.0	14.8	15.0	15.2
21	15.0	13.5	13.0	24.6	31.0	28.0	20.0	18.5	20.5
22	17.0	16.8	14.8	21.6	24.2	24.0	16.5	16.7	19.0
23	15.0	13.0	13.0	19.8	22.2	21.5	16.0	11.0	16.4
24	11.0	8.7	8.5	18.5	22.2	20.0	12.7	10.0	14.0
25	11.0	10.8	11.4	21.5	23.5	24.8	15.4	15.0	16.7
26	13.5	11.2	12.4	24.0	30.0	30.2	19.2	20.0	20.1
27	19.0	15.5	13.7	25.2	29.2	25.8	20.8	18.0	20.9
28	20.5	20.0	22.5	26.4	29.8	28.5	23.8	21.0	24.1
29	20.0	18.4	14.3	23.4	28.0	25.0	21.0	20.0	21.3
30	18.6	16.5	17.5	23.5	28.8	29.0	24.0	23.5	22.7
31									0.0
total	484.4	447.7	433.5	660.1	763.2	total	568.9	total	574.0
Average	16.1	14.9	14.5	22.0	25.4	Average	19.0	Average	19.1

- **December**

Date	Dry ambient temperature (°C)								
	Time								
	0	3	6	9	12	15	18	21	Average
1	24.5	23.8	23.2	26.3	29.2	30.7	27.0	20.8	25.7
2	13.4	20.8	19.8	25.0	25.3	24.7	16.0	15.2	20.0
3	14.4	16.2	16.3	21.0	26.0	22.4	20.5	20.0	19.6
4	18.0	15.0	12.8	13.0	18.5	16.7	14.8	11.0	15.0
5	8.3	7.8	7.8	15.0	20.0	17.5	11.4	9.0	12.1
6	10.0	9.0	7.0	17.5	23.0	24.5	16.2	14.6	15.2
7	12.6	11.5	12.0	20.5	23.7	23.5	14.8	13.5	16.5
8	13.0	10.5	10.0	22.4	26.0	27.8	16.7	14.0	17.6
9	16.7	14.2	10.5	24.8	28.7	29.6	24.3	21.5	21.3
10	16.8	14.0	14.5	22.0	23.0	20.0	18.0	17.0	18.2
11	16.5	16.4	15.8	17.0	18.0	17.0	15.5	13.8	16.3
12	13.4	13.5	11.5	14.7	18.0	17.3	14.8	8.5	14.0
13	10.0	9.5	10.0	14.0	17.2	17.9	9.2	9.6	12.2
14	9.2	9.2	8.5	14.8	19.2	18.0	15.8	12.0	13.3
15	12.7	11.0	11.5	17.0	15.3	15.5	13.4	12.1	13.6
16	11.4	9.8	8.5	10.5	13.6	12.8	8.5	8.3	10.4
17	7.5	6.7	5.8	11.7	14.0	12.5	8.5	6.4	9.1
18	4.3	3.5	4.8	13.4	18.4	19.0	13.0	12.0	11.1
19	12.5	15.0	16.3	20.2	27.5	28.2	18.7	20.5	19.9
20	18.7	18.3	14.4	23.0	26.5	21.3	13.7	12.0	18.5
21	11.2	9.5	8.7	18.0	22.4	20.8	16.8	15.5	15.4
22	14.6	15.0	15.5	21.6	27.5	27.7	18.0	17.0	19.6
23	15.7	18.6	18.0	25.8	30.6	29.3	23.2	20.5	22.7
24	15.5	16.0	16.2	20.0	21.0	20.0	14.5	17.5	17.6
25	11.8	11.0	11.5	15.5	17.5	16.8	12.0	11.0	13.4
26	8.0	6.3	6.0	13.5	17.3	16.0	8.6	6.0	10.2
27	8.2	8.4	8.8	10.0	12.7	11.0	11.0	11.0	10.1
28	14.2	14.5	10.0	11.7	15.2	13.9	14.5	11.3	13.2
29	9.6	9.0	7.2	12.3	15.8	16.3	8.0	6.6	10.6
30	6.3	4.8	3.5	12.2	16.8	17.0	9.5	11.0	10.1
31	8.0	6.8	8.6	14.7	19.8	17.8	12.7	9.5	12.2
total	387.0	375.6	355.0	539.1	647.7	623.5	459.6	408.7	474.5
Average	12.5	12.1	11.5	17.4	20.9	20.1	14.8	13.2	15.3

3-D Zawya City relative humidity 2010

- **January**

Date	Relative humidity (%)								
	Time								
	0	3	6	9	12	15	18	21	Average
1	42	58	57	43	39	48	51	51	48.6
2	52	59	66	63	61	71	93	97	70.3
3	93	87	85	64	52	61	94	94	78.8
4	84	80	82	51	38	34	66	64	62.4
5	58	51	59	35	24	25	35	37	40.5
6	40	46	46	34	35	33	70	69	46.6
7	76	71	56	35	30	42	57	48	51.9
8	48	45	35	39	42	44	48	59	45.0
9	59	77	59	43	41	42	48	46	51.9
10	53	65	65	47	50	54	64	84	60.3
11	77	80	56	52	50	48	75	62	62.5
12	55	56	55	53	63	77	80	93	66.5
13	93	89	80	59	45	55	61	61	67.9
14	74	77	81	60	53	63	74	70	69.0
15	89	92	99	80	67	62	71	80	80.0
16	83	93	83	94	91	87	91	83	88.1
17	87	85	88	88	90	96	92	94	90.0
18	86	86	88	81	74	78	90	94	84.6
19	96	98	94	93	92	82	85	97	92.1
20	97	99	97	84	71	70	96	92	88.3
21	91	90	85	78	73	71	80	71	79.9
22	75	72	76	79	79	79	81	93	79.3
23	96	95	97	73	60	65	91	97	84.3
24	99	96	96	77	63	58	75	79	80.4
25	82	79	79	63	57	59	66	76	70.1
26	74	66	66	62	52	49	63	84	64.5
27	84	81	76	60	59	59	81	88	73.5
28	88	93	94	82	74	84	99	97	88.9
29	99	99	100	95	95	76	89	97	93.8
30	99	82	85	58	48	48	56	63	67.4
31	55	70	72	58	53	51	66	71	62.0
total	2384	2417.0	2357.0	1983.0	1821.0	1871.0	2288.0	2391.0	2189.0
Average	76.9	78.0	76.0	64.0	58.7	60.4	73.8	77.1	70.6

- **February**

Date	Relative humidity (%)								
	Time								
	0	3	6	9	12	15	18	21	Average
1	73	77	64	53	42	59	73	71	64
2	68	73	70	69	68	67	76	76	70.9
3	75	82	84	72	73	96	97	81	82.5
4	91	84	83	58	43	44	66	77	68.3
5	75	71	65	53	48	50	71	97	66.3
6	95	93	90	61	47	61	95	100	80.3
7	88	90	92	70	64	63	77	79	77.9
8	75	81	91	73	73	75	84	80	79.0
9	79	73	79	63	53	52	87	87	71.6
10	87	94	85	67	48	49	65	72	70.9
11	68	69	67	59	53	48	54	57	59.4
12	78	74	73	60	55	74	93	97	75.5
13	98	97	97	57	52	69	89	69	78.5
14	68	72	70	84	76	59	76	100	75.6
15	100	100	98	66	52	76	83	60	79.4
16	64	64	63	33	38	41	49	52	50.5
17	57	59	67	41	33	33	47	52	48.6
18	59	74	70	42	38	44	56	65	56.0
19	63	61	56	31	30	34	45	76	49.5
20	70	47	51	57	57	63	91	97	66.6
21	91	74	66	48	42	57	83	67	66.0
22	63	64	59	56	23	27	52	50	49.3
23	65	55	51	32	27	41	55	57	47.9
24	58	57	60	60	65	60	91	71	65.3
25	60	75	75	54	4	54	69	62	56.6
26	63	57	56	28	23	34	61	54	47.0
27	69	71	79	52	39	57	79	72	64.8
28	57	51	50	25	22	27	39	50	40.1
total	2057	2039	2011	1524	1288	1514	2003	2028	1808
Average	73.5	72.8	71.8	54.4	46.0	54.1	71.5	72.4	64.6

- **March**

Date	Relative humidity (%)								
	Time								
	0	3	6	9	12	15	18	21	Average
1	48	41	40	27	73	76	83	97	60.6
2	100	100	63	65	70	91	88	84	82.6
3	83	62	47	29	27	42	36	49	46.9
4	36	92	94	53	45	54	76	81	66.4
5	63	72	84	54	62	58	78	84	69.4
6	75	66	83	61	38	73	90	86	71.5
7	88	90	85	81	64	81	77	39	75.6
8	57	92	85	74	84	74	91	94	81.4
9	88	67	66	42	32	27	50	73	55.6
10	81	89	88	75	74	66	77	87	79.6
11	93	92	63	44	52	70	77	73	70.5
12	82	87	93	55	51	39	76	52	66.9
13	46	47	85	74	74	85	84	79	71.8
14	73	64	67	66	63	58	67	64	65.3
15	71	78	73	81	61	51	66	88	71.1
16	91	91	89	87	77	60	86	97	84.8
17	97	97	97	60	57	68	72	93	80.1
18	94	95	49	37	53	70	71	71	67.5
19	73	78	83	46	36	34	67	77	61.8
20	69	69	68	37	20	33	43	60	49.9
21	48	66	33	35	38	51	64	50	48.1
22	69	61	50	29	20	28	35	42	41.8
23	43	43	44	24	41	78	92	96	57.6
24	98	98	92	74	69	72	87	73	82.9
25	71	65	62	33	26	35	78	48	52.3
26	49	45	39	30	30	28	44	48	39.1
27	78	95	95	81	74	77	89	94	85.4
28	94	94	85	65	57	69	87	95	80.8
29	98	99	97	45	46	43	62	68	69.8
30	56	53	45	29	22	23	78	88	49.3
31	96	96	98	49	50	64	83	81	77.1
total	2308	2384	2242	1642	1586	1778	2254	2311	2063.1
Average	74.5	76.9	72.3	53.0	51.2	57.4	72.7	74.5	66.6

- **April**

Date	Relative humidity (%)								
	Time								
	0	3	6	9	12	15	18	21	Average
1	84	81	79	55	54	53	71	66	67.9
2	71	86	89	64	63	64	80	87	75.5
3	91	94	96	48	60	56	55	52	69.0
4	53	39	38	24	20	22	28	34	32.3
5	80	87	90	75	73	70	80	88	80.4
6	85	94	94	65	66	69	81	82	79.5
7	79	80	82	39	46	63	32	51	59.0
8	74	80	88	71	52	72	85	87	76.1
9	90	92	90	70	69	71	81	90	81.6
10	87	86	82	80	60	65	73	89	77.8
11	88	94	94	58	49	51	63	74	71.4
12	68	61	60	30	34	38	48	46	48.1
13	62	75	69	59	52	45	89	95	68.3
14	98	99	98	74	61	52	35	36	69.1
15	41	72	80	48	59	57	70	52	59.9
16	48	69	90	71	83	82	88	94	78.1
17	95	97	98	82	70	72	82	70	83.3
18	94	90	86	68	48	66	87	93	79.0
19	95	94	89	73	66	71	80	94	82.8
20	98	98	98	59	56	69	77	81	79.5
21	82	85	74	41	50	52	57	64	63.1
22	56	59	58	29	23	22	29	32	38.5
23	35	25	27	30	73	74	78	93	54.4
24	95	97	94	55	54	56	77	74	75.3
25	90	89	71	53	61	64	77	84	73.6
26	82	82	81	75	72	71	84	97	80.5
27	97	98	97	70	66	71	84	91	84.3
28	91	85	79	72	84	89	92	96	86.0
29	98	97	95	72	62	72	83	97	84.5
30	98	98	97	65	60	66	77	89	81.3
total	2405	2483	2463	1775	1746	1845	2123	2278	2139.75
Average	80.2	82.8	82.1	59.2	58.2	61.5	70.8	75.9	71.3

- **May**

Date	Relative humidity (%)								
	Time								
	0	3	6	9	12	15	18	21	Average
1	89	92	79	38	40	44	65	91	67.3
2	88	73	55	21	36	28	34	49	48.0
3	35	46	54	29	31	46	49	69	44.9
4	65	51	51	15	28	18	24	31	35.4
5	71	85	84	74	67	69	80	90	77.5
6	92	91	90	35	30	44	51	54	60.9
7	59	41	45	34	29	35	38	51	41.5
8	56	80	86	82	78	77	87	89	79.4
9	97	94	95	37	49	66	83	76	74.6
10	68	66	50	25	15	16	21	23	35.5
11	23	26	34	15	37	66	77	87	45.6
12	91	93	87	67	36	51	81	90	74.5
13	86	81	81	50	60	62	78	80	72.3
14	82	85	82	60	42	60	85	70	70.8
15	60	57	73	36	36	42	51	70	53.1
16	74	72	42	21	27	67	76	83	57.8
17	92	95	84	42	52	50	64	71	68.8
18	83	89	79	51	50	58	64	80	69.3
19	83	82	65	41	46	52	69	76	64.3
20	73	75	69	63	61	45	58	69	64.1
21	72	80	60	55	51	59	69	89	66.9
22	92	92	71	57	52	56	65	75	70.0
23	74	65	62	30	35	61	50	66	55.4
24	65	59	82	71	51	75	87	85	71.9
25	83	76	81	74	65	68	81	90	77.3
26	91	94	95	68	51	42	54	74	71.1
27	68	68	53	21	28	25	36	38	42.1
28	42	47	38	24	17	29	34	31	32.8
29	32	37	33	22	30	64	60	37	39.4
30	67	88	79	64	66	78	78	82	75.3
31	80	80	78	66	60	47	50	78	67.4
total	2233	2260	2117	1388	1356	1600	1899	2144	1874.6
Average	72.0	72.9	68.3	44.8	43.7	51.6	61.3	69.2	60.5

- **June**

Date	Relative humidity (%)								
	Time								
	0	3	6	9	12	15	18	21	Average
1	66	74	45	36	43	40	51	65	52.5
2	74	79	66	37	35	42	49	51	54.1
3	45	56	55	40	42	58	71	64	53.9
4	67	74	66	60	50	56	69	78	65.0
5	79	91	78	57	60	66	71	86	73.5
6	91	93	85	60	60	54	63	81	73.4
7	88	90	72	39	39	36	42	45	56.4
8	51	48	38	23	23	26	35	50	36.8
9	75	91	75	50	50	39	36	64	60.0
10	57	50	56	34	32	29	36	41	41.9
11	46	37	44	26	34	28	45	24	35.5
12	28	46	52	23	24	24	44	56	37.1
13	77	89	78	37	65	71	64	80	70.1
14	77	86	75	51	55	58	47	57	63.3
15	47	41	40	29	25	40	24	41	35.9
16	42	53	66	51	67	71	73	78	62.6
17	79	70	78	49	41	30	44	78	58.6
18	87	91	80	53	37	29	64	91	66.5
19	86	90	80	66	63	66	73	79	75.4
20	78	88	80	50	57	63	71	79	70.8
21	86	93	79	74	59	57	58	75	72.6
22	77	81	68	53	53	63	71	77	67.9
23	87	91	77	60	59	61	71	88	74.3
24	89	91	81	42	53	55	72	74	69.6
25	71	76	60	46	40	53	63	62	58.9
26	62	61	58	26	78	63	57	69	59.3
27	78	89	77	54	60	72	83	83	74.5
28	91	90	87	58	56	57	75	91	75.6
29	95	96	94	68	51	64	80	91	79.9
30	95	97	95	40	56	63	78	93	77.1
total	2171	2302	2085	1392	1467	1534	1780	2091	1852.8
Average	72.4	76.7	69.5	46.4	48.9	51.1	59.3	69.7	61.8

- **July**

Date	Relative humidity (%)								
	Time								
	0	3	6	9	12	15	18	21	Average
1	97	97	94	54	47	61	66	91	75.9
2	93	94	60	43	43	43	60	78	64.3
3	72	78	60	36	36	31	39	44	49.5
4	58	62	52	63	40	52	62	87	59.5
5	93	95	36	64	50	45	57	90	66.3
6	93	94	79	52	58	64	77	92	76.1
7	94	93	98	66	62	70	79	92	81.8
8	91	89	79	63	60	71	84	95	79.0
9	99	98	98	69	65	68	77	87	82.6
10	91	88	79	48	56	56	65	71	69.3
11	75	72	67	45	45	52	63	69	61.0
12	68	76	68	39	43	45	64	73	59.5
13	59	63	51	35	41	37	55	59	50.0
14	56	56	47	35	34	36	38	43	43.1
15	44	43	36	24	25	22	31	35	32.5
16	40	53	47	21	28	43	72	88	49.0
17	91	95	96	54	53	44	74	88	74.4
18	93	96	96	59	43	46	84	89	75.8
19	93	96	88	56	55	70	81	92	78.9
20	91	94	89	62	64	71	81	88	80.0
21	96	97	89	44	51	30	45	56	63.5
22	58	73	58	31	29	34	48	48	47.4
23	54	63	57	41	34	32	57	69	50.9
24	77	88	69	40	39	40	70	84	63.4
25	85	75	73	65	59	66	69	84	72.0
26	90	92	79	56	53	54	61	66	68.9
27	82	87	73	49	49	55	66	79	67.5
28	84	94	83	42	53	53	66	75	68.8
29	78	85	78	36	46	46	53	68	61.3
30	74	82	77	43	47	55	74	88	67.5
31	89	90	76	46	56	59	76	84	72.0
total	2458	2558	2232	1481	1464	1551	1994	2352	2011.3
Average	79.3	82.5	72.0	47.8	47.2	50.0	64.3	75.9	64.9

- **August**

Date	Relative humidity (%)								
	Time								
	0	3	6	9	12	15	18	21	Average
1	88	91	89	70	55	63	69	86	76.4
2	93	95	83	39	43	52	70	83	69.8
3	88	91	82	46	38	51	52	59	63.4
4	77	95	88	61	69	70	70	86	77.0
5	84	93	90	63	59	65	71	84	76.1
6	91	93	91	59	58	65	70	96	77.9
7	91	93	83	44	52	50	66	65	68.0
8	74	87	79	54	59	66	81	89	73.6
9	94	96	87	61	58	61	75	90	77.8
10	95	96	93	51	49	60	70	90	75.5
11	96	96	91	65	59	56	69	82	76.8
12	94	97	94	46	50	49	70	66	70.8
13	73	68	53	27	31	29	41	42	45.5
14	44	53	49	32	28	27	35	43	38.9
15	37	40	43	38	24	20	33	26	32.6
16	35	57	47	33	46	47	63	52	47.5
17	69	76	53	53	57	43	62	66	59.9
18	67	64	65	47	42	36	61	60	55.3
19	72	75	66	50	34	51	76	90	64.3
20	94	96	95	71	62	57	73	89	79.6
21	87	94	95	56	36	45	54	64	66.4
22	69	73	74	46	24	71	86	92	66.9
23	92	93	92	66	60	66	81	89	79.9
24	96	98	98	60	62	60	80	92	80.8
25	94	96	87	50	44	43	69	90	71.6
26	96	94	95	66	60	66	81	89	80.9
27	97	96	89	66	59	68	81	91	80.9
28	95	97	89	48	47	51	66	78	71.4
29	85	92	85	48	64	69	77	89	76.1
30	95	98	94	56	50	51	64	73	72.6
31	81	85	83	60	57	60	71	71	71.0
total	2543	2668	2502	1632	1536	1668	2087	2362	2124.8
Average	82.0	86.1	80.7	52.6	49.5	53.8	67.3	76.2	68.5

- **September**

Date	Relative humidity (%)								
	Time								
	0	3	6	9	12	15	18	21	Average
1	84	90	85	49	41	57	66	65	67.1
2	65	68	62	34	35	35	40	82	52.6
3	59	67	72	41	43	62	80	83	63.4
4	94	87	88	71	92	79	76	84	83.9
5	88	96	96	64	57	62	76	86	78.1
6	94	98	89	56	51	49	65	70	71.5
7	66	71	72	35	41	38	57	35	51.9
8	53	70	64	34	30	44	53	71	52.4
9	78	79	83	55	50	57	74	82	69.8
10	86	92	78	67	64	63	63	82	74.4
11	88	82	74	50	51	55	66	86	69.0
12	92	81	75	61	55	54	73	86	72.1
13	92	93	84	56	60	56	69	84	74.3
14	90	97	85	72	55	50	61	72	72.8
15	70	88	81	55	51	57	71	96	71.1
16	97	91	84	68	63	63	81	91	79.8
17	91	92	91	57	59	59	72	84	75.6
18	80	85	80	45	43	47	60	70	63.8
19	78	88	93	44	35	31	67	81	64.6
20	82	94	95	60	59	55	81	87	76.6
21	91	94	91	55	50	70	76	76	75.4
22	83	79	78	42	39	41	69	88	64.9
23	88	86	89	64	66	66	76	88	77.9
24	93	94	93	58	37	57	60	95	73.4
25	93	83	74	60	59	62	75	81	73.4
26	82	92	95	43	48	61	77	57	69.4
27	76	87	93	61	26	55	77	88	70.4
28	89	90	90	78	72	80	87	92	84.8
29	89	88	88	77	70	66	70	79	78.4
30	71	70	67	54	46	58	70	73	63.6
total	2482	2572	2489	1666	1548	1689	2088	2394	2116
Average	82.7	85.7	83.0	55.5	51.6	56.3	69.6	79.8	70.5

- **October**

Date	Relative humidity (%)								
	Time								
	0	3	6	9	12	15	18	21	Average
1	91	88	86	55	48	51	70	90	72.4
2	86	93	91	44	42	48	69	79	69.0
3	79	82	88	43	40	44	69	77	65.3
4	63	69	58	32	27	43	62	50	50.5
5	53	64	79	32	23	25	36	37	43.6
6	58	61	58	23	30	38	75	95	54.8
7	93	96	98	84	68	74	84	98	86.9
8	95	97	95	60	59	62	73	72	76.6
9	75	83	84	78	63	43	74	68	71.0
10	70	71	74	39	28	29	50	55	52.0
11	39	82	72	62	56	58	77	47	61.6
12	33	41	63	32	19	39	56	57	42.5
13	63	70	70	61	31	72	82	82	66.4
14	71	60	48	36	34	56	72	88	58.1
15	88	90	76	41	33	42	74	86	66.3
16	74	67	61	28	40	53	74	84	60.1
17	90	93	85	37	66	87	93	93	80.5
18	90	92	85	59	65	57	68	83	74.9
19	80	84	76	52	42	49	57	62	62.8
20	63	68	72	48	39	44	73	77	60.5
21	80	78	85	63	49	60	68	69	69.0
22	77	83	85	54	56	65	74	73	70.9
23	77	83	89	48	36	55	60	59	63.4
24	56	62	63	53	70	62	73	71	63.8
25	76	82	91	68	70	70	87	98	80.3
26	90	87	87	46	41	67	78	90	73.3
27	67	70	61	50	51	53	59	53	58.0
28	58	57	71	53	52	57	59	68	59.4
29	75	77	80	50	43	53	76	89	67.9
30	88	91	88	51	34	50	72	84	69.8
31	95	91	62	34	25	29	45	39	52.5
total	2293	2412	2381	1516	1380	1635	2139	2273	2003.6
Average	74.0	77.8	76.8	48.9	44.5	52.7	69.0	73.3	64.6

- **November**

Date	Relative humidity (%)								
	Time								
	0	3	6	9	12	15	18	21	Average
1	42	41	46	32	23	37	56	63	42.5
2	61	62	66	44	35	36	76	83	57.9
3	74	74	71	48	41	55	75	97	66.9
4	94	93	97	71	67	67	79	95	82.9
5	89	87	84	69	49	57	80	86	75.1
6	86	85	91	63	47	42	50	56	65.0
7	58	67	84	65	61	62	66	87	68.8
8	75	73	70	48	39	43	52	52	56.5
9	56	49	45	31	29	28	34	43	39.4
10	52	47	37	29	23	21	41	49	37.4
11	50	50	53	41	45	69	80	79	58.4
12	58	66	66	56	54	58	63	62	60.4
13	72	90	79	89	74	88	85	94	83.9
14	93	94	94	64	47	58	82	92	78.0
15	93	94	83	54	37	52	79	89	72.6
16	92	94	85	69	61	68	79	77	78.1
17	92	95	95	82	50	56	84	94	81.0
18	86	81	77	45	28	26	73	82	62.3
19	79	73	75	42	39	48	83	95	66.8
20	93	91	96	68	48	65	86	87	79.3
21	78	77	75	38	24	40	68	71	58.9
22	81	74	70	36	29	29	54	47	52.5
23	53	55	50	37	28	35	54	69	47.6
24	69	70	71	43	35	44	84	90	63.3
25	78	75	64	37	33	36	75	63	57.6
26	65	73	65	33	24	21	62	45	48.5
27	46	67	59	29	27	40	53	62	47.9
28	77	34	27	28	27	29	44	48	39.3
29	50	57	78	41	35	54	57	40	51.5
30	44	49	44	29	23	27	39	35	36.3
31									
total	2136	2137	2097	1461	1182	1391	1993	2132	1816.1
Average	71.2	71.2	69.9	48.7	39.4	46.4	66.4	71.1	60.5

- **December**

Date	Relative humidity (%)								
	Time								
	0	3	6	9	12	15	18	21	Average
1	29	28	27	25	66	16	20	38	31.1
2	40	38	35	29	27	44	76	68	44.6
3	76	98	89	85	57	88	95	92	85.0
4	85	61	55	77	58	59	60	79	66.8
5	89	91	82	63	48	61	89	93	77.0
6	87	80	78	48	37	37	82	80	66.1
7	81	72	70	43	32	33	80	59	58.8
8	55	66	66	34	28	26	63	62	50.0
9	43	60	75	30	25	27	38	45	42.9
10	50	57	53	40	63	57	73	58	56.4
11	57	56	55	54	47	52	67	66	56.8
12	74	75	72	61	49	47	61	75	64.3
13	62	64	64	50	74	74	89	85	70.3
14	88	87	90	56	58	66	71	86	75.3
15	86	91	88	65	71	74	88	96	82.4
16	89	87	93	81	52	55	65	65	73.4
17	65	64	67	51	52	52	62	62	59.4
18	68	65	53	35	32	41	61	58	51.6
19	54	43	41	35	22	21	44	34	36.8
20	36	35	46	28	30	44	86	95	50.0
21	89	93	94	69	54	72	94	92	82.1
22	76	65	60	47	31	35	71	61	55.8
23	57	38	39	26	21	26	47	48	37.8
24	61	60	61	40	33	36	46	43	47.5
25	47	49	47	34	31	35	54	52	43.6
26	59	66	67	42	33	40	72	82	57.6
27	62	58	76	82	72	94	96	95	79.4
28	71	68	90	89	83	90	75	93	82.4
29	89	90	83	60	52	50	93	93	76.3
30	91	94	95	61	42	47	85	69	73.0
31	80	88	78	61	48	56	87	93	73.9
total	2096	2087	2089	1601	1428	1555	2190	2217	1907.9
Average	67.6	67.3	67.4	51.6	46.1	50.2	70.6	71.5	61.5

Appendix 5-A

Table 5-A1 Summary of MED-TVC sensitivity study

Performance Parameters	Effect of Temperature (°C)	Effect of salinity (g/kg)	Effect of motive Steam (bar)
Gain output ratio GOR	1.46	0.03	1.32
Concentration factor	0.11	0.00	0.00
Specific Heat consumption	1.44	0.03	0.00
Fresh Water production	1.47	0.03	3.75
Sea water feed flow	6.69	0.30	7.94
Sea water rejected flow	10.06	0.47	10.76
Average Effect spray flow	1.70	0.04	3.75
Total pumps power consumption	3.67	0.14	5.40
Rejected below down flow	1.81	0.04	3.75
Steam flow	0.00	0.00	0.00
Condensate flow	0.00	0.00	5.00
Condenser area	6.70	0.06	7.94
Minimum separation factor	-100.000000	0.00	5.00
Exergy efficiency	1.62	5.86	3.90
Total exergy destruction	2.47	5.86	1.16

Appendix 6-A
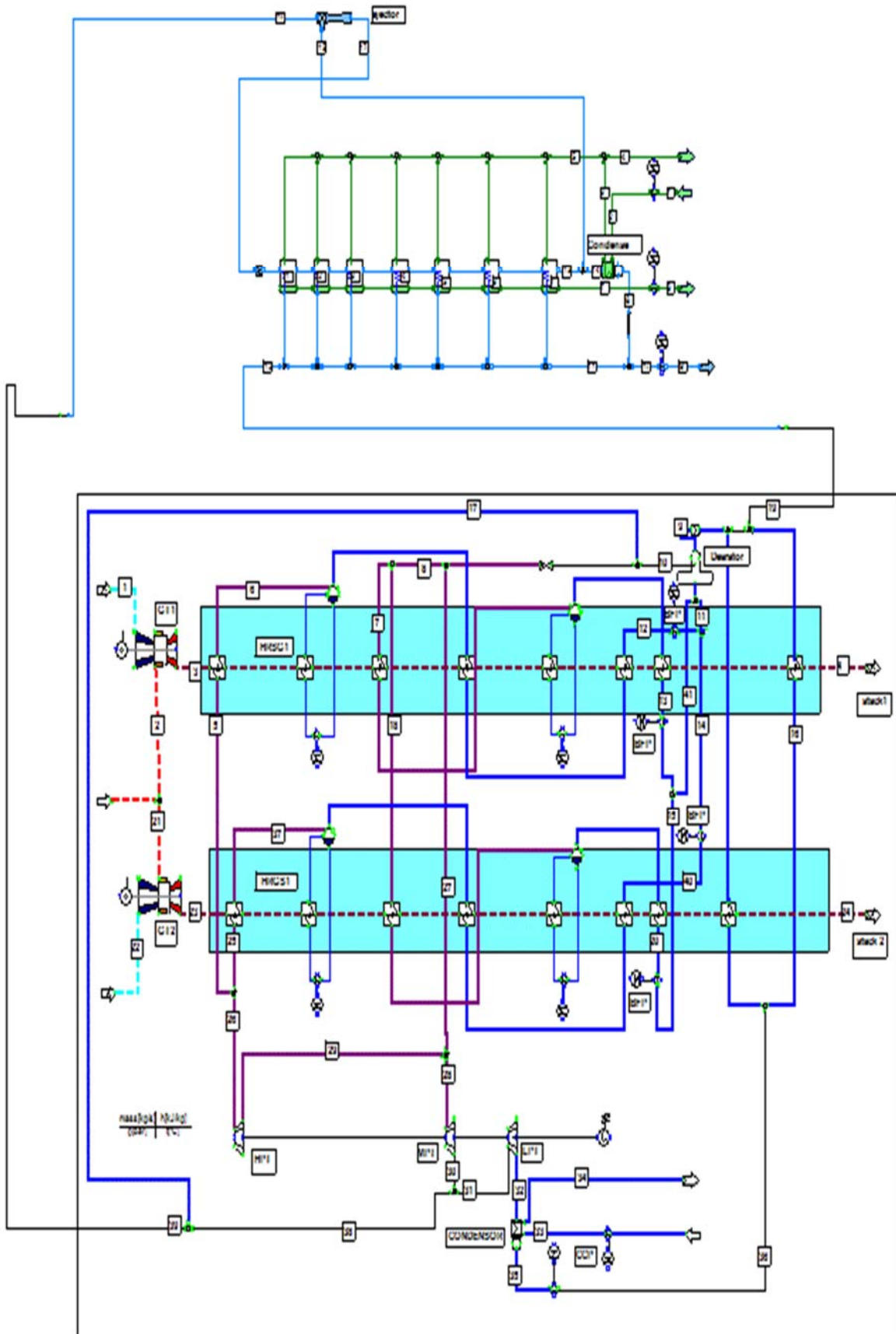
CCPP+AC+MED-TVC

Appendix 7-A

Multi Effect Desalination with Thermal Vapour Compression (MED-TVC)

Appendix 7-B

Two-pass RO